

**MICROWAVE ASSISTED SYNTHESIS OF  
MCM-41 TYPE MESOPOROUS MATERIALS  
AND  
DIFFUSION OF ORGANIC VAPORS IN POROUS MEDIA:  
MCM-41 AND CARBON NANOTUBES**

by

**ASLI ERGÜN**

Submitted to the Graduate School of Engineering and Natural Sciences

in partial fulfillment of

the requirements for the degree of

Doctor of Philosophy

Sabanci University

February 2011

MICROWAVE ASSISTED SYNTHESIS OF  
MCM-41 TYPE MESOPOROUS MATERIALS  
AND  
DIFFUSION OF ORGANIC VAPORS IN POROUS MEDIA:  
MCM-41 AND CARBON NANOTUBES

APPROVED BY:

Prof. Dr. Yuda Yürüm  
(Dissertation Supervisor)



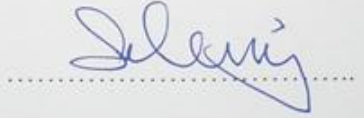
Prof. Dr. Selahattin Gültekin



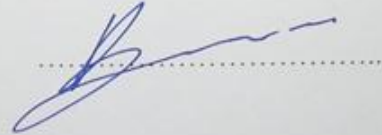
Prof. Dr. Ferhat Yardım



Assist. Prof. Selmiye Alkan Gürsel



Assist. Prof. Burç Mısırlıoğlu



DATE OF APPROVAL: .....03/02/2011.....

© ASLI ERGÜN 2011

ALL RIGHTS RESERVED.

MICROWAVE ASSISTED SYNTHESIS OF  
MCM-41 TYPE MESOPOROUS MATERIALS  
AND  
DIFFUSION OF ORGANIC VAPORS IN POROUS MEDIA:  
MCM-41 AND CARBON NANOTUBES

ASLI ERGÜN

Materials Science and Engineering, PhD Dissertation, 2011

Supervisor: Prof. Dr. Yuda Yürüm

Keywords: Microwave heating, diffusion, uptake measurements, mesoporous sieves, carbon nanotubes

ABSTRACT

In this study a novel synthesis technique of MCM-41 has been successfully applied for the production of pure and metal incorporated MCM-41 type mesoporous molecular sieves under microwave radiation by using a household microwave oven operated at several different combinations of power and time. High quality MCM-41 hexagonal mesoporous materials of good thermal stability were obtained in 30 minutes at 120 Watt by microwave assisted hydrothermal autoclave heating with specific surface area value of  $1438 \text{ m}^2/\text{g}$  and average pore diameter of 3.49 nm.

The effect of metal incorporation into the MCM-41 mesoporous molecular sieves was studied in detail with transition metals such as copper, nickel, cobalt and iron. Impregnation and microwave assisted direct synthesis techniques were used in the

production of MCM-41 type catalytic materials and the physical and structural properties of these were investigated.

The incorporation of metal into MCM-41 structure was investigated using different Si/Metal mol ratios as 25, 50, 75 and 100. Development of the hexagonal mesoporous structure was confirmed by X-ray diffraction (XRD) and N<sub>2</sub> physisorption and Fourier transform infrared (FT-IR), while the metal dispersion were characterized by energy dispersion spectroscopy (EDS) and transmission electron microscopy (TEM). Thermal stabilities of the samples were characterized by thermal gravimetric analyzer (TGA).

Diffusion of organic volatile chemicals in pure MCM-41, metal incorporated MCM-41 (Si/Metal mol ratio: 25) and carbon nanotubes were investigated. Diffusion coefficients, mode of transport and activation energies of diffusion of alcohols (methanol, ethanol, n-propanol, n-butanol) and aromatic solvents (benzene, toluene, ethylbenzene, propylbenzene, o-xylene, m-xylene, p-xylene) into the porous media were measured in 26-32 °C temperature range with a macroscopic measurement technique.

As the molecular weight of the alcohols and aromatics increased, diffusion coefficients into MCM-41 and CNTs decreased, activation energy for diffusion increased, and the time necessary to reach equilibrium increased. The diffusion of alcohols and aromatics into MCM-41 and CNTs obeyed the anomalous transport mechanism. Diffusion rate constants slightly increased with increasing temperature. The diffusion coefficients of volatile molecules into the CNTs were at least 10 times higher than that of diffusion coefficients into MCM-41.

MCM-41 TİPİ MEZOGÖZENEKLİ MALZEMELERİN  
MİKRODALGA YÖNTEMİYLE SENTEZİ  
VE  
GÖZENEKLİ ORTAMLARDA ORGANİK BUHARLARIN DİFÜZYONU:  
MCM-41 VE KARBON NANOTÜP

ASLI ERGÜN

Malzeme Bilimi ve Mühendisliği, Doktora Tezi, 2011

Tez Danışmanı: Prof. Dr. Yuda Yürüm

Anahtar Kelimeler: Mikrodalga ısıtma, difüzyon, alınımlar, mezogözenekli  
elekler, karbon nanotüp

**ÖZET**

Bu çalışmada, yeni bir sentez tekniği kullanılarak saf ve metal eklentili MCM-41 tipi mezogözenekli moleküler eleklerin çeşitli güç ve zaman kombinasyonlarında çalıştırılan ev tipi mikrodalga içerisinde mikrodalga radyasyonu altında sentezlenmesi başarıyla gerçekleştirilmiştir. Yüksek kalite ve ısıl kararlılıktaki MCM-41 hekzagonal mezogözenekli elekler, mikrodalga destekli hidrotermal otoklav ısıtması yöntemiyle spesifik yüzey alanı 1438 m<sup>2</sup>/g ve gözenek çapı 3.49 nm olarak 30 dakika ve 120 Watt'ta elde edilmiştir.

MCM-41 mezogözenekli moleküler eleklerin yapısına metal yüklenmesinin etkisi geçiş metalleri olan bakır, nikel, kobalt ve demir kullanılarak detaylı olarak incelenmiştir. Emdirme ve mikrodalgayla direkt sentez yöntemleri kullanılarak MCM-41 tipi katalitik malzemeler üretilmiş ve bu malzemelerin fiziksel ve yapısal özellikleri incelenmiştir.

Metallerin MCM-41 yapısına katılımı 25, 50, 75 ve 100 olarak belirlenen farklı Si/Metal oranları kullanılarak incelenmiştir. Hekzagonal mezogözenekli yapısının oluşması X-ışını difraksiyonu (XRD), N<sub>2</sub> fiziksel yerleşmesi ve Fourier-transform kızılötesi spektroskopisi ile, metal dağılımlar energy dağılım spektroskopisi (EDS) ve geçirimli electron mikroskobu (TEM) ile tasdik edilmiştir. Malzemelerin ısı kararlılık özellikleri ısı gravimetrik analizör (TGA) ile karakterize edilmiştir.

Uçucu organik kimyasalların saf MCM-41, metal eklentili MCM-41 ve karbon nanotüplerde (KNT) difüzyonu incelenmiştir. Alkollerin (metanol, etanol, n-propanol, n-butanol) ve aromatiklerin çözücülerin (benzen, tolüen, etilbenzen, propilbenzen, o-ksilen, m-ksilen, p-ksilen) mezogözenekli ortamda difüzyon katsayısı, difüzyon mekanizması ve aktivasyon enerjileri 26-32 °C sıcaklık aralığında makroskopik yöntem kullanılarak ölçülmüştür.

Hem MCM-41'de hem de KNT'lerde alkollerin ve aromatiklerin molekül ağırlıkları arttıkça difüzyon katsayısının azaldığı, aktivasyon enerjisi ve dengeye ulaşmak için gerekli olan zamanın arttığı gözlenmiştir. Alkollerin ve aromatiklerin MCM-41 ve KNT'lerdeki alkol ve aromatiklerin difüzyon mekanizması düzensiz difüzyondur. Difüzyon hız sabitleri sıcaklık arttıkça yükselmektedir. Uçucu moleküllerin KNT'lerdeki difüzyon katsayıları MCM-41'inkilere oranla en az 10 kat yüksektir.

**«»To my family«»**

## **ACKNOWLEDGEMENTS**

I would like to express my sincere gratitude to my advisor Prof. Dr. Yuda Yürüm. It is only with his guidance, support, and encouragement that I have been able to complete this process, and I am grateful for all of the opportunities that he has provided me. Through his actions he has shown me how research should be done and how an academician should be, and it has been a privilege to study under his guidance.

I would like to express my special thanks to the members of Faculty of Engineering and Natural Sciences of Sabancı University who kindly shared the knowledge and experience with me. The staff of Sabancı University also deserves to be acknowledged for their contributions to this work. I would like to thank Sibel Pürçüklü for her endless support.

I would like to thank both the present and past laboratory group members in our research group who made the journey pleasurable and rewarding. I would also like to thank all my friends who support me and encourage me.

I would like to especially thank my parents, my grandparents and my parents-in-law for their endless love and selfless support over the years. I am grateful for everything they have done for me. Lastly and mostly, I would like to thank my husband Hüseyin Ergün for walking through the journey together with me and sharing the new perspective over these years.

## TABLE OF CONTENTS

ACKNOWLEDGEMENTS .....	IX
TABLE OF CONTENTS.....	X
LIST OF FIGURES .....	XIII
LIST OF TABLES.....	XVI
LIST OF SYMBOLS AND ABBREVIATIONS .....	XVIII
CHAPTER 1. INTRODUCTION .....	1
CHAPTER 2. STATE OF THE ART .....	3
2.1 MCM-41.....	3
2.1.1 Historical Background .....	4
2.1.2 Structural Properties .....	8
2.1.3 Synthesis Methods .....	10
2.1.4 Characterization Methods .....	31
2.2 CARBON NANOTUBES .....	36
2.2.1 Historical Background .....	36
2.2.2 Structural Properties .....	37
2.2.3 Synthesis Methods .....	39
2.2.4 Characterization Methods .....	41
2.3 DIFFUSION IN POROUS MEDIA .....	45
2.3.1 Theory .....	47
2.3.2 Activation Energy .....	53
2.3.3 Mode of Transport .....	54
CHAPTER 3. EXPERIMENTAL.....	55
3.1 MATERIALS .....	55
3.1.1 Chemicals Used in MCM-41 Synthesis.....	55
3.1.2 Carbon Nanotubes.....	55
3.1.3 Chemicals Used in Diffusion Experiments.....	57

3.2 MICROWAVE ASSISTED SYNTHESIS OF MCM-41 .....	58
3.2.1 Pure MCM-41 .....	58
3.2.2 Metal Incorporated MCM-41 .....	60
3.3 CHARACTERIZATION OF MCM-41 .....	63
3.3.1 N <sub>2</sub> Sorption Analysis .....	63
3.3.2 XRD .....	63
3.3.3 SEM and EDS .....	63
3.3.4 TEM .....	64
3.3.5 FT-IR .....	64
3.3.6 TGA .....	64
3.4 DIFFUSION EXPERIMENTS .....	65
CHAPTER 4. RESULTS AND DISCUSSION .....	67
4.1 SYNTHESIS OF MCM-41 BY MICROWAVE RADIATION .....	67
4.2 SYNTHESIS OF METAL INCORPORATED MCM-41 .....	78
4.2.1 Cu-MCM-41 .....	79
4.2.2 Ni-MCM-41 .....	89
4.2.3 Co-MCM-41 .....	99
4.2.4 Fe-MCM-41 .....	108
4.3 DIFFUSION EXPERIMENTS .....	116
4.3.1 Diffusion in MCM-41 .....	117
4.3.2 Diffusion in Metal Incorporated MCM-41 .....	126
4.3.3 Diffusion in CNT .....	137
CONCLUSIONS .....	146
REFERENCES .....	151
APPENDIX A .....	168
A.1 EXXON MOBIL PATENTS ON SELECTED APPLICATIONS OF M41S MOLECULAR SIEVES .....	168
APPENDIX B .....	170
B.1 CALCULATING DIFFUSION COEFFICIENTS .....	170
B.2 CALCULATING DIFFUSION RATE CONSTANTS AND DIFFUSION EXPONENTS .....	172

APPENDIX C .....	173
C.1 DIFFUSION MEASUREMENTS IN MCM-41 .....	173
C.2 DIFFUSION MEASUREMENTS IN METAL INCORPORATED MCM-41 ..	174
C.3 DIFFUSION MEASUREMENTS IN CNT .....	176
APPENDIX D.....	177
CURRICULUM VITAE.....	177

## LIST OF FIGURES

<b>Figure 2-1</b> M41S family of materials.....	4
<b>Figure 2-2</b> Number of publications citing Kresge et al., Nature, 1992.....	7
<b>Figure 2-3</b> a) hexagonal pores and b) functionalized pores .....	8
<b>Figure 2-4</b> Zeolite versus MCM-41 .....	9
<b>Figure 2-5</b> Formation mechanisms proposed by Beck et al.....	11
<b>Figure 2-6</b> Representation of the cooperative formation mechanism .....	13
<b>Figure 2-7</b> Molecular formula of frequently used cationic surfactants.....	15
<b>Figure 2-8</b> Anionic surfactants.....	16
<b>Figure 2-9</b> Adsorption desorption isotherm of MCM-41 .....	31
<b>Figure 2-10</b> X-ray diffraction pattern of high-quality calcined MCM-41 .....	33
<b>Figure 2-11</b> a) The structure of hexagonal MCM-41 and b) The unit cell of the solid phase .....	33
<b>Figure 2-12</b> SEM image of MCM-41 .....	34
<b>Figure 2-13</b> Transmission electron micrograph of MCM-41 featuring 4.0 nm sized pores, hexagonally arranged .....	35
<b>Figure 2-14</b> a) Unit cell of SWCNT and b) chirality of SWCNT .....	37
<b>Figure 2-15</b> a) armchair nanotube b) zigzag nanotube and c) chiral nanotube.....	38
<b>Figure 2-16</b> CVD experimental set-up.....	40
<b>Figure 2-17</b> Growth mechanism of CNTs .....	41
<b>Figure 2-18</b> TEM image of SWNTs grown at 750 °C using Fe-Co-MCM-41 catalyst	42
<b>Figure 2-19</b> SEM images of CNTs synthesized using Fe-Co-MCM-41 catalyst .....	42
<b>Figure 2-20</b> Raman spectrum.....	43
<b>Figure 2-21</b> Transport mechanisms in porous media: (a) gaseous or molecular flow, (b) Knudsen flow, (c) surface diffusion, (d) multilayer diffusion, (e) capillary condensation, (f) configurational diffusion.....	50
<b>Figure 3-1</b> SEM image of Baytubes C 150 HP .....	57
<b>Figure 3-2</b> Schematic representation of synthesis techniques .....	62
<b>Figure 3-3</b> Set-up of diffusion experiments .....	66
<b>Figure 4-1</b> XRD patterns of MCM-41 (80/10, 80/20, 80/30, 80/60).....	68
<b>Figure 4-2</b> N <sub>2</sub> sorption isotherms of MCM-41 a) 80/10 b) 80/20 c) 80/30 d) 80/60 .....	70
<b>Figure 4-3</b> XRD patterns of MCM-41 (120/10, 120/20, 120/30, 120/60).....	71

<b>Figure 4-4</b> N <sub>2</sub> sorption isotherms of MCM-41 a) 120/10 b) 120/20 c) 120/30 d)120/60 .....	73
<b>Figure 4-5</b> SEM images of MCM-41 (120/30) by inlens detector.....	75
<b>Figure 4-6</b> SEM images of MCM-41 a) 80/60 b) 80/120 by secondary electron detector .....	75
<b>Figure 4-7</b> FTIR spectra of MCM-41 synthesized at 120 W in 30 minutes a) uncalcined b)calcined.....	76
<b>Figure 4-8</b> XRD patterns of Cu-MCM-41-DS-25 (80/30 and 80/60).....	79
<b>Figure 4-9</b> N <sub>2</sub> sorption isotherms of Cu-MCM-41-DS-25 a) 80/30 b) 80/60.....	80
<b>Figure 4-10</b> SEM images of Cu-MCM-41-DS-25 a) 80/30 b) 80/60.....	81
<b>Figure 4-11</b> XRD patterns of Cu-MCM-41 (120/30) with different Si/Cu mol ratios prepared by microwave assisted direct synthesis.....	81
<b>Figure 4-12</b> N <sub>2</sub> sorption isotherms direct synthesized Cu-MCM-41 (120/30) samples a) Si/Cu:25 b) Si/Cu:50 c) Si/Cu: 75 d) Si/Cu:100.....	83
<b>Figure 4-13</b> SEM images of Cu-MCM-41 (120/30) a) Si/Cu:25 b) Si/Cu:75.....	85
<b>Figure 4-14</b> TEM of Cu-MCM-41-DS-25 (120/30).....	85
<b>Figure 4-15</b> XRD patterns of Cu-MCM-41(120/30) with different Si/Cu mol ratios prepared by microwave assisted impregnation synthesis.....	86
<b>Figure 4-16</b> N <sub>2</sub> sorption isotherms of impregnated Cu-MCM-41 (120/30) samples a) Si/Cu:25 b) Si/Cu:50 c) Si/Cu:75 d) Si/Cu:100.....	87
<b>Figure 4-17</b> XRD patterns of Ni-MCM-41-DS-25 (80/30 and 80/60).....	89
<b>Figure 4-18</b> N <sub>2</sub> sorption isotherms of Ni-MCM-41-DS-25 a) 80/30 b) 80/60.....	90
<b>Figure 4-19</b> SEM image of Ni-MCM-41-DS-25 (80/30).....	90
<b>Figure 4-20</b> XRD patterns of Ni-MCM-41 (120/30) with different Si/Ni mol ratios prepared by microwave assisted direct synthesis.....	91
<b>Figure 4-22</b> SEM images of Ni-MCM-41 (120/30) a) Si/Ni: 25 b) Si/Ni:50 c) Si/Ni:75 d) Si/Ni:100 by inlens detector.....	92
<b>Figure 4-21</b> N <sub>2</sub> sorption isotherms of direct synthesized Ni-MCM-41 (120/30) samples a) Si/Ni:25 b) Si/Ni:50 c) Si/Ni:75 d) Si/Ni:100.....	93
<b>Figure 4-23</b> TEM of Ni-MCM-41-DS-25 (120/30).....	95
<b>Figure 4-24</b> XRD patterns of Ni-MCM-41(120/30) with different Si/Ni mol ratios prepared by microwave assisted impregnation synthesis.....	96
<b>Figure 4-25</b> N <sub>2</sub> sorption isotherms of impregnated Ni-MCM-41 (120/30) samples a) Si/Ni:25 b) Si/Ni:50 c) Si/Ni:75 d) Si/Ni:100.....	97

<b>Figure 4-26</b> XRD patterns of Co-MCM-41 (120/30) with different Si/Co mol ratios prepared by microwave assisted direct synthesis .....	99
<b>Figure 4-28</b> Pore size distribution of Co-MCM-41-DS-25 (120/30).....	100
<b>Figure 4-27</b> N <sub>2</sub> sorption isotherms of direct synthesized Co-MCM-41 (120/30) samples a) Si/Co:25 b) Si/Co:50 c) Si/Co:75 d) Si/Co:100.....	101
<b>Figure 4-29</b> SEM images of Co-MCM-41 (120/30) a) Si/Co: 25 b) Si/Co:50 c) Si/Co:75 d) Si/Co:100.....	103
<b>Figure 4-30</b> TEM of Co-MCM-41-DS-25 (120/30) .....	104
<b>Figure 4-31</b> XRD patterns of Co-MCM-41(120/30) with different Si/Co mol ratios prepared by microwave assisted impregnation synthesis .....	105
<b>Figure 4-32</b> N <sub>2</sub> sorption isotherms of impregnated Co-MCM-41 (120/30) samples a) Si/Co:25 b) Si/Co:50 c) Si/Co:75 d) Si/Co:100.....	106
<b>Figure 4-33</b> XRD patterns of Fe-MCM-41 (120/30) with different Si/Fe mol ratios prepared by microwave assisted direct synthesis .....	108
<b>Figure 4-34</b> N <sub>2</sub> sorption isotherms of direct synthesized Fe-MCM-41 (120/30) samples a) Si/Fe:25 b) Si/Fe:50 c) Si/Fe:75 d) Si/Fe:100 .....	110
<b>Figure 4-35</b> TEM of Fe-MCM-41-DS-25 (120/30).....	112
<b>Figure 4-36</b> XRD patterns of Fe-MCM-41(120/30) with different Si/Fe mol ratios prepared by microwave assisted impregnation synthesis .....	113
<b>Figure 4-37</b> N <sub>2</sub> sorption isotherms of impregnated Fe-MCM-41 (120/30) samples a) Si/Fe:25 b) Si/Fe:50 c) Si/Fe:75 d) Si/Fe:100 .....	114
<b>Figure 4-38</b> Diffusion coefficients of volatile alcohols in MCM-41 .....	118
<b>Figure 4-39</b> Diffusion coefficients of volatile aromatics in MCM-41.....	120
<b>Figure 4-40</b> Diffusion coefficients of volatile alcohols in Cu-MCM-41 .....	128
<b>Figure 4-41</b> Diffusion coefficients of volatile alcohols in Ni-MCM-41.....	128
<b>Figure 4-42</b> Diffusion coefficients of volatile alcohols in Co-MCM-41 .....	129
<b>Figure 4-43</b> Diffusion coefficients of volatile alcohols in Fe-MCM-41.....	129
<b>Figure 4-44</b> Diffusion coefficients of volatile alcohols in CNT .....	138
<b>Figure 4-45</b> Diffusion coefficients of volatile aromatics in CNT.....	140

## LIST OF TABLES

<b>Table 2-1</b> Overview of MCM-41-like materials .....	17
<b>Table 2-2</b> Comparison of the currently available microwave systems for synthetic applications .....	25
<b>Table 3-1</b> Structural properties of Baytubes® C 150 HP.....	56
<b>Table 3-2</b> Parameters of the microwave synthesis of pure MCM-41 .....	59
<b>Table 3-3</b> Summary of the metal incorporated experiments .....	61
<b>Table 4-1</b> Physical and structural properties of MCM-41 type catalytic materials synthesized by microwave assisted direct synthesis method.....	74
<b>Table 4-2</b> Physical and structural properties of Cu-MCM-41 type catalytic materials synthesized by microwave assisted direct synthesis method.....	84
<b>Table 4-3</b> Physical and structural properties of Cu-MCM-41 type catalytic materials synthesized by microwave assisted impregnation method .....	88
<b>Table 4-4</b> Physical and structural properties of Ni-MCM-41 type catalytic materials synthesized by microwave assisted direct synthesis method.....	94
<b>Table 4-5</b> Physical and structural properties of Ni-MCM-41 type catalytic materials synthesized by microwave assisted impregnation method .....	98
<b>Table 4-6</b> Physical and structural properties of Co-MCM-41 type catalytic materials synthesized by microwave assisted direct synthesis method.....	102
<b>Table 4-7</b> Physical and structural properties of Co-MCM-41 type catalytic materials synthesized by microwave assisted impregnation method .....	107
<b>Table 4-8</b> Physical and structural properties of Fe-MCM-41 type catalytic materials synthesized by microwave assisted direct synthesis method.....	111
<b>Table 4-9</b> Physical and structural properties of Fe-MCM-41 type catalytic materials synthesized by microwave assisted impregnation method .....	115
<b>Table 4-10</b> Diffusion rate constants, diffusion exponents, and transport mechanism of alcohols in MCM-41 .....	121
<b>Table 4-11</b> Diffusion rate constants, diffusion exponents, and transport mechanism of aromatics in MCM-41.....	123
<b>Table 4-12</b> Activation energies of volatile alcohols in MCM-41 .....	125
<b>Table 4-13</b> Activation energies of volatile aromatics in MCM-41 .....	125

<b>Table 4-14</b> Diffusion rate constants, diffusion exponents, and transport mechanism of alcohols in Cu-MCM-41 .....	130
<b>Table 4-15</b> Diffusion rate constants, diffusion exponents, and transport mechanism of alcohols in Ni-MCM-41.....	132
<b>Table 4-16</b> Diffusion rate constants, diffusion exponents, and transport mechanism of alcohols in Co-MCM-41 .....	133
<b>Table 4-17</b> Diffusion rate constants, diffusion exponents, and transport mechanism of alcohols in Fe-MCM-41.....	134
<b>Table 4-18</b> Activation energies of volatile alcohols in metal incorporated MCM-41 .	136
<b>Table 4-19</b> Diffusion rate constants, diffusion exponents, and transport mechanism of alcohols in CNT .....	142
<b>Table 4-20</b> Diffusion rate constants, diffusion exponents, and transport mechanism of aromatics in CNT.....	143
<b>Table 4-21</b> Activation energies of volatile alcohols in CNT .....	144
<b>Table 4-22</b> Activation energies of volatile aromatics in CNT .....	145

## LIST OF SYMBOLS AND ABBREVIATIONS

$a$	: characteristic lattice parameter
$C$	: capacity
$C_i$	: concentration of species $i$
$d$	: interlayer spacing
$D$	: diffusion coefficient
$D_{\text{pore}}$	: pore diameter
$\delta$	: pore wall thickness
$E_a$	: activation energy
$\epsilon_r$	: dielectric coefficient (permittivity)
$f$	: frequency
$k$	: diffusion rate constant
$J$	: flux
$M_t$	: mass of solvent diffused at time $t$
$M_\infty$	: mass of solvent diffused at steady state
$\mu$	: chemical potential
$n$	: diffusion exponent
$P$	: Pressure
$P_0$	: Reference pressure
$\Psi$	: thermodynamic correction factor
$R^2$	: correlation coefficient
$\sigma$	: dielectric conductivity
$T$	: temperature

AFM	: Atomic Force Microscopy
AMS	: Anionic-surfactant-templated Mesoporous Silica
BET	: Brunauer Emmett Teller
BJH	: Barrett Joyner Halenda
CNT	: Carbon Nanotube
CTABr	: Cetyltrimethyl ammonium bromide
CVD	: Chemical Vapor Deposition
DFT	: Density Functional Theory
EDS	: Energy Dispersive Spectroscopy
FSM	: Folded-sheet Mesoporous Material
FT-IR	: Fourier Transformed Infrared Spectroscopy
HMS	: Hexagonal Ordered Silica
IUPAC	: International Union of Pure and Applied Chemistry
LCT	: Liquid Crystal Templating
M41S	: Mobil Family of Materials
MCM	: Mobil Composition of Matter – Mobile Crystalline Material
MSU	: Michigan State University material
MWCT	: Multi-walled Carbon Nanotubes
SBA	: Santa Barbara Amorphous type material
SEM	: Scanning Electron Microscopy
STM	: Scanning Tunneling Microscopy
SWCT	: Single-walled Carbon Nanotubes
TBOS	: Tetrabutyl orthosilicate

TEM : Transmission Electron Microscopy  
TEOS : Tetraethyl orthosilicate  
TMOS : Tetramethyl orthosilicate  
TGA : Thermal Gravimetric Analyzer  
XRD : X-ray Diffraction

## CHAPTER 1. INTRODUCTION

Many applications in adsorption, separation and catalysis require nanostructures whose pore size can be controlled and architecture be adjusted upon requisites. Following the discovery of MCM-41, and multi wall carbon nanotubes (MWCT) in 1991, which possesses nanopores that are both regularly ordered and well defined, extensive scientific studies concentrated on miscellaneous aspects of chemical and physical processes in nanopores were set off.

Since their discovery, MCM-41 mesoporous molecular sieves are synthesized with conventional hydrothermal synthesis. However production of these materials with environmentally friendly techniques is an important issue to meet the requirements of green chemistry. In recent years studies suggest that microwave energy may have a unique ability in materials syntheses. Specifically, syntheses of zeolites, mixed oxide and mesoporous molecular sieves by employing microwave energy have attracted great attention. Reduction of synthesis time, by over an order of magnitude make continuous production possible to replace batch synthesis as well as lowering the cost of the process. In addition to this, more uniform and defect-free products can be synthesized by microwave radiation than conventional hydrothermal synthesis.

At present, microwave irradiation technique is widely applied to the synthesis of mesoporous molecular sieves but most investigations aimed at synthesizing pure silica MCM-41. The application of pure silica mesoporous molecular sieve to various kinds of catalytic reactions is limited due to electro-neutral surface structure with little acidic center. The catalytic performance of MCM-41 can be improved by incorporation of transition metals into the structure. Few articles considering the metal incorporation into

MCM-41 mesoporous molecular structure under microwave radiation have been reported recently. In this study, detailed investigations of microwave-assisted hydrothermal autoclave heating for the production of MCM-41 mesoporous materials were presented. Furthermore, incorporation of transition metals into the mesoporous structure was investigated by using two different techniques such as microwave assisted direct synthesis and impregnation method.

Understandings of the fundamental diffusion properties of organic molecules in the nanopores are significantly important in heterogeneous catalysis, gas–solid reactions and adsorptive separations since the molecular transport processes in nanopores are the crucial steps. It is therefore important to investigate the diffusion of molecules in these materials and analyze the factors limiting their performance.

MCM-41 molecular sieves and carbon nanotubes (CNT) with tubular shape and high surface/weight ratio make them attractive candidates for gas adsorption, and catalysis. In this study, diffusion of organic volatile solvents such as alcohols and aromatics were investigated in detail.

## CHAPTER 2. STATE OF THE ART

### 2.1 MCM-41

Due to the recent demands in technology and industrial applications, the discovery of new materials is an essential objective of material science research. There has been a growing interest to develop materials with greater pore sizes from the microporous scale to the mesoporous scale.

The classification of materials in terms of their pore sizes according to International Union of Pure and Applied Chemistry (IUPAC) is, [1]:

1. Microporous materials ( pore diameters  $\leq 2$  nm)
2. Mesoporous materials (2 nm < pore diameters < 50 nm)
3. Macroporous materials ( pore diameters  $\geq 50$  nm)

One such microporous material is zeolite with pore sizes in the range of 0.3 to 1.5 nm. Their acidic form makes them the most important heterogeneous acid catalysts used in industry. Their natural form on the other hand, have many applications in wastewater cleaning, agriculture, fertilizers, aquaculture, animal health, animal nourishment, gas separation, solar refrigeration, gas cleaning, deodorization, solid electrolytes, construction materials, and cleaning of radioactive wastes [2]. However, the microporous structure of zeolites has drawback dealing with larger molecules. Mesoporous materials have a clear advantage over zeolites in which larger molecules can be diffused and catalyzed.

### 2.1.1 Historical Background

The developing needs both in industry and research have had inevitable impact on discovering new materials with greater pore sizes. In 1988, a crystalline microporous material, VPI-5, with regular pores larger than 1 nm was synthesized [3, 4]. Following that, larger-pore crystalline materials were developed, such as AlPO-4, Cloverite, JDF-20, ULM-5, UDT-1, ULM-16, CIT-5, ND-1, FDU-4, NTHU-1... etc. [4].

Concurrently, scientists from Mobil Oil Corporation had discovered even more larger-pore (2-10 nm) mesoporous molecular sieves, designated as M41S and patented in 1991 and 1992 [5-9]. M41S is the acronym of the family of mesoporous materials discovered by Mobil researchers. Most well-known members are MCM-41 with hexagonal phase, MCM-48 with cubic phase and MCM-50 with lamellar phase (Figure 2-1) [10-14]. The acronym of **MCM** refers to **Mobil Composition of Matter**; also it stands for **Mobil Crystalline Material**. The number refers to the experiment number.

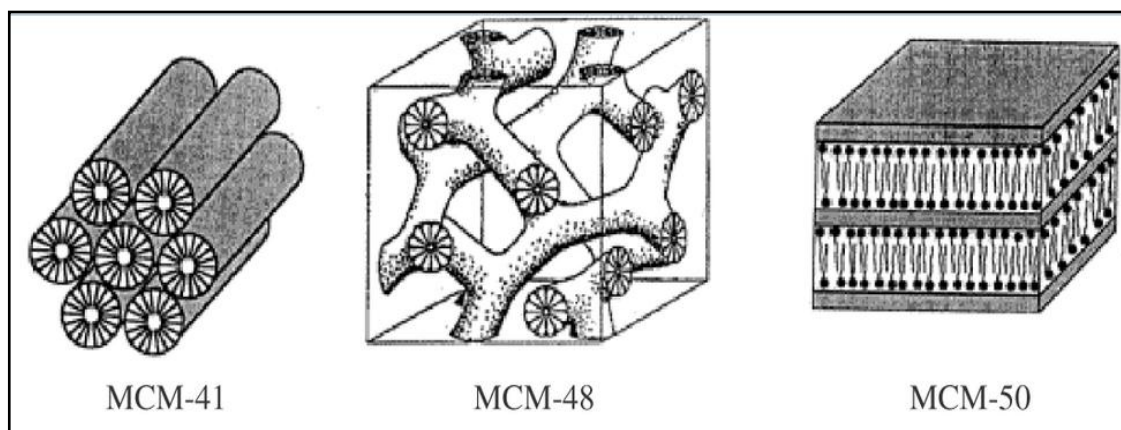


**Figure 2-1** M41S family of materials [12]

Before their declaration, a patent describing the procedure for the preparation of low-density silica was already filed in 1969 [15]. However, due to the lack of analysis and characterization, the remarkable properties of these materials were not recognized until 1997 when Di Renzo et al. [16] reproduced the synthesis reported in the patent and found that it leads to a material identical to mesoporous MCM-41. Nevertheless, the developed synthesis techniques and discoveries of Mobil researchers opened a new field of mesoporous materials.

Also in the early 1990s, the discovery of mesoporous silica nanoparticles by Kuroda's group in Japan [17, 18] led to the development of new alkylammonium-clay intercalation complexes which have been subjected to hydrothermal treatment followed by calcination. The resulting material produced a highly ordered mesoporous powder with a honeycomb structure referred to as FSM-n (folded-sheet mesoporous material) where n refers to the number of carbon atoms in the surfactant alkylchain used to synthesize the material which is identical to MCM-41. Even though the Japanese publication was a year earlier than was the Mobil patent, the pathway described in the publication by Yanagisawa et al. [17] was difficult to realize, however, the early publications of Mobil group described a more generalizable pathway.

Pinnavaia et al. [19, 20] have developed two additional approaches for the synthesis of mesoporous materials based on neutral surfactants to prepare HMS (hexagonal ordered silica) and MSU (Michigan State University material) [21]. Also, silica nanoparticles with much larger pores (4.6 to 30 nm) were produced at the University of California aptly named the Santa Barbara Amorphous, or SBA-15 with a hexagonal array of pores [22].

The discovery of M41S family of materials arises from the effort to discover new porous materials which can selectively convert high molecular weight, bulky petroleum molecules into more valuable fuel and lubricant products by Mobil researchers. In the mid-1980s, researchers in Mobil Research and Development Corporation in Paulsboro, NJ laboratory were working on layered-type materials and converting them into stable porous catalysts by pillaring. In the mid-1980s to late-1980s, researchers in what was then called Paulsboro Laboratory approached synthesizing large pore frameworks by combining the concept of pillared layer materials and formation of zeolites and result was MCM-22 composed of crystalline layers linked together by weak chemical bonds that become stronger after thermal treatment [23]. A pillared layered material designated as MCM-36 was also identified after delimitating the crystalline layers of MCM-22 [24, 25].

The layered zeolites precursors such as MCM-22 had higher activity and porosity compared to the other layered precursors. This approach, interrupting the synthesis to isolate the layered zeolites precursors, was investigated in detail. In order to optimize the synthesis conditions, the synthesis was interrupted each time in many experiments

for X-ray diffraction characterization to observe the crystallinity. The interruptions were either performed by adding alkyltrimethylammonium salt at high pH or a reactive silica i.e. tetramethyl ammonium salt, was added as a potential pillaring agent. These new synthesis mixtures were treated at around 100 °C in an attempt to form zeolites-layered hybrid materials. In these experiments, researchers recognized some very unusual properties: one broad low angle peak at about  $2^\circ 2\theta$ ; high BET surface area values greater than 1000 m<sup>2</sup>/g; and high hydrocarbon sorption capacities, abnormally high when compared to zeolites. Aside from its interruptive capacity, cetyltrimethylammonium hydroxide was directly added to develop high efficiency swelling and used as a structure-directing-agent in zeolite-like synthesis. The products again showed the unusual properties as described above. Thus, both techniques resulted in the new mesoporous products with each remarkable sorption properties that researchers at analytical laboratories initially believed that their test equipment was broken or miscalibrated [26].

The researchers used many characterization techniques before declaring their discovery. First, from the XRD pattern, they initially assumed that they synthesized some kind of layered silicate precursor with crystalline domain sizes below XRD detectability. After TEM analysis, they observed the uniform hexagonal channels. When <sup>29</sup>Si NMR data showed that the walls were amorphous, reserachers determined that the materials lacked typical crystalline framework. After determining that XRD patterns were generated by ordering of the pores instead of crystalline walls, they were eventually convinced that a new class of materials had been discovered. After this discovery, many Exxon Mobil patents were filed on catalytic applications and other applications. A summary of selected patents is given in Table A.1 and Table A.2 in Appendix A [26].

The M41S family of materials differs from zeolites in many ways: i.e., they contain amorphous walls and little or no Brønsted acidity. Even though the walls are amorphous, there are silanol groups with uniform density within the channels which provide sites for the functionalization of species within the channels. These functionalized products can be used in designing new catalyst/sorption materials for new applications in catalysis and other areas such as drug delivery, water cleaning, fiber optic, tissue engineering etc.

As far as catalysis is concerned, crystalline mesoporous materials have shown promising performances in a number of acid- and redox-based processes. The observed improvement compared to more conventional catalysts often stems from increased surface area and greater accessibility of active sites.

A growing interest in the M41S mesoporous materials since their discovery in 1992 is evidenced in Figure 2.2. There is a tremendous increase in the number of publications per year from 1998 to 2010. Separate sessions at international symposia entirely dedicated to mesoporous materials as well as meetings dedicated entirely to this subject even organized.

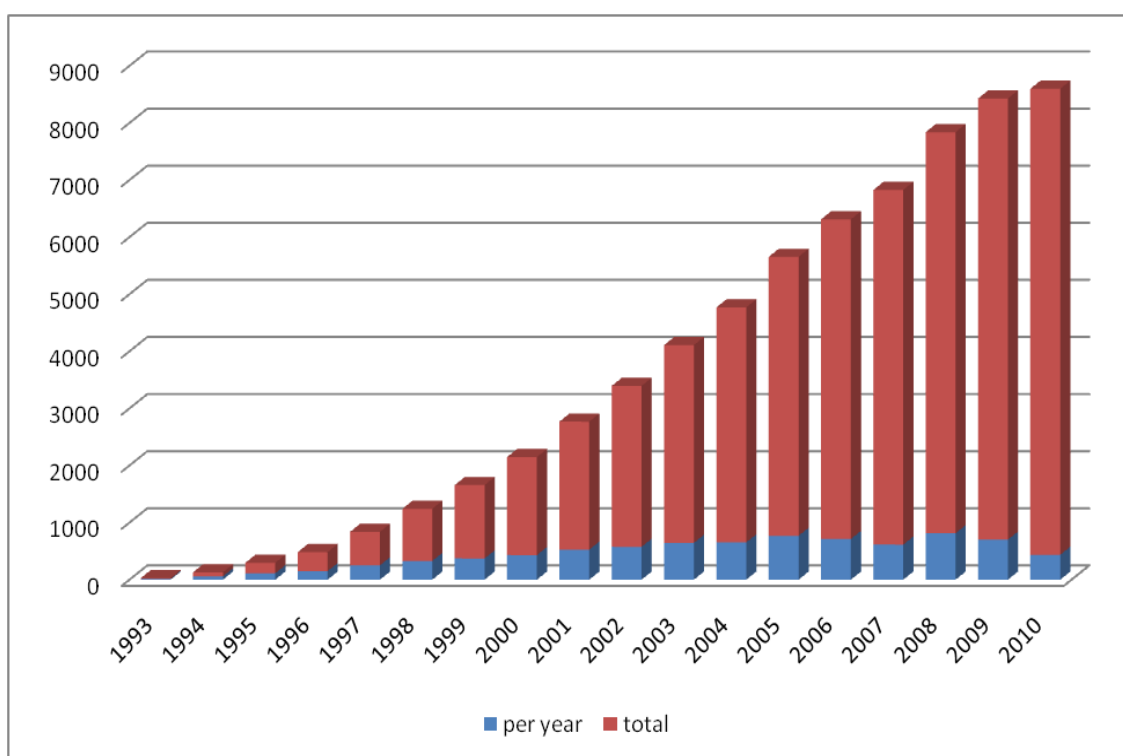


**Figure 2-2** Number of publications citing Kresge et al., Nature, 1992 [5] from Scifinder

Although MCM-41, MCM-48 and MCM-50 are synthesized from the same materials, they show very different structural properties. Undoubtedly, MCM-41 is the most popular mesoporous molecular sieve that is widely studied by researchers. Detailed descriptions, properties, and syntheses of MCM-41 mesoporous materials are given in the following titles.

### 2.1.2 Structural Properties

MCM-41 is as described previously, a mesoporous silica walled material which has a regularly ordered two-dimensional hexagonal pore arrangement and narrow pore size distribution. The channels of MCM-41 are not connected and the walls are amorphous silica. In other words, MCM-41 mesoporous molecular sieves exhibit order on the mesoscopic-scale but disorder on the atomic scale.

In general, pure silica MCM-41 mesoporous molecular sieve has little catalytic activity due to some defects, for example, its surface is almost electro-neutral with little acidic center. However, its catalytic performance can be further extended since the walls can be functionalized by incorporation of transition metals to enhance the electron-transfer efficiency to design new catalysts/sorption systems [27]. The pore diameters can be arranged from 1.5 to 10 nm by varying the alkyl chain length of the surfactants (Figure 2.3).

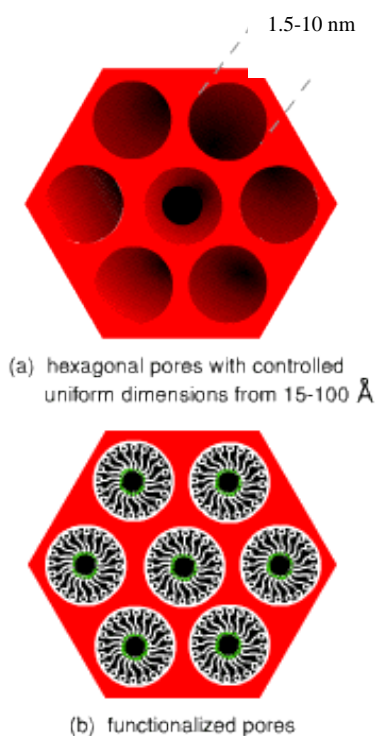


**Figure 2-3** a) hexagonal pores and b) functionalized pores [28]

MCM-41 mesoporous molecular sieves have received increasing scientific interest with their:

1. Highly ordered meso-structure,
2. Uniformly distributed pore size
3. High surface area ( $1500 \text{ m}^2/\text{g}$ ),
4. High pore volume ( $1 \text{ cm}^3/\text{g}$ ),
5. Designable chemical composition and functionalizable surface, and
6. Controllable size and morphology,

all which make them promising candidates for use as catalyst and support.

Due to MCM-41's larger pores, it has advantages over zeolites, such as (Figure 2.3):

- Separates larger molecules
- Performs catalysis on larger molecules (i.e. hydrocracking large molecular weight molecules into gasoline)

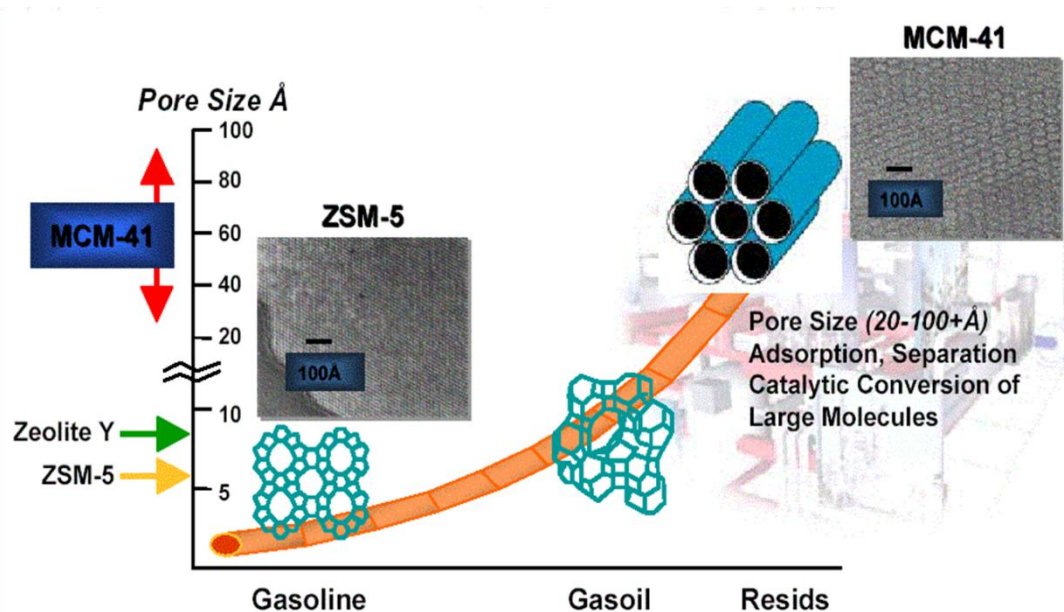


**Figure 2-4** Zeolite versus MCM-41 [28]

### 2.1.3 Synthesis Methods

The syntheses of MCM-41 materials occur under moderate temperatures, below 120 °C, in a basic solution of silicate source with cationic surfactants under conventional heating or microwave radiation.

For the synthesis of MCM-41, four main reagents are required; (1) a solvent (water and/or ethanol), (2) a silica source (tetraethyl orthosilicate (TEOS), sodium silicate solution, tetramethyl orthosilicate (TMOS), tetrabutyl orthosilicate (TBOS)), (3) an ionic (anionic or cationic) or neutral surfactant, (4) base [29].

The formation of mesoporous materials has been considered to be highly dependent on the interaction between organic (surfactants) and inorganic (silica oligomers) species. The reaction can occur in basic medium in which the base is the catalyst and surfactant/silica mol ratio may vary as given below. In the synthesis, the inorganic species first hydrolyze and condense into an oligomeric silica sol, followed by a sol-gel transition due to the further condensation, then accompanied by the self-assembly of surfactants and inorganic species to finally form mesostructures. The mixture is stirred, aged at room temperature and placed in a static autoclave for several hours under conventional synthesis route or microwaved in shorter crystallization time. The surfactant template is removed by calcination under air atmosphere and the obtained product washed with distilled water, filtered, and dried.

In the M41S family, MCM-41 is formed with the highest concentration of silica, i.e., lowest surfactant/silica molar ratio. As the surfactant/silica molar ratio is varied, the resulting products can be grouped into four main categories [15]:

1. Surfactant/silica < 1 : Hexagonal (MCM-41)
2. Surfactant/Silica = 1-1.5 : Cubic (MCM-48)
3. Surfactant/Silica = 1.2-2 : Lamellar (MCM-50)
4. Surfactant/Silica > 2 : Cubic octamer

Detailed information about formation mechanism, templating techniques in terms of type of surfactants, and type of heating mode is given in the following sections.

### 2.1.3.1 Formation Mechanisms

After their discovery, researchers focused on the formation mechanism of M41S family of materials. The mesostructure of M41S materials depends greatly on the surfactant concentration and hydrophobic chain length and on the presence of organic swelling agents dissolved in the hydrophobic spaces. Mobil scientists proposed two possible pathways for the formation of mesoporous molecular sieves as can be seen in Figure 2.5 [5, 6, 14, 15]:

1. The liquid-crystal phase is intact before the silicate species are added
2. The addition of silicate results in the ordering of the subsequent silicate encased surfactant micelles

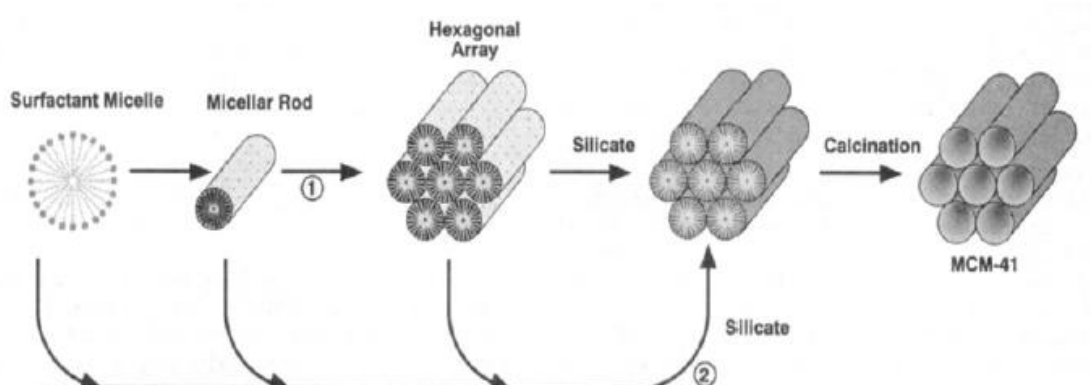


**Figure 2-5** Formation mechanisms proposed by Beck et al.

For either pathway, the resultant composition would produce an inorganic material that mimics known liquid-crystal phases. For pathway 1, which is called *liquid crystal templating mechanism*, to be operative, the surfactant molecules must exist in sufficient concentration for a liquid-crystal structure to form. This liquid-crystal structure serves as the templating agent and the inorganic silicate anions solely serve to counterbalance the charge of these fully ordered surfactant aggregates. The liquid crystal templating mechanism has been a matter of debate, since no preformed surfactant liquid crystalline phase exists in the synthesis precursor of mesoporous materials in the hydrothermal synthesis. The concentration of surfactant required for the formation of liquid crystal is very high, which could not be obtained in the dilute precursor solutions.

For pathway 2, which is as called *the cooperative formation mechanism*, surfactant is only part of the template. The presence of a silicate anion species not only serves to balance the surfactant cations but also participates in the formation and ordering of the liquid-crystal phase.

The cooperative formation mechanism of mesoporous silica was further advanced by Davis et al [30, 31] and Stucky et al, [13, 32]. Davis and co-workers proposed a “silicate rod assembly” mechanism. Two or three monolayers of silicate species first deposit on isolated surfactant micellar rods. The long surfactant-silicate rods spontaneously aggregate and eventually pack into a long-range ordered hexagonal arrangement. This mechanism is, however, unconvincing due to the difficulty of assembling long rods. It is also not as popular as the cooperative formation mechanism, first proposed by Stucky and co-workers and accepted by most researchers.

Stucky’s theory was inspired by the lamellar-to-hexagonal phase transformation [33]. Figure 2.6 presents the process of formation of MCM-41 mesoporous silica from aqueous solution of surfactant (cetyltrimethylammonium bromide, CTABr) and silica source. In an early stage, an ion-exchange occurs preferentially between silicate oligomers and CTABr in the precursor solution and a CTA-silica complex is thus formed. The self-assembly of CTA-silica then naturally enables the formation of a silicatropic liquid crystal (SLC) phase. A low-curvature lamellar phase is first formed because of the highly charged silica species and the matching charge density. When the condensation of silicate proceeds, the negative charge density of oligosilicate is dramatically reduced. This causes a rearrangement of surfactant and consequently a mesophase transformation to a high-curvature hexagonal one. The final phase is determined by the reaction coordinate when the solidification of the SLC is achieved.

In other words the ion pairs then self-organize into a mesophase, having most often a liquid-crystal structure, i.e., hexagonal, lamellar, or cubic. The structure of the mesophase depends on the composition of the mixture, the pH, and the temperature.

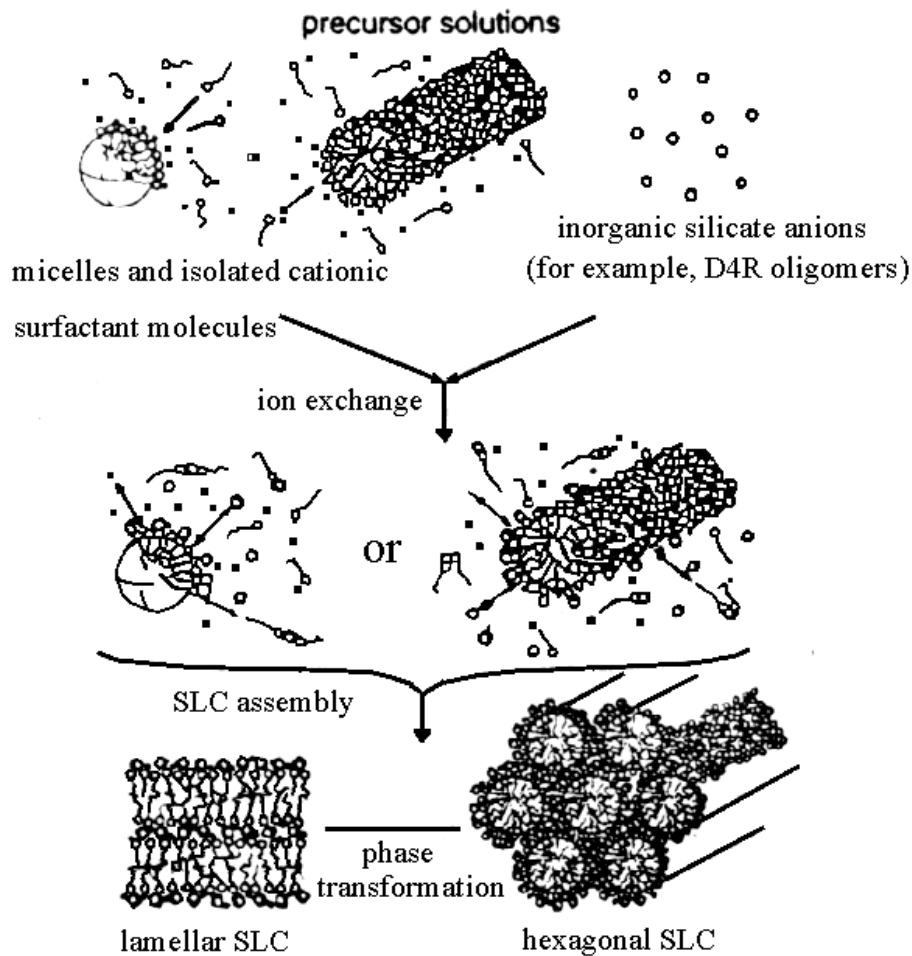


**Figure 2-6** Representation of the cooperative formation mechanism [32]

The formation mechanisms, *i.e.* liquid crystal templating and cooperative formation, are valid when using different synthesis methods. It is known that the free energy of mesostructure formation ( $\Delta G_{\text{meso}}$ ) is mainly composed of four terms given in equation (2.1); including the contributions of the organic-inorganic interactions ( $\Delta G_{\text{inter}}$ ), the condensation of inorganic framework ( $\Delta G_{\text{inorg}}$ ), the micellization of surfactant ( $\Delta G_{\text{org}}$ ) and the free energy change of the solution ( $\Delta G_{\text{sol}}$ ) [34].

$$\Delta G_{\text{meso}} = \Delta G_{\text{inter}} + \Delta G_{\text{inorg}} + \Delta G_{\text{org}} + \Delta G_{\text{sol}} \quad (2.1)$$

In the process of hydrothermal mesostructure formation,  $\Delta G_{\text{inter}}$  dominates the overall free energy change, and in this case cooperative formation mechanism is valid. The controlling factor of the mesophase determination is the organic/inorganic interaction.

### 2.1.3.2 Effect of Surfactants

The formation occurs through a liquid-crystal templating (LCT) mechanism which was discussed earlier where an organic species functions as a central structure, surrounded by inorganic oxides forming a framework. Long-chain surfactant molecules arrange themselves assisted by a micelle self-assembly to form liquid-crystalline phases. Silicate species deposit between surfactant 'rods' and then condense to form an inorganic network, with a hexagonal ordering dictated by the interaction between the surfactant and silicate species. After removal of the surfactant templates, a mesoporosity is obtained with pore size of 2-10 nm. In general, the overall LCT mechanism is governed by two factors: (i) the dynamics of surfactant molecules to form assemblies, micelles, and ultimately crystalline structure, functioning as template; and (ii) the ability of the inorganic oxide to undergo hydrolysis and polycondensation reactions leading to a network surrounding the organic template.

A wide variety of ionic surfactant molecules with different sizes, shapes, functionalities and charges has been shown to be able to effectively function as pore structure directing agents. These surfactant molecules can be classified based on their head group chemistry and charge as follows:

*Cationic surfactants:* the hydrophilic group carries a positive charge, e.g., tetraalkylammonium salts  $(C_nH_{2n+1})(CH_3)_3NX$ ,  $n = 6, 8, 9, 10, 12, 14, 16, 18, 20, 22$ ;  $X = OH, Cl, Br, HSO_4$ ; and  $(C_nH_{2n+1})(C_2H_5)_3N$ ,  $n = 12, 14, 16, 18$ .

Molecular formula of frequently used cationic quaternary ammonium surfactants are shown in Figure 2.7.

Alkyltrimethyl quaternary ammonium surfactant	$\text{H}_3\text{C}-(\text{CH}_2)_{n-1}-\overset{\text{R}_1}{\underset{\text{R}_3}{\text{N}^+}\text{R}_2}[\text{Br}^-] \quad \text{R}_1, \text{R}_2, \text{R}_3 = \text{CH}_3, \text{C}_2\text{H}_5, \text{C}_3\text{H}_7$ $n = 8 - 22$ $\text{H}_3\text{C}-(\text{CH}_2)_{n-1}-\overset{\text{CH}_3}{\underset{\text{CH}_3}{\text{N}^+}(\text{CH}_2)_{m-1}-\text{CH}_3}[\text{Br}^-]$ $n = 8 - 22; m = 2 - 22$ $\text{H}_3\text{C}-(\text{CH}_2)_{n-1}-\overset{\text{CH}_3}{\underset{\text{CH}_3}{\text{N}^+}(\text{CH}_2)_m-\text{R}}[\text{Br}^-] \quad \text{R} = \text{---}\langle\bigcirc\rangle\text{---}, \text{---}\langle\bigcirc\rangle\text{---}, \text{---OH, etc}$ $n = 8 - 22; m = 0 - 3$
Gemini surfactant ( $\text{C}_{n-s-m}$ )	$\text{H}_3\text{C}-(\text{CH}_2)_{n-1}-\overset{\text{H}_3\text{C}}{\underset{\text{H}_3\text{C}}{\text{N}^+}}(\text{CH}_2)_s-\overset{\text{CH}_3}{\underset{\text{CH}_3}{\text{N}^+}}(\text{CH}_2)_{m-1}-\text{CH}_3[2\text{Br}^-]$ $n = 8 - 22; s = 2 - 6; m = 1 - 22$
( $\text{C}_{n-s-1}$ )	$\text{H}_3\text{C}-(\text{CH}_2)_{n-1}-\overset{\text{H}_3\text{C}}{\underset{\text{H}_3\text{C}}{\text{N}^+}}(\text{CH}_2)_s-\overset{\text{CH}_3}{\underset{\text{CH}_3}{\text{N}^+}}(\text{CH}_3)[2\text{Br}^-]$ $n = 8 - 22; s = 2 - 6$
(18B <sub>4-3-1</sub> )	$\text{H}_3\text{C}-(\text{CH}_2)_{17}-\text{O}-\langle\bigcirc\rangle-\text{O}-(\text{CH}_2)_4-\overset{\text{CH}_3}{\underset{\text{CH}_3}{\text{N}^+}}(\text{CH}_2)_3-\overset{\text{CH}_3}{\underset{\text{CH}_3}{\text{N}^+}}(\text{CH}_3)[2\text{Br}^-]$
Bolaform surfactant ( $\text{R}_n$ )	$\text{H}_3\text{C}-\overset{\text{H}_3\text{C}}{\underset{\text{H}_3\text{C}}{\text{N}^+}}(\text{CH}_2)_n-\text{O}-\langle\bigcirc\rangle-\langle\bigcirc\rangle-\text{O}-(\text{CH}_2)_n-\overset{\text{CH}_3}{\underset{\text{CH}_3}{\text{N}^+}}(\text{CH}_3)[2\text{Br}^-]$ $n = 4, 6, 8, 10, 12$
Tri-headgroup cationic surfactant ( $\text{C}_{m-s-p-1}$ )	$\text{H}_3\text{C}-(\text{CH}_2)_m-\overset{\text{H}_3\text{C}}{\underset{\text{H}_3\text{C}}{\text{N}^+}}(\text{CH}_2)_s-\overset{\text{CH}_3}{\underset{\text{CH}_3}{\text{N}^+}}(\text{CH}_2)_p-\overset{\text{CH}_3}{\underset{\text{CH}_3}{\text{N}^+}}(\text{CH}_3)[3\text{Br}^-]$ $m = 14, 16, 18; s = 2; p = 3$
Tetra-headgroup rigid bolaform surfactant ( $\text{C}_{n-m-m-n}$ )	$\text{H}_3\text{C}-\overset{\text{H}_3\text{C}}{\underset{\text{H}_3\text{C}}{\text{N}^+}}(\text{CH}_2)_n-\overset{\text{CH}_3}{\underset{\text{CH}_3}{\text{N}^+}}(\text{CH}_2)_m-\text{O}-\langle\bigcirc\rangle-\langle\bigcirc\rangle-\text{O}-(\text{CH}_2)_m-\overset{\text{H}_3\text{C}}{\underset{\text{H}_3\text{C}}{\text{N}^+}}(\text{CH}_2)_n-\overset{\text{CH}_3}{\underset{\text{CH}_3}{\text{N}^+}}(\text{CH}_3)[4\text{Br}^-]$ $n = 2, 3, 4; m = 8, 10, 12$

**Figure 2-7** Molecular formula of frequently used cationic surfactants [35]

Quaternary cationic surfactants,  $\text{C}_n\text{H}_{2n+1}\text{N}(\text{CH}_3)_3\text{Br}$  ( $n = 8-22$ ), are generally efficient for the synthesis of ordered mesoporous silicate materials. Commercially available cetyltrimethylammonium bromide is often used. Gemini surfactants, bolaform surfactants, multiheadgroup surfactants, and recently reported cationic fluorinated surfactants can also be used as templates to prepare various mesostructures [12, 36-38]. In the first reports of mesoporous silicates from Mobil Company, structure directing agents were the cationic surfactants. These have excellent solubility, high critical micelle temperature values, and can be widely used in acidic and basic media.

Stucky and co-workers proposed four general synthetic routes, which are  $S^+I$ ,  $S^-I^+$ ,  $S^+X^-I^+$ , and  $S^-X^+I^-$  ( $S^+$  = surfactant cations,  $S^-$  = surfactant anions,  $I^+$  = inorganic precursor cations,  $I^-$  = inorganic precursor anions,  $X^+$  = cationic counterions, and  $X^-$  = anionic counterions) [12,13]. To yield mesoporous materials, it is important to adjust the chemistry of the surfactant headgroups, which can fit the requirement of the inorganic components. Under basic conditions, silicate anions ( $I^-$ ) match with surfactant cations ( $S^+$ ) through Coulomb forces ( $S^+I^-$ ), the result is M41S family of materials.

Anionic salt surfactants include carboxylates, sulfates, sulfonates, phosphates, etc. given in Figure 2.8.

*Anionic surfactants:* the hydrophilic group carries a negative charge, e.g., sulfates ( $C_nH_{2n+1}OSO_3$  with  $n = 12, 14, 16, 18$ ), sulfonates ( $C_{16}H_{33}SO_3H$  and  $C_{12}H_{25}C_6H_4SO_3Na$ ), and phosphates ( $C_{12}H_{25}OPO_3H_2$ ,  $C_{14}H_{29}OPO_3K$ ).

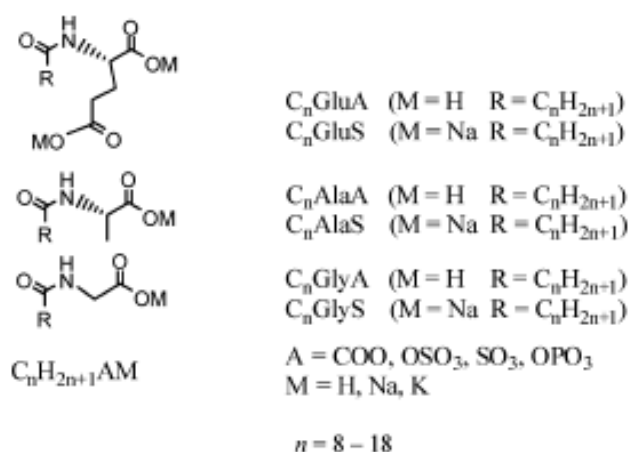


**Figure 2-8** Anionic surfactants [39]

In previous research, anionic surfactants as the template always gave rise to disordered mesophases or no mesostructure could be obtained. A possible reason is that under acidic condition anionic surfactant could be largely protonated, while under basic conditions, the interactions of counter-cations with surfactant and silicate ions are very weak.

To solve this problem, Che *et al* first introduced co-structure-directing agent (Amino silane or quarternary ammonium silane) into the anionic surfactant templating system, and a family of highly ordered mesoporous silicas AMS (anionic-surfactant-templated mesoporous silica) has been achieved [39, 40].

Depending on the synthesis conditions, and the silica source or the type of surfactant used, many other mesoporous materials (HMS, MSU, SBA,...) can be synthesized with properties different than those of MCM-41. A short summary of other MCM-41-like silica based mesoporous structures are represented in Table 2.1.

**Table 2-1** Overview of MCM-41-like materials [35]

Route	Interactions	Symbols	Medium	Products	Pore range	References
S <sup>+</sup> I	electrostatic Coulomb force	S <sup>+</sup> , cationic surfactants I <sup>-</sup> , anionic silicate species	basic	MCM-41, MCM-48, MCM-50	2-10	6
				SBA-6, SBA-2, SBA-8	5-30	36, 43, 44
S <sup>+</sup> I <sup>+</sup>	electrostatic Coulomb force	S <sup>-</sup> , anionic surfactants, I <sup>+</sup> , transition metal ions, i.e. Al <sup>3+</sup>	aqueous	mesoporous alumina, etc.		12
S <sup>+</sup> X <sup>+</sup> I <sup>+</sup>	electrostatic Coulomb force, double layer H bond	S <sup>+</sup> , cationic surfactants ; I <sup>+</sup> , silicate species; X <sup>-</sup> , Cl <sup>-</sup> , Br <sup>-</sup> , I <sup>-</sup> , SO <sub>4</sub> <sup>2-</sup> , NO <sub>3</sub> <sup>-</sup>	acidic	SBA-1, SBA-2, SBA-3	5-30	12, 43, 45
S <sup>-</sup> N <sup>+</sup> I	electrostatic Coulomb force	S <sup>-</sup> , anionic surfactants (lab-made) ; N <sup>+</sup> , cationic amino group of TMAPS or APS; I <sup>-</sup> , anionic silicate species	basic	AMS- <i>n</i>		39, 40, 46- 49
S <sup>-</sup> X <sup>+</sup> I	electrostatic Coulomb force, double layer H bond	S <sup>-</sup> , anionic phosphate surfactants I <sup>+</sup> , transition metal ions, WO <sub>4</sub> <sup>2-</sup> , Mo <sub>2</sub> O <sub>7</sub> <sup>2-</sup> ; X <sup>+</sup> , Na <sup>+</sup> , K <sup>+</sup> , Cr <sup>3+</sup> , Ni <sup>2+</sup> , etc.	basic	W, Mo oxides		12, 50
S <sup>0</sup> I <sup>0</sup> (N <sup>0</sup> I <sup>0</sup> )	H bond	S <sup>0</sup> , nonionic surfactants, oligomeric alkyl PEO surfactants, and triblock copolymers; N <sup>0</sup> , organic amines, C <sub>n</sub> H <sub>2n+1</sub> NH <sub>2</sub> , H <sub>2</sub> NC <sub>n</sub> H <sub>2n+1</sub> NH <sub>2</sub> ; I <sup>0</sup> , silicate and aluminate species	neutral	HMS, MSU, disordered worm-like mesoporous silicates	2-10	21, 51
S <sup>0</sup> H <sup>+</sup> X <sup>-</sup> I <sup>+</sup>	electrostatic Coulomb force, double layer H bond	S <sup>0</sup> , nonionic surfactants ; I <sup>+</sup> , silicate species; X <sup>-</sup> , Cl <sup>-</sup> , Br <sup>-</sup> , I <sup>-</sup> , SO <sub>4</sub> <sup>2-</sup> , NO <sub>3</sub> <sup>-</sup>	Acidic pH < 2	SBA- <i>n</i> ( <i>n</i> = 11, 12, 15, 16), FDU- <i>n</i> ( <i>n</i> =1, 5, 12), KIT- <i>n</i> ( <i>n</i> =5, 6)		22, 52-57
N <sup>0</sup> ...I <sup>+</sup>	coordination bond	N <sup>0</sup> , organic amines; I <sup>+</sup> , transition metal (Nb, Ta)	acidic	Nb, Ta oxides		12
S <sup>+</sup> I	covalent bond	S <sup>+</sup> , cationic surfactants containing silicate, e.g., C <sub>16</sub> H <sub>33</sub> N(CH <sub>3</sub> ) <sub>2</sub> OSi(OC <sub>2</sub> H <sub>5</sub> ) <sub>3</sub> Br; I <sup>-</sup> , silicate species	basic	mesoporous silica		58, 59

### 2.1.3.3 Structure Control, Surface Modification and Functionalization

The pore sizes of M41S materials are easily adjustable from ca. 2 to about 10 nm in three different ways: (1) by changing the length of the alkyl chain of the surfactant molecule,[5, 6]; (2) by adding expander molecules such as 1,3,5-trimethylbenzene [5-7,13], which dissolve in the hydrophobic region of the micelles, thus increasing their size; or (3) by aging a sample prepared at low temperature (e.g., 70 °C) in its mother liquor at higher temperature (e.g., 150 °C) for different periods of time [41]. Moreover, the pore size of MCM-41 silicates may be adjusted by post-synthesis silylation [42].

The pH plays a crucial role in the synthesis of M41S materials. By controlling the pH of the initial synthesis mixture, MCM-41 with increased wall thicknesses of 1.6 and 2.7 nm was prepared [60–62]. Apart from this technique of controlling the synthesis conditions, a postsynthesis treatment of the as-synthesized sample can further improve the quality of the MCM-41 [63, 64]. Furthermore, pH adjustments during synthesis using some acids have been shown to significantly increase the long-range order of MCM-41 and hence improve the stability. Furthermore, high quality MCM-41 was prepared by changing the initial mother liquor with water. As a consequence of this treatment, the lowered pH of the synthesis mixture results in a restructuring of the local atomic arrangement of the silicate wall creating a high quality MCM-41 [65].

MCM-41 has little acidity compared to zeolites to be used directly in many industrial applications. However, their catalytic activity can be improved by employing several different techniques of surface modification. The most applied technique is metal incorporation into the structure by adding metal solution into the synthesis solution. It is a one-pot synthesis, identified as direct synthesis. Another method is modifying the surface after desired structure is synthesized. The hydroxyl groups may be employed as anchor sites for the attachment of elemental precursors, resulting in a monolayer of active sites. A third method is incorporation of metals into the structure by the wetness impregnation technique.

When trivalent cations such as  $\text{Al}^{3+}$ ,  $\text{B}^{3+}$ ,  $\text{Ga}^{3+}$ ,  $\text{Fe}^{3+}$  substitute for silicon in the walls of the mesoporous silica, the framework possesses negative charges that can be compensated by protons and solids can be used in acidic reactions. When other cations such as  $\text{Ti}^{4+}$ ,  $\text{V}^{4+}$ ,  $\text{Sn}^{4+}$ ,  $\text{Zr}^{4+}$  are introduced, the electroneutrality is maintained and the

corresponding mesoporous materials are used rather in specific reactions like in redox catalysis.

Aluminum is the studied element for the modification of MCM-41 materials due to its acidic behavior, and the acid sites of Al-MCM-41 have been characterized [66-68]. Tetrahedral aluminum is assumed to be incorporated into the wall structure, while octahedral aluminum is regarded as extra framework species. Generally, cationic surfactants have been applied in the syntheses of mesoporous aluminosilicate materials [69-75]. The significance of different aluminum sources has also been investigated [69, 76, 77], but the conclusions are not accurate which is probably due to different synthesis conditions.

Titanium [78-89] and vanadium-modified [90, 91] mesoporous materials are interesting redox catalysts, and several synthesis reports are available. Other transition metals that have been incorporated into mesoporous structures are, e.g. copper [92], nickel [93], cobalt [94], chromium [95], iron [96], gallium [97, 98] and manganese [99, 100], boron [101, 102], palladium [103].

Encapsulation of organic polymers such as polyaniline, methyl methacrylate within the channels of MCM-41 is reported [104-106]. Polymerization of semiconducting polymers within the channels of MCM-41 is a promising method for the preparation of electronic and optoelectronic devices.

In general, the internal surface of MCM-41 mesoporous molecular sieves is hydrophobic. This hydrophobic nature of these materials makes them attractive candidates for selective adsorbents for the removal of volatile organic compounds and other organic compounds in gas streams or wastewater [107].

The adsorption characteristics of MCM-41 for polar molecules strongly depend on the surface silanol groups (SiOH) [108]. There are several different types of SiOH groups on the MCM-41 surfaces [109] which allow various modifications of MCM-41 for catalysis, adsorption, and novel composites [110].

The sorption capacity of polar molecules can be further reduced by silylation, substitution of the surface hydroxyl groups with trimethylchlorosilane groups to create even more hydrophobic environment which results in selective removal of organic compounds from streams or wastewater [110].

#### 2.1.3.4 Microwave Assisted Synthesis

Microwaves (0.3GHz–300GHz) lie in the electromagnetic radiation region between radiowave and infrared frequencies with relatively large wavelengths (1 mm-1 m). For the last 50 years, microwave energy has been used for heating food materials [111] and now it has been realized that this technique may find potential useful applications in the synthesis of nanoporous materials.

In 1967, microwaves were used to heat polymers [112]. However, their first usage in chemical transformations dates back to 1981 [113]. At that same time, zeolites and microwaves together attracted the attentions of researchers, not in the synthesis but dehydration of zeolites [114-117]. In 1988, Mobil researches published the first data on zeolite synthesis by microwave radiation in a patent briefly describing the synthesis conditions of zeolites Na-A and ZSM-5 [118]. Mobil Oil researchers firstly claimed that microwave energy was successfully applied in the crystallization for several zeolites. According to their patent, crystalline zeolites could be synthesized by employing microwave energy with the help of a heat transfer agent, which is sympathetic to microwave energy. To date, several types of zeolites such as NaA (LTA), CoAPO-44, CoAPO-5, AlPO4-5, zeolite A, zeolite Y and ZSM-5 have been prepared by microwave heating of the precursor gels. In 1998, Cundy reviewed a detailed article on the syntheses and modification of zeolites by microwave radiation which covered different aspects of microwave synthesis that differ from conventional hydrothermal methods [119].

Recently, Yürüm and coworker studied the microwave assisted synthesis of AlPO4-5 and achieved to obtain high quality crystals in relatively shorter crystallization times [120].

Microwave assisted synthesis of zeolites have been investigated and the success of obtaining these materials opened a new route for the synthesis of MCM-41 type mesoporous materials. Before detailing microwave assisted synthesis of MCM-41, description and working principle of microwave radiation will be discussed.

The principles and working mechanism of microwaves are based on simple laws. The heating effect of microwave results through a mechanism called dielectric heating [121-127]. According to this mechanism, the mobility of dipoles plays an important role in that orientation ability becomes critical due to the direction of the electric field. Molecules with permanent dipole moment partly or completely align themselves through rotation with the direction of electric field. Since the molecules can rotate in time with field frequencies of  $10^6$  Hz in gases or liquids, their inability to follow the inversion of the electric field at an indefinite time results in phase shifts and dielectric losses. Apart from the dielectric coefficient, the size of the excited molecule becomes crucial. Due to the fast changing electric field of the microwave radiation, electric field energy is transferred to the medium and converted into kinetic or thermal energy because the change in polarity of the electric field is much faster than the rotation of the medium molecules around their dipole center causing a phase lag. Highly conductive solids or, polar liquids exhibit large dielectric losses; hydrocarbons and low polarity solvents show little heating effect.

The dielectric coefficient (permittivity)  $\epsilon_r$ , a constant that shows the ability of a medium to interact and absorb microwave energy, is characteristic for each material and its state. It is related to the ability to save electric energy (capacity, C) with the following equation:

$$\epsilon_r = \frac{C}{C_0} \quad (2.2)$$

At high frequencies,  $\epsilon_r$  is extended by the imaginary part as a complex number according to equation (2.3) where  $i^2 = -1$ .

$$\epsilon_r = \epsilon_r' + i\epsilon_r'' \quad (2.3)$$

The dielectric loss factor  $\epsilon_r''$  (dynamic dielectric coefficient) is obtained by comparing the irradiated microwave energy to the energy that has coupled with the sample.  $\epsilon_r''$  depends on the dielectric conductivity  $\sigma$  and on the frequency according to equation (2.4).

$$\epsilon_r'' = \frac{\sigma}{2\pi f} \quad (2.4)$$

The coupling of microwave energy in the medium depends on the dielectric properties of the substance to be heated, i.e. it depends on the quantity of microwave radiation that fails to penetrate the substance. The degree of energy coupling in the reaction system is related on both  $\epsilon_r'$  and  $\epsilon_r''$  and is called dissipation factor D.

$$D = \tan \delta = \frac{\epsilon_r''}{\epsilon_r'} \quad (2.5)$$

$$\tan \delta \sim \frac{1}{x} \quad (2.6)$$

The dissipation factor defines the ability of a medium at a given frequency and temperature to convert electromagnetic energy into heat. It can also be regarded as a measure of the penetration depth (x) of microwave radiation into a material and is inversely proportional with x given in equation (2.6).

Dissipation factor depends on many factors [125]:

1. Temperature
2. Ion concentration
3. Ion size
4. Dielectric constant
5. Microwave frequency
6. Viscosity of reaction medium

The penetration depth and dissipation factor are strongly dependent on temperature however penetration depths were only measured for a few materials in a very small range of temperatures [127-128]. As a result, special attention must be given for designing chemical reactors for industrial applications.

The interaction of microwave radiation with matter can be classified as [129]:

1. Absorption
2. Transmission
3. Reflection

Microwaves are a nonionizing form of radiation energy that cannot break chemical bonds but transfer energy selectively to various substances. Materials with high dielectric coefficients (dipole moment), polar substances and salts, absorb the microwaves and result in a rapid heating of the medium. In such materials, the dielectric loss factor increases and the penetration depth of microwaves in medium decreases. Microwaves couple directly with molecules in the reaction mixture with rapid rise in temperature; dipole rotation and ionic conduction being two most important fundamental mechanisms for transfer of energy from microwaves to the molecules being heated. Essentially, polar molecules try to align themselves with the rapidly changing electric field of the microwave, and coupling ability, among others, is determined by the polarity of the molecules. If microwave radiation is reflected by the material surface, there is no or only a small coupling energy in the system i.e. metals with high conductivity. This type of materials can be used for shielding microwave ovens. Some materials (such as hydrocarbons, glass, and ceramics) are nearly transparent to microwave, and therefore behave as good insulators in a microwave oven since they are heated only to a very limited extent.

The energy input ( $Q_{mv}$ ) and the energy necessary to reach desired temperature ( $Q_{th}$ ) are determined from the following equations:

$$Q_{mv} = P_{mv} t \quad (2.7)$$

$$Q_{th} = mc_p \Delta T \quad (2.8)$$

The efficiency factor ( $\eta$ ) is the ratio of required heat over used energy input that describes the effectiveness of the conversion of microwave energy into thermal energy is given in equation (2.9).

$$\eta = \frac{Q_{th}}{Q_{mv}} \quad (2.9)$$

Using these equations and thermodynamic data of the medium, it is possible to calculate the required energy input to reach the necessary temperature for the reaction to occur.

There are two types of microwave oven used for chemical synthesis: domestic and laboratory-scale. In domestic microwave ovens, it is not so easy to reach the desired synthesis conditions since the only controllable parameters are power and time. The temperature remains undetermined and it is manipulated with on and off switching of the microwave oven. In a laboratory-type microwave oven, it is possible to control the temperature with the temperature feedback which keeps the temperature constant by manipulating microwave power. In this system, temperature and pressure are kept constant with a precision of  $\pm 1\text{K}$  and  $\pm 0.5\text{ bar}$ , respectively, states not easily reached by conventional heating. The former has the advantage of economy but lacks flexibility in control and reaction monitoring. The latter is more expensive but is purpose-built, has extensive facilities for programming and allows stirring of the reaction mixture and the continuous monitoring and control of temperature and pressure. These oven types are usually multimode oven with non-uniform electric field distribution. There are also microwave ovens that operate with a monomode device in which microwave energy is piped into a reactor through waveguides. However, the amount of monomode radiation depends on several parameters such as reactor size and material, insertion position in the waveguide, constitution and amount of reaction mixture [130, 131]. So in theory there are no great differences between multimode and monomode radiation. In 2004, Gum et al. suggest that microwave ovens should be classified according to their radiation intensity and power density. They summarize the properties of currently available microwave ovens that are used for synthetic applications (Table 2-2).

Household microwave ovens mostly operate by pulsed microwave radiation while there are some advanced systems that operate by continuous (unpulsed) irradiation. In the pulsed systems, pulses with maximum available power are applied according to the preset irradiation and time. In the pulsed systems actual preset power is applied [131].

Microwaves are widely used in telecommunication so the usage of microwaves for other applications is strictly restricted due to international standards [132, 133]. The frequency used in most devices is 2.45 GHz, including most household microwave ovens.

**Table 2-2** Comparison of the currently available microwave systems for synthetic applications

Manufacturer	Type	Irradiation modus	Max. power	Cavity volume	Max. power density in empty cavity	Reaction scale
<b>Sharp</b>	domestic MW oven R-220A	Multimode	800 W, pulsed	15.7 L	around 50 W L <sup>-1</sup>	max. 100 g in dry reactions
<b>Personal Chemistry</b>	Emrys™ Creator	Monomode	300 W, unpulsed	< 1 L	> 300 W L <sup>-1</sup>	< 20 g
<b>CEM</b>	Discovery™	Monomode	300 W, unpulsed	< 1 L	> 300 W L <sup>-1</sup>	< 50 g
<b>MLS/Milestone</b>	ETHOS™ MR	Multimode	1000 W, pulsed or unpulsed	42.8 L	around 23 W L <sup>-1</sup>	up to 3000 g depending on reactor

There are three types of methods for the measurement of temperature in a microwave oven:

- 1) Shielded thermocouples
- 2) IR-sensors
- 3) Fiber optics

Even though shielded thermocouples are the least expensive tools, they have some limitations. First of all, they are unsuitable for high temperature synthesis (300 °C); and reaction volumes should be at least 30 ml since they have significant amount of volume due to shielding. By using IR-sensors, temperature can be measured indirectly from the reactor wall with a temperature range of -40 to 1000 °C. However, they have errors because temperature can only be measured from the outside wall of the container that is the coldest point of the reaction mixture. The third and most expensive method is temperature measurement by fiber optics with high precision. The disadvantage compared to IR sensors is the narrow operating temperature range of 0 to 330 °C [131].

Tompsett and coworkers published a review article [134] based on microwave synthesis of nanoporous materials and proposed the advantages of microwave assisted synthesis:

- 1) Reduced synthesis time (more rapid nucleation) [135-142]
- 2) More uniform dimension and composition of product [143-146]
- 3) More variable compositions can be produced[147,148]

Microwave assisted synthesis have achieved some enhancements in the synthesis of nanoporous materials when compared to the efficiency of conventional synthesis, but many important factors must be taken into account during synthesis. Important differences between the conventional chemical reactions in the liquid phase and the same reactions conducted under microwave irradiation can be summarized as [131, 134]:

- 1) Dielectric properties and concentration of the medium
- 2) Reactor geometry: batch volume, shape, etc...
- 3) Process: stirring, ramp rate, heat dissipating agents, etc...
- 4) Microwave frequency
- 5) Activation energy (energy efficiency)
- 6) Template interactions
- 7) Temperature control

Synthesis of nanoporous materials with microwave radiation provides efficient and selective production of many materials. Microwave radiation also achieves the goal of green energy requirements recommended by American Chemical Society [149]: “use methods that minimize the energy required for a reaction to take place. For example, ...catalysts or microwave radiation...”. However further research is required in order to understand the mechanism and achieve reproducibility which can be established by interdisciplinary research of chemists, physicians and engineers.

During the last years, syntheses of MCM-41 mesoporous molecular sieves with microwave energy have been investigated. In 1996, Bein and Wu [150] shortly reported that molecular sieve MCM-41 was synthesized in a microwave heating environment in which they employed only water solvent as a reaction medium of microwave preparation. According to their study, the variation of crystallinity with various reaction conditions suggests that the formation mechanism of MCM-41 under microwave heating is similar to that observed with conventional oven heating. They performed the experiments in a Teflon autoclave operated in Questron microwave oven at 160 °C for 1 minute, followed by heating at 150 °C for 80 minutes. They concluded that for that specific gel composition, the best temperature to synthesize ordered mesoporous materials was between 140 °C and 160 °C. They claimed that condensation rate was not sufficient at lower temperatures while continued heating resulted in decomposition of already formed structure at higher temperatures.

Two years later Kim and co-workers [151] published the synthesis data of mesoporous material MCM-41 under microwave heating conditions depending on synthetic parameters. In particular, they focused on investigating the effect of ethylene glycol as another dielectric medium on the crystallinity and the morphology of materials prepared by microwave-induced heating operating in CEM MDS-2000 at 2.45 GHz at 0-100% of microwave full power ( $630 \pm 50$ ) and was controlled by pressure change up to 200 psi with a fiber optic probe of phosphor sensor. They performed the experiments in a Teflon autoclave and heated the solution in two steps. The first was nucleation applied at 100-150 °C for 1-30 min; the second, at 100 °C for 30 min under 60 W of microwave power for crystallization.

Kim et al. [152] also published another article with more specific microwave conditions as first heating at 120 °C for 10 min under 480 W of microwave power for nucleation and 100 C for 30 minutes under 60 W of microwave power for crystallization.

Papp et. al compared four different syntheses techniques of MCM-41 mesoporous molecular sieves [153] as thermal treatment in polypropylene bottles, in static autoclaves, in a stirred autoclave in ovens, and in microwave reactors heated with microwave radiation at 95 °C for different times. Microwave assisted syntheses were performed at 70% CEM MDS 2000 in 4 hours. They were able to synthesize highly-ordered MCM-41 and assumed that stimulation of water molecules around the silicon atoms by microwave radiation (vibration and rotation) was the reason of accelerated condensation process of the framework in contrast to propylene bottles or autoclaves.

Park et al. reported the monitoring of the rapid silicate condensation onto the surfactant micelles during microwave assisted MCM-41 formation by fluorescence and electron spin resonance spectroscopy [154-156]. In this spectroscopic technique, pyrene as a fluorescence probe and 4-(N,N-dimethyl-N-hexadecyl)ammonium-2,2,6,6-tetramethyl piperidinyloxy iodide (CAT16) as a spin probe were dissolved into the micelle solutions. These probes allowed to monitor the supramolecular interaction between the anionic silicate and cationic surfactant molecules. During microwave radiation it was observed that the fast increase in hydrophobicity and microviscosity of the probes resulted from the accelerated condensation of silicates onto the micelle surfaces. They proposed that the fast dissolution of the precursor gel aside with microwave-susceptible head groups of surfactant molecules resulted in rapid formation of MCM-41.

Many of the articles on microwave assisted synthesis mainly focused on the decrease in reaction time. However, another advantage of microwave radiation implies that control on particle size distribution and macroscopic morphology could also be achieved in the synthesis of nanostructured materials [157, 158].

Recently Jhung et. al [159] published a book chapter on microwave-induced synthesis and fabrication of nanoporous materials and Cao Yuan et.al.[160] published an article on the advances in microwave assisted synthesis of ordered mesoporous materials covering pure and metal incorporated MCM-41 and SBA-15 mesoporous molecular sieves.

Microwave irradiation technique was widely applied to the synthesis of mesoporous molecular sieves but most investigation aimed at the synthesis of pure MCM-41. Nowadays, there has been a growing interest in the microwave preparation of metal incorporated MCM-41 mesoporous materials. In 1999, Wha-Seung Ahn and co-workers synthesized the titanium substituted MCM-41 mesoporous materials by microwave and compared the results with conventionally synthesized Ti-MCM-41 materials [161]. In their study CEM MDS-2100 microwave was used with heating periods of 10 minutes to 5 hours at 373-393 K. They achieved synthesis of titanium containing mesoporous materials with an average pore diameter of 3 nm and specific surface area of around 900 m<sup>2</sup>/g by microwave radiation within 2 hr instead of producing the same material with conventional heating within 24 hours. The number of articles corresponding to metal incorporation by using microwave radiation steadily increased from 2007 to 2010. Gläser and coworker studied the synthesis and catalytic performance of Cr substituted MCM-41 and MCM-48 which has been reported for the first time and compared the results with conventional heating [162]. The microwave assisted syntheses of Cr-MCM-41 and Cr-MCM-48 were completed within 1-2 hr with CEM MDS-2000 at 100 °C and 150 °C respectively, whereas the conventional hydrothermal method took at least 12-24 hours for completion. Gläser et al. claimed that the Cr content within the samples were up of 2.0 wt% and the long-range order was somewhat enhanced for the samples prepared using microwave.

Hengbo Yin and coworkers investigated the effect of copper, nickel and cobalt doping on the pore structure of pure MCM-41 mesoporous molecular sieve under 220 W microwave radiation for 2.5 hr. They achieved synthesis of long-range and well-ordered Ni-MCM-41 mesoporous molecular sieves with different amount of Ni content. As in the conventional synthesis method, the specific surface area and pore volume of the samples obtained by microwave heating decreased with increasing the amount of nickel and mesoporous ordering of the samples became poor [163,164]. They investigated the synthesis of Cu-MCM-41 mesoporous molecular sieves with different metal content with microwave irradiation method and same results as in the Ni-MCM-41 samples were observed such as decrease in specific surface area, pore volume and regularity with the increase of metal content [164] For the case of cobalt incorporated samples, they also investigated the calcination temperature for both microwave assisted and conventionally synthesized samples and concluded that the thermal stability of Co-

MCM-41 mesoporous molecular sieve obtained by microwave heating was enhanced compared to that of Co-MCM-41 obtained by hydrothermal method. Among all the samples, Co-MCM-41 mesoporous molecular sieves had the highest specific surface area values [164,165]. Recently, Yin et al. studied the microwave synthesis of Ce-incorporated mesoporous molecular sieves by microwave radiation at 220 W for 2.5 hours [166]. In all experiments Yin and coworkers used National NN-S570MFS type microwave oven.

Besides using microwave energy for the synthesis of pure and metal incorporated MCM-41, it has been proposed by Duan et al. that microwave energy can also be used for removing the surfactant from zeolites- $\beta$  porous materials [167]. They also investigated the calcination step of MCM-41. Traditionally, the calcination step of MCM-41 is carried out around 500 °C for 10 hours or longer. In their two-step calcination procedure, Duan and coworkers first calcined the materials for 2 hours at a lower temperature determined by decomposition of the template and then heated linearly to 550 C at a rate of 1 C/min and maintained at 500 C for 6 hours. The obtained MCM-41 mesoporous materials resulted in a better long-range structure and more acid sites.

The use of microwave energy as an energy source for synthesizing MCM-41 mesoporous molecular sieves is an important issue, but there are some points that should be considered seriously. Gum et al. claim that the information in publications covering the use of microwave energy are incomplete: scientists dealing with microwaves have experienced measurement and physical problems which lack the reproducibility of the products. Many articles do not give basic description of the equipment used, i.e. the type of microwave or its country of manufacture is often not mentioned. Also the power used during synthesis is defined in terms of full power or as preset power, a categorization makes conclusions about achieved temperatures impossible. It is also worth mentioning that in microwave-assisted reaction, the medium plays an important role: the polarity and the amount of the components in reaction mixture determines the absorption and the quality of the output product. When all of these issues are considered, it is crucial to describe the reaction parameters in detail since these data will be used in future for large-scale productions with microwave energy [168].

## 2.1.4 Characterization Methods

MCM-41 is honeycomb structure results in hexagonal packing of unidimensional cylindrical pores. Reliable characterization of the porous hexagonal structure requires the use of three independent techniques [4]: X-ray diffraction (XRD), transmission electron microscopy (TEM) and adsorption analysis.

### 2.1.4.1 N<sub>2</sub> Sorption Analysis

Adsorption techniques are used to determine the porosity and specific surface area of materials. The most common adsorbate is N<sub>2</sub> (at 77K).

For MCM-41, typical sorption measurements follow the type IV isotherm, as illustrated in Figure 2-9, with a high porosity (1 cm<sup>3</sup>/g) and a large surface area of about 1400 m<sup>2</sup>/g [169]. At low relative pressures ( $P/P_0 < 0.2$ ), the formation of a monolayer of adsorbed molecules is the prevailing process. At higher pressures ( $P/P_0 > 0.2$ ), the adsorption in mesopores leads to multilayer formation until condensation occurs, enabling a sharp increase for the adsorption volume. As the mesopores are filled, the adsorption continues on the external surface. The isotherms are usually reversible for pores smaller than a critical size and exhibit a sharp inflection at  $P/P_0 = 0.25-0.45$ , depending on the pore size of the material. This process corresponds to capillary condensation of N<sub>2</sub> in the mesopores. The sharpness of the inflection reflects the uniformity of the pore sizes and the height indicates the pore volume. A hysteresis effect is often observed for N<sub>2</sub> adsorption-desorption isotherms when the pore diameter is larger than approximately 40 Å [170].

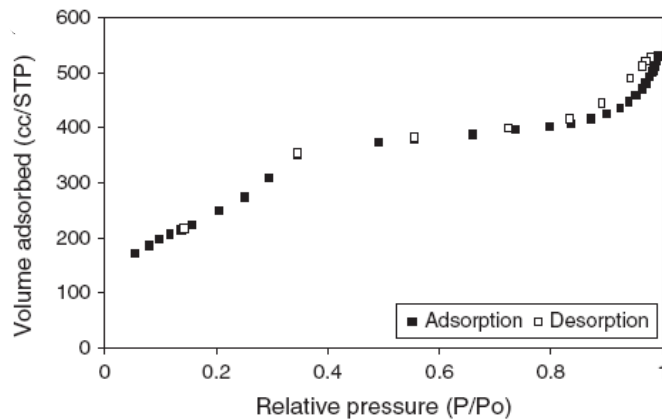


**Figure 2-9** Adsorption-desorption isotherm of MCM-41 [169]

The steps in the isotherm (Figure 2-9) qualitatively reflect a narrow and uniform distribution of the pore size, while its height indicates the pore volume. Desorption occurs via evaporation of the adsorbate from mesopores and usually takes place at a pressure lower than that of capillary condensation, resulting in hysteresis. For disordered samples, the step of the isotherm becomes less sharp for the samples with the largest pores, suggesting a widening of the pore size distribution. The hysteresis is, in general, attributed to the different sizes of the pore mouths and pore bodies or to the different adsorption and desorption behaviors in near-cylindrical pores. Materials with uniform pore sizes and shapes exhibit type H1 hysteresis (i.e., parallel adsorption and desorption branches), whereas those with non-uniform pore sizes and shapes give type H2 hysteresis (e.g., pore blocking, percolation effects, tensile strength, i.e. cavitation effects). In the latter case, condensation takes place in each section at the relative pressure provided by the Kelvin equation, but evaporation from the pore body cannot occur while the pore mouth remains filled. On the other hand, in the former case, the meniscus is cylindrical during condensation and hemispherical during evaporation.

#### **2.1.4.2 X-ray Diffraction Measurements**

XRD provides direct information of the pore architecture of the materials. For MCM-41 mesoporous materials, the diffraction patterns only have reflection peaks in the low-angle range, meaning  $2\theta$  less than  $10^\circ$ . No reflections are seen at higher angles which indicate that the pore walls are mainly amorphous. The ordering lies in the pore structure, and the low-angle diffraction peaks can be indexed according to different lattices [170].

MCM-41 exhibits an XRD pattern containing typically 3-5 peaks which can be indexed to a hexagonal lattice as (100), (110), (200), (210), and (300) (Figure 2-10). Since the materials are not crystalline at the atomic level, no reflections at higher angles are observed. By X-ray diffraction it is not possible to quantify the purity of the material [171].

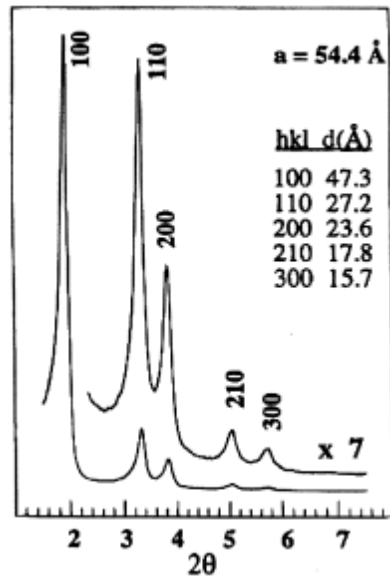


**Figure 2-10** X-ray diffraction pattern of high-quality calcined MCM-41 [172]

The schematic representation of the structure of hexagonal MCM-41 and the unit cell of the solid phase is given in Figure 2-11 [173].

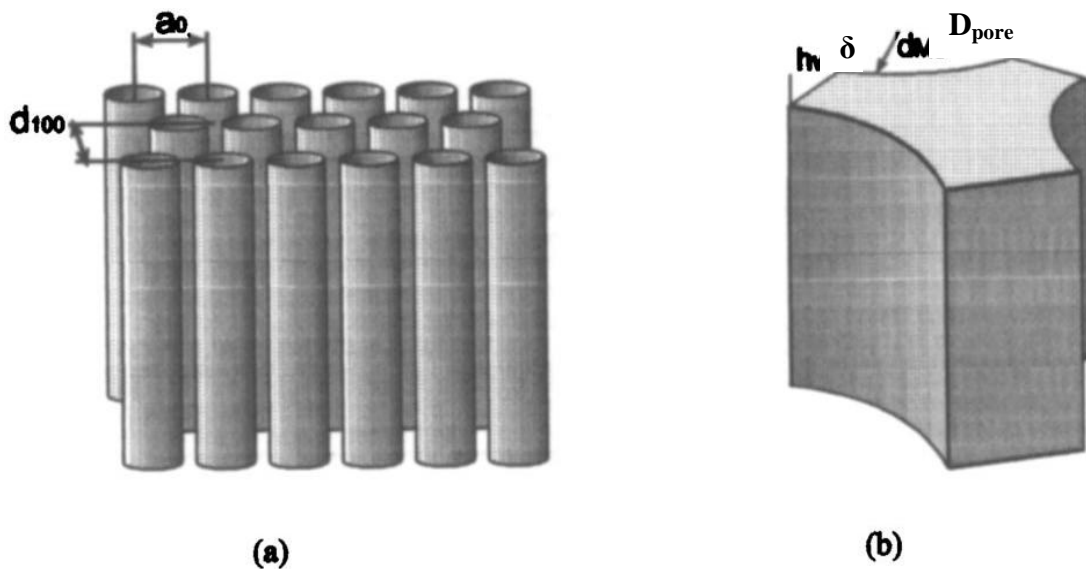


**Figure 2-11** a) The structure of hexagonal MCM-41 and b) The unit cell of the solid phase

The internal structure of MCM-41, constructed from an ordered array of cylindrical walls is characterized by XRD values of  $d_{100}$  and the following formula:

$$a = \frac{2}{\sqrt{3}} d_{100} \quad (2.10)$$

where  $a$  is the characteristic lattice parameter which is defined as the repeating distance between two pore centers.

It can also be expressed as the distance between the nearest centers of cylindrical pores with a pore size of  $D_{pore}$  where  $D_{pore}$  is calculated from the desorption branch of  $N_2$  isotherm and derived by BJH method.

$$a = D_{pore} + \delta \quad (2.11)$$

where  $\delta$  is the wall thickness.

So, the value of  $\delta$  is defined as :

$$\delta = a - D_{pore} \quad (2.12)$$

#### 2.1.4.3 Scanning Electron Microscopy

Scanning Electron Microscopy (SEM) has advantages over Transmission Electron Microscopy (TEM) for the determination of crystal morphology and fine surface structures with large depth of focus. The surface topology of the sample can be observed by SEM at different contrast in the image. In addition to this, when compared to TEM, SEM is an easy-to-handle tool, especially in sample preparation [174]. In order to observe morphology of mesoporous materials by SEM, carbon coating can be applied to overcome charging problems.

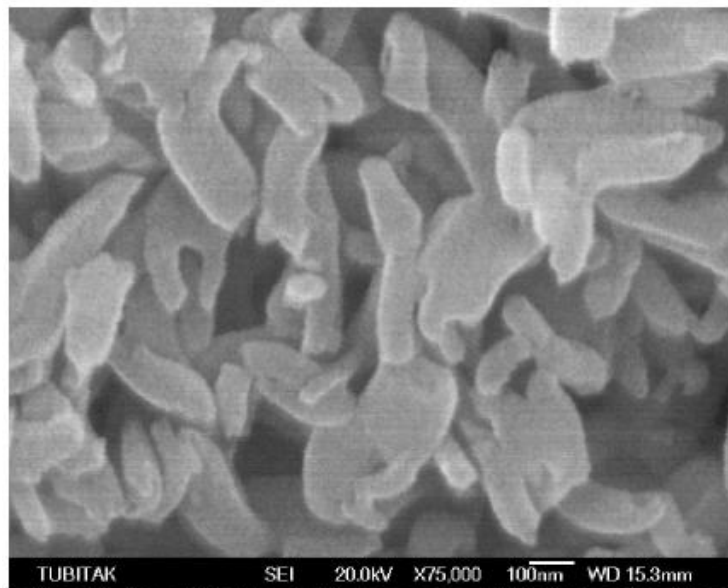


**Figure 2-12** SEM image of MCM-41 [169]

#### 2.1.4.4 Transmission Electron Microscopy

TEM is the pre-eminent method for determining dislocations' and other crystallographic character defect and for performing chemical and crystallographic analysis of micrometer and smaller precipitates as well as other microstructures [175].

To elucidate the pore structure of MCM-41 analysis, transmission electron microscopy is frequently used (Figure 2-13) [171]. Beside  $N_2$  sorption, TEM is an alternative way of estimating pore size and pore wall thickness and it gives detailed information about the homogeneity of the sample.

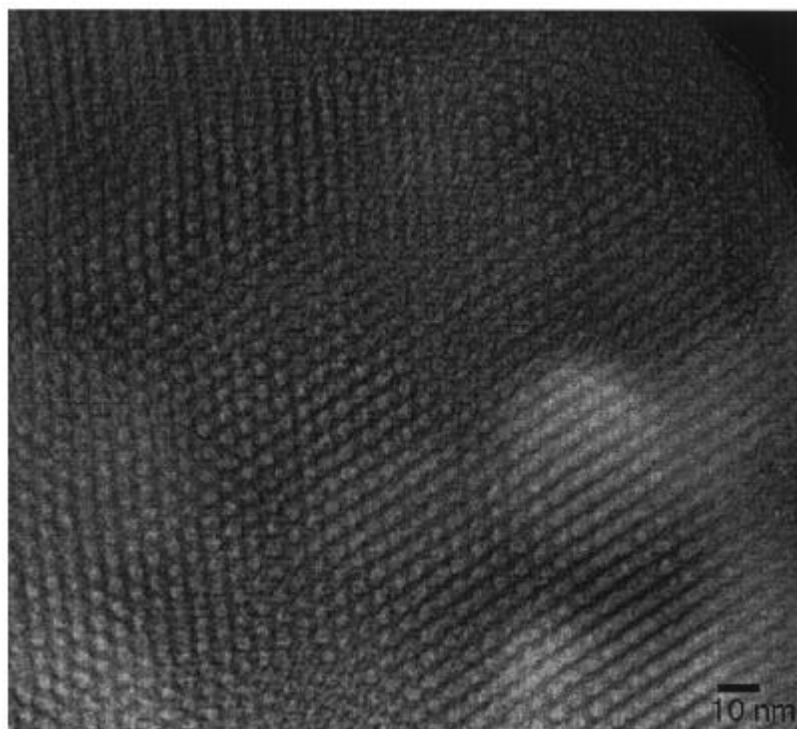


**Figure 2-13** Transmission electron micrograph of MCM-41 featuring 4.0 nm sized pores, hexagonally arranged [171]

Due to focus problem, TEM analysis should be done carefully to investigate the exact pore sizes and pore wall thicknesses. Chen and coworkers proved that the exact pore size and wall thickness values are strongly depended on the focus conditions [176]. In addition to this, many MCM-41 samples contain disordered regions such as lamellar and fingerprint structures [177] so during TEM analysis micrographs should be taken from various parts of the samples.

## 2.2 Carbon Nanotubes

### 2.2.1 Historical Background

In 1985, Rick Smalley et al. [178] discovered fullerenes. The first discovered fullerene was  $C_{60}$  with a bucky ball shape consisting of 60  $sp^2$  hybridized C atoms bonded together in pentagons and hexagons. 5 years later Smalley proposed the existence of tubular fullerene which could be made by elongating a  $C_{60}$  molecule [179]. In 1991, Dresselhaus announced the existence of carbon nanotubes capped with fullerene hemispheres at either end [180]. In the same year Iijima reported the TEM image of multi-walled carbon nanotubes (MWCNs) for the first time [181]. Two years later Iijima and coworkers [182] and Bethune and coworkers [183] proposed the existence of single-walled carbon nanotubes (SWNTs) simultaneously and independently.

Actually in 1960, Bacon published an article investigating the structure of carbon nanowhiskers with SEM and he proposed a scroll-like structure [184]. In 1970s nanotubes were directly produced and imaged by Endo by HRTEM during his investigation of producing carbon fibers at 1000 °C [185]. He observed the carbon fibers with a hollow core and a catalyst particle at the end which he discovered later that the catalyst particle was iron oxide that is today a well-known catalyst in carbon nanotubes production. The carbon nanotubes were observed many years ago. However not until the discovery of  $C_{60}$  and other fullerene structures did researchers realized their importance.

The formation mechanism was first observed by Bacon [184]. He proposed that a graphene sheet rolled up like a scroll and form carbon nanotubes. Iijima was first to recognize the potential helicities and chiralities of carbon nanotubes.

The first mass production of MWCTs was achieved by Ebbesen and Ajayan [186] by using arc discharge method to produce several grams of MWCTs with purity %75. Nowadays most research focuses on large scale production of SWCTs with high purity and low cost since they can be produced with much higher crystalline quality than MWCTs.

### 2.2.2 Structural Properties

Two types of nanotubes have been distinguished so far, namely the single-walled carbon nanotube and the multi-walled carbon nanotube. A SWCT is generated by folding back a graphene sheet on itself and forming a seamless cylinder with constant radius. In SWCTs there are no dangling bonds so ends are closed off by hemispherical caps. These caps can be opened by experimental techniques.

A single-wall carbon nanotube is conveniently characterized in terms of its diameter  $d_t$ , its chiral angle  $\theta$  and its one-dimensional unit cell, as shown in Figure 2-14a.

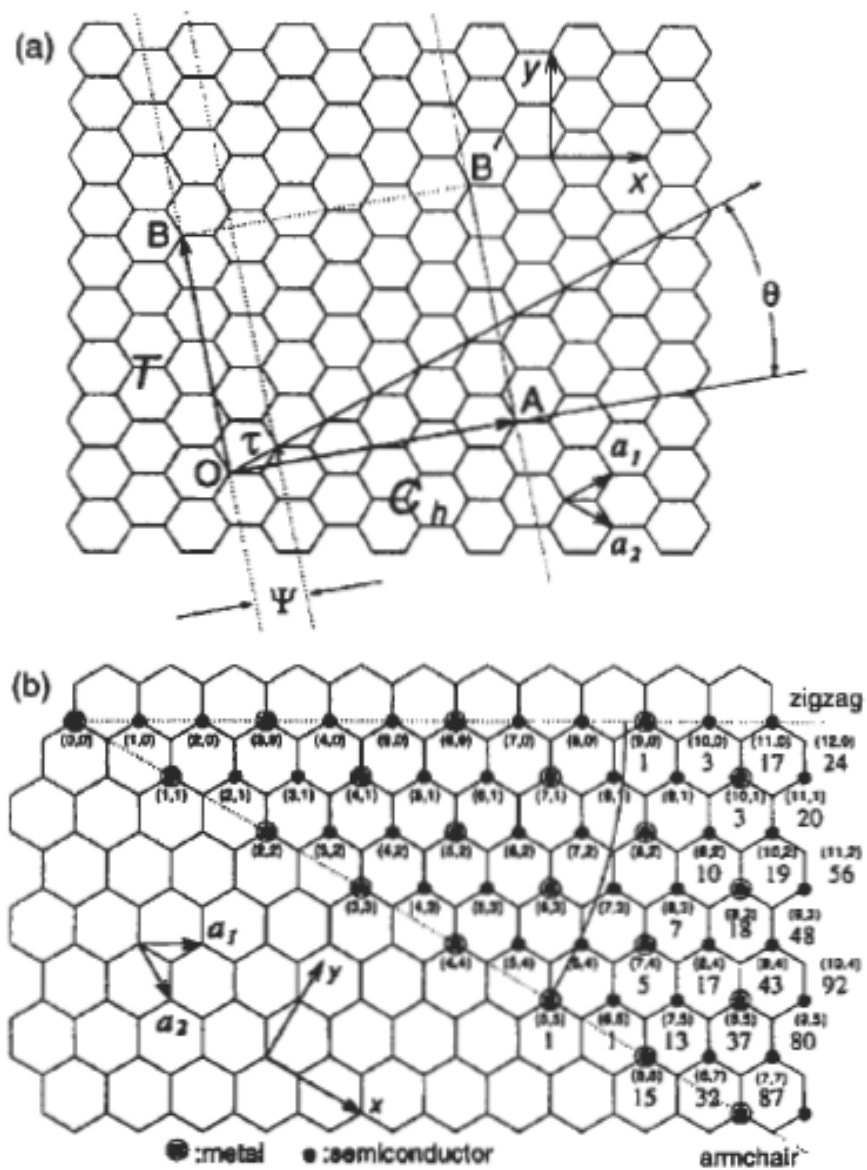
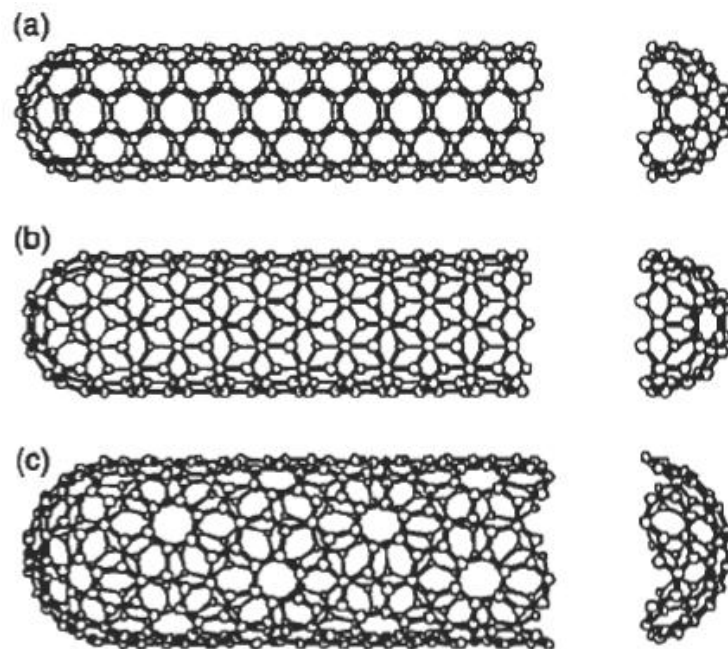


Figure 2-14 a) Unit cell of SWCT and b) chirality of SWCT [187]

The chiral vector  $\vec{OA}$  or  $\vec{C}_h = na_1 + ma_2$  is defined on the honeycomb lattice of carbon atoms by unit vectors  $a_1$  and  $a_2$  of a graphene layer and the chiral angle  $\theta$  with respect to the zigzag axis ( $\theta = 0^\circ$ ). Also shown are the lattice vector  $\vec{OB} = T$  of the one-dimensional nanotube unit cell, the rotation angle  $\Psi$  and the translation  $\tau$  [187].

Possible chiral vectors  $\vec{C}_h$  specified by the pairs of integers  $(n, m)$  angle is used to separate carbon nanotubes into three classes according to their electronic properties as armchair ( $n = m = 30^\circ$ ), zigzag ( $m = 0, n > 0, \theta = 0^\circ$ ) and chiral ( $0 < |m| < n, 0 < \theta < 30^\circ$ ) as given in Figure 2-14b and Figure 2-15.



**Figure 2-15** a) armchair nanotube b) zigzag nanotube and c) chiral nanotube

According to theoretical calculations, the encircled dots denote metallic nanotubes, while the small dots are for semiconducting nanotubes (Figure 2-14b) [187]. Therefore, armchair carbon nanotubes are metallic (a degenerate semimetal with zero band gap), zigzag and chiral nanotubes can be semimetals with a finite band gap if  $n-m/3 = I$  ( $I$  being an integer and  $m \neq n$ ) or semiconductors in other cases [188].

The nanotube diameter is inversely proportional with the band gap for the semimetallic and semiconductor nanotubes resulting in a unique electronic behavior for each

nanotube [189, 190]. Combining different diameters and chiralities bring about many nanotubes with different mechanical, electrical, piezoelectric and optical properties.

Measurements of the nanotube diameter  $d_t$  and chiral angle  $\theta$  are conveniently made by scanning tunneling microscopy and high resolution TEM [187].

### **2.2.3 Synthesis Methods**

There are different methods of carbon nanotube production, i.e. electric arc-discharge, laser ablation and chemical vapor deposition (CVD). Among others, the CVD route seems to be the most promising for large-scale industrial applications, due to its opportunity to upscale both the preparation and the purification methods.

#### **2.2.3.1 Arc discharge synthesis**

The first recognized method of producing carbon nanotubes was arc discharge method. In this method, low voltage (~12-25 V) and high-current (50-120 amps) power supplies are used in which an arc is produced across a 1-mm gap between two graphite electrodes with 5 to 20 mm diameter under inert atmosphere specially formed by He or Ar at a pressure of 100 to 1000 torr [188]. Iijima used this method to produce MCNTs for the first time [181] that the nanotubes were formed on the cathode. Later Iijima produced the SWCNTs by this method by adding metal catalyst (Fe/C) to the anode in methane/argon environment while Bethune produced SWCNTs by Co/C anode under He environment [182, 183]. It has been found that Ar/He gas ratio had an effect on the diameter of SWCNTs [191] while the total gas pressure had an effect on the yield of SWCNTs [192]. Arc discharge synthesis is an inexpensive production technique but the products need further purification before use.

#### **2.2.3.2 Laser Ablation Synthesis**

In 1996, Smalley et al. [193] achieved first large-scale production of SWCNTs by laser ablation technique at 1200 °C. In this technique a pulsed or continuous-wave laser can be used over a metal impregnated graphite source in a tube furnace with an inert atmosphere. The SWCNTs are formed on the nano-sized metal catalysts in the plasma plume with many side products, mostly graphitic and amorphous carbon.

In both arc-discharge and laser ablation technique, SWCNTs are formed when a metal-impregnated graphite is used and MWCNTs are formed when pure graphite is used.

### 2.2.3.3 Chemical Vapor Deposition Synthesis

In 1993, Endo et al. [194] first achieved to synthesize MWCTs by chemical vapor deposition technique while in 1996, SWCT production was achieved using CO as carbon feedstock [195]. In this method, carbon source is flow over catalyst nanoparticles in a temperature range of 500-1200 °C to produce single-walled carbon nanotubes (Figure 2-16). Depending on the synthesis conditions and catalyst particle size, the yield can exceed % 99 and the final product can be free of amorphous carbon [188].

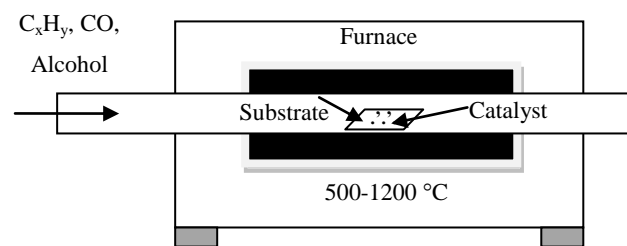


**Figure 2-16** CVD experimental set-up

The first used carbon feedstock used in CVD technique was carbon monoxide [195]. Later further investigations show that methane [196], ethylene [197], acetylene [198], ethanol, methanol [199], benzene [200] ...etc can also be used as carbon feedstock.

The catalysts used in CVD method are Fe, Co, and Ni regardless of the feedstock. Bimetallic and trimetallic mixtures of Fe, Co, and Ni with elements such as Y, Mo, Ru, and Pt increase the efficiency of reaction leading to high yields under certain conditions [201, 202].

The growth of CNTs by the CVD method divided into two types depending on the location of catalysts as gas phase growth and substrate growth. In gas phase growth the catalyst formation and nanotube growth occur in air while in substrate growth catalyst nanoparticles are deposited on a substrate [188]. In substrate growth, CNT will undergo either base growth or tip growth in which the catalyst particle remains attached to the surface of the substrate for the first case and the catalyst particle shoots into the air while the nanotube is extruding in the latter case (Figure 2-17).

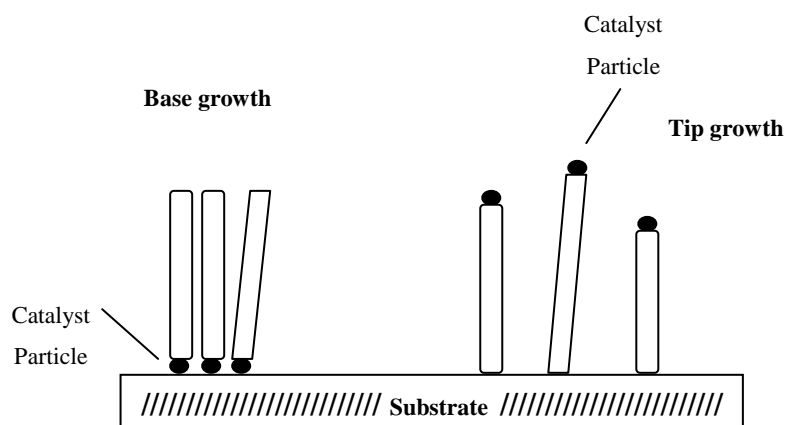


**Figure 2-17** Growth mechanism of CNTs

These two mechanisms are observed for the growth of carbon fibers, SWCNTs, and MWCNTs depending on the synthesis conditions, and catalysts sizes.

The smallest single-walled CNT (0.4 nm) was synthesized in the channel of zeolite AlPO<sub>4</sub>-5 single crystal [203]. Hence the microporous molecular sieves are the frequently used as catalyst supports in the synthesis of CNTs with CVD method mesoporous molecular sieves such as M41S materials are a kind of new catalyst supports with many interesting properties. Recently, metal-substituted MCM-41 materials have utilized for the synthesis of SWNTs by Haller and co-workers [204, 205] and Ramesh et al. [206], but still they have reported the CNTs with low yield. Pandurangan and coworker synthesized of SWNTs with high yield using Fe, Co and Fe–Co incorporated over mesoporous MCM-41 molecular sieves as a catalytic template [207].

## 2.2.4 Characterization Methods

### 2.2.4.1 Electron microscopy

Scanning electron microscopy (SEM) and transmission electron (TEM) microscopy are really effective equipments for morphologic analysis of carbon nanotubes. Due to its higher resolution TEM is favorable over SEM which enables imaging of single-walled or multi-walled carbon nanotubes, as well as number of walls, bundles etc. For more detailed information, high resolution transmission electron microscope is needed (HRTEM). For qualitative analysis TEM is generally used, especially to have information about the purity and quality of CNT samples [208]. For quantitative analysis, differential scanning calorimetry or near-infrared spectroscopy techniques are

used [209-212]. TEM measurements are utilized to study the interplay between structures, electronic properties, and local perturbations.

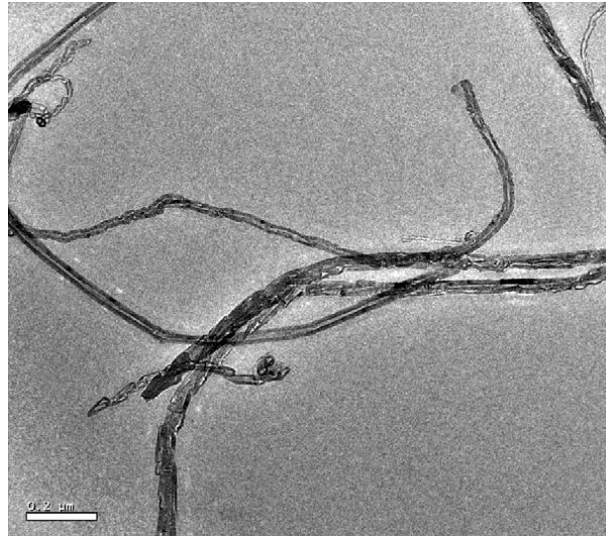


**Figure 2-18** TEM image of SWNTs grown at 750 °C using Fe-Co-MCM-41 catalyst [213]

SEM on the other hand, a powerful tool for pre-analysis of the overall structure due to its wider availability, ease of use, and simpler sample preparation [208]. The nanotube powder as well as individual tubes on the substrate can be observed by SEM.

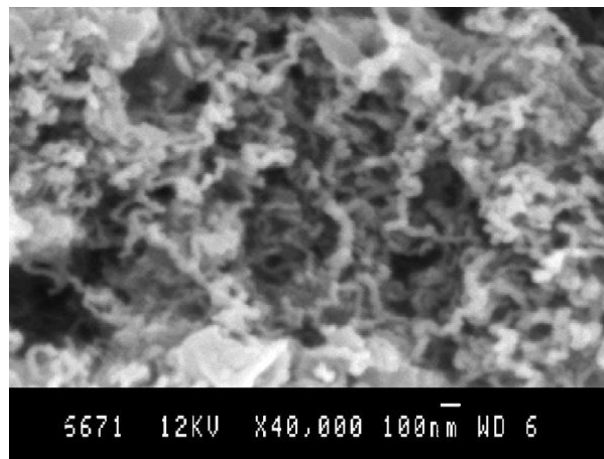


**Figure 2-19** SEM images of CNTs synthesized using Fe-Co-MCM-41 catalyst [213]

### 2.2.4.2 Raman Spectroscopy

Raman spectroscopy is one the most sensitive characterization tool for carbon nanotube structure [214, 215] which depends on the excitation laser energy. Nanotubes in resonance with that energy give high Raman signal. In addition to this, Raman intensity depends on light polarization which is characteristic of nanotubes and gives information about nanotube orientation.

There are two dominant Raman features, radial breathing mode (RBM) at low frequencies and tangential mode (G band) at high frequencies. There are also weak features, such as disorder-induced D band.

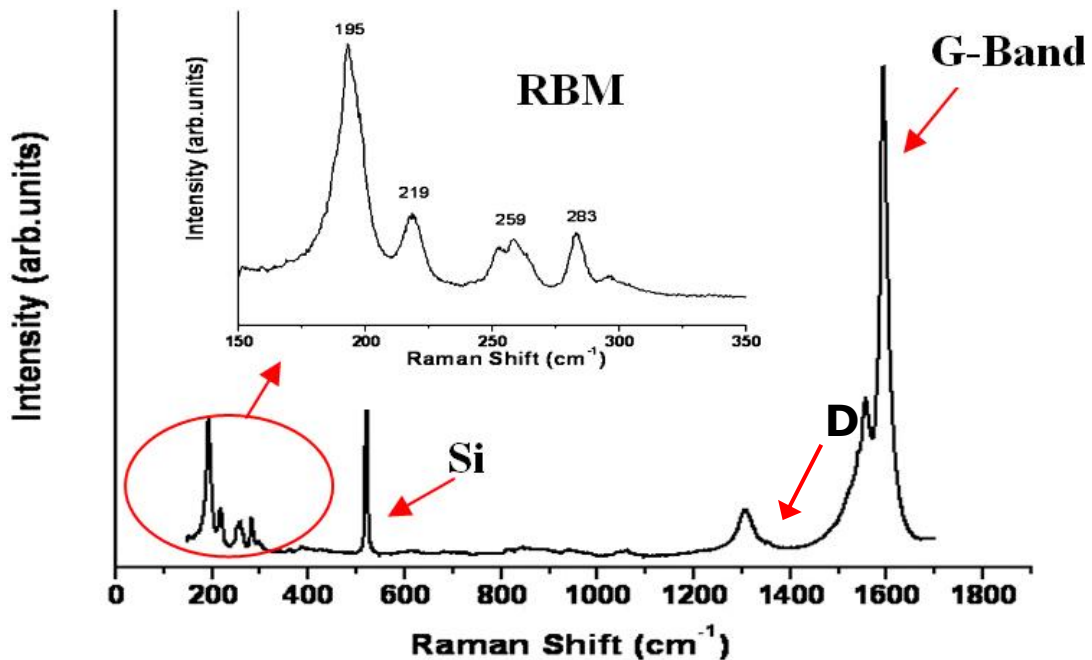


Figure 2-20 Raman spectrum [216]

RBM is unique to carbon nanotubes and is not observed for other carbon structures. It is used to observe nanotube diameter with higher accuracy as the diameter gets smaller. Analysis of RBM intensity as a function of laser energy can be used to analyze the optical transition energy of specific (n, m) tubes on bundles isolated in aqueous solution [217, 218] or on Si substrates [214, 215].

The G band in graphite has a single sharp peak at 1582 cm<sup>-1</sup> so the G band in SWCNTs is composed of two stronger peaks (G<sup>+</sup> and G<sup>-</sup>) related to the circumferential (TO) and axial (LO) atomic vibrations [219]. There is a relation between the splitting of these two peaks and tube-wall curvature. But the most important data is observed from the G<sup>-</sup> peak

that correlates to the tube type and doping. For semiconducting tubes, the TO mode has lower frequency than LO mode, and for metallic tubes, it is vice versa.

The D band is observed when there is symmetry breaking on the  $sp^2$  bonding lattices for nanotubes. Its observation is related to either the presence of defects or to the presence of amorphous-carbon material in the structure. According to the  $I_D/I_G$  intensity ratio, the amount of defects can be predicted since the D band intensity gets larger which results in larger  $I_D/I_G$  ratio. D band data is also used for more detailed analysis, such as the dependence of atomic edge structure observed at graphene edges [220].

#### **2.2.4.3 Scanning Probe Microscopy**

The most general scanning probe microscopes that are used to characterize CNTs are atomic force microscopy (AFM) and scanning tunneling microscopy (STM). After their discovery, many researchers used AFM and STM to observe the structure of CNTs [221-225]. However, it was not until 1998 that these data can be correlated between the structure and electronic properties of CNTs [226-228]. After that these techniques are directly used to analyze either metallic or semiconducting feature of nanotubes. STM can also be used to analyze the effect of structural defects on electronic properties [229, 230].

Many other characterization techniques such as near-infrared spectroscopy, thermogravimetric analysis, differential scanning calorimetry, small-angle X-ray dispersion are important for bulk sample characterization.

## 2.3 Diffusion in Porous Media

There are a variety of usages for porous solids, including but not limited to adsorbents, membranes and catalysts. Therefore, the comprehension of fundamental diffusion properties of organic molecules within nanopores is essential for industrial purposes. Moreover, molecular transport processes within nanopores have been an important problem of interest for adsorptive separations, gas–solid reactions and heterogeneous catalysis for a long time.

Diffusion of molecules in porous materials is essential for analyzing the factors limiting their performance. Realizing such an understanding requires knowledge of the adsorptive properties of the materials and the extent to which transport of molecules within the pores involves surface diffusion as well as gas-phase diffusion [231-236]. Furthermore, the dimensions of the pores and of the diffusing molecules, and the interactions of the latter with the pore surfaces, are clearly important issues. The experimental determination of diffusion coefficients is also an important issue. Traditionally, diffusion coefficients have been determined by macroscopic methods in which concentration gradients are present within a sample, under either steady-state or unsteady-state conditions [237, 238]. A microscopic method, nuclear magnetic resonance, has the feature that diffusional information can be obtained in the absence of concentration gradients, i.e., under equilibrium conditions [229, 240]. The differences frequently observed in diffusion parameters obtained by different methods are not clearly understood. The main features of macroscopic and microscopic methods as well as the discrepancies in diffusivity parameters have been discussed extensively by leading investigators in the field [241-243].

A number of different techniques are available for studying the diffusion in porous structures. The techniques can be summarized as follows:

- [1] Macroscopic techniques
  - 1.1 Membrane permeation
  - 1.2 Uptake methods
  - 1.3 Chromatographic methods
  - 1.4 Positron emission profiling
  - 1.5 Tapered element oscillating microbalance technique

## [2] Microscopic techniques

- 2.1 Pulsed Field Gradient NMR
- 2.2 Quasi-Elastic Neutron Scattering
- 2.3 Interference microscopy

The most common technique is to follow the time response of an adsorbate-adsorbent system after changing the pressure or composition of the surrounding atmosphere. By analyzing the response curves the contributing diffusion coefficients can then be calculated [244]. A number of different sorption techniques are nowadays available, which all have their advantages and disadvantages. A special class of techniques form the ones in which labelled molecules are used, as these techniques are capable of measuring the diffusion under equilibrium conditions and can thus probe the *tracer-* or self-diffusivity. More recently, two new techniques have been introduced to directly probe the self-diffusivity in these materials called pulse-field gradient NMR (PFG-NMR) [245] and Quasi-Elastic Neutron Scattering (QENS) [246]. Both techniques are capable of measuring the meansquare displacement of the molecules inside the pores.

Seferinoglu and Yürüm measured the diffusion coefficients of pyridine in raw and acid-washed low rank coals with a simple and precise gravimetric method [247, 248]. They observed that the diffusion of pyridine in the coal was increased with increasing temperature.

Yürüm and coworkers also studied diffusion of organic volatile substances into natural zeolites using the same method [249, 250]. They investigated that, as the molecular weight of the solvent increased, the coefficients of diffusion decreased, the time necessary to reach equilibrium increased, and the activation energies increased. In addition to these, they observed that for all volatile solvents, the diffusion coefficients increased linearly with an increase in temperature.

### 2.3.1 Theory

Diffusion is the random migration of molecules or small particles in which movement occurs due to thermal energy [251-269]. In a more simple way, diffusion is the result of chaotic movement of atoms, molecules or small particles where fewer elements of its own type are located. Diffusion of gases in porous media is a very important topic since this effect plays an important role in catalysis, gas chromatography, and gas separation processes.

Two types of diffusion can be distinguished: *transport* diffusion resulting from a concentration gradient, and *self* -diffusion which takes place in a system which is at equilibrium. Adolf Fick and Thomas Graham started the quantitative study of diffusion in 1850-1855. According to his studies, Fick concluded that diffusion law is isomorphic to the Fourier law of heat transfer. Consequently, he proposed his first law of diffusion describing diffusion process macroscopically. The flux due to transport diffusion can be described using Fick's First Law of Diffusion given in equation (2.13):

$$\bar{J} = -D \bar{\nabla} C \quad (2.13)$$

in which the matter flux,  $\bar{J}$  is linearly related with concentration gradient,  $\bar{\nabla} C$  and  $D$  is the Fickian diffusion coefficient or transport diffusion coefficient.

Transport diffusion results from a gradient concentration however self-diffusion occurs in the absence of a chemical potential gradient. The differences in the microphysical situations between these two phenomena result in different diffusion coefficients (transport diffusion coefficient,  $D$  and self-diffusion coefficient,  $D^*$ ). Although transport and self-diffusion generally occur by essentially the same microscopic principle, usually these coefficients for transport and self-diffusion are not the same.

Diffusion equation can also be expressed in terms of chemical potential of materials where  $L$  is the phenomenological Onsager coefficient:

$$\bar{J} = -L \bar{\nabla} \mu \quad (2.14)$$

Fick's second equation defines the diffusion where  $D$  does not depend on  $C$  (equation 2.15):

$$\frac{\partial C}{\partial t} = -D\nabla^2 C \quad (2.15)$$

In microporous and mesoporous materials, such as silica, alumina and activated carbon, pores are typical. So assuming that the framework atoms are stable, diffusion phenomena of the mobile species can be calculated within the fixed coordinates of solid porous materials. If we consider the diffusion into a porous solid as a special case of binary diffusion where the diffusivity of the solid atoms is zero, then interdiffusion coefficient will be simply the diffusivity of mobile species.

In order to calculate the corrected diffusion coefficient, the following equations are used:

$$J_i = v_i C_i \quad (2.16)$$

where  $v$  is the average drift velocity. It is defined as:

$$\bar{v}_i = b_i \bar{F}_i \quad (2.17)$$

Where  $b$  is the molecular mobility and  $F$  is the force applied on particles where it is assumed that the only driving force is a concentration gradient.  $F$  is defined as:

$$\bar{F}_i = -\nabla \mu_i \quad (2.18)$$

And chemical potential is defined as:

$$\mu_i = \mu_i^0 + RT \ln P_i \quad (2.19)$$

where  $P$  is the partial pressure of the component  $i$ .

So combining these equations result in:

$$J_i = RTb \left( \frac{d \ln P_i}{d \ln C_i} \right) \left( \frac{d C_i}{dx} \right) \quad (2.20)$$

$$D_i = RTb \left( \frac{d \ln P_i}{d \ln C_i} \right) = D_0 \left( \frac{d \ln P_i}{d \ln C_i} \right) = D_0 \Psi \quad (2.21)$$

For microporous materials, there is no clear distinction between molecules on the surface and the molecules in the gas phase because adsorption in micropores is a volume filling process [270]. So,  $D_0$  is defined as the corrected diffusion coefficient where  $P_i$  is the sorptive gas pressure and  $C_i$  is the concentration of the sorbed phase and  $\Psi$  is a thermodynamic correction factor which defines the nonlinearity between pressure and concentration of the adsorbent [258]. For macroporous materials diffusion is not affected by the adsorption process where  $\Psi$  equals to 1 so that diffusion coefficient is the corrected diffusion coefficient.

Experimental diffusion studies in the zeolites with several different methods, such as steady-state methods [271], uptake methods [272-281] to calculate Fickian diffusion coefficients and microscopic methods [282] to calculate self-diffusion coefficients. In experimental studies, the corrected diffusivity is calculated where transport diffusion is measured [277]. In these experiments, first Fickian diffusion coefficients,  $D$  are calculated then by using  $D$ , corrected diffusion coefficients,  $D_0$  are obtained which are approximately equal to self-diffusion coefficients,  $D^*$  [283].

When we consider the porous materials, it is observed that zeolites with micropores have overlapping surface forces of opposed pore walls and MCM-41 with mesoporous have surface forces and capillary forces while materials with macroporous have little effect of pore wall forces in contribution of diffusion phenomena.

There are four well-known diffusion types:

1. Gaseous or molecular diffusion
2. Knudsen diffusion
3. Liquid diffusion
4. Atomic diffusion in solids

When we consider the transport mechanism in porous media there are 6 types of diffusion (Figure 2-21):

1. Gaseous or molecular flow
2. Knudsen flow
3. Surface diffusion
4. Multilayer diffusion
5. Capillary condensation
6. Configurational diffusion

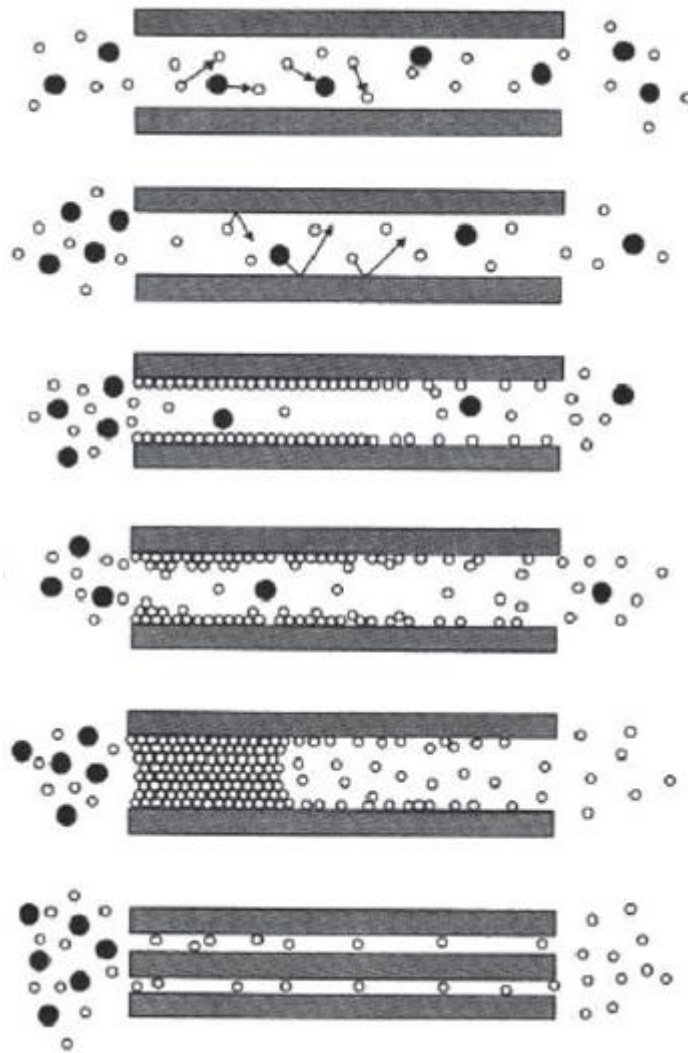


**Figure 2-21** Transport mechanisms in porous media: (a) gaseous or molecular flow, (b) Knudsen flow, (c) surface diffusion, (d) multilayer diffusion, (e) capillary condensation, (f) configurational diffusion [284]

In gaseous flow pore diameter is larger than the mean free path so the collisions between molecules are more frequent than those between molecules and pore walls [285-288].

In Knudsen diffusion, mean free path of the molecules increases or the pore diameter decreases, so the molecules move in such a way that they collide with pore walls and flow independently without disturbing others [286, 288]. Surface diffusion is the result of adsorption of diffusing molecules on the pore walls [171, 287, 289]. An extension of this mechanism is multilayer diffusion that is the transition regime between the capillary and surface diffusion. Capillary condensation is the result of condensing diffusing

molecules within the pore until the molecules fill the pore and evaporation of molecules at the other end of the pore. The last mechanism is configurational diffusion, which is active when pore diameters are so small that only small molecules can diffuse through the pores [258, 171].

According to the pore diameter, different type of diffusion mechanism roles. For macropores, collisions between molecules are much dominant than the collisions with the wall that molecular diffusion take place. When the pore size decreases, the number of collisions with the wall increases so that Knudsen diffusion is the dominant mechanism in which the mobility now starts to depend on the pore size of the material. As the pore size gets smaller and smaller like zeolites or related materials, configurational diffusion regime plays an important role [258].

In a porous adsorbent system, the diffusion of the volatile species in the porous material can be done by uptake measurements assuming spherical sorbent particles with stable particle sizes. In order to calculate the Fickian diffusion coefficient in radial coordinates the following formula with specific boundary conditions should be solved [263, 290]:

$$\frac{\partial C_A}{\partial t} = D \left( \frac{\partial^2 C_A}{\partial r^2} + \frac{2}{r} \frac{\partial C_A}{\partial r} \right) \quad (2.22)$$

(I)	@ t>0	$C_A = C_\infty$	for r = r <sub>0</sub>
(II)	@ t = 0	$C_A(r) = C = \text{constant}$	for 0 < r < r <sub>0</sub>

in which  $C_A$  is the concentration (mol/m<sup>3</sup>),  $D$  is the diffusion coefficient constant through the process (m<sup>2</sup>/s),  $t$  is time (s),  $r$  is the distance from the particle center (m),  $C$  is the initial concentration (mol/cm<sup>3</sup>) and  $r_0$  is the particle radius (m).

Solving equation (2.22) for gas phase diffusion in spherical system gives [291-293]:

$$\frac{M_t}{M_\infty} = 1 - \frac{6}{\pi^2} \sum_{n=1}^{\infty} \frac{1}{n^2} \exp\left(-Dn^2\pi^2 \frac{1}{a^2}\right) \quad (2.23)$$

where  $M_t$  and  $M_\infty$  are the amount of solvent diffused at time  $t$  and at steady state, respectively into the spherical solute particles with radius  $a$ .

The solution to equation (2.23) is given by equation (2.24) [294]:

$$\frac{M_t}{M_\infty} = 6 \left( \frac{Dt}{a^2} \right)^{1/2} \left[ \pi^{-1/2} + 2 \sum_{n=1}^{\infty} \text{ierfc} \left( \frac{na}{\sqrt{Dt}} \right) \right] - 3 \frac{Dt}{a^2} \quad (2.24)$$

For small times equation (2.24) becomes:

$$\frac{M_t}{M_\infty} = 6 \left( \frac{Dt}{\pi a^2} \right)^{1/2} - 3 \frac{Dt}{a^2} \quad (2.25)$$

Neglecting the contribution of the second term in equation (2.25), value of diffusion coefficient D is found from the slope of  $M_t/M_\infty$  vs  $t^{1/2}$ .

When the collisions of the molecules with the container walls are more frequent than the intermolecular gaseous collisions, Knudsen diffusion will be dominant and it will be demonstrated that the net flow of molecules in gas flow direction will be proportional to molecular flux gradient. To be more specific, for porous catalysts, the Knudsen diffusion coefficient will be expressed as follows for a capillary of circular cross-section and radius r [295]:

$$D_K = \frac{2}{3} r \sqrt{\frac{8RT}{\pi M}} \quad (2.26)$$

where M is the molecular weight of diffusing gas. This equation has some limitations because most of the catalyst particles do not have straight cylindrical capillaries. So a more specific formula may be applied which strongly depends on the pore geometry in terms of porosity ( $\Psi$ ), specific surface area ( $A_s$ ) and particle density ( $\rho_p$ , mass per unit total particle volume including volume occupied by space):

$$D_K = \frac{16}{3} \frac{\Psi}{\rho_p A_s} \sqrt{\frac{RT}{\pi M}} \quad (2.27)$$

The porosity can be calculated by using particle density ( $\rho_p$ ) and true density of the solid ( $\rho_s$ ). The ratio of  $\rho_p/\rho_s$  will give the fraction of solid present in the particles and  $1-(\rho_p/\rho_s)$  is the porosity.

The effective diffusivity in the region of the molecular flow ( $D_e$ ) and Knudsen flow ( $D_{eK}$ ) for the porous solid can be calculated from the following formula by using a geometric factor including porosity and tortuosity ( $\tau$ ):

$$D_e = D \frac{\Psi}{\tau}$$

$$D_{eK} = D_K \frac{\Psi}{\tau}$$
(2.28)

Tortuosity is the ratio of path length which must be traversed by molecules diffusing between two points within a pellet to the direct linear separation between those points.

### 2.3.2 Activation Energy

Activation energy of diffusion is also called energy barrier for diffusion. Activation energy of diffusion is calculated from the following equation [258]:

$$D = D_0 e^{-E_A/RT}$$

$$\ln D = \ln D_0 - \frac{E_A}{RT}$$
(2.29)

where  $D_0$  ( $\text{m}^2/\text{s}$ ) is the pre-exponential factor and  $E_A$  is the activation energy for diffusion ( $\text{J/mol}$ ) [296].

According to this formula, activation energy,  $E_A$  can be determined by measuring the diffusion coefficients at different temperatures.

Diffusion as a process that takes place in the form of a series of jumps [297] where  $D_0$  is related to the elementary rate at which particles aim to jump to a nearby adsorption site. The exponential is an expression of the change when the particles manage to overcome  $E_A$ , the free energy barrier, between these neighboring sites. The temperature dependence in diffusion systems is explained with this simple theory.

### 2.3.3 Mode of Transport

In order to analyze the sorption data a comprehensive equation is used to describe the kinetics of diffusion:

$$\frac{M_t}{M_\infty} = kt^n \quad (2.30)$$

where  $M_t$  and  $M_\infty$  denote the amount of solvent diffused in the macromolecular structure at time  $t$  and at steady state, respectively.  $t$  is the release time,  $k$  is the rate constant which depends on structural characteristics of the system, and  $n$  is an exponent characteristic of the mode of transport of the solvent in the porous structure depends on diffusion mechanism and particle geometry. In the graph of  $\ln(M_t/M_\infty)$  versus  $\ln(t)$ ,  $\ln(k)$  is the intercept and  $n$  is the slope [298].

In macromolecular systems sorption mechanism are defined in terms of two limiting cases of Fickian diffusion and Case II transport [299].

For  $n > 0.5$ , non-Fickian diffusion is observed, while  $n = 0.5$  represents the Fickian diffusion mechanism. The value of  $n = 1$  provides Case II transport mechanism and the values between 0.5 and 1 indicates anomalous transport. The values of  $n$  can be used for initial approximation for the nature of the process since it is structure sensitive.

For an infinite plan sheet, the values of  $n$  would be 0.5 and 1 for Fickian and Case II respectively. For the case of an infinite cylinder,  $n$  values would be 0.45 and 0.89 for Fickian and Case II respectively [299]. Different  $n$  values can be found in the literature [300].

In a porous structure, they may be different sections which affect the diffusion behavior of the system. So,  $n$  values could be used only as a rough estimation of the nature of the process.

A preliminary analysis of sorption data results in equation 2.30, however, this equation can only be used up to 60% of the final weight of diffused molecules, and moreover, it does not give comprehensive information like inflections or penetrant loss over time [300].

## CHAPTER 3. EXPERIMENTAL

### 3.1 Materials

#### 3.1.1 Chemicals Used in MCM-41 Synthesis

In the synthesis of MCM-41 mesoporous materials, an aqueous solution of sodium silicate, containing 27 wt. % SiO<sub>2</sub> (Aldrich) was used as the silica source and hexadecyltrimethylammonium bromide (CTABr, (C<sub>16</sub>H<sub>33</sub>)N(CH<sub>3</sub>)<sub>3</sub>Br), Merck 99% pure) was used as the surfactant. Metal sources used in metal incorporated synthesis of MCM-41 mesoporous materials were:

- Iron (III) nitrate nonahydrate (Merck ≥ 99 % pure),
- Cobalt (II) nitrate hexahydrate (Fluka ≥ 98 % pure),
- Nickel(II) nitrate hexahydrate, and
- Copper (II) nitrate trihydrate

#### 3.1.2 Carbon Nanotubes

Carbon nanotubes named as “Baytubes® C 150 HP” from Bayer Company were purchased for diffusional studies. The structural properties of carbon nanotubes were given in Table 3-1.

Baytubes® are agglomerates of multi-wall carbon nanotubes with low outer diameter, narrow diameter distribution and an ultra-high aspect ratio (length-to-diameter ratio). Baytubes® show excellent tensile strength and E-modulus, as well as exceptional thermal and electrical conductivity.

**Table 3-1** Structural properties of Baytubes® C 150 HP

<b>Property</b>	<b>Value</b>	<b>Unit</b>	<b>Method</b>
<b>C-Purity</b>	> 99	%	Elementary analysis
<b>Free amorphous carbon</b>	Not detectable	%	TEM
<b>Number of walls</b>	3 - 15	-	TEM
<b>Outer mean diameter</b>	13 - 16	nm	TEM
<b>Outer diameter distribution</b>	5 - 20	nm	TEM
<b>Inner mean diameter</b>	4	nm	TEM
<b>Inner diameter distribution</b>	2 - 6	nm	TEM
<b>Length</b>	>1	μm	SEM
<b>Bulk density</b>	140 – 230	kg/m <sup>3</sup>	EN ISO 60
<b>Loose agglomerate size</b>	0.1 – 1	mm	PSD
<b>Average agglomerate size</b>	0.5	mm	PSD
<b>Length of Baytubes</b>	0.2 – 1	μm	TEM
<b>BET surface area</b>	220-250	m <sup>2</sup> /g	N <sub>2</sub> sorption analyzer

Baytubes® are produced in a high-yield catalytic process based on chemical vapor deposition. The process yields easy to handle agglomerates with high apparent density. The optimized process results in a high degree of purity (low concentration of residual catalyst and absence of free amorphous carbon). SEM image of Baytubes® was given in Figure 3.1.

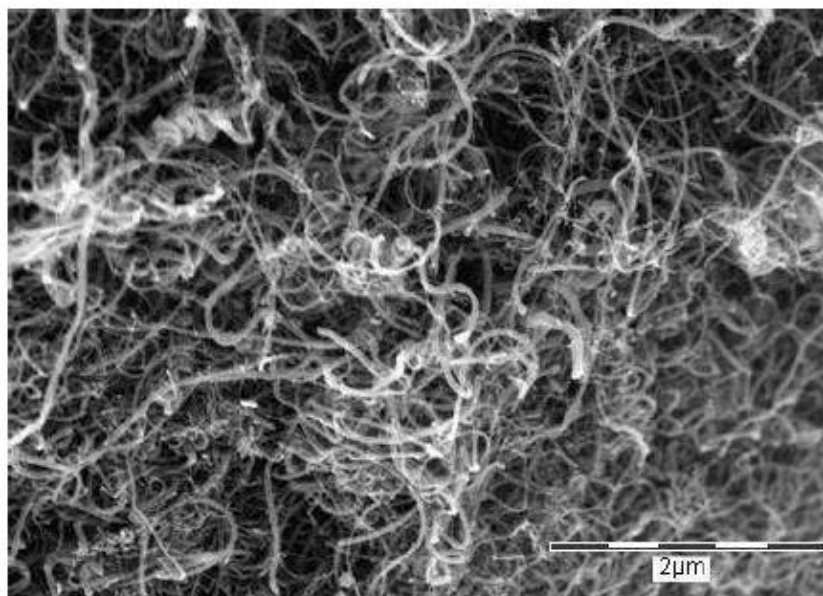


**Figure 3-1** SEM image of Baytubes C 150 HP

### 3.1.3 Chemicals Used in Diffusion Experiments

The alcohols used in diffusion experiments were:

- Methanol (Labkim, 99.9% pure),
- ethanol (Labkim, 99.8% pure),
- 1-propanol (Lab-Scan, 99.5% pure),
- n-butanol (Ideal)

The aromatic solvents used in diffusion experiments were:

- Benzene (Merck, 99.8% pure),
- Ethylbenzene (Merck,  $\geq 99\%$  pure),
- Propylbenzene Fluka  $\geq 98\%$  pure),
- Toluene (Merck,  $\geq 99\%$  pure),
- o-xylene (Merck,  $\geq 99\%$  pure),
- m-xylene (Merck,  $\geq 99\%$  pure),
- p-xylene (Merck,  $\geq 99\%$  pure)

The chemicals purchased for diffusion experiments in mesoporous medium were used as received.

## **3.2 Microwave Assisted Synthesis of MCM-41**

### **3.2.1 Pure MCM-41**

The synthesized procedure was a modified method described in [3]. 6.6 gr of hexadecyltrimethylammonium bromide was dissolved slowly in 43 ml of deionized water at 40 °C and 5.65 ml of sodium silicate solution was added dropwise to the clear solution with continuous stirring at the same temperature. After stirring for 1 hours, the pH of the mixture was adjusted to 11 by adding sufficient amount of 1 M H<sub>2</sub>SO<sub>4</sub>. The resulting gel is stirred for 1 hour before being transferred to a 120 ml Teflon bottle and placed in a domestic microwave (Delonghi, Max. power: 800 W, Max. adjustable time: 30 minutes).

For finding the optimum synthesis conditions, the microwave power and reaction time were combined in several ways. Summary of the experiments were given in Table 3.2. The optimum synthesis condition was devised as 30 minutes and 120 W.

The resultant solid was recovered by filtration, washed thoroughly with distilled water until the pH got neutralized and dried at room temperature. Before calcination step the solid was kept at 40°C for 24 hours. The as-synthesized MCM-41 was finally calcined inside a quartz filter installed quartz tube (120 cm long x 1 cm diameter) which was placed in a tubular furnace, by heating from ambient temperature to 550 °C at a rate of 1 °C/min and kept at 550 °C for 6 hours in a flow of dry air.

**Table 3-2** Parameters of the microwave synthesis of pure MCM-41

<b>Sample ID</b>	<b>Power (W)</b>	<b>Time (min)</b>
<b>MCM-41-80-1</b>	80	1
<b>MCM-41-80-10</b>	80	10
<b>MCM-41-80-20</b>	80	20
<b>MCM-41-80-30</b>	80	30
<b>MCM-41-80-60</b>	80	60
<b>MCM-41-80-120</b>	80	120
<b>MCM-41-120-1</b>	120	1
<b>MCM-41-120-10</b>	120	10
<b>MCM-41-120-20</b>	120	20
<b>MCM-41-120-30</b>	120	30
<b>MCM-41-120-60</b>	120	60
<b>MCM-41-120-120</b>	120	120

## **3.2.2 Metal Incorporated MCM-41**

### **3.2.2.1 Impregnation**

For impregnation method sodium silicate and surfactant mixture was heated in microwave oven as described above. After washing and drying steps required amount of metal was dissolved in 10 ml of distilled water and the solution was added to the dried as-synthesized MCM-41 to obtain different Si/metal mole ratios as 25, 50, 75 and 100. In the impregnation technique, the metal solution was mixed with about 2 gr of as-synthesized MCM-41 (average product yield before calcination) in order to keep the Si/Metal mole ratio reliable. After overnight stirring the excess liquid portion was removed by centrifuge. After drying at 40 C in an oven, the solid product was calcined in the tubular furnace, by heating from ambient temperature to 550 °C at a rate of 1 °C/min and kept at 550 °C for 6 hours in a flow of dry air.

### **3.2.2.2 Direct Synthesis**

In the direct synthesis method, the required amount of metal was dissolved in 10 ml of distilled water and the solution was added into the sodium silicate and surfactant mixture before pH adjustment as described above in pure MCM-41 synthesis. The metal solutions were prepared in such a way that Si/metal mole ratios were 25, 50, 75 and 100 for each metal. After adjusting the pH to 11, the resulting gel was stirred for 1 hour before being transferred to a 120 ml Teflon bottle and placed in the microwave and reacted for 30 minutes at 120 W. The resultant solid was recovered by filtration, washed thoroughly with distilled water until the pH got neutralized and dried at room temperature. Before calcination step the solid was kept at 40°C for 24 hours. The product was finally calcined in the tubular furnace, by heating from ambient temperature to 550 °C at a rate of 1 °C/min and kept at 550 °C for 6 hours in a flow of dry air.

Four different type of metal were incorporated into the MCM-41 structure with two different methods and four different Si/Metal mole ratios. In Table 3.3 the experiments were summarized.

**Table 3-3** Summary of the metal incorporated experiments

		<b>Direct Synthesis Method</b>				<b>Impregnation Method</b>			
<b>Type of metal</b>		Fe	Co	Ni	Cu	Fe	Co	Ni	Cu
<b>Si/Metal mole ratio</b>	25	25	25	25	25	25	25	25	25
	50	50	50	50	50	50	50	50	50
	75	75	75	75	75	75	75	75	75
	100	100	100	100	100	100	100	100	100
<b>Power/time (W/min)</b>	120/30	120/30	80/60	80/60	120/30	120/30	120/30	120/30	120/30
			120/30	120/30					

Schematic representation of direct and impregnation synthesis techniques were given in Figure 3.2.

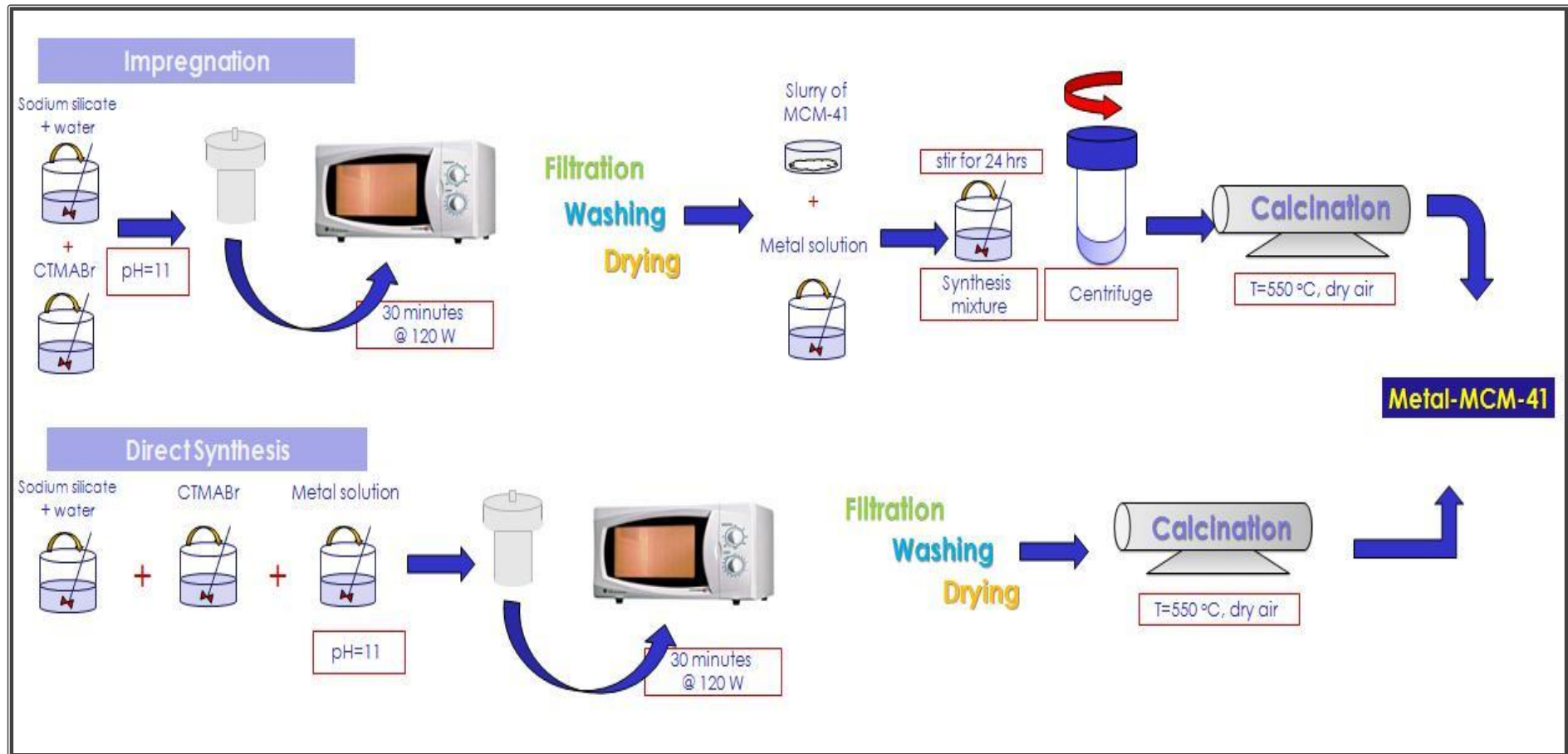


Figure 3-2 Schematic representation of synthesis techniques

### **3.3 Characterization of MCM-41**

Development of the hexagonal mesoporous structure was confirmed by X-ray diffraction (XRD) and N<sub>2</sub> physisorption and Fourier transform infrared (FT-IR), while the metal dispersion were characterized by energy dispersion spectroscopy (EDS) and transmission electron microscopy (TEM). Thermal stabilities and structural morphology of the samples were characterized by thermal gravimetric analyzer (TGA) and Scanning Electron microscopy (SEM) respectively.

#### **3.3.1 N<sub>2</sub> Sorption Analysis**

The surface area and porosity properties of the mesoporous materials were determined using NOVA 2200e Surface Area and Pore Size Analyzer by Quantachrome Instruments Co., USA. The measurement was performed at the liquid nitrogen boiling point of 77 K. The samples were outgassed at 150 °C overnight. The BET surface area was determined by a multipoint BET method using the adsorption data in the relative pressure (P/P<sub>0</sub>) range of 0.05–0.3. The pore volume and pore size distributions were calculated using a procedure developed by BJH method.

#### **3.3.2 XRD**

XRD measurements of the samples were done with an X-ray powder diffractometer (Bruker AXS-D8 advance powder diffractometer fitted a Siemens X-ray gun and equipped with Bruker axS Diffrac Plus software) at room temperature. The measurements were performed in the 2 $\theta$  range of 2°- 7° at 40 kV and 40 mA, using Cu-K $\alpha$  radiation with a wavelength of 1.5406 Å. In all measurements, the step size was 0.01°, and data collection period was 1 second in each step. The samples were outgassed before XRD measurements.

#### **3.3.3 SEM and EDS**

Leo G34-Supra 35VP scanning electron microscope coupled with and energy dispersive spectrometer software was used for images and elemental analysis respectively. The samples were coated with carbon by Emitech T950 Turbo Evaporator before SEM and EDS analyses in order to maintain a conductive layer on the surface to prevent charging.

The gun chamber pressure was about  $10^{-11}$  mbar. The column was equipped with a secondary electron detector, back-scattered electron detector, and in-lens detector for secondary electron detection. Imaging was done at the extractor voltage of 5.2 keV, and the accelerating voltage range of 2-5 keV using secondary electron detector.

### **3.3.4 TEM**

High Resolution transmission electron microscopy (TEM) analyses were performed by JEOL 2100 LaB6 HRTEM in TUBITAK MAM Electron Microscopy Laboratories of Material Institute.

### **3.3.5 FT-IR**

Structural analyses were done by Nicolet iS10 Fourier transform infrared spectroscopy with KBR pellet technique. The effective range was from 400 to 4000  $\text{cm}^{-1}$ .

### **3.3.6 TGA**

Thermal stabilities of the samples were characterized by Netsch 449C thermal gravimetric analyzer. The thermal behavior of the samples were analyzed by heating the samples up to 1000 °C from room temperature with a heating rate of 10 °C/min under nitrogen atmosphere in pure alumina crucibles.

### 3.4 Diffusion Experiments

Diffusional behaviors of alcohols (methanol, ethanol, propanol, n-butanol) and aromatics (benzene, ethylbenzene, propylbenzene, toluene, o-xylene, m-xylene, p-xylene) in mesoporous media were investigated in detail in an adiabatic isothermal setup. A Sartorius CP 124S analytical balance with 4-digit accuracy was placed in a Memmert model 300 laboratory oven.

Approximately 0.2 g of degassed MCM-41, or metal incorporated MCM-41 or CNT was evenly distributed in a Petri dish and the balance was tared. A total amount of 200 ml solvent was evenly poured into four Petri dishes and placed in the closest vicinity of the balance pan. The temperature of the experiment was set, and the system was closed. After the temperature reached a constant set value between 26 and 32 °C, the weight increase of the sorbent as a result of vapor uptake was recorded every 5 s with the aid of Sartorius Connect software installed on the PC. The experiment was continued until uptake measurement reached to equilibrium.

The effect of temperature and chain length of solvents on the diffusion character were investigated at four different temperatures, 26, 28, 30 and 32 °C namely. The aims of this work are to determine realistic diffusion coefficients in mesoporous MCM-41 materials and CNTs, mode of transport, and activation energies of some alcohols into mesoporous channels of MCM-41 and CNT.



PC with SartoConnect software

Sartorius CP 124S Analytical Balance

Memmert Modell 300 Oven

**Figure 3-3** Set-up of diffusion experiments

## CHAPTER 4. RESULTS AND DISCUSSION

### 4.1 Synthesis of MCM-41 by Microwave Radiation

Microwave assisted synthesis of MCM-1 molecular sieves is a promising method due to the advantages such as more rapid nucleation, more uniform dimension and composition of product as well as saving energy [134]. Also it was informed that the formation mechanism of MCM-41 under microwave heating is similar to that observed with conventional oven heating [150]. In this study, MCM-41 was synthesized by using domestic microwave oven at several different combinations of power and time. The optimum reaction time and microwave power was determined after the trial of several combinations.

In the literature, the synthesis temperature and duration varied between 100-160 °C and 30-240 min., respectively [150-156]. In the present survey, microwave assisted hydrothermal autoclave heating was applied for the synthesis of mesoporous materials. The first set of direct synthesis experiments were done at 80 Watt for 1, 10, 20, 30, 60 and 120 minutes. X-ray diffraction graphs and N<sub>2</sub> sorption analysis were given in Figure 4-1 and Table 4-1 respectively to understand the formation of ordered structure.

The XRD pattern of MCM-41 point out the high level of ordered structure of mesoporous channels with amorphous silica walls [5]. The characteristic Bragg peaks were at low angles and typically 3-5 peaks which can be indexed to a hexagonal lattice as (100), (110), (200), (210), and (300) [6]. The sample prepared at 10 minutes did not show the characteristic Bragg peaks of MCM-41 structure. For the case of 20 minutes synthesis time, it was observed that the ordered structure was started to form and two reflections were observed at 2 $\theta$  values of 2.68 and 4.42. When we increased the synthesis time to 30 minutes, a sharp Bragg peak corresponding to d<sub>100</sub> and two reflections were observed at 2 $\theta$  values of 2.48, 4.20 and 4.80. For 60 minutes treated

sample, the highest intensity was observed corresponding to  $d_{100}$  at  $2\theta$  value of 2.47 and two more reflections at 4.19 and 4.65.

The samples prepared at 80 Watt for 1 minute and 120 minutes did not give any Bragg peaks by XRD analysis. The reason for the initial case was that the time was not enough to initiate the formation of ordered structure and also it was evidence that no crystalline MCM-41 was formed before the microwave treatment. For the latter case over heating resulted in phase deformation.

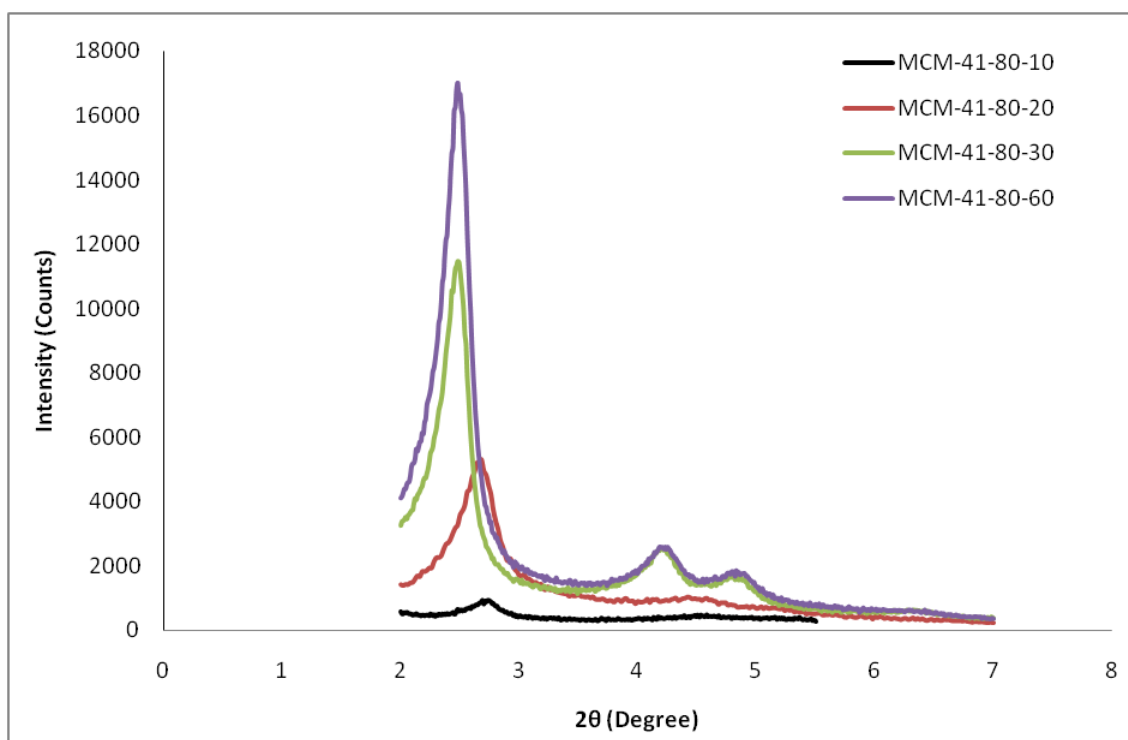


**Figure 4-1** XRD patterns of MCM-41 (80/10, 80/20, 80/30, 80/60)

The  $N_2$  adsorption isotherms of samples prepared at 80 Watt for 20, 30 and 60 minutes showed isotherms of type IV with a sharp inflection around  $P/P_0 = 0.25-0.35$ , characteristic of MCM-41 (Figure 4-2) [169]. For the sample prepared in 10 minutes, the sharp inflection was not observed. The specific surface area (BET), pore volume and average pore diameter ( $D_{pore}$ ) evaluated from the desorption branch of  $N_2$  isotherm by BJH theory,  $d_{100}$ , lattice parameter ( $a$ ), and pore wall thickness ( $\delta$ ) of these samples as calculated from the  $N_2$  desorption isotherms were presented in Table 4-1.

The characteristic lattice parameter  $a$ , which was defined as the repeating distance between the two pore centers, was evaluated from equation (2.10) [173]:

$$a = \frac{2}{\sqrt{3}} d_{100} \quad (2.10)$$

and the pore wall thickness ( $\delta$ ) values were evaluated from equation (2.12) [173]:

$$\delta = a - D_{pore} \quad (2.12)$$

BET surface area values increased with the increase of time as 558, 1211, 1385 and 1390 m<sup>2</sup>/g for 10, 20, 30 and 60 minutes respectively. Pore diameters remained unchanged which may be explained by using the same surfactant for all samples. There was slight increase in pore wall thicknesses and lattice parameters as the samples became more organized. There was also a noticeable increase in the pore volume of sample prepared in 60 minutes compared to other samples, which had the highest regularity according to XRD data. For instance, pore volumes were 0.18, 0.45, 0.39 and 1.10 cm<sup>3</sup>/g, respectively.

In the literature, Bein and coworker [150] reported that, using cetyltrimethyl ammonium bromide as surfactant, microwave treatment of the sample at 150 C for 60 minutes resulted in the formation of MCM-41 mesoporous sieves with 800-1000 m<sup>2</sup>/g specific surface area values.

MCM-41 materials were prepared at 100-120 °C within 40 minutes in ethylene glycol solution using the same surfactant under microwave radiation [152]. The BET surface areas and pore volumes of MCM-41 materials formed by this ethylene glycol method were 700-1150 m<sup>2</sup>/g and 0.60-0.78 cm<sup>3</sup>/g, respectively.

In this study, MCM-41 mesoporous material was obtained at 80 Watt, 60 minutes with specific surface area value of 1390 m<sup>2</sup>/g and pore volume of 1.10 cm<sup>3</sup>/g which were higher than the values reported in the literature.

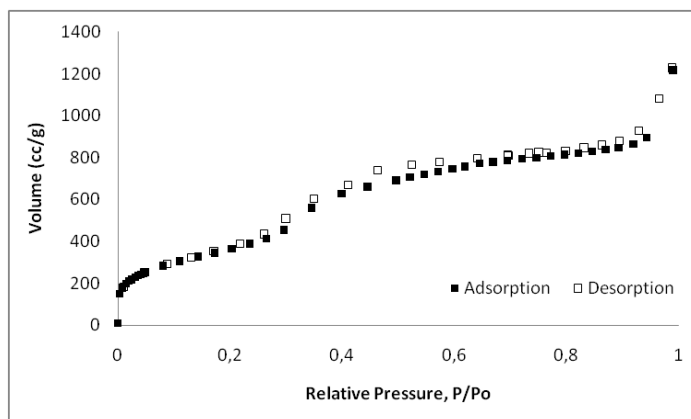
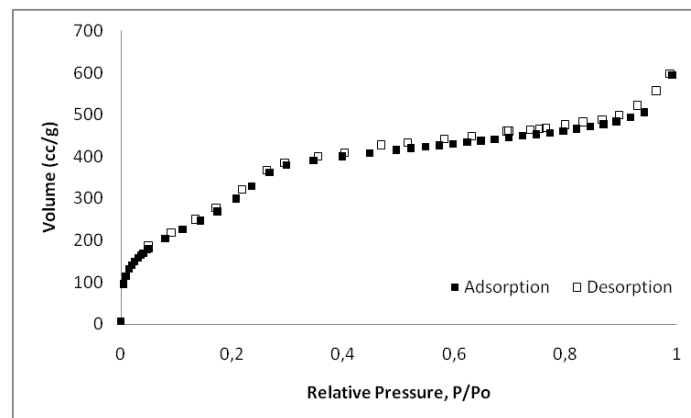
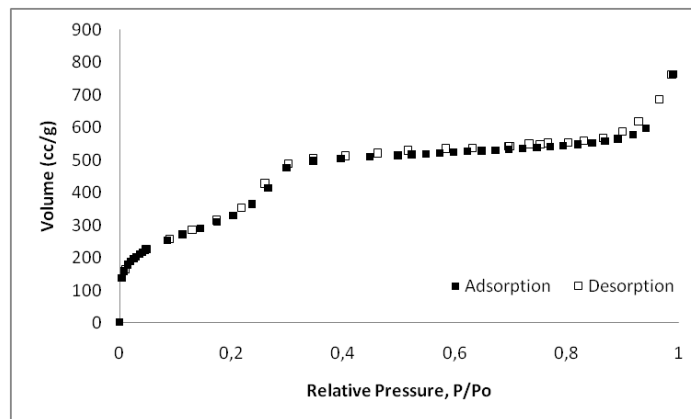
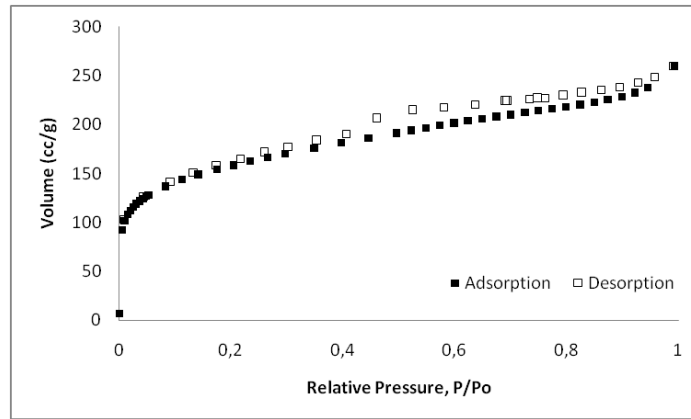


**Figure 4-2** N<sub>2</sub> sorption isotherms of MCM-41 a) 80/10 b) 80/20 c) 80/30 d) 80/60

The second set of experiments was performed at 120 Watt for 1, 10, 20, 30, 60 and 120 minutes. X-ray diffraction graphs and N<sub>2</sub> sorption analysis were given in Figure 4-3 and Table 4-1 respectively to understand the formation of ordered structure.

When we observe the XRD data of these samples, the formation of ordered structure started even in the case of 20 minutes sample with three remarkable peaks at 2 $\theta$  values of 2.51, 4.15 and 4.69. Since the ordering started earlier, it was also decomposed earlier than the 80 Watt samples. When the synthesis time reached 60 minutes, a decrease was observed in the intensity of XRD peaks compared to the sample prepared at 30 minutes. Also no peaks were observed for the samples prepared ad 1 minute and 120 minute duration.

The sample prepared at 120 Watt in 30 minutes gave the most ordered structure according to XRD data. The three peaks were observed at 2 $\theta$  values of 2.50, 4.26 and 4.82, respectively.

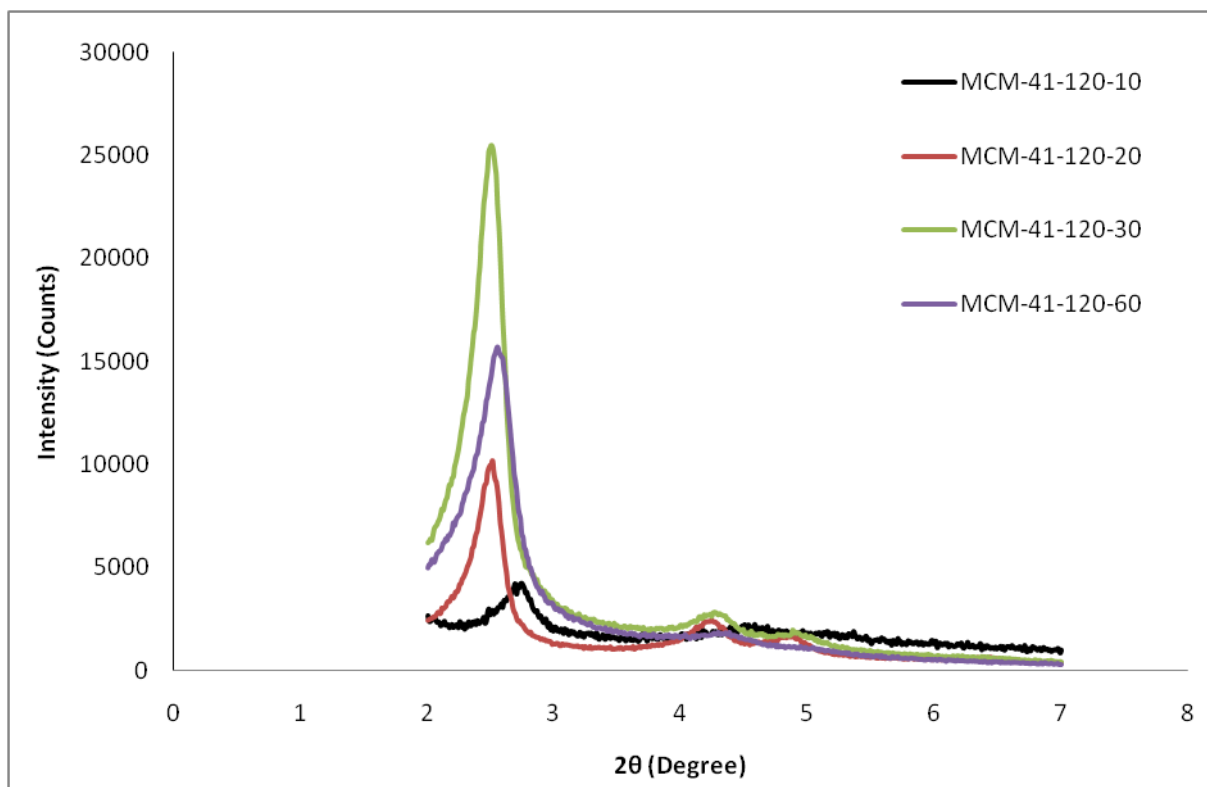


**Figure 4-3** XRD patterns of MCM-41 (120/10, 120/20, 120/30, 120/60)

The specific surface area (BET), pore volume and average pore diameter ( $D_{pore}$ ) evaluated from the desorption branch of  $N_2$  isotherm by BJH theory,  $d_{100}$ , lattice parameter (a), and pore wall thickness ( $\delta$ ) of these samples as calculated from the  $N_2$  desorption isotherms were presented in Table 4-1.

The  $N_2$  adsorption isotherms of samples prepared at 120 Watt for 10, 20, 30 and 60 minutes all showed isotherms of type IV with a sharp inflection around  $P/P_0 = 0.25-0.35$ , characteristic of MCM-41 (Figure 4-4). BET surface area values increased with the increase of time as 688, 1343, and 1438  $m^2/g$  for 10, 20, and 30 minutes respectively. Then it started to decrease to 1210  $m^2/g$  for the sample prepared at 60 minutes.

Pore diameters were 4.46, 4.02, 3.49 and 4.02 nm for the sample prepared 10, 20, 30 and 60 minutes, respectively. There was also a noticeable decrease in the pore volume of sample prepared in 10 minutes compared to other samples, which had the lowest regularity according to XRD data. For instance, pore volumes were 0.28, 0.71, 0.53 and 0.58  $cm^3/g$ , for the sample prepared 10, 20, 30 and 60 minutes respectively.

Pore wall thicknesses of the samples were 0.37, 0.88 and 0.35 nm for the sample prepared 20, 30 and 60 minutes, respectively. As the samples became more organized, pore wall thickness values became higher as for the sample prepared at 120 Watt in 30 minutes.

The BET surface area of the samples increased from 688 to 1438  $m^2/g$  when the time reached from 10 minutes to 30 minutes. The increase in the pore volume was not as high as the samples prepared at 80 Watt, but still there was an increase when the reaction time increased. Pore diameter value of the sample prepared at 120 Watt in 30 minutes was close to the samples prepared at 80 W in 60 minutes, another evidence that using the same surfactant would not affect the pore size when ordered hexagonal mesoporous structure was formed.

The sample prepared at 120 Watt in 30 minutes had the highest specific surface area value compared to other samples obtained under microwave radiation in this study and reported in the literature.

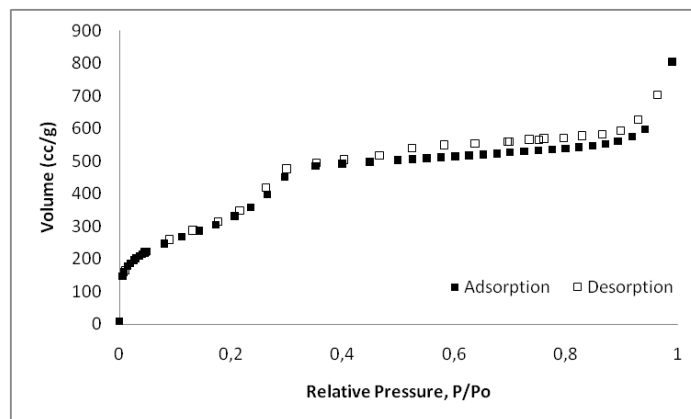
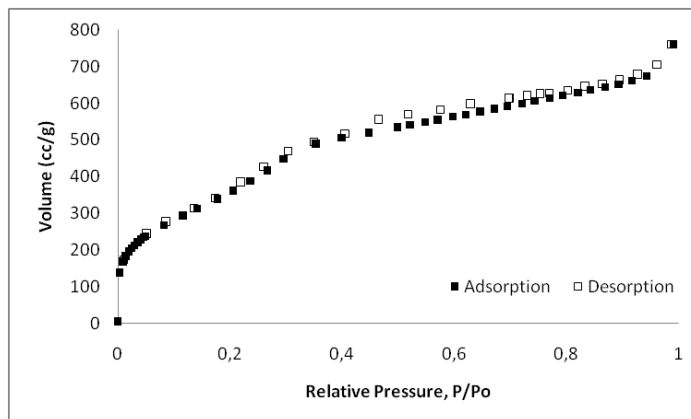
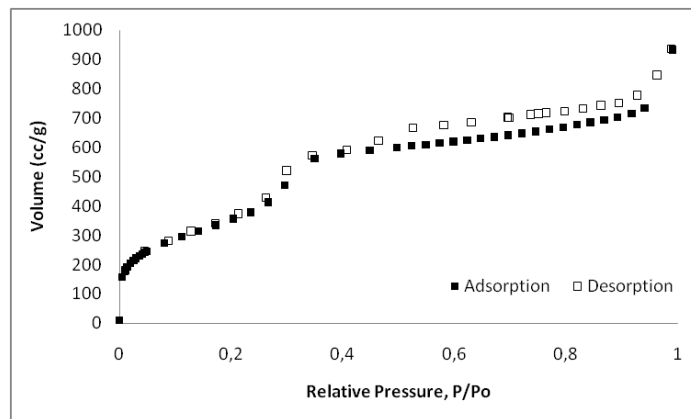
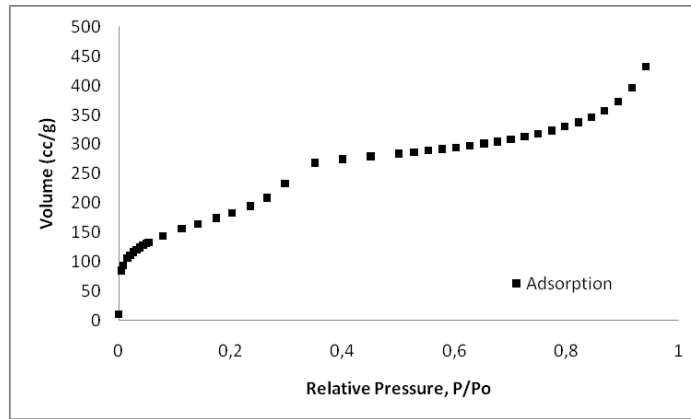


**Figure 4-4** N<sub>2</sub> sorption isotherms of MCM-41 a) 120/10 b) 120/20 c) 120/30 d) 120/60

**Table 4-1** Physical and structural properties of MCM-41 type catalytic materials synthesized by microwave assisted direct synthesis method

Sample ID (Power/Time) (Watt/Min.)	BET Surface Area (m <sup>2</sup> /g)	BJH Des. Pore Volume (cm <sup>3</sup> /g)	BJH Des. Pore Diameter (nm)	d <sub>100</sub> (nm)	Lattice Parameter “a” (nm)	Pore Wall Thickness “δ” (nm)
MCM-41 (80/10)	558	0.18	3.48	3.54	4.09	0.79
MCM-41 (80/20)	1211	0.45	3.47	3.54	4.09	0.79
MCM-41 (80/30)	1385	0.39	3.50	3.65	4.21	0.89
MCM-41 (80/60)	1390	1.10	3.50	3.65	4.22	0.89
MCM-41 (120/10)	688	0.28	4.46	3.54	4.09	-
MCM-41 (120/20)	1343	0.71	4.02	3.63	4.19	0.37
MCM-41 (120/30)	1438	0.53	3.49	3.64	4.20	0.88
MCM-41 (120/60)	1210	0.58	4.02	3.61	4.16	0.35

The morphologies of samples prepared at 120 W in 30 minutes and at 80 W in 60 and 120 minutes were given in Figure 4-5 and Figure 4-6 respectively by using SEM.

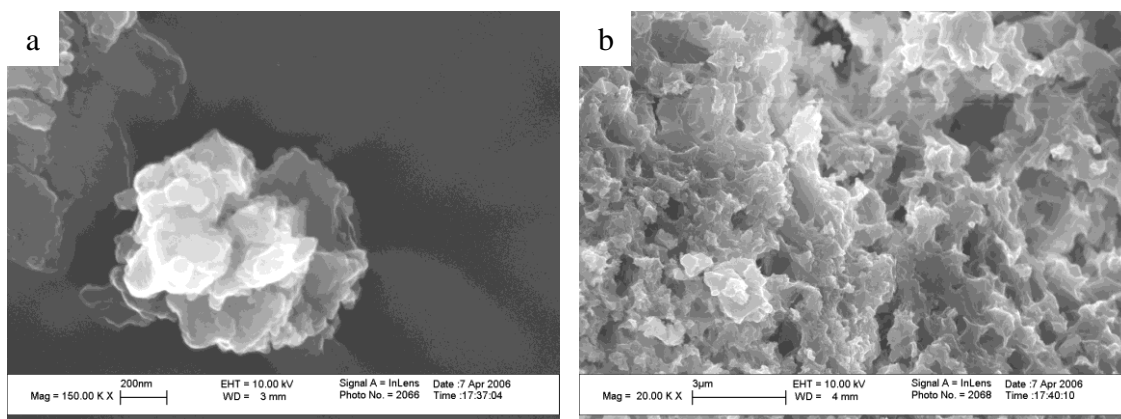


**Figure 4-5** SEM images of MCM-41 (120/30) by inlens detector

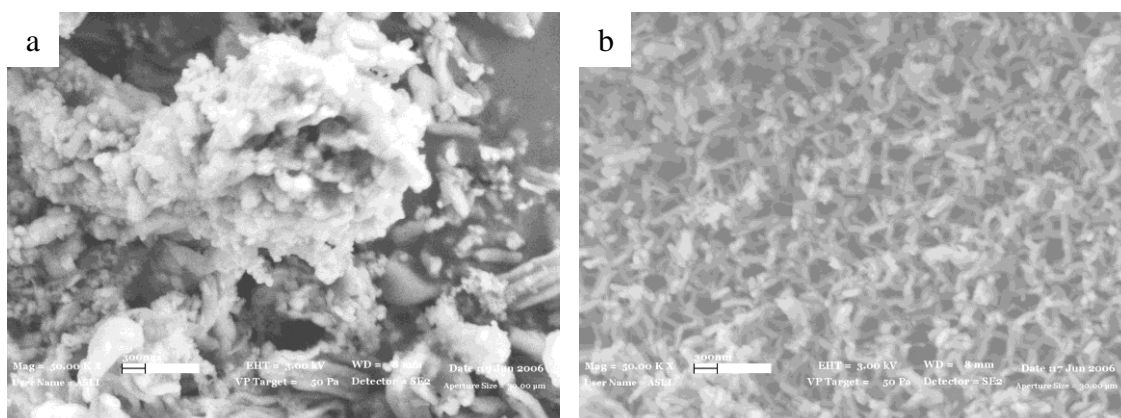


**Figure 4-6** SEM images of MCM-41 a) 80/60 b) 80/120 by secondary electron detector

The thermal gravimetric analyses of MCM-41 samples were done by heating the samples from room temperature to 1000 °C with a heating rate of 10 °C/min under air atmosphere. At 950 °C, MCM-41 lost 23% by weight while it only lost 7% by weight around 120 °C which was in good agreement with the literature [301, 302]. The TGA thermogram of MCM-41(120/30) was given in Appendix A, Figure A.1.

The structural analysis of the samples were also done by FTIR technique. The FTIR spectra uncalcined and calcined sample prepared at 120 W in 30 minutes were given as an example in Figure 4-7a. In the uncalcined sample, the bands at 2922, 2852 and 1478  $\text{cm}^{-1}$  were the characteristic bands of surfactant alkyl chain. These bands disappeared after the calcination step. In Figure 4-7b the band at 3407  $\text{cm}^{-1}$  was characteristic band of Si-OH and water molecules adsorbed; the band at 1632  $\text{cm}^{-1}$  were from vibration of water molecules adsorbed. The band at 1065  $\text{cm}^{-1}$  is from asymmetric extension

vibration of Si–O–Si. There were no other peaks that were related to the surfactant which showed that the calcination step was perfectly performed [303, 304].

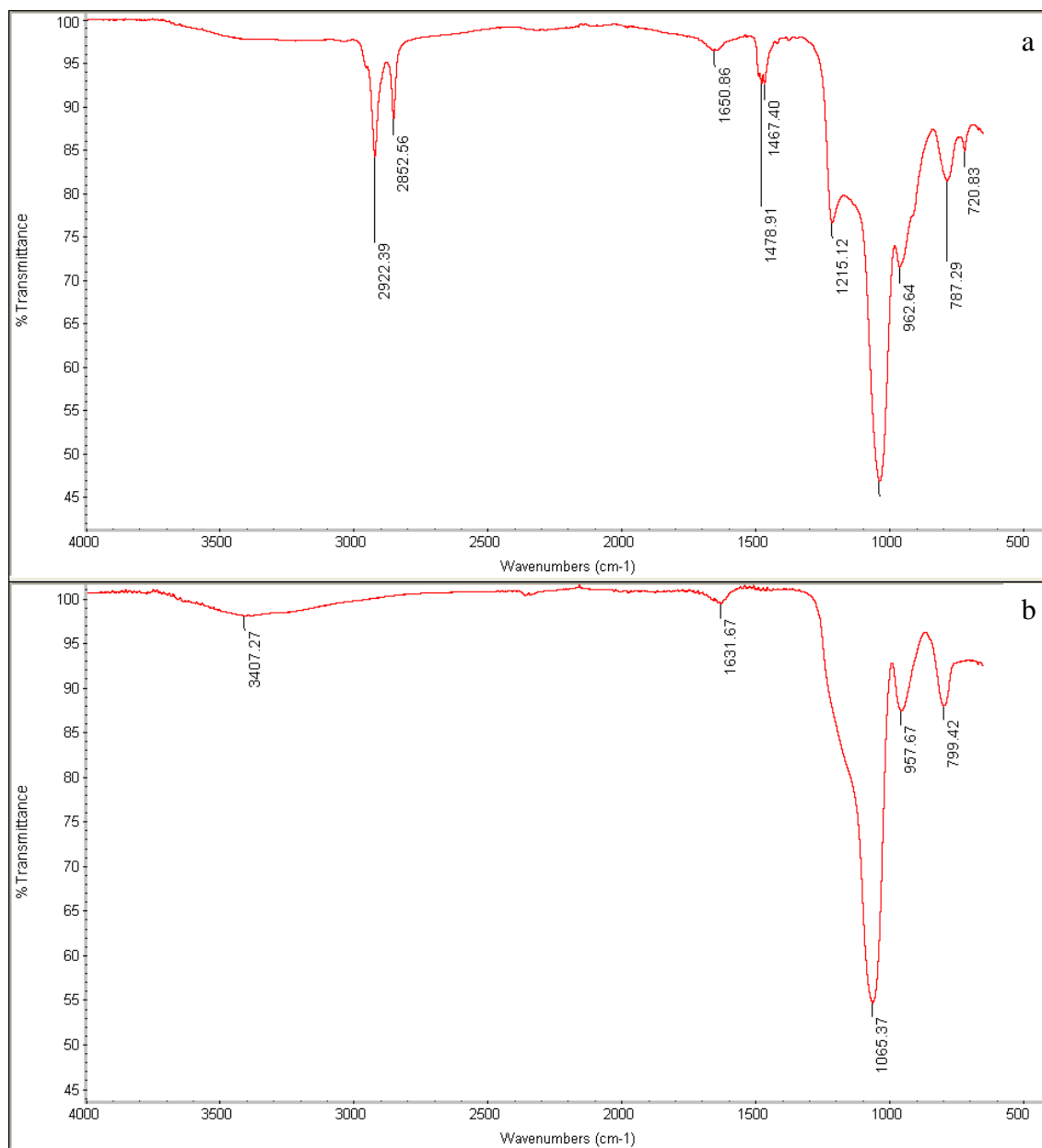


**Figure 4-7** FTIR spectra of MCM-41 synthesized at 120 W in 30 minutes a) uncalcined b) calcined

As a conclusion, high quality hexagonal mesoporous materials of good thermal stability were obtained in 30 minutes by microwave assisted heating. The variation of crystallinity with various reaction conditions suggests that the formation mechanism of MCM-41 under microwave heating was similar to that observed with conventional oven heating. Apparently, the effect of the microwave heating was to accelerate the condensation reactions of the silicate network. It is thought that the microwave radiation, by stimulating the water molecules around the silicon atoms via vibration and rotation, causes the condensation process of the framework to accelerate.

The specific surface area values were found to be very high especially for the sample obtained at 120 W and 30 minutes. The pore volumes, average pore diameters were close to each other, showing reproducibility. Lattice diameter and pore wall thicknesses were in agreement with the published values in literature.

There was no temperature control in our microwave system, so when the heating time was too long (or temperature was too high) continued heating resulted in decomposition of the already formed structure. A hexagonal phase was already formed after heating the gel at 80 Watt for 20 minutes. Increasing the microwave power and time first increase the crystallinity then decrease it after heating for two hours. Continued microwave action may cause the meta stable MCM-41 material to collapse into a denser phase in the reaction solution, for example by destroying the surfactant [150].

It was important to note that the first aim of the synthesis of mesoporous material by microwave heating was the significant effect to reduce synthesis time. This goal was achieved with the synthesis of MCM-41 by microwave induced heating at 120 Watt for 30 minutes with highly ordered structure.

For all metal incorporated samples this optimum condition was applied in both direct synthesis and impregnation techniques. For the case of Cu and Ni samples, at the highest metal amount (Si/Metal:25), direct synthesis experiments were performed at 80 Watt for 30 and 60 minutes in order to see whether the incorporation of metal would result in a better orientation at lower energy. The results that correspond to above discussion were given in the following title.

## 4.2 Synthesis of Metal Incorporated MCM-41

Si-MCM-41 mesoporous materials lack intrinsic catalytic applicability by themselves, but can be modified with organic functional groups or heterogenized with transition metals in order to make them suitable for various applications.

The synthesis of transition metals such as Cu [305-309], Ni [310-314], Co [315-319] and Fe [320-324] containing mesoporous molecular sieves by different methods has already been investigated. However, there has been very few data published about microwave assisted synthesis of metal incorporated MCM-41 mesoporous molecular sieves [161-166].

In this research, the effect of metal incorporation into the MCM-41 hexagonal structure by microwave radiation was studied in detail with transition metals such as copper, nickel, cobalt and iron. Two different techniques were used (impregnation and direct synthesis) to investigate the effects of synthesis procedures on the physical and structural properties of the synthesized catalytic materials.

The incorporation of metal into MCM-41 structure was investigated using different Si/Metal mol ratios as 25, 50, 75 and 100. Development of the hexagonal mesoporous structure was confirmed by X-ray diffraction (XRD) and N<sub>2</sub> physisorption and Fourier transform infrared (FT-IR), while the metal dispersion were characterized by energy dispersion spectroscopy (EDS) and transmission electron microscopy (TEM). Thermal stabilities of the samples were characterized by Netsch 449C Thermal Gravimetric Analyzer (TGA).

The materials with highest metal content (Si/Me: 25) were used in diffusion experiments. With redox properties it was expected to enhance the intraparticle diffusion when compared to zeolites, due to their special characteristics such as higher surface area and higher pore diameter [325]. With microwave radiation, materials with relatively high Metal/Si mole ratios as well as high order were obtained in a shorter time.

## 4.2.1 Cu-MCM-41

### 4.2.1.1 Microwave Assisted Direct Synthesis Results

Cu-MCM-41 mesoporous molecular sieves were synthesized by microwave assisted direct synthesis technique with different amounts of Si/Cu mole ratios as 25, 50, 75, and 100 at 120 Watt in 30 minutes. In addition to those experiments, two more trials were performed at 80 Watt for 30 and 60 minutes as well for the highest amount of Cu content (Si/Cu: 25) in order to see the effect of metal introduction into the reaction solution. As can be seen from Figure 4-8, the samples prepared at 80 Watt for 30 and 60 minutes had diffraction peak of  $d_{100}$  at  $2\theta$  value of  $2.397^\circ$  and  $2.402^\circ$  respectively which were shifted to the lower angles with respect to MCM-41 as Cu incorporated into the structure.

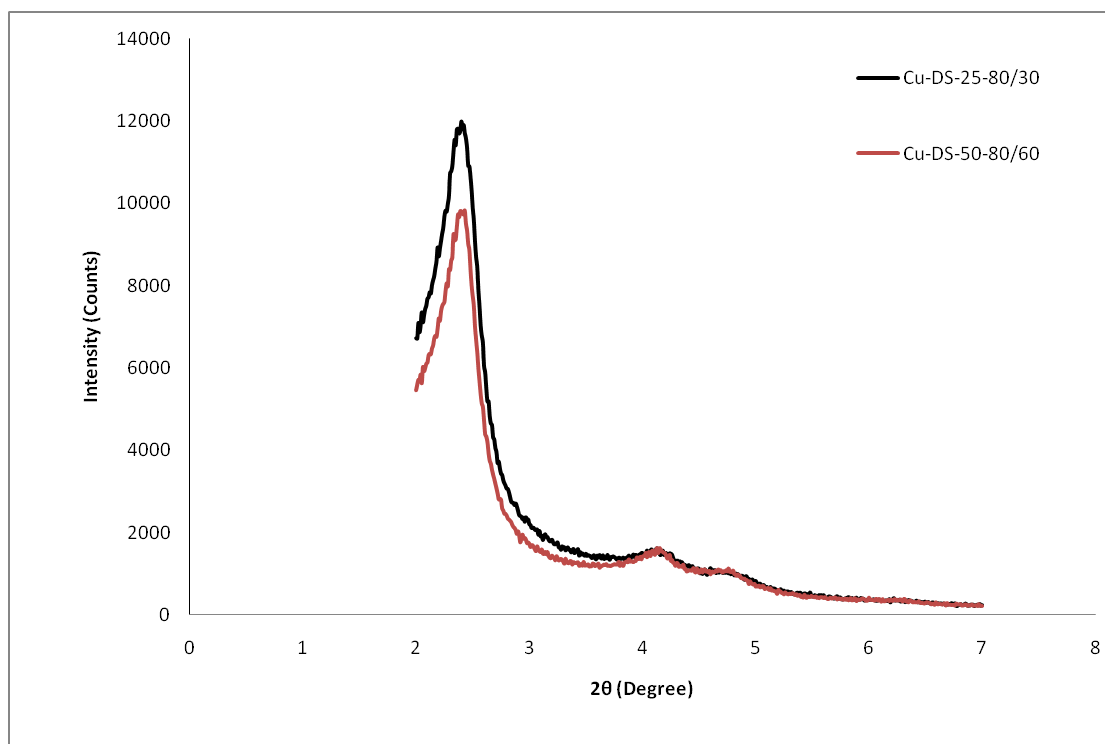


**Figure 4-8** XRD patterns of Cu-MCM-41-DS-25 (80/30 and 80/60)

Lattice parameters and pore wall thickness values of these samples were higher than pure MCM-41 as 4.25 and 0.93 nm respectively. The surface area values were increased from 649 to 721  $\text{m}^2/\text{g}$  when time increased from 30 to 60 minutes. No significant effect was observed at 80 Watt in the ordering of the structure. The pore diameter and pore volume values were also very close to each other (Table 4-2).

The specific surface areas of the samples were determined using the nitrogen-desorption data from the relative equilibrium pressure interval of 0.05–0.3  $P/P_0$  according to the standard BET procedure. In Figure 4-9,  $N_2$  sorption isotherms of Cu-MCM-41 samples prepared at 80 Watt were given:

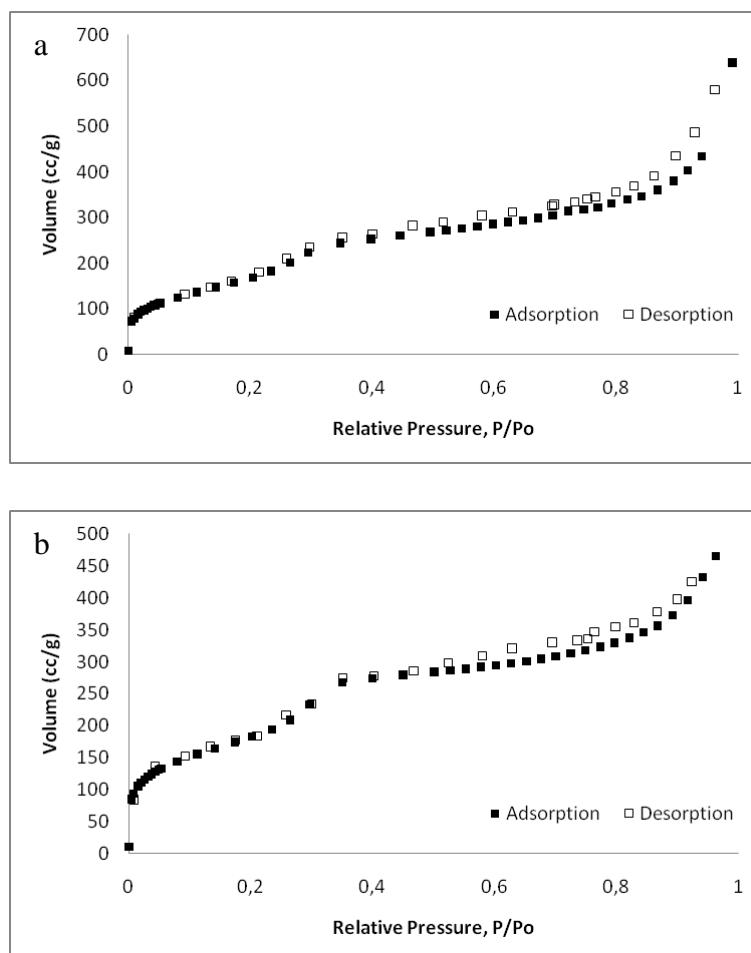


**Figure 4-9**  $N_2$  sorption isotherms of Cu-MCM-41-DS-25 a) 80/30 b) 80/60

The samples had typical Type IV isotherms with hysteresis loop caused by capillary condensation in mesopores. The abruptness between the relative pressure of 0.3–0.4 were not so sharp which showed the lack of uniform pore size distribution.

The morphology of samples prepared at 80 Watt in 30 minutes and 80 Watt in 60 minutes were observed by SEM and given in Figure 4-10.

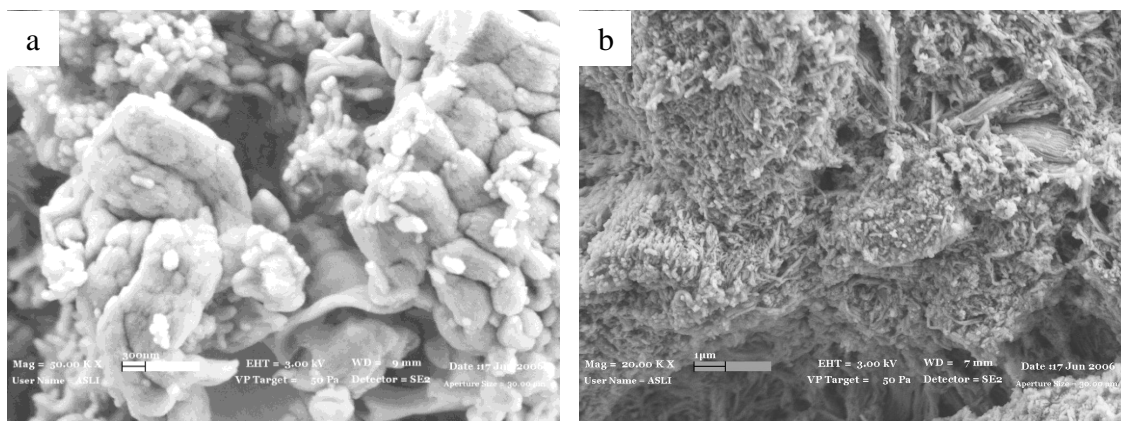


**Figure 4-10** SEM images of Cu-MCM-41-DS-25 a) 80/30 b) 80/60

The XRD patterns of Cu incorporated samples prepared at 120 Watt for 30 minutes were given in Figure 4-11. As the amount of Cu incorporated into the structure increased, the main peak in the XRD patterns shifted to the lower angles which leads to higher lattice parameters as expected. Mainly 3 peaks were observed for all samples which could be indexed as (100), (110) and (200) planes on hexagonal unit cell respectively. The sharp Bragg peaks corresponding to  $d_{100}$  were observed at  $2\theta$  values of 2.361, 2.499, 2.486, and 2.504° for Si/Cu mole ratios of 25, 50, 75 and 100 respectively.

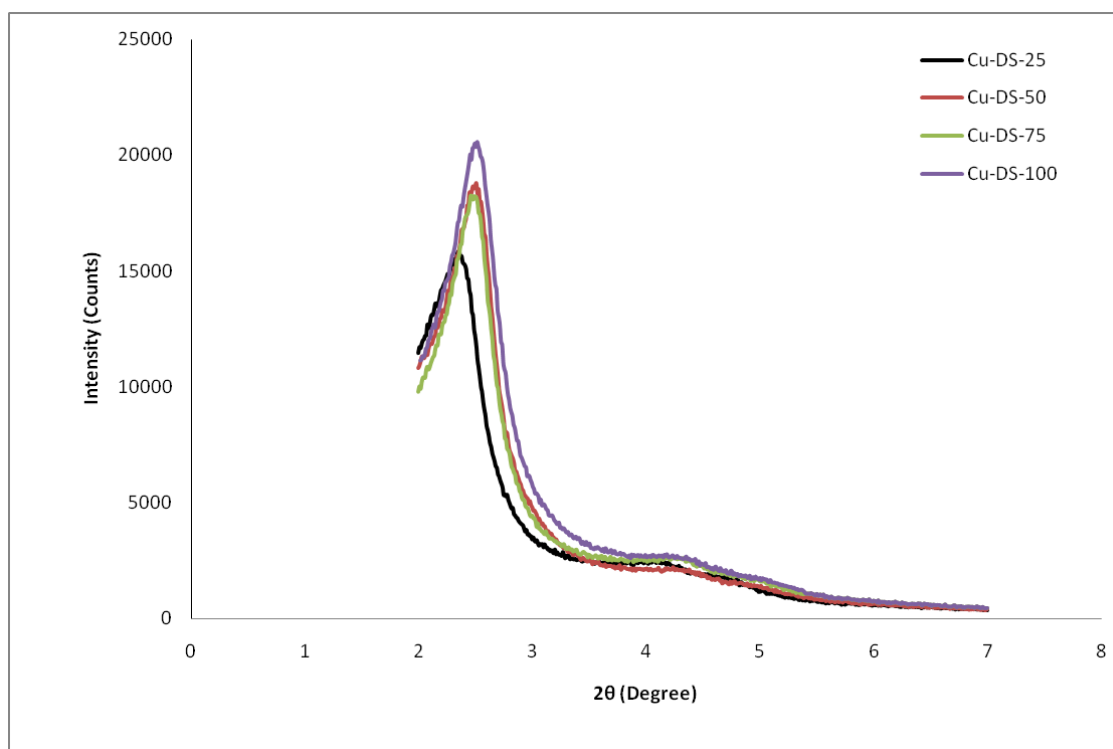


**Figure 4-11** XRD patterns of Cu-MCM-41 (120/30) with different Si/Cu mol ratios prepared by microwave assisted direct synthesis

In the high angle range of XRD patterns, no peaks were observed corresponding to large metal or metal oxide particles.

In Figure 4-12 N<sub>2</sub> adsorption-desorption isotherms for the Cu incorporated samples synthesized at 120 Watt-30 minutes were given. All samples had typical Type IV isotherm as expected of mesoporous materials. Between P/P<sub>0</sub> 0.3-0.4 a well defined step occurs especially for the samples with low metal content.

Surface area values increased from 941 to 1368 m<sup>2</sup>/g as the Si/Cu mole ratios increased. Pore diameter values increased as the Cu content decreased which may be due to the fewer blockages of pores with metal incorporation. The increase in pore wall thickness was also an evidence of the metal incorporation into the walls of mesoporous matrix as the metal content increased (Table 4-2).

The sample with highest metal content (Si/Cu:25) prepared at 120 Watt in 30 minutes gave much better results than the samples prepared at 80 Watt in 30 and 60 minutes. Lattice parameter increased from 4.25 to 4.32 nm and wall thickness increased from 0.93 to 1.40 nm which reinforce the idea of better metal incorporation into the mesoporous structure. The surface area value also increased from 649 to 941 m<sup>2</sup>/g.

The lattice parameters of Cu incorporated MCM-41 type mesoporous materials were greater than that of pure MCM-41. This was consisted with the Metal-O bonds being longer than that of Si-O bonds and gave an evidence of the metal incorporation into the framework.

It was also observed that the lattice parameters increased with the metal content which indicated that the metal content incorporated in the framework increased with increasing amount of metal salt added in the synthesis gel.

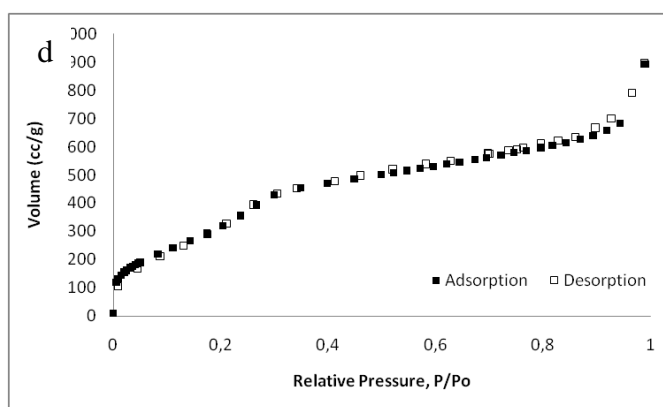
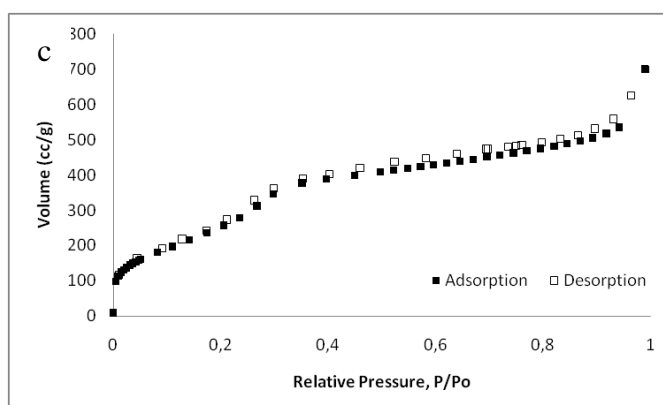
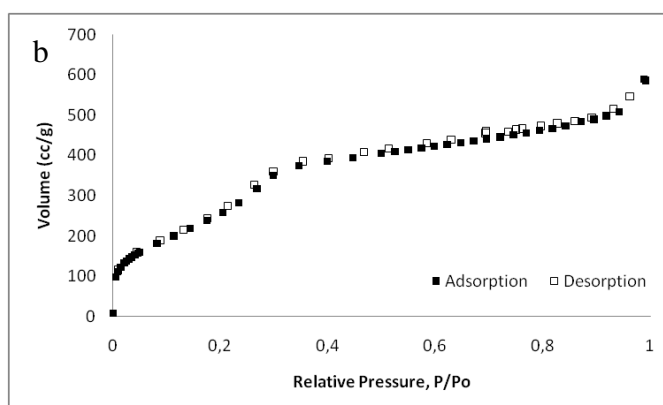
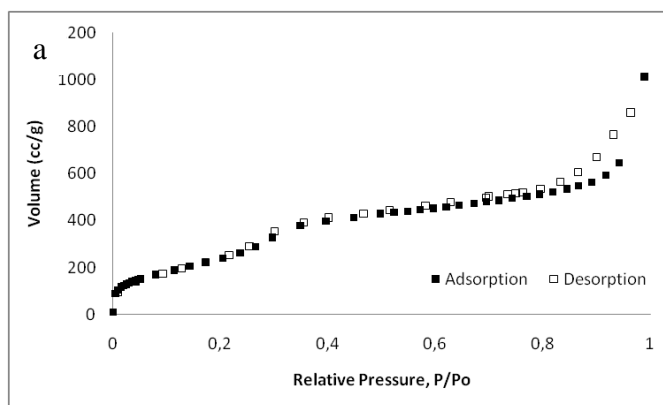


**Figure 4-12** N<sub>2</sub> sorption isotherms direct synthesized Cu-MCM-41 (120/30) samples  
 a) Si/Cu:25 b) Si/Cu:50 c) Si/Cu:75 d) Si/Cu:100

**Table 4-2** Physical and structural properties of Cu-MCM-41 type catalytic materials synthesized by microwave assisted direct synthesis method

Sample ID (Power/Time) (Watt/Min.)	Si/Metal (mole ratio) EDS	BET Surface Area (m <sup>2</sup> /g)	BJH Des. Pore Volume (cm <sup>3</sup> /g)	BJH Des. Pore Diameter (nm)	d <sub>100</sub> (nm)	Lattice Parameter “a” (nm)	Pore Wall Thickness “δ” (nm)
Cu-MCM-41 (80/30) DS 25	22	649	0.72	3.49	3.68	4.25	0.93
Cu-MCM-41 (80/60) DS 25	24	721	1.06	3.50	3.68	4.24	0.92
Cu-MCM-41 (120/30) DS 25	21	941	1.00	3.07	3.74	4.32	1.40
Cu-MCM-41 (120/30) DS 50	44	1067	1.14	3.46	3.53	4.08	0.79
Cu-MCM-41 (120/30) DS 75	63	1010	0.61	3.46	3.55	4.10	0.81
Cu-MCM-41 (120/30) DS 100	81	1368	0.79	3.49	3.53	4.07	0.75

The metal content in the samples were determined by EDS with a Si/Cu mol ratio in the range of 21-81. The Si/Cu mol ratios were in good agreement with the initial values.

Some examples to show the morphology of Cu-MCM-41 samples prepared at 120 Watt in 30 minutes were given in Figure 4-13.

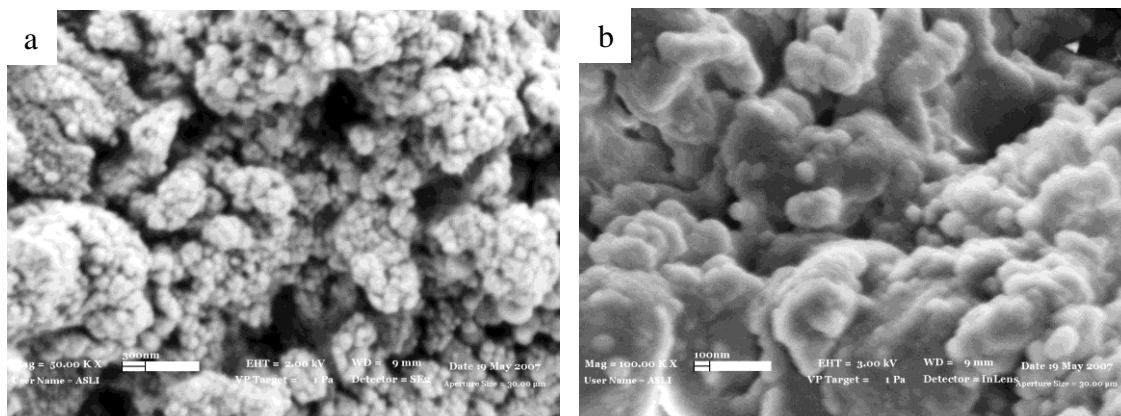


**Figure 4-13** SEM images of Cu-MCM-41 (120/30) a) Si/Cu:25 b) Si/Cu:75

TEM analysis of the highest metal incorporated sample (Si/Cu: 25) revealed that the catalyst particles were distributed into the structure with particle sizes less than 100 nm (Figure 4-14).

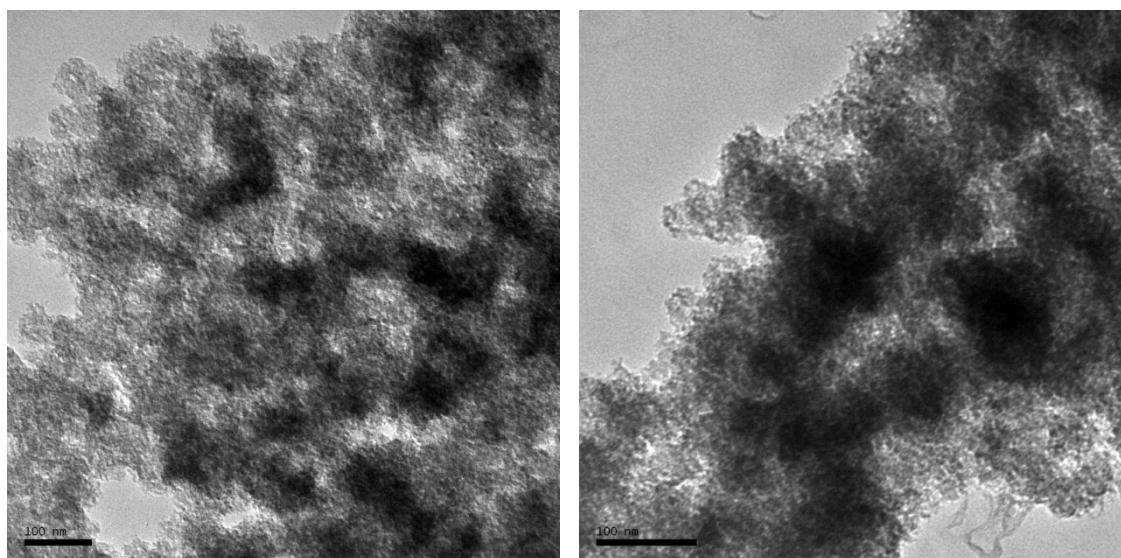


**Figure 4-14** TEM of Cu-MCM-41-DS-25 (120/30)

#### 4.2.1.2 Impregnation Results

The XRD patterns of the samples prepared by impregnation technique were given in Figure 4-15. Well defined XRD patterns with 3 distinct peaks were observed for all samples. The peaks corresponding to  $d_{100}$  shift to lower angles as metal impregnation increased except Si/Cu: 50 sample.  $2\theta$  values of the sharp peak were observed at 2.190, 2.326, 2.568 and 2.470 as the Si/Cu mol ratio increased from 25 to 100 respectively.

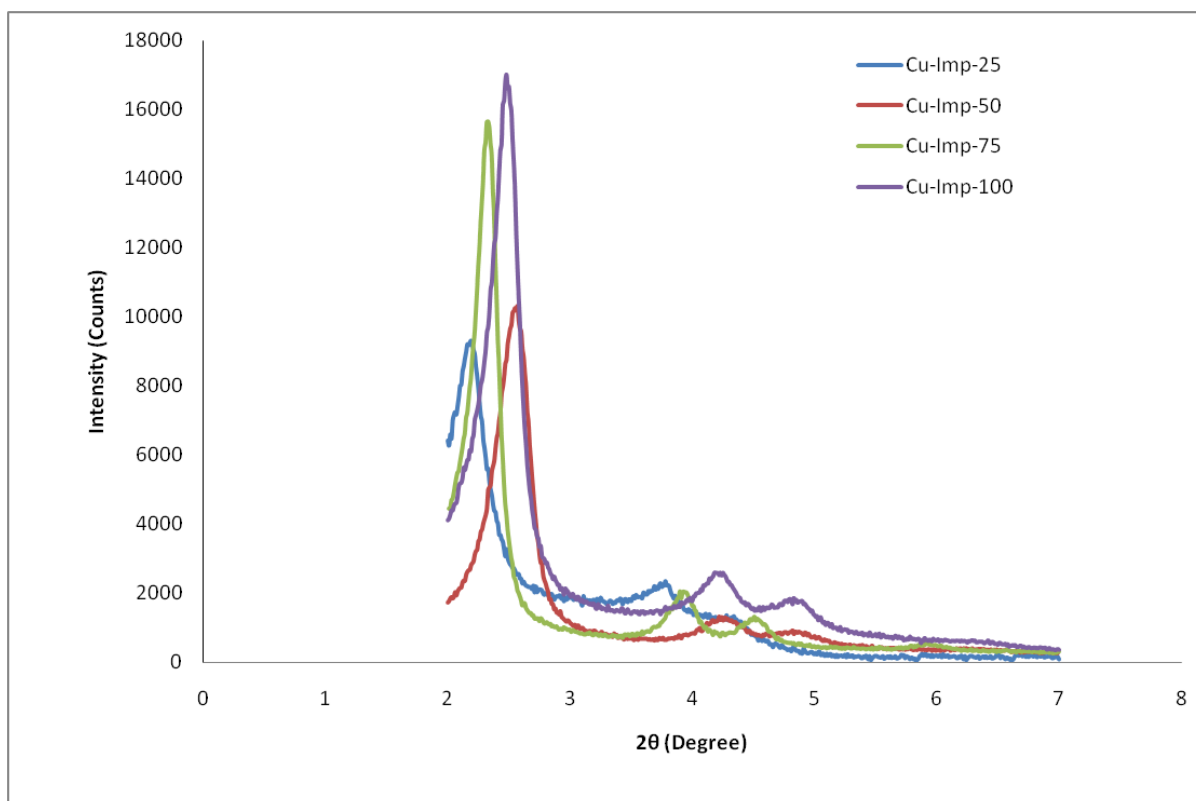


**Figure 4-15** XRD patterns of Cu-MCM-41(120/30) with different Si/Cu mol ratios prepared by microwave assisted impregnation synthesis

No peaks were observed in the high angle XRDs of the Cu impregnated mesoporous sieves which indicated the absence of large crystalline metal or metal oxide particles on the silica surface.

All the samples prepared by impregnation method had Type IV isotherms indicating the mesoporous structure. Capillary condensation of nitrogen was observed at relative pressures between 0.3 and 0.4 (Figure 4-16).

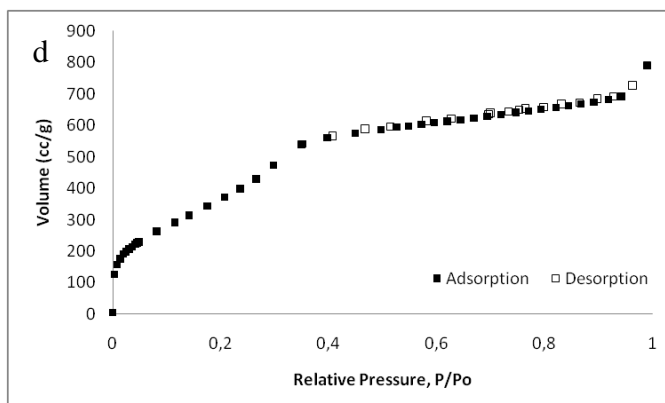
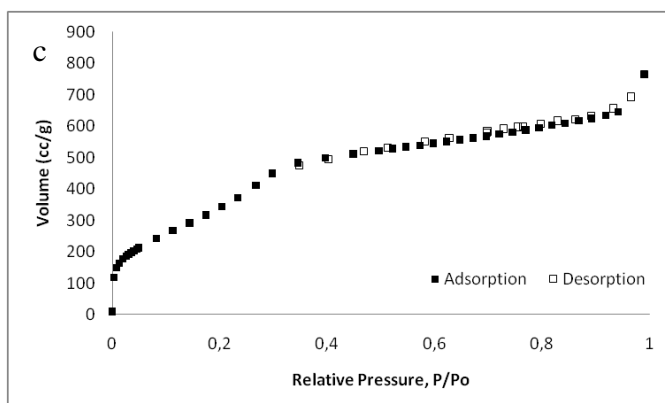
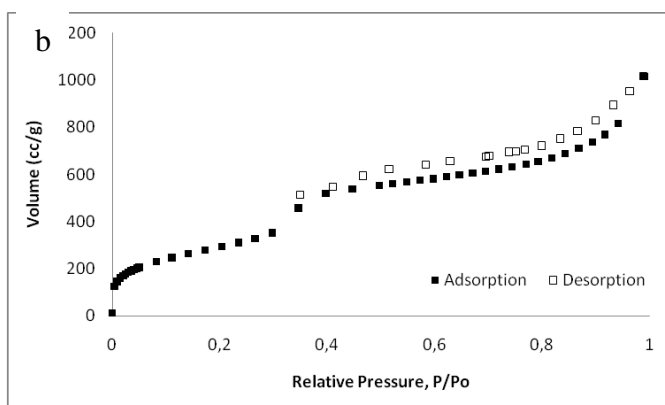
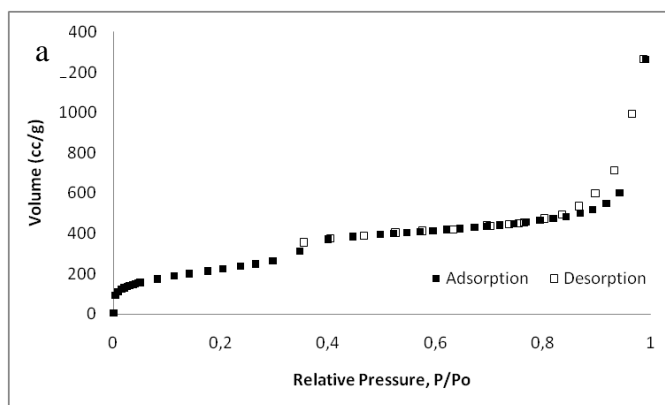


**Figure 4-16** N<sub>2</sub> sorption isotherms of impregnated Cu-MCM-41 (120/30) samples  
 a) Si/Cu:25 b) Si/Cu:50 c) Si/Cu:75 d) Si/Cu:100

The surface area increased from 837 to 1481 m<sup>2</sup>/g as the Si/Cu mol ratio increased from 25 to 100. The pore diameter decreased and pore wall thickness values of the samples increased as the amount of metal impregnated to the structure increased which was related to the metal incorporation. However pore volume of the samples decreased from 1.59 cm<sup>3</sup>/g to 0.46 as the initial Cu amount decreased (Table 4-3). This might occur because as the amount of metal increased, pore size distribution of the samples became wider with some pores even close to 10 nm due to high metal loading. Once the metal content decreased, the pore size distribution became narrower and pore volume of these samples decreased.

**Table 4-3** Physical and structural properties of Cu-MCM-41 type catalytic materials synthesized by microwave assisted impregnation method

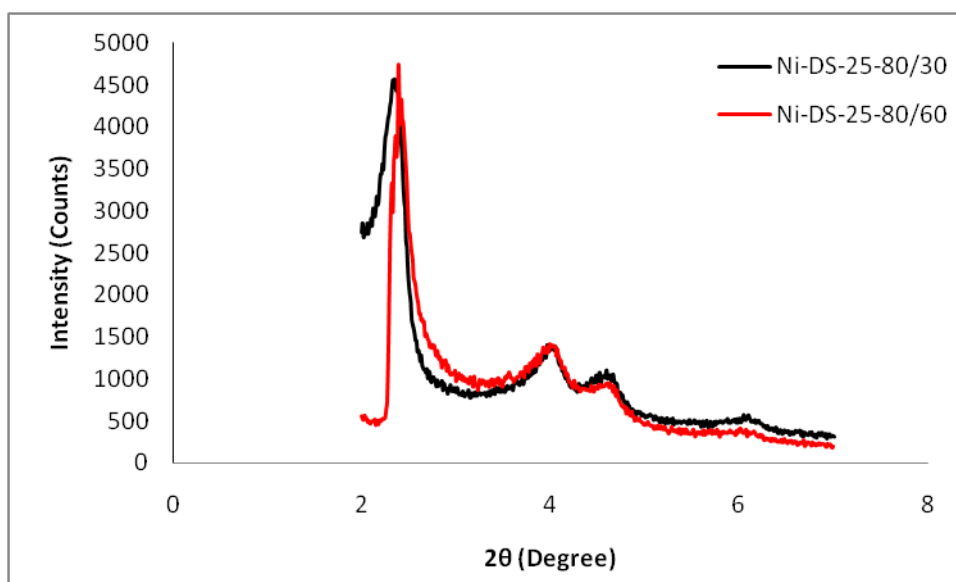
Sample ID (Power/Time) (Watt/Min.)	Si/Metal (mole ratio) EDS	BET Surface Area (m <sup>2</sup> /g)	BJH Des. Pore Volume (cm <sup>3</sup> /g)	BJH Des. Pore Diameter (nm)	d <sub>100</sub> (nm)	Lattice Parameter “a” (nm)	Pore Wall Thickness “δ” (nm)
Cu-MCM-41 (120/30) Imp. 25	9	837	1.59	3.08	4.04	4.66	1.74
Cu-MCM-41 (120/30) Imp. 50	15	1108	0.95	3.29	3.80	4.38	1.26
Cu-MCM-41 (120/30) Imp. 75	22	1399	0.55	3.49	3.44	3.97	0.65
Cu-MCM-41 (120/30) Imp. 100	33	1481	0.46	3.52	3.65	4.21	0.87

The metal content in the samples were determined by EDS with a Si/Cu mol ratio in the range of 9-33. The Si/Cu mol ratios showed that higher amount of metal were incorporated into the structure than that of direct synthesized samples.

## 4.2.2 Ni-MCM-41

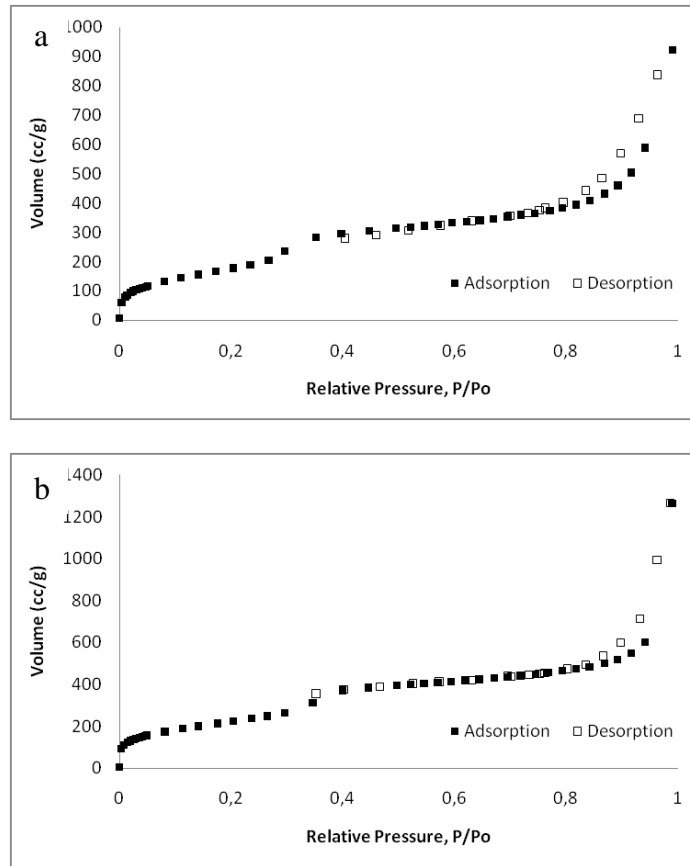
### 4.2.2.1 Microwave Assisted Direct Synthesis Results

Long-range and ordered Ni-MCM-41 mesoporous molecular sieves with different amount of nickel were successfully synthesized by microwave assisted direct synthesis using nickel nitrate hexahydrate as the nickel source. In order to see the effect of microwave power on the incorporation of metal into the structure, additional experiments were performed at 80 Watt for two different durations for the highest amount of metal content. The XRD patterns of the Ni incorporated MCM-41 sample with the highest metal content prepared at 80 Watt in 30 minutes and 80 Watt in 60 minutes were given in Figure 4-17.



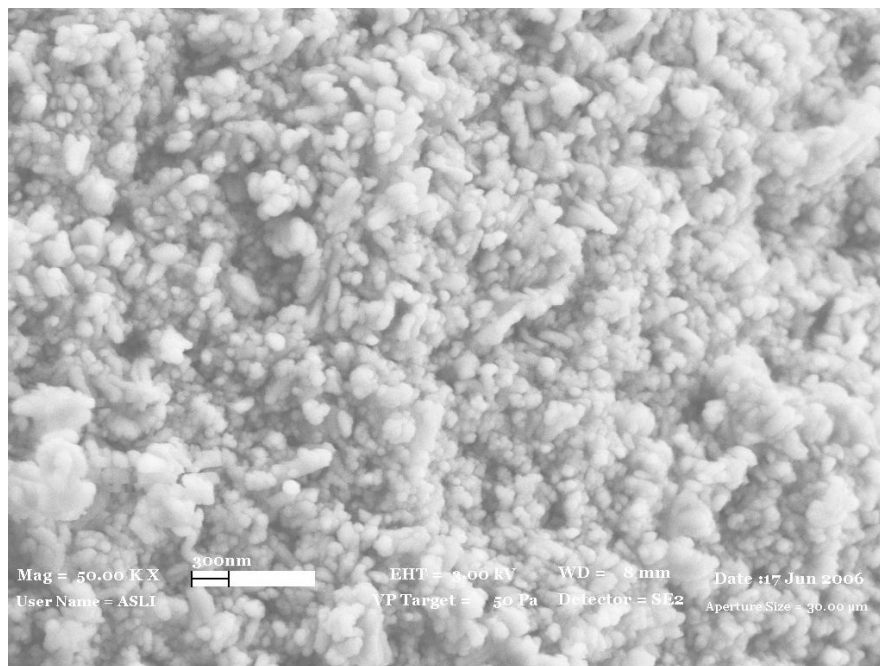
**Figure 4-17** XRD patterns of Ni-MCM-41-DS-25 (80/30 and 80/60)

From the XRD analysis, it was easily observed that the duration had no significant effect on the formation of ordered structures at 80 Watt. There was a slight increase in the surface area from 738 to 873 m<sup>2</sup>/g when the time increased from 30 to 60 minutes (Table 4-4). From the N<sub>2</sub> sorption isotherms, no sharp inflection was observed around P/P<sub>0</sub> = 0.25–0.35 (Figure 4-18).



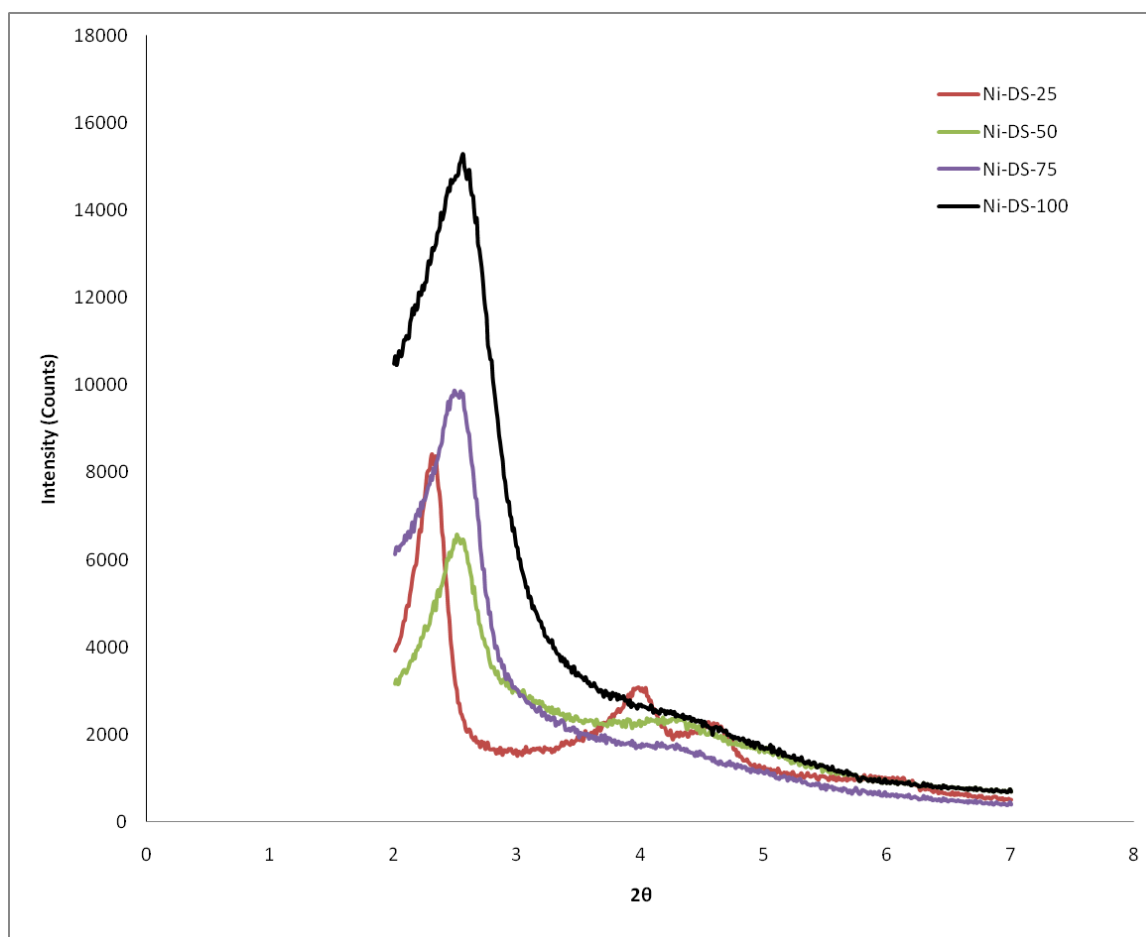
**Figure 4-18** N<sub>2</sub> sorption isotherms of Ni-MCM-41-DS-25 a) 80/30 b) 80/60

The morphology of Ni-MCM-41 prepared at 80 Watt in 30 minutes was given in Figure 4-19.



**Figure 4-19** SEM image of Ni-MCM-41-DS-25 (80/30)

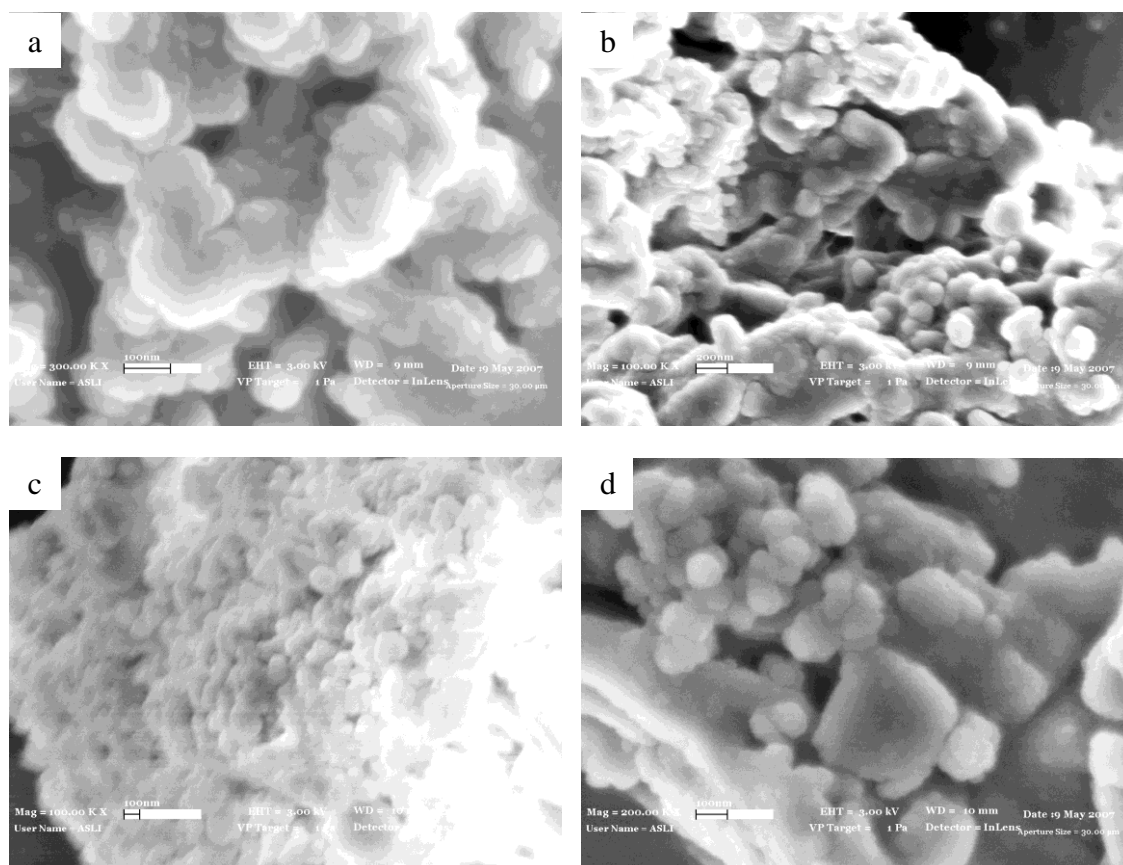
For the case of Ni incorporated MCM-41 mesoporous molecular sieves obtained at 120 W at 30 minutes, a strong low angle diffraction pattern was observed at around  $2.315^\circ$  for  $2\theta$  and this was assigned to a (100) reflection from a hexagonal arrangement of mesopores for Si/Ni ol ratio of 25. Propagation of the metal loading leads to a gradual reduction of intensity and a shift towards the lower angles of the peak in the (100) (Figure 4-20). The aforementioned reduction of intensity was in prospect, as introducing metal based nanoparticles into the pores causes an increase in the phase cancelation, and to this respect, reduced scattering intensities for the Bragg reflections. No peaks were observed in the high angle XRDs of the Ni incorporated mesoporous sieves which indicated the absence of large crystalline metal or metal oxide particles on the silica surface.



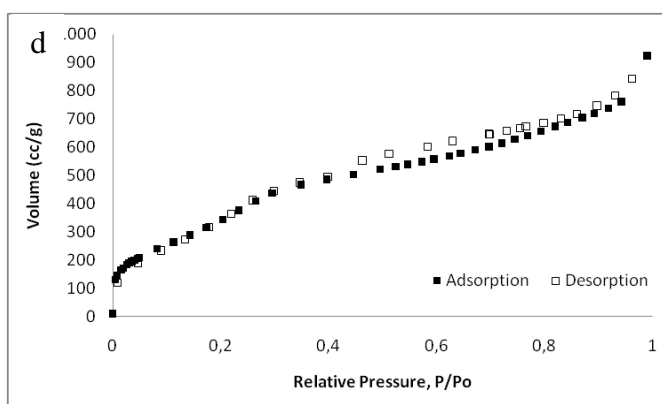
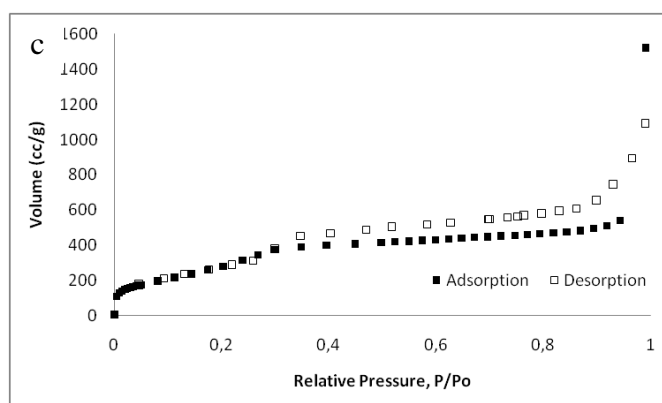
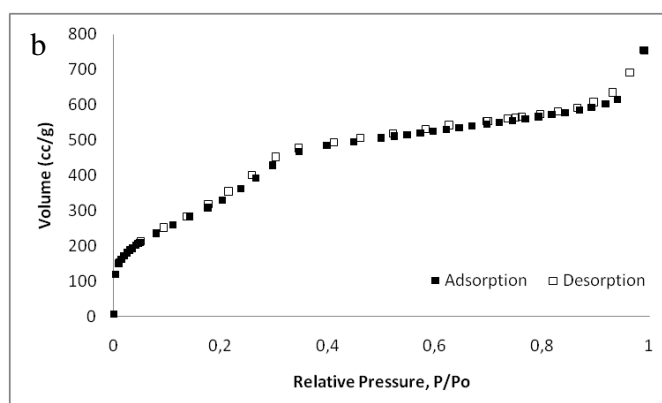
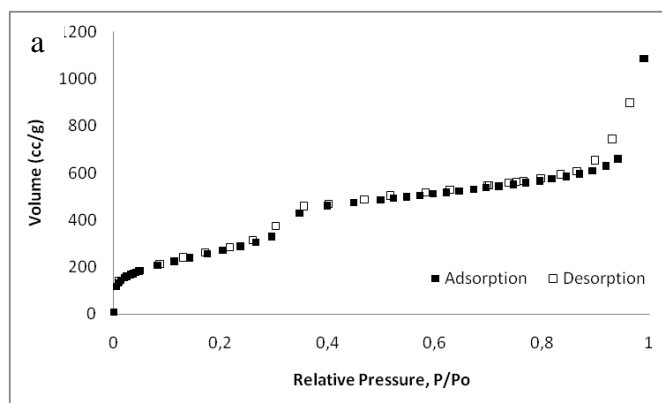
**Figure 4-20** XRD patterns of Ni-MCM-41 (120/30) with different Si/Ni mol ratios prepared by microwave assisted direct synthesis

Figure 4-21 showed the N<sub>2</sub> adsorption-desorption isotherms for the nickel incorporated mesoporous materials. All samples had typical type IV isotherms as expected for mesoporous materials. At P/P<sub>0</sub> 0.3, a well defined step occurs, representing the spontaneous filling of the mesopores due to capillary condensation. The shape of the isotherms becomes less inclined with increasing the Ni content. Nitrogen physisorption data showed a decrease in pore volume, average pore diameter and surface area values with increasing nickel content in accordance with expectations as the amount of metal species increased within the pores. In Table 4-4, the results corresponding to the discussion were given in detail. The sample with highest metal content had the lowest surface area value of 1047 m<sup>2</sup>/g and lowest pore diameter of 3.07 nm. It also had the highest pore wall thickness value of 1.48 nm which indicated the incorporation of metal particles on to the walls of silica material.

SEM images of Ni incorporated samples prepared at 120 Watt in 30 minutes with different Si/Ni mol ratios were given in Figure 4-22.



**Figure 4-21** SEM images of Ni-MCM-41 (120/30) a) Si/Ni: 25 b) Si/Ni:50 c) Si/Ni:75 d) Si/Ni:100 by inlens detector



**Figure 4-22** N<sub>2</sub> sorption isotherms of direct synthesized Ni-MCM-41 (120/30) samples  
 a) Si/Ni:25 b) Si/Ni:50 c) Si/Ni:75 d) Si/Ni:100

**Table 4-4** Physical and structural properties of Ni-MCM-41 type catalytic materials synthesized by microwave assisted direct synthesis method

Sample ID (Power/Time) (Watt/Min.)	Si/Metal (mole ratio) EDS	BET Surface Area (m <sup>2</sup> /g)	BJH Des. Pore Volume (cm <sup>3</sup> /g)	BJH Des. Pore Diameter (nm)	d <sub>100</sub> (nm)	Lattice Parameter “a” (nm)	Pore Wall Thickness “δ” (nm)
Ni-MCM-41 (80/30) DS 25	19	738	1.16	3.47	3.86	4.46	1.17
Ni-MCM-41 (80/60) DS 25	21	873	1.59	3.08	3.67	4.24	1.32
Ni-MCM-41 (120/30) DS 25	18	1047	1.13	3.07	3.81	4.40	1.48
Ni-MCM-41 (120/30) DS 50	33	1393	1.93	3.49	3.49	4.03	0.71
Ni-MCM-41 (120/30) DS 75	55	1238	0.90	3.51	3.52	4.06	0.73
Ni-MCM-41 (120/30) DS 100	76	1431	0.90	3.47	3.46	3.99	0.70

The metal content in the samples were determined by EDS with a Si/Ni mol ratio in the range of 18-76. The Si/Ni mol ratios were in good agreement with the initial values.

TEM analysis of the sample with highest metal content (Si/Ni: 25) confirmed the production of nano scale metal particles on the mesoporous host. In Figure 4-23 nanoparticles with  $100 < \text{nm}$  size could be clearly observed.

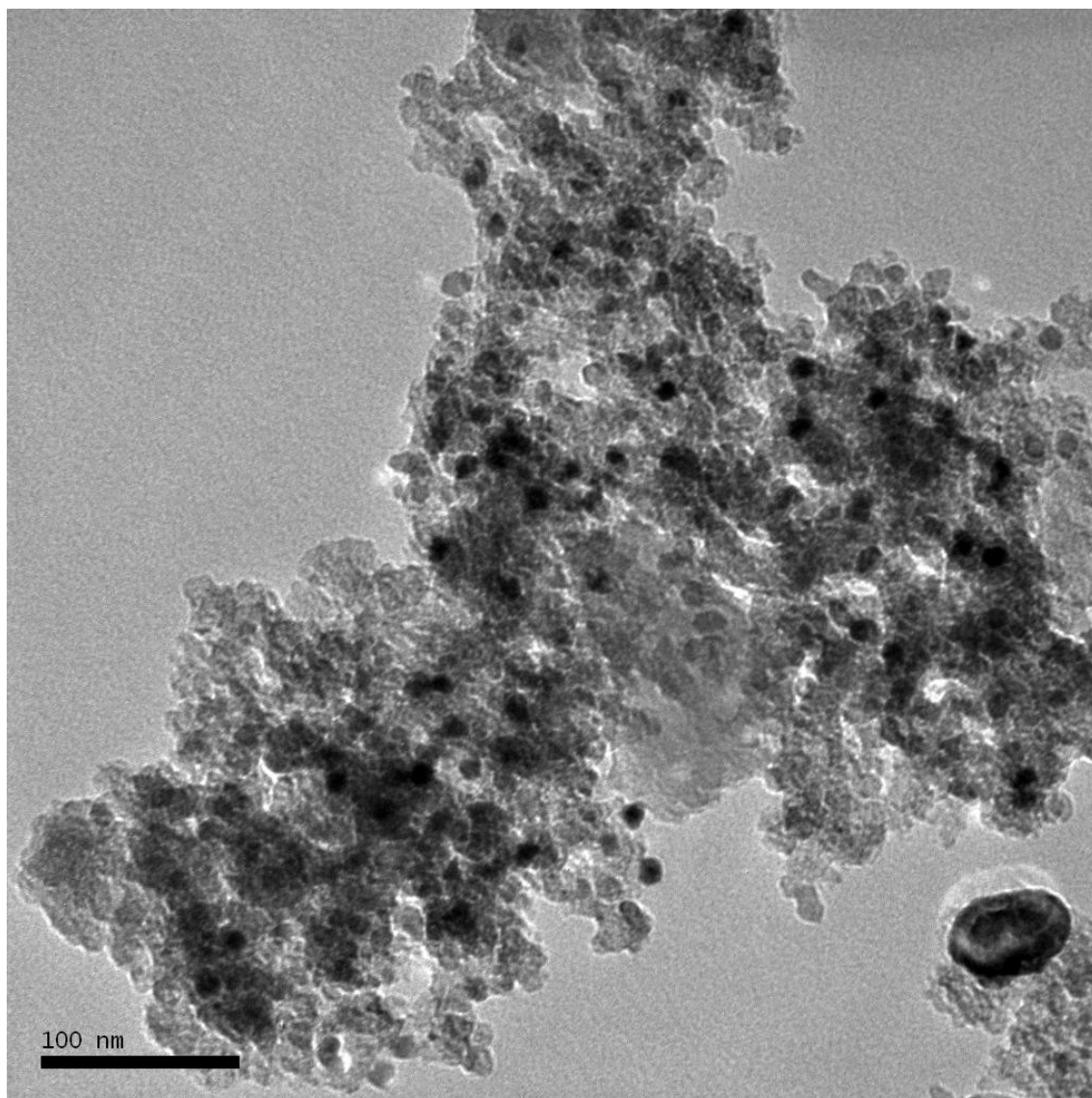


**Figure 4-23** TEM of Ni-MCM-41-DS-25 (120/30)

#### 4.2.2.2 Impregnation Results

In the XRD patterns of Ni-MCM-41 materials prepared by microwave assisted impregnation synthesis, the characteristic sharp Bragg peak corresponding to  $d_{100}$  and two to three other reflections were detected (Figure 4-24). For instance, the major peak and the reflections were observed at  $2\theta$  values of 2.257, 3.868, 4.456 and 5.879 with the Ni-MCM-41 sample with highest metal content (Si/Ni:25). The  $d_{100}$  spacings and corresponding values of lattice parameter “a” were reported in Table 4-5. As the amount of metal content decreased, the peaks shifted to higher angles as  $2\theta$  values of 2.312, 2.468 and 2.540 for Si/Ni mol ratio of 50, 75 and 100 respectively.

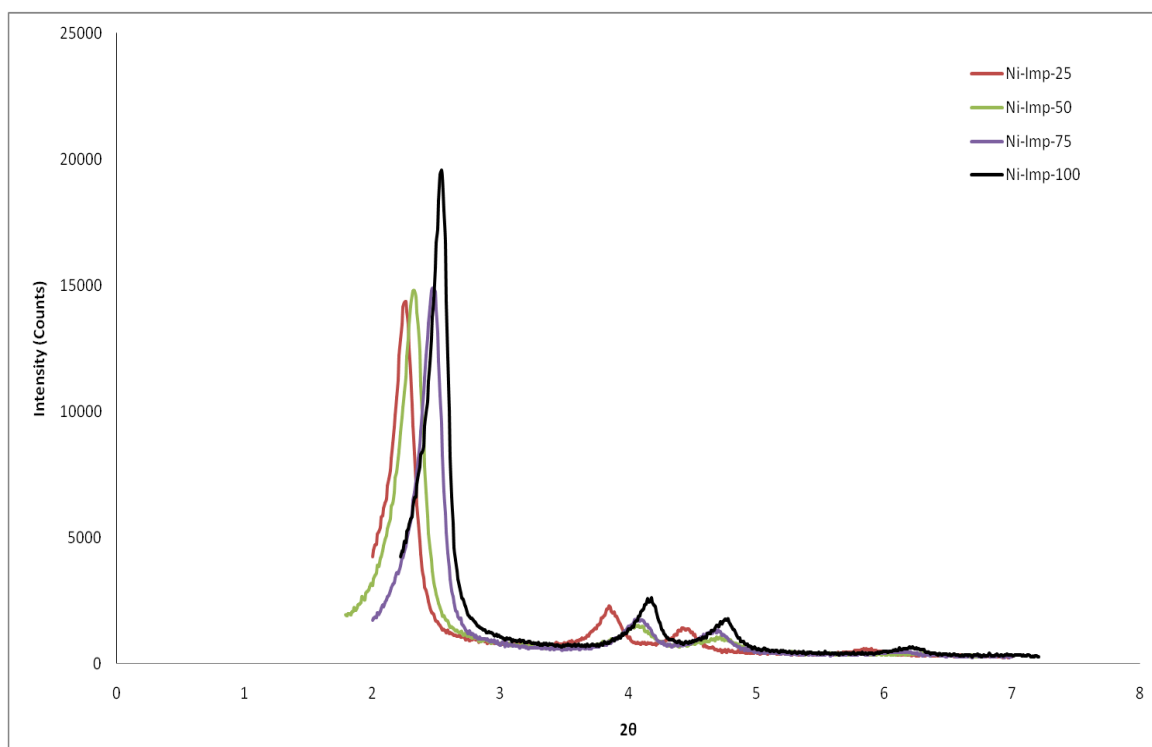


**Figure 4-24** XRD patterns of Ni-MCM-41(120/30) with different Si/Ni mol ratios prepared by microwave assisted impregnation synthesis

The samples prepared by impregnation showed a type IV isotherm, which are characteristic of mesoporous materials. The nitrogen adsorption-desorption isotherms of samples prepared by impregnation technique were given in Figure 4-25.

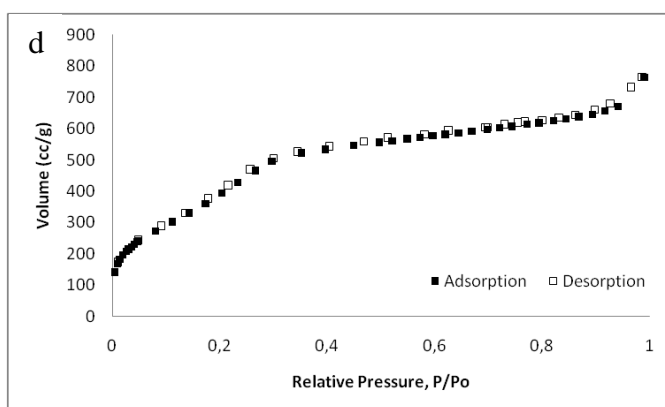
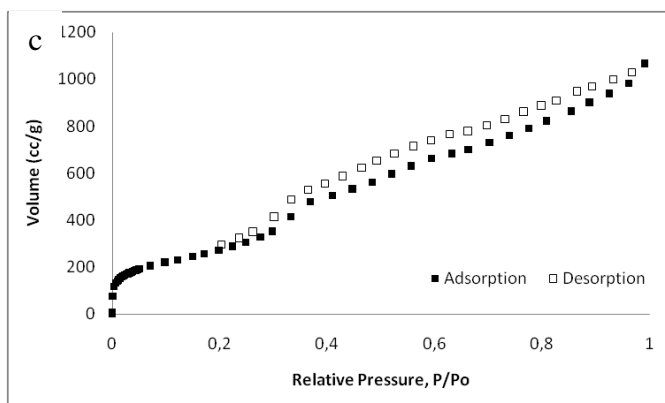
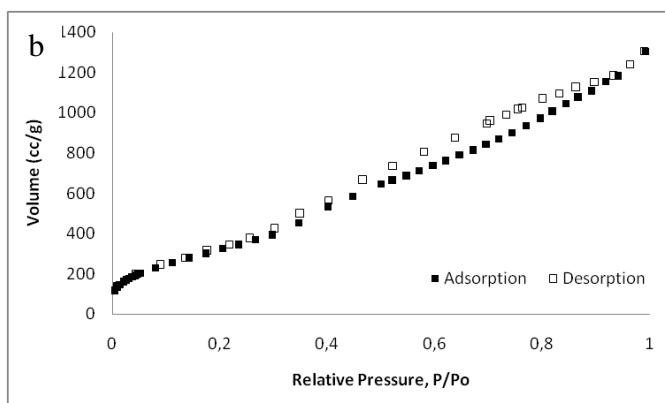
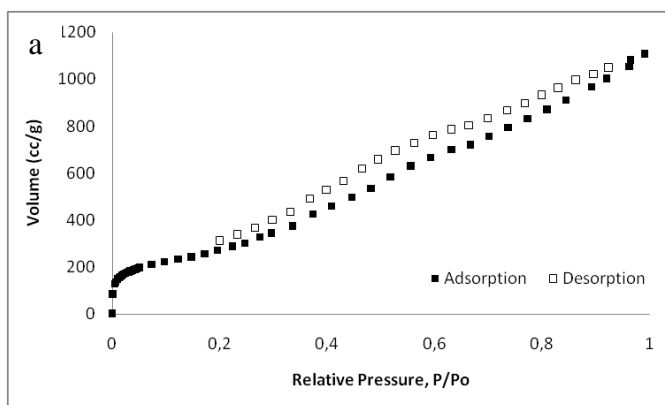


**Figure 4-25** N<sub>2</sub> sorption isotherms of impregnated Ni-MCM-41 (120/30) samples  
 a) Si/Ni:25 b) Si/Ni:50 c) Si/Ni:75 d) Si/Ni:100

The specific surface area values of Ni impregnated materials were found to be as high as 1485 m<sup>2</sup>/g. The pore diameters were close to each other showing the reproducibility of synthesizing materials by using the same surfactant. The lattice parameters decreased from 4.52 nm to 4.17 nm as well as the pore wall thickness values decreased from 1.11 nm to 0.84 nm as the metal content decreased.

**Table 4-5** Physical and structural properties of Ni-MCM-41 type catalytic materials synthesized by microwave assisted impregnation method

Sample ID (Power/Time) (Watt/Min.)	Si/Metal (mole ratio) EDS	BET Surface Area (m <sup>2</sup> /g)	BJH Des. Pore Volume (cm <sup>3</sup> /g)	BJH Des. Pore Diameter (nm)	d <sub>100</sub> (nm)	Lattice Parameter “a” (nm)	Pore Wall Thickness “δ” (nm)
Ni-MCM-41 (120/30) Imp. 25	11	1085	1.46	3.58	3.91	4.52	1.11
Ni-MCM-41 (120/30) Imp. 50	19	1271	1.87	3.49	3.77	4.35	1.04
Ni-MCM-41 (120/30) Imp. 75	29	1060	1.23	3.58	3.66	4.23	0.83
Ni-MCM-41 (120/30) Imp. 100	42	1485	0.49	3.50	3.61	4.17	0.84

The metal content in the samples were determined by EDS with a Si/Ni mol ratio in the range of 11-42. The Si/Cu mol ratios showed that higher amount of metal were incorporated into the structure than that of direct synthesized samples

## 4.2.3 Co-MCM-41

### 4.2.3.1 Microwave Assisted Direct Synthesis Results

The XRD patterns of the Co-MCM-41 materials clearly showed the characteristic Bragg peaks of MCM-41 structure corresponding to (100) and the three reflections. It is observed that, when the metal content of the sample increased (Si/Co ratio decreased), the intensity of the XRD graphs decreased as shown in Figure 4-26. For instance, for Co-MCM-41 material synthesized by microwave assisted direct synthesis with highest metal content (Si/Co:25), Bragg peak corresponding to  $d_{(100)}$  and three reflections were observed at  $2\theta$  values of 2.37, 4.08, 4.66, and 6.20 respectively. For the case of lowest metal content (Si/Co:100), corresponding  $2\theta$  values were 2.46, 4.20, 4.72, and 6.22 respectively. It is observed that as the incorporation of the metal content into MCM-41 structure increased, the interplanar spacing values ( $d_{(100)}$ ) increased (Table 4-6).

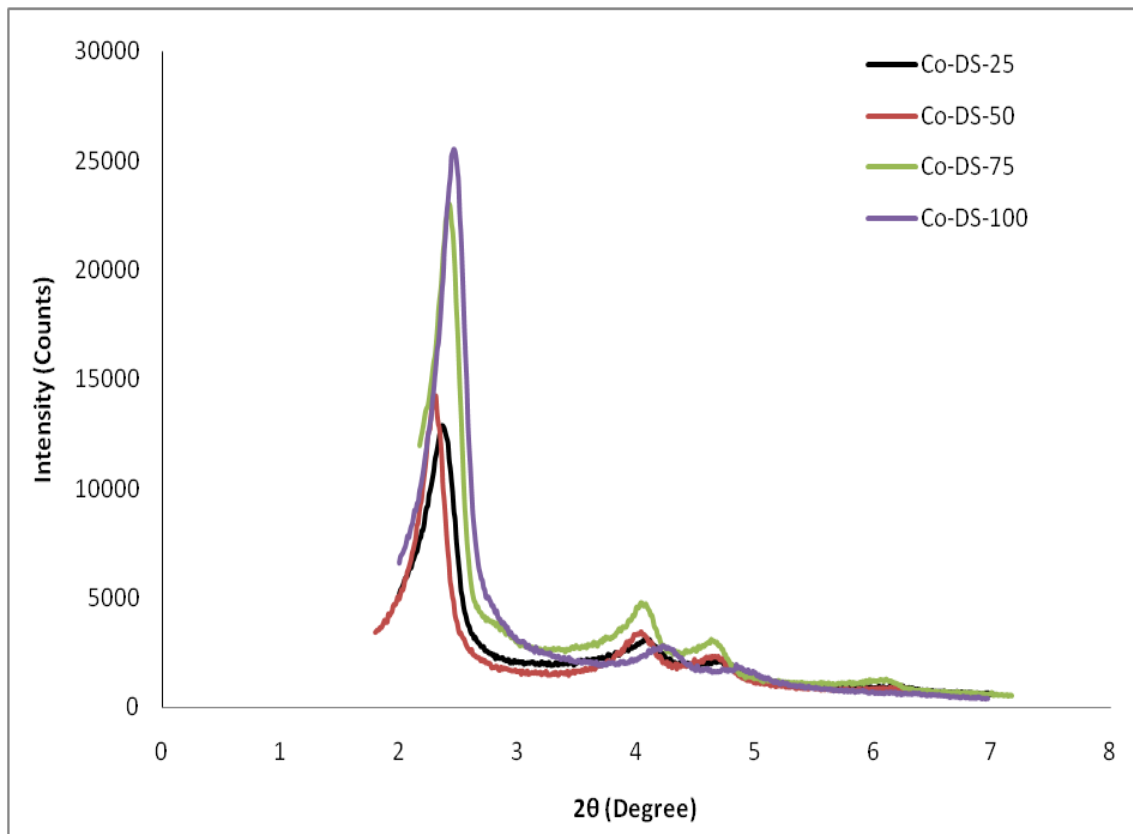


**Figure 4-26** XRD patterns of Co-MCM-41 (120/30) with different Si/Co mol ratios prepared by microwave assisted direct synthesis

The N<sub>2</sub> adsorption isotherms of all Co-MCM-41 type mesoporous catalytic materials prepared by microwave assisted direct synthesis showed Type IV isotherm with a sharp inflection around  $P/P_0 = 0.25-0.35$ , which is the characteristic of MCM-41 type ordered mesoporous materials (Figure 4-27). The specific surface area, pore volume and the average pore diameter of these samples as calculated from the N<sub>2</sub> adsorption isotherms are presented in Table 4-6.

The highest metal loaded Co-MCM-41 synthesized by direct synthesis technique showed a broad pore size distribution as given in Figure 4-28.

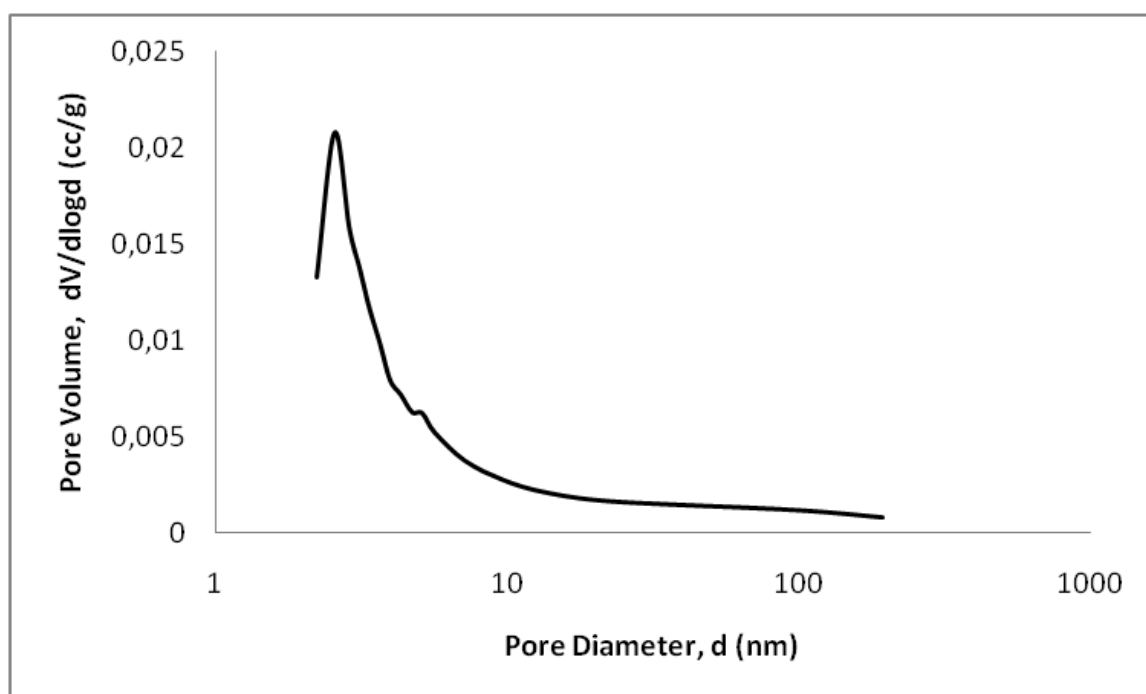


**Figure 4-27** Pore size distribution of Co-MCM-41-DS-25 (120/30)

The materials prepared by microwave assisted direct synthesis method had surface area values higher than 1000 m<sup>2</sup>/g evaluated from BET theory. Metal incorporation into the mesoporous structure with this technique increased the lattice parameter of the samples as Si/Co ratio decreased. Pore wall thickness evaluated from equation (2.12) was 2.06 nm for the highest metal incorporation (Co-DS-25). For other samples, pore wall thickness values were around 1 nm.

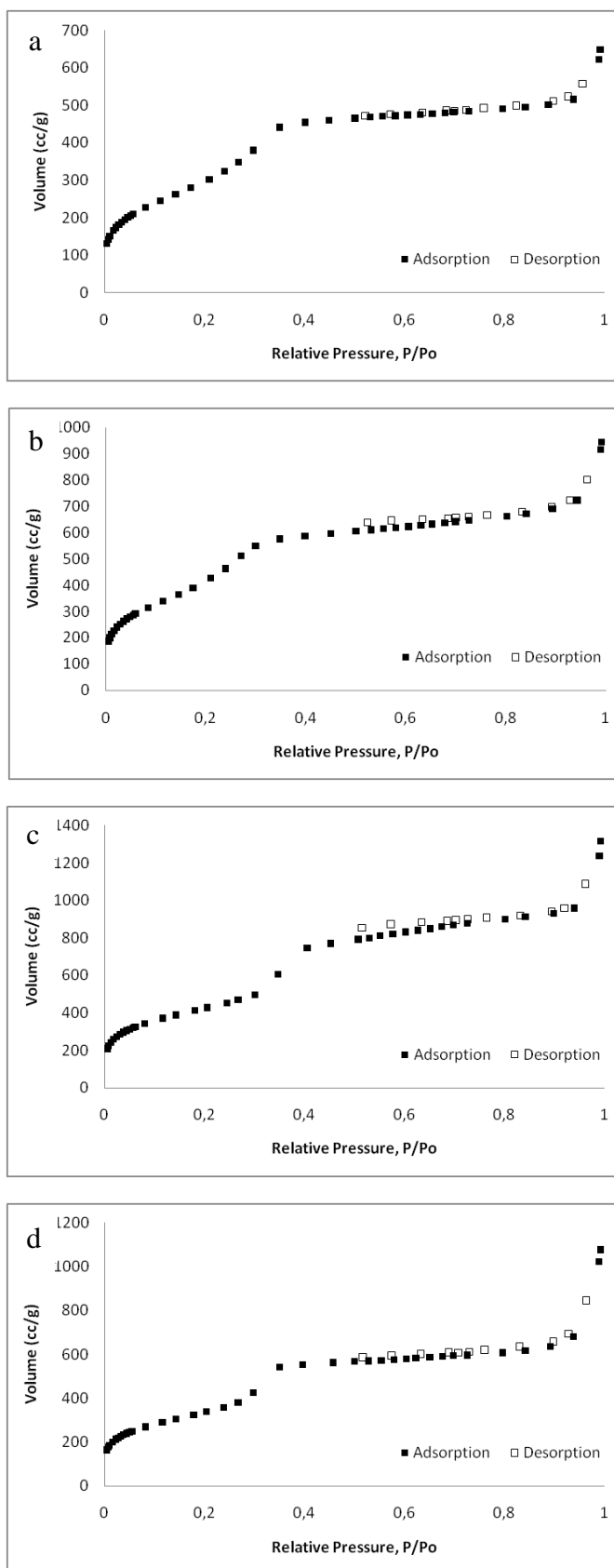


**Figure 4-28** N<sub>2</sub> sorption isotherms of direct synthesized Co-MCM-41 (120/30) samples  
a) Si/Co:25 b) Si/Co:50 c) Si/Co:75 d) Si/Co:100

**Table 4-6** Physical and structural properties of Co-MCM-41 type catalytic materials synthesized by microwave assisted direct synthesis method

Sample ID (Power/Time) (Watt/Min.)	Si/Metal (mole ratio) EDS	BET Surface Area (m <sup>2</sup> /g)	BJH Des. Pore Volume (cm <sup>3</sup> /g)	BJH Des. Pore Diameter (nm)	d <sub>100</sub> (nm)	Lattice Parameter “a” (nm)	Pore Wall Thickness “δ” (nm)
Co-MCM-41 (120/30) DS 25	19	1151	0.30	3.41	3.72	4.30	1.06
Co-MCM-41 (120/30) DS 50	36	1499	0.63	3.40	3.77	4.35	1.12
Co-MCM-41 (120/30) DS 75	56	1546	1.06	3.44	3.69	4.26	1.00
Co-MCM-41 (120/30) DS 100	73	1305	0.92	3.04	3.66	4.23	1.34

The metal content in the samples were determined by EDS with a Si/Co mol ratio in the range of 19-73. The Si/Co mol ratios were in good agreement with the initial values.

Incorporation of high cobalt content into the mesoporous structure lead to a decrease in surface area and pore volume values due to the blockage of metals inside the channels. In the N<sub>2</sub> sorption analysis of Co-DS-25 material (Figure 4-27), the hysteresis between adsorption and desorption isotherms was smaller than other samples. Also pore diameter of Co-DS-25 was 3.41 nm, while other samples with lower metal content had pore diameter value between 3-3.4 nm.

The morphology of the Co incorporated MCM-41 materials synthesized by microwave assisted direct synthesis technique was given in Figure 4-29.

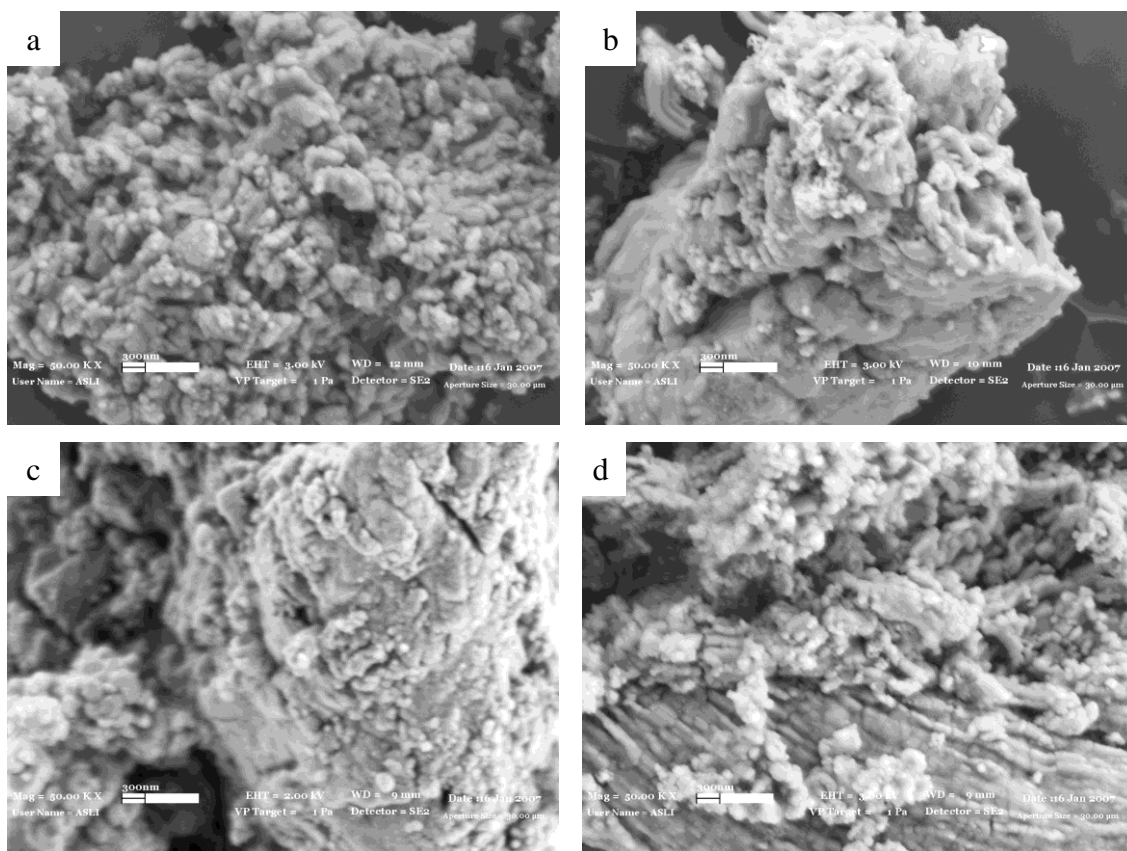


**Figure 4-29** SEM images of Co-MCM-41 (120/30) a) Si/Co: 25 b) Si/Co:50 c) Si/Co:75 d)Si/Co:100

No peaks were observed at high angle XRDs of the metal incorporated mesoporous materials which indicates the absence of large crystalline metal or metal oxide particles on the silica surface.

The lattice parameters of Co incorporated MCM-41 type mesoporous materials were greater than that of pure MCM-41. This was consisted with the Metal-O bonds being longer than that of Si-O bonds and gave an evidence of the metal incorporation into the framework.

It was also observed that the lattice parameters increased with the metal content which indicated that the metal content incorporated in the framework increased with increasing amount of metal salt added in the synthesis gel.

The morphology of the Co-MCM-41 catalysts were investigated by TEM at 100 nm and the metal particles were well distributed within the catalyst with an average pore size below 20 nm. The TEM picture of Co-MCM-41 with the highest metal content (Si/Fe 25) was given in Figure 4-30.

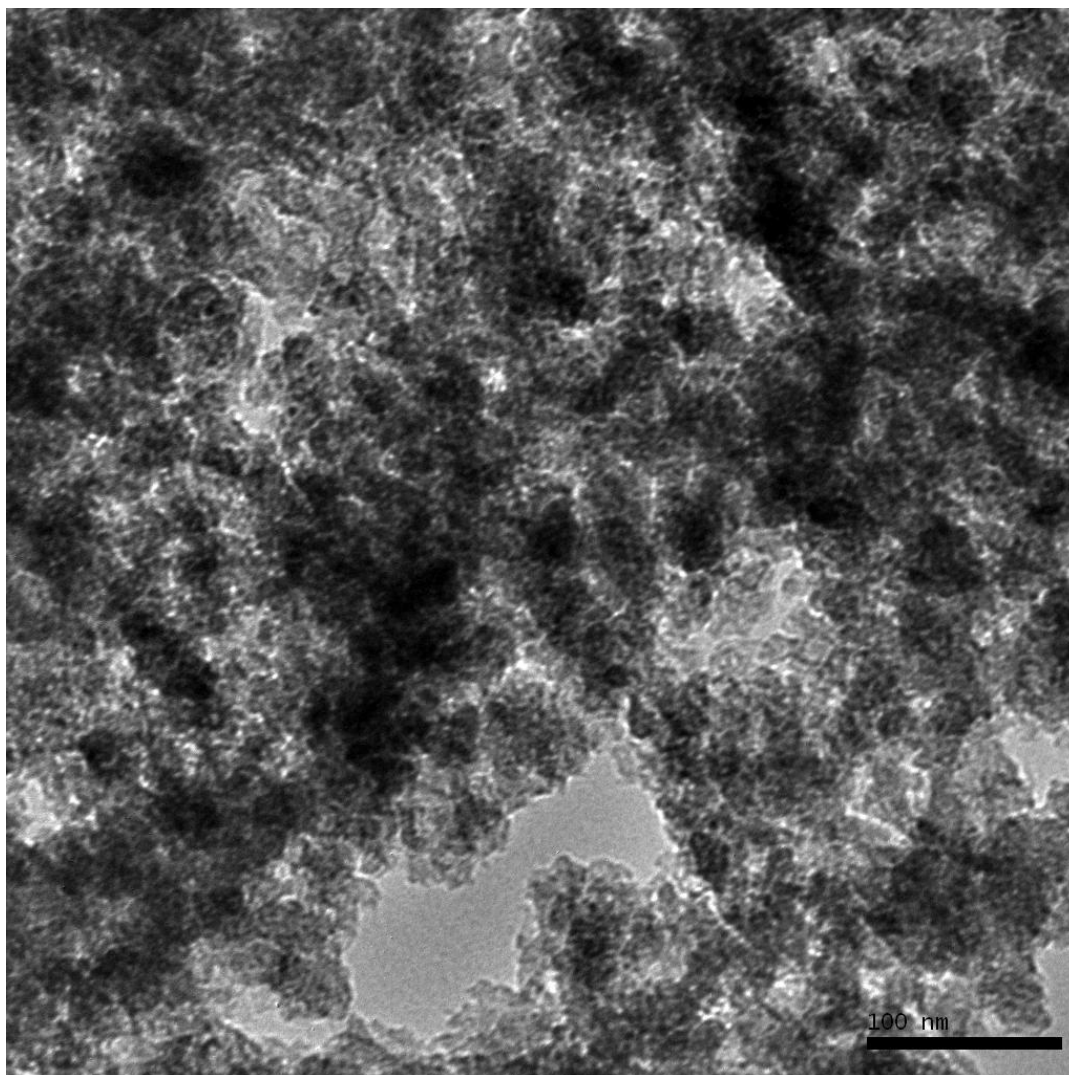


**Figure 4-30** TEM of Co-MCM-41-DS-25 (120/30)

### 4.2.3.2 Impregnation Results

Cobalt incorporated materials were also obtained from microwave assisted impregnation techniques with different initial Si/Co mole ratios as 25, 50, 75 and 100. The XRD patterns of the impregnated Co-MCM-41 materials clearly showed the characteristic Bragg peaks of MCM-41 structure corresponding to  $d_{(100)}$  and the three reflections for the case of low metal impregnated samples (Figure 4-31). For the case of Co-Imp-25, the highest metal content in the mesoporous structure, Bragg peak corresponding to  $d_{(100)}$  and one reflection were observed at  $2\theta$  values of 2.08, and 3.82 respectively. For the case of lowest metal content (Si/Co mol ratio 100, Imp-100), corresponding  $2\theta$  values were 2.37, 4.05, 4.59, and 6.12 respectively. The interplanar spacing values and lattice parameters increased as the amount of Co content impregnated into the structure decreased (Table 4-7).

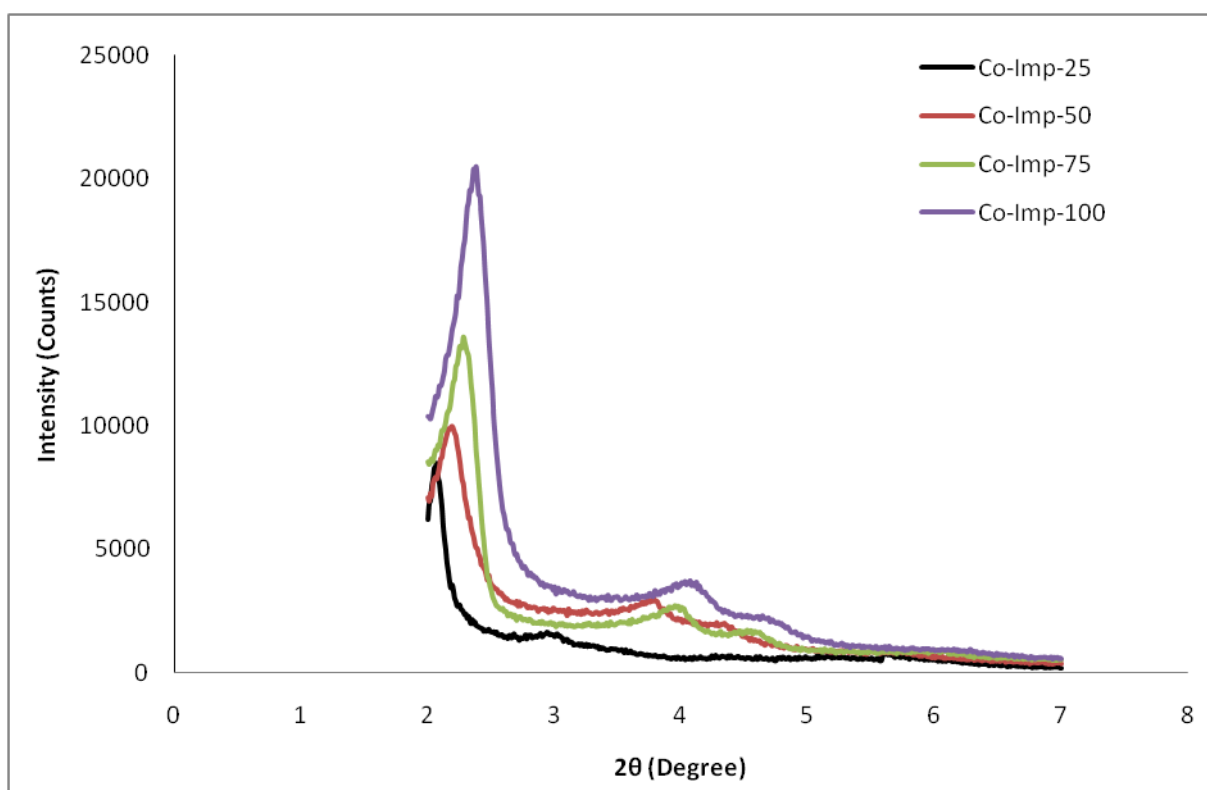


**Figure 4-31** XRD patterns of Co-MCM-41(120/30) with different Si/Co mol ratios prepared by microwave assisted impregnation synthesis

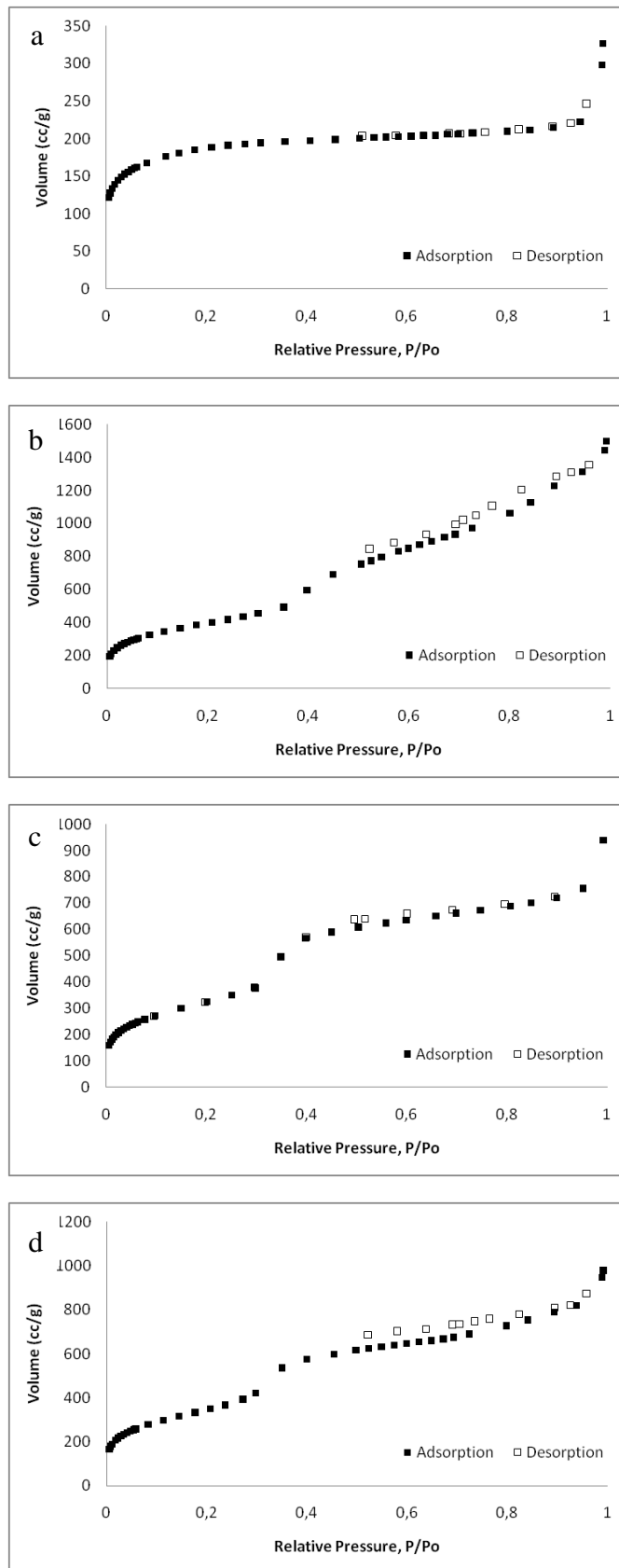


**Figure 4-32** N<sub>2</sub> sorption isotherms of impregnated Co-MCM-41 (120/30) samples  
a) Si/Co:25 b) Si/Co:50 c) Si/Co:75 d) Si/Co:100

**Table 4-7** Physical and structural properties of Co-MCM-41 type catalytic materials synthesized by microwave assisted impregnation method

Sample ID (Power/Time) (Watt/Min.)	Si/Metal (mole ratio) EDS	BET Surface Area (m <sup>2</sup> /g)	BJH Des. Pore Volume (cm <sup>3</sup> /g)	BJH Des. Pore Diameter (nm)	d <sub>100</sub> (nm)	Lattice Parameter “a” (nm)	Pore Wall Thickness “δ” (nm)
Co-MCM-41 (120/30) Imp. 25	14	656	0.22	3.10	4.09	4.72	1.78
Co-MCM-41 (120/30) Imp. 50	27	1420	2.25	3.05	4.04	4.66	1.77
Co-MCM-41 (120/30) Imp. 75	35	1182	0.72	3.40	3.88	4.48	1.25
Co-MCM-41 (120/30) Imp. 100	41	1307	0.80	3.43	3.72	4.30	1.04

The metal content in the samples were determined by EDS with a Si/Co mol ratio in the range of 24-41. The Si/Co mol ratios were higher than samples obtained from direct synthesis method.

## 4.2.4 Fe-MCM-41

### 4.2.4.1 Microwave Assisted Direct Synthesis Results

The XRD patterns of Fe incorporated calcined mesoporous catalysts prepared at 120 Watt for 30 minutes were given in Figure 4-33. As the amount of Fe incorporated into the structure increased, the main peak in the XRD patterns shifted to the lower angles which leads to higher lattice parameters as expected. It is observed that the intense peak at  $2.2 - 2.5^\circ$  ( $2\theta$ ) due to (100) plane confirmed the hexagonal meso-structure of the materials. The sharp Bragg peaks corresponding to  $d_{100}$  were observed at  $2\theta$  values of  $2.31, 2.25, 2.36,$  and  $2.51^\circ$  for Si/Fe mole ratios of 25, 50, 75 and 100 respectively.

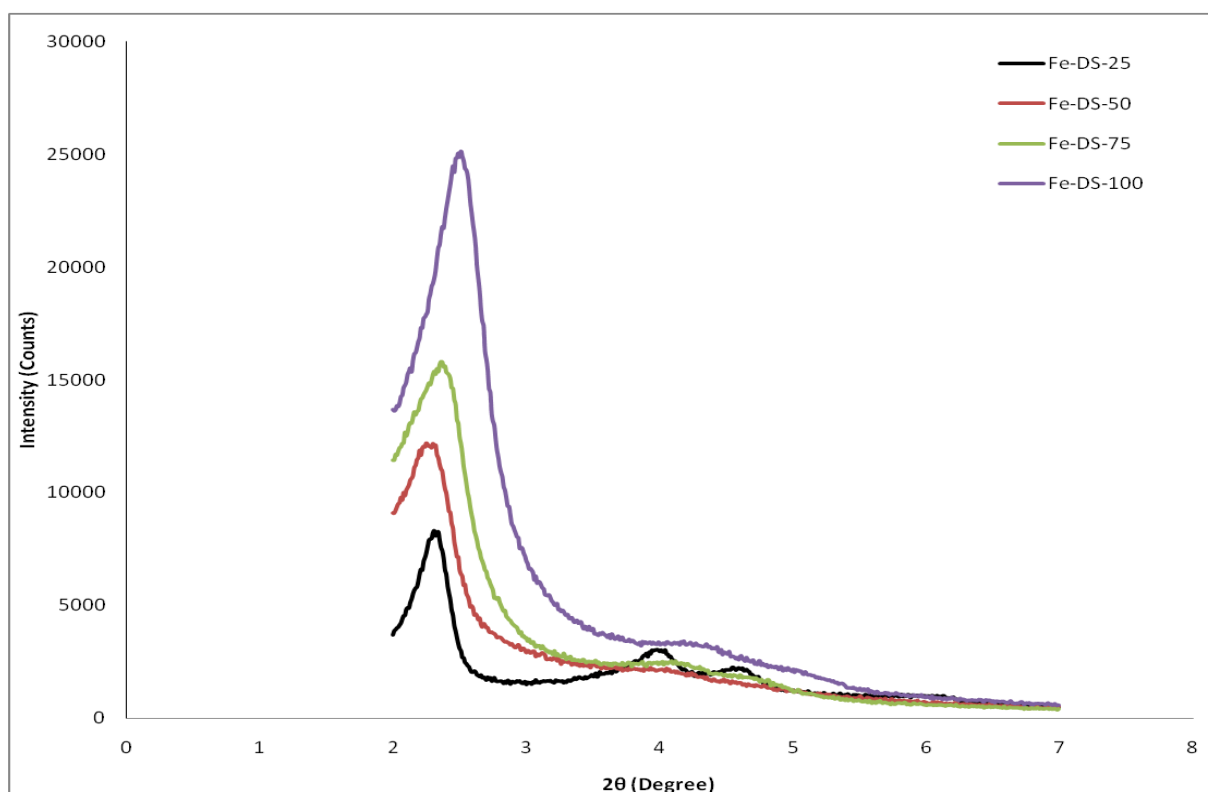


**Figure 4-33** XRD patterns of Fe-MCM-41 (120/30) with different Si/Fe mol ratios prepared by microwave assisted direct synthesis

Adsorption isotherms of the samples were given in Figure 4-34, with a hysteresis loop of a typical type IV isotherm, indicating capillary condensation in the mesopores. The isotherms of all samples showed a sharp inflection step at  $P/P_0$  of  $\sim 0.3-0.4$ , characteristic of condensation of uniform mesoporous materials.

The isotherm corresponding to  $P/P_0 < 0.3$  represents the monolayer adsorption of  $N_2$  on the walls of the mesopore, while that with  $P/P_0 > 0.4$  represents the multilayer adsorption on the outer surface of the materials. The point at which the inflection begins is related to the capillary condensation within the uniform mesopores.

Nitrogen physisorption data showed a decrease in pore volume, average pore diameter and surface area values with increasing iron content in accordance with expectations as the amount of metal species increased within the pores. In Table 4-8, the results corresponding to the discussion were given in detail. The sample with highest metal content had the lowest surface area value of  $1299 \text{ m}^2/\text{g}$  and lowest pore diameter of  $3.07 \text{ nm}$ .

Hengbo Yin and coworkers investigated the effect of copper, nickel and cobalt doping on the pore structure of pure MCM-41 mesoporous molecular sieve under  $220 \text{ W}$  microwave radiation for  $2.5 \text{ hr}$ . They achieved synthesis of long-range and well-ordered Ni-MCM-41 mesoporous molecular sieves with different amount of Ni content. As in the conventional synthesis method, the specific surface area and pore volume of the samples obtained by microwave heating decreased with increasing the amount of nickel and mesoporous ordering of the samples became poor [163,164]. They investigated the synthesis of Cu-MCM-41 mesoporous molecular sieves with different metal content with microwave irradiation method and same results as in the Ni-MCM-41 samples were observed such as decrease in specific surface area, pore volume and regularity with the increase of metal content [164] For the case of cobalt incorporated samples, they also investigated the calcination temperature for both microwave assisted and conventionally synthesized samples and concluded that the thermal stability of Co-MCM-41 mesoporous molecular sieve obtained by microwave heating was enhanced compared to that of Co-MCM-41 obtained by hydrothermal method. Among all the samples, Co-MCM-41 mesoporous molecular sieves had the highest specific surface area values [164,165].

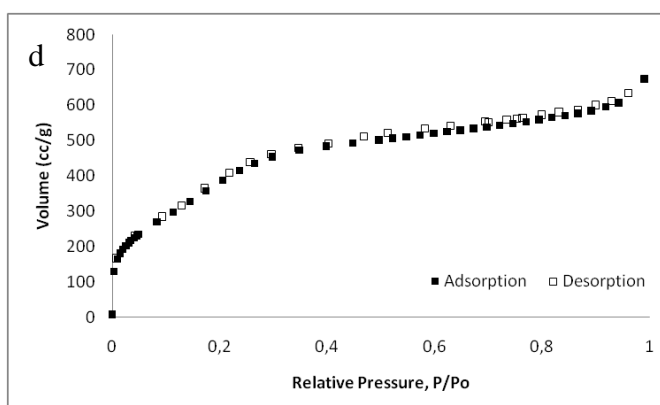
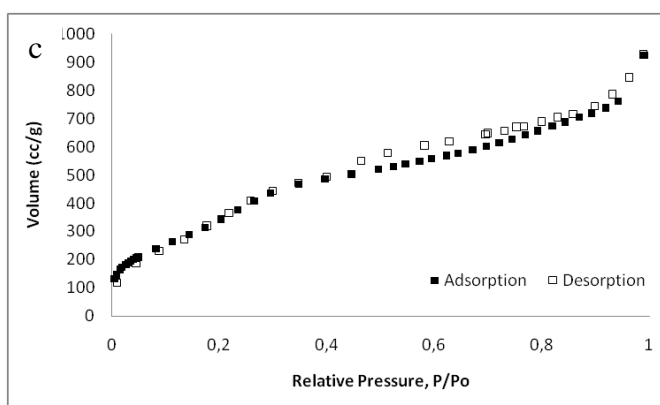
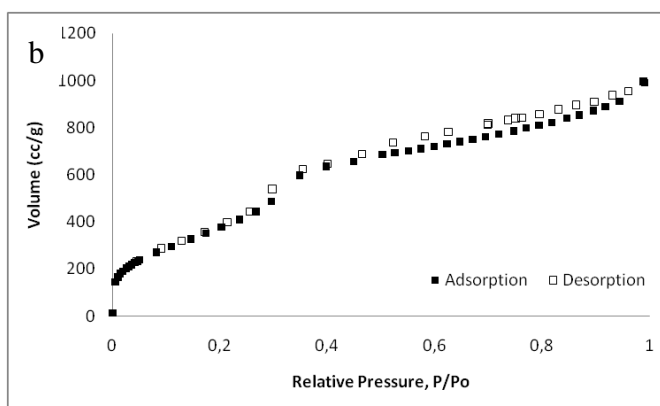
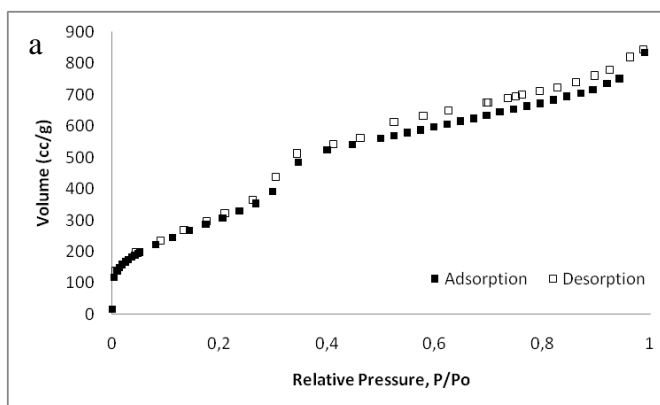


**Figure 4-34** N<sub>2</sub> sorption isotherms of direct synthesized Fe-MCM-41 (120/30) samples  
 a) Si/Fe:25 b) Si/Fe:50 c) Si/Fe:75 d) Si/Fe:100

**Table 4-8** Physical and structural properties of Fe-MCM-41 type catalytic materials synthesized by microwave assisted direct synthesis method

Sample ID (Power/Time) (Watt/Min.)	Si/Metal (mole ratio) EDS	BET Surface Area (m <sup>2</sup> /g)	BJH Des. Pore Volume (cm <sup>3</sup> /g)	BJH Des. Pore Diameter (nm)	d <sub>100</sub> (nm)	Lattice Parameter “a” (nm)	Pore Wall Thickness “δ” (nm)
Fe-MCM-41 (120/30) DS 25	21	1229	0.66	4.01	3.78	4.36	0.56
Fe-MCM-41 (120/30) DS 50	43	1582	0.84	3.99	3.87	4.47	0.67
Fe-MCM-41 (120/30) DS 75	60	1496	0.90	3.47	3.77	4.35	1.06
Fe-MCM-41 (120/30) DS 100	76	1546	0.38	3.50	3.65	4.21	0.89

In this study we investigated the Fe incorporation into MCM-41 structure by microwave radiation for the first time. The obtained results were in good agreement with the results reported in the literature for other transition metals.

The metal content in the samples were determined by EDS with a Si/Fe mol ratio in the range of 11-76. The Si/Fe mol ratios were in good agreement with the initial values.

The morphology of the Fe-MCM-41 catalysts were investigated by TEM at 100 nm and the metal particles were well distributed within the catalyst with an average pore size below 20 nm. The TEM picture of Fe-MCM-41 with the highest metal content (Si/Fe 25) was given in Figure 4-35.

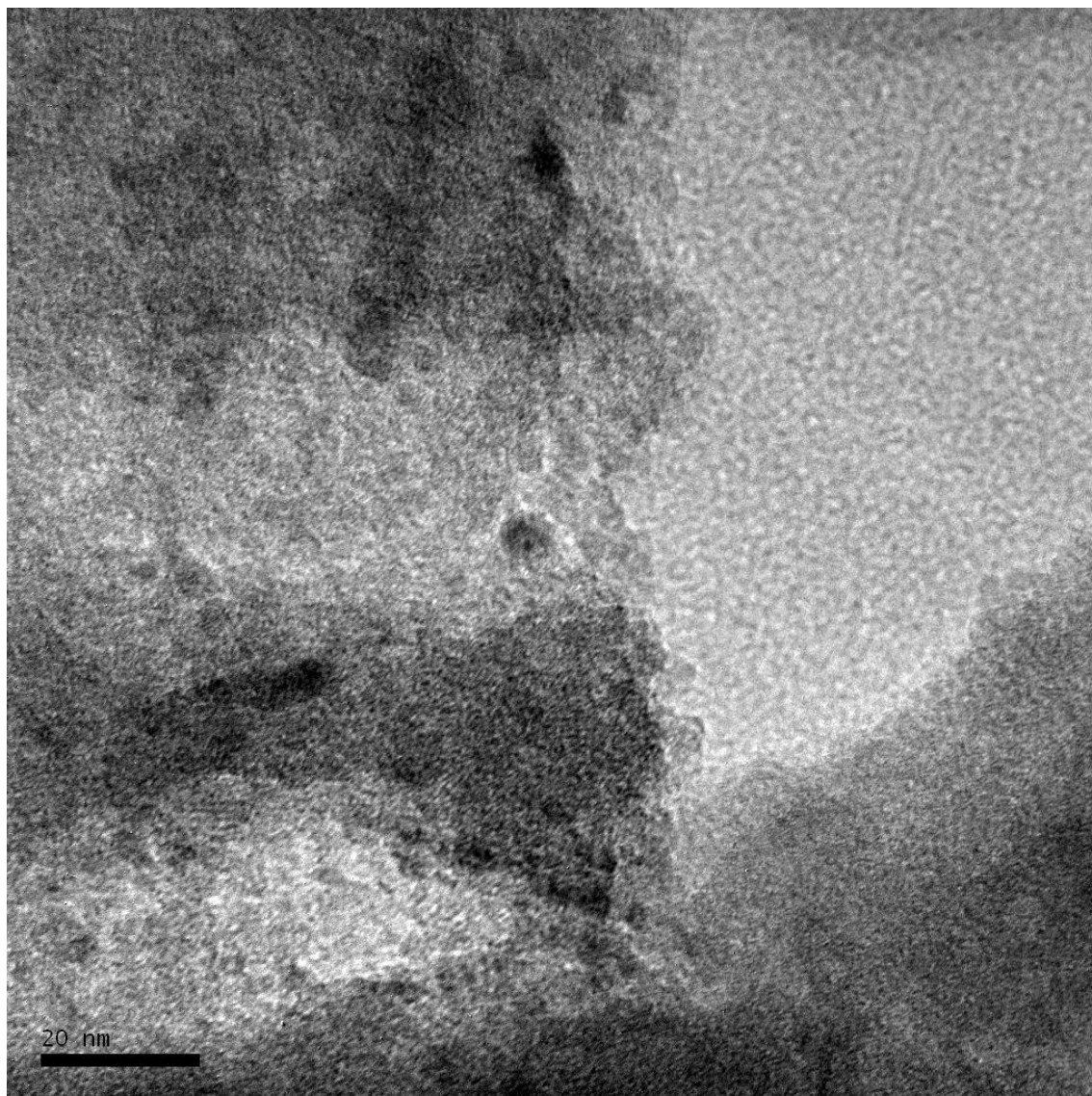


**Figure 4-35** TEM of Fe-MCM-41-DS-25 (120/30)

#### 4.2.4.2 Impregnation Results

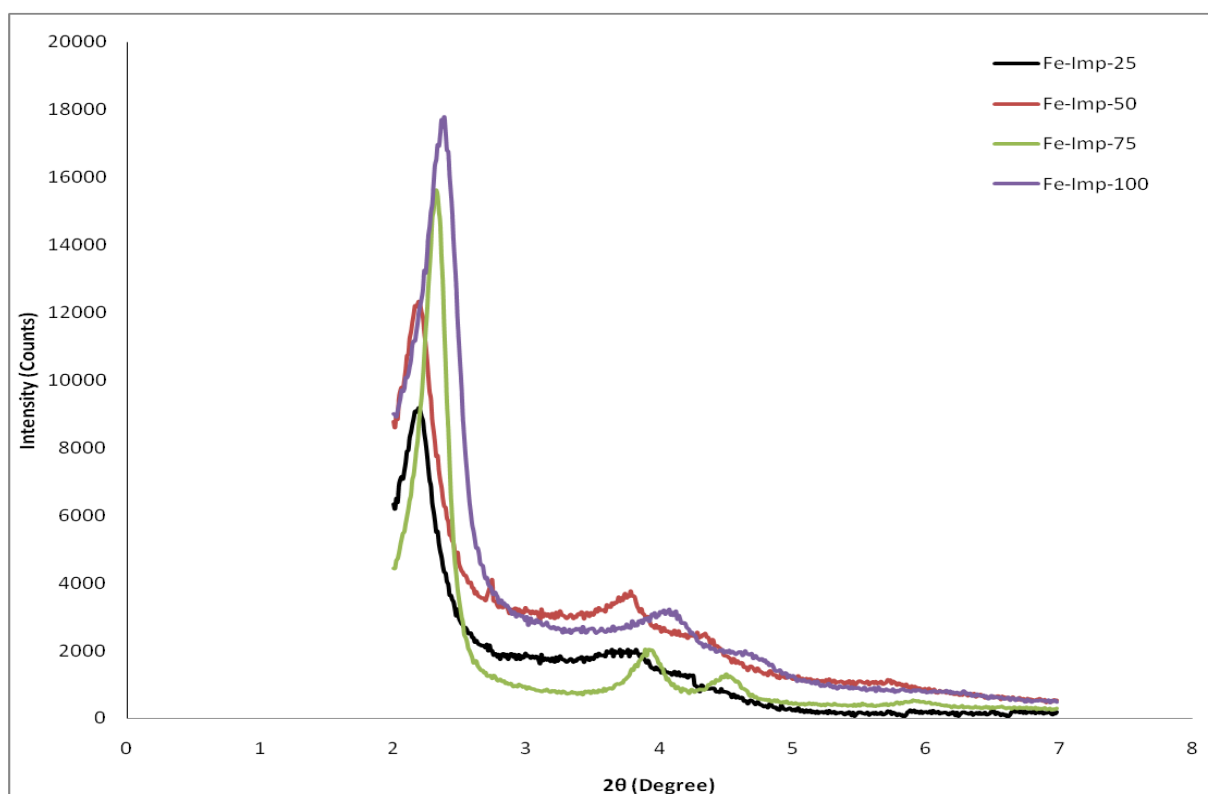


**Figure 4-36** XRD patterns of Fe-MCM-41(120/30) with different Si/Fe mol ratios prepared by microwave assisted impregnation synthesis

The XRD patterns of Fe incorporated samples prepared by impregnation technique were given in Figure 4-36. As the amount of Fe incorporated into the structure increased, the main peak in the XRD patterns shifted to the lower angles which leads to higher lattice parameters as expected. Mainly 3 peaks were observed for all samples which could be indexed as (100), (110) and (200) planes on hexagonal unit cell respectively. The sharp Bragg peaks corresponding to  $d_{100}$  were observed at  $2\theta$  values of 2.19, 2.20, 2.31, and 2.38° for Si/Fe mole ratios of 25, 50, 75 and 100 respectively.

No peaks were observed in the high angle XRDs of the Fe impregnated mesoporous sieves which indicated the absence of large crystalline metal or metal oxide particles on the silica surface.

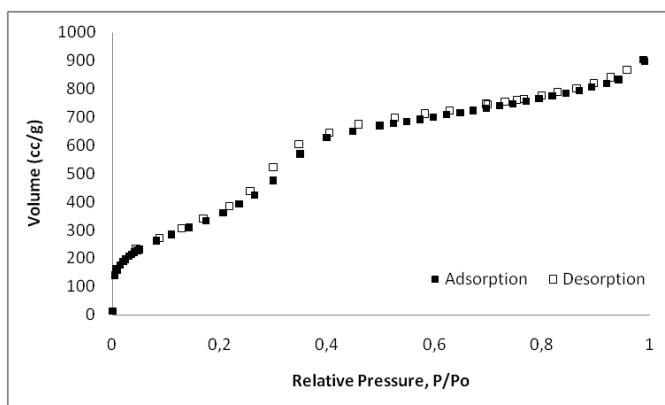
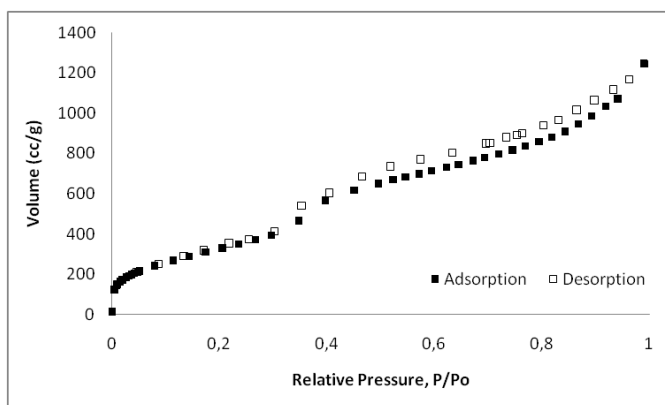
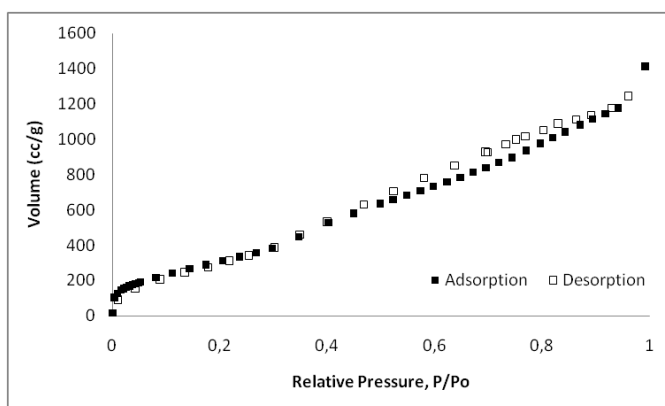
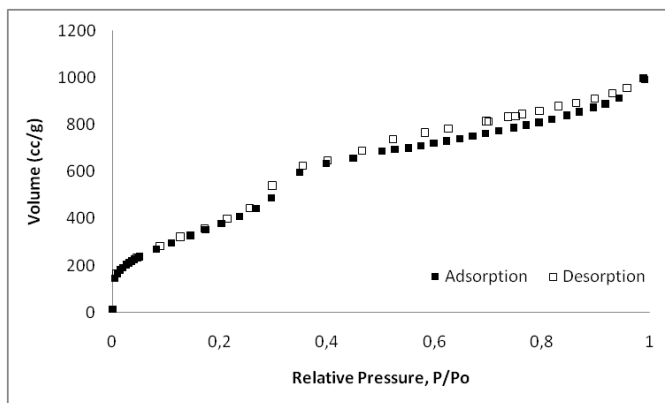


**Figure 4-37** N<sub>2</sub> sorption isotherms of impregnated Fe-MCM-41 (120/30) samples  
 a) Si/Fe:25 b) Si/Fe:50 c) Si/Fe:75 d) Si/Fe:100

**Table 4-9** Physical and structural properties of Fe-MCM-41 type catalytic materials synthesized by microwave assisted impregnation method

Sample ID (Power/Time) (Watt/Min.)	Si/Metal (mole ratio) EDS	BET Surface Area (m <sup>2</sup> /g)	BJH Des. Pore Volume (cm <sup>3</sup> /g)	BJH Des. Pore Diameter (nm)	d <sub>100</sub> (nm)	Lattice Parameter “a” (nm)	Pore Wall Thickness “δ” (nm)
Fe-MCM-41 (120/30) Imp. 25	18	995	1.25	3.48	3.87	4.47	1.16
Fe-MCM-41 (120/30) Imp. 50	31	1262	1.48	3.49	3.88	4.48	1.17
Fe-MCM-41 (120/30) Imp. 75	37	1274	1.09	3.49	3.78	4.36	1.05
Fe-MCM-41 (120/30) Imp. 100	49	1520	0.56	3.46	3.73	4.31	1.02

The metal content in the samples were determined by EDS with a Si/Fe mol ratio in the range of 8-29. The Si/Cu mol ratios showed that higher amount of metal were incorporated into the structure than that of direct synthesized samples

The obtained catalytic materials showed promising pore diameter and surface area values as high as 3.49 nm and 1520 m<sup>2</sup>/g respectively. The synthesis time was reduced to 30 minutes in which it took at least 12-24 hours in hydrothermal synthesis. In impregnation, high metal loading lead to low surface area values (995 m<sup>2</sup>/g) and deformation of crystallinity.

For the same amount of metal loading, direct synthesis superimposed the products obtained by impregnation with high ordering and more homogeneous metal dispersion. For both synthesis techniques, surface area decreased as metal content increased.

### 4.3 Diffusion Experiments

In heterogeneous catalysis and adsorption applications it is critical to have a perception how a molecule behaves in nanoporous medium- its adsorption and diffusion behavior within the system. In MCM-41, pores are not interconnected and the surface contains hydroxyl groups which may experience specific interactions with molecules susceptible of having hydrogen bonds. Modifications of the surface of these materials could be achieved by grafting of hydrophobic groups [326]. So, specific surface interaction effects on the properties of the confined compounds may be of interest to catalyst researchers since MCM-41 nanoporous materials has an advantage for application in chemical industry.

In this study we observed the diffusion behavior of single chain alcohols and aromatic solvents in MCM-41 by macroscopic method. Also, diffusion of alcohols in metal incorporated MCM-41 with Si/Metal mol ratio of 25, were studied in detail to understand the effect of metal in diffusion process.

Beside MCM-41, CNTs with the same inner mean pore diameter of MCM-41 (4 nm) were used in alcohols and aromatic solvent uptake measurements. Atomically detailed calculations have predicted that the diffusivities of light gases inside the pores of carbon nanotubes can be orders of magnitude faster than comparable diffusivities for gases adsorbed in polymeric pores, zeolites, or other nanoporous materials [327-330]. These extremely high diffusivities can be attributed to the extraordinary smoothness of the potential-energy surface defined by carbon nanotubes.

The diffusion coefficients, mode of transport and activation energies of aromatic solvents into the porous channels of MCM-41 and CNTs were investigated in 26-32 °C temperature range. The diffusion coefficients were measured from the slope of graphs of  $Mt/M_\infty$  versus  $t^{1/2}$ .

For the calculation of diffusion coefficients, the following assumptions are made [250]: the diffusion mechanism obeys Fick's law of diffusion, the crystallites possess a spherical shape, the concentration profile of the sorbed gas in these spheres shows radial symmetry, the diffusion is assumed to be isotropic; it can be described by a single diffusion coefficient rather than a diffusion tensor, and the diffusion coefficient does not depend on sorbate concentration.

### 4.3.1 Diffusion in MCM-41

#### 4.3.1.1 Diffusion Coefficients in MCM-41

Due to high surface area, adsorption capacity and mesoporous structure MCM-41 has high potential as an adsorbent for small and bulky adsorbate molecules. Adsorption of N<sub>2</sub> [5, 331-335] and water [30, 331, 336, 337] on MCM-41 has been thoroughly investigated. There are also some studies based on heavier hydrocarbons, such as benzene [338, 339], toluene [340], cyclopentane [341, 342], cyclohexane [176, 343-345], propane [346], and methane [347] on MCM-41. However, there are very few studies on the diffusion properties of MCM-41.

In this study, diffusion of volatile alcohols and aromatic solvents in the mesoporous media of MCM-41 were done by using materials synthesized by microwave assisted direct synthesis method at 120 Watt and in 30 minutes. The materials had specific surface area values of around 1400 m<sup>2</sup>/g and pore diameters around 4 nm by using cetyltrimethyl ammonium bromide as the surfactant and agglomerate sizes around 0.5 μm.

The diffusion coefficients of methanol, ethanol, n-propanol and n-butanol at 26, 28, 30 and 32 °C were presented in Figure 4-38. Raw data were given in Appendix C, Table C-1. It is observed that the lower the molecular weight of alcohols, the higher the diffusion coefficients, thus higher amounts of low molecular weight alcohols diffused relative to high molecular weight alcohols due to steric hindrances at the same temperature. For example, diffusion coefficients of methanol, ethanol, n-propanol and n-butanol were 4.01 x 10<sup>-13</sup>, 1.83 x 10<sup>-13</sup>, 8.26 x 10<sup>-14</sup> and 2.51 x 10<sup>-14</sup> m<sup>2</sup>/g at 26 °C, respectively.

Increasing the temperature increased the kinetic energy of the molecules which result to an increase in the diffusion coefficient. For instance, the diffusion coefficients of methanol at 26, 28, 30, and 32 °C were measured as 4.01 x 10<sup>-13</sup>, 4.38 x 10<sup>-13</sup>, 8.43 x 10<sup>-13</sup>, 9.99 x 10<sup>-13</sup> m<sup>2</sup>/s respectively.

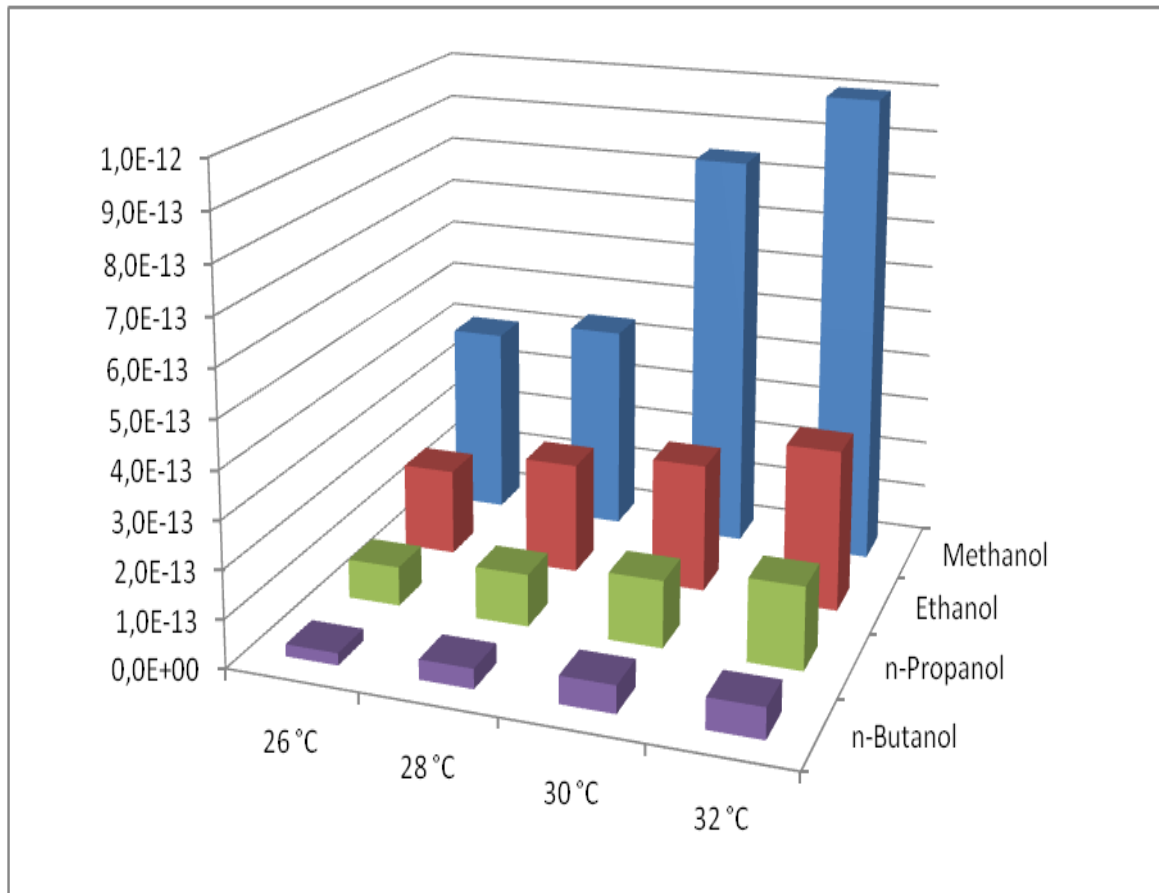


**Figure 4-38** Diffusion coefficients of volatile alcohols in MCM-41

Sakintuna and Yürüm [249] studied the diffusion of low carbon chain alcohols in natural zeolites with 40.2 % micropores, 57.9 % mesopores and 1.9 % macropores and 59 m<sup>2</sup>/g surface area. The diffusion coefficients of methanol, ethanol, propanol and n-butanol were 10 times lower than those measured in the present work. It is clearly seen that, larger pore diameter and higher surface area values of MCM-41 make diffusion more suitable for volatile substances.

Wang et al. [348] studied the diffusion of N<sub>2</sub> and CO<sub>2</sub> in  $\gamma$ -alumina within limited volume of a stiff container. The diffusion coefficients were in the order of 10<sup>-7</sup> m<sup>2</sup>/g.

Diffusion coefficients of benzene, toluene, ethylbenzene, propylbenzene, o-xylene, m-xylene and p-xylene at 26, 28, 30 and 32 °C were presented Figure 4-39. Raw data were given in Appendix C, Table C-2. The experimental results were presented in two groups: benzene, toluene, ethylbenzene and propylbenzene as one group and benzene, toluene, o-xylene, m-xylene, p-xylene as another according to organic structures.

Diffusion coefficients of benzene were the highest one in both groups and increased from  $3.96 \times 10^{-14}$  to  $9.52 \times 10^{-14} \text{ m}^2/\text{g}$  as the temperature increased from 26 to 32 °C. As the molecular weight of aromatic solvent increased, diffusion coefficients decreased. For instance, diffusion coefficients of benzene, toluene, ethylbenzene and propylbenzene were  $3.96 \times 10^{-14}$ ,  $3.79 \times 10^{-14}$ ,  $3.74 \times 10^{-14}$  and  $3.26 \times 10^{-14} \text{ m}^2/\text{g}$  at 26 °C, respectively and o-xylene, m-xylene and p-xylene were  $3.68 \times 10^{-14}$ ,  $3.42 \times 10^{-14}$ ,  $3.11 \times 10^{-14}$ , at 26 °C, respectively.

As the chain length of the attachment to the benzene ring increased, the diffusion coefficients slightly decreased, i.e. ethylbenzene and propylbenzene. Within the xylenes, there were no significant differences between diffusion coefficients at the same temperatures. It can be concluded that, the diffusion of isomeric molecules within the mesoporous channels were not affected by the branching, the deterministic behavior was again the molecular weight of the molecule.

Hoang et al. [349] investigate the diffusion of aromatic solvents (*n*-Heptane, toluene and oxylene) in bi-porous nano-materials using zero length column (ZLC) method and compared the results with pure silicate crystal. The diffusion coefficients were in the order of  $10^{-16} \text{ m}^2/\text{g}$  at 70 °C and increased with temperature. The coefficients were higher than the pure silicate due to the presence of mesoporous channels.

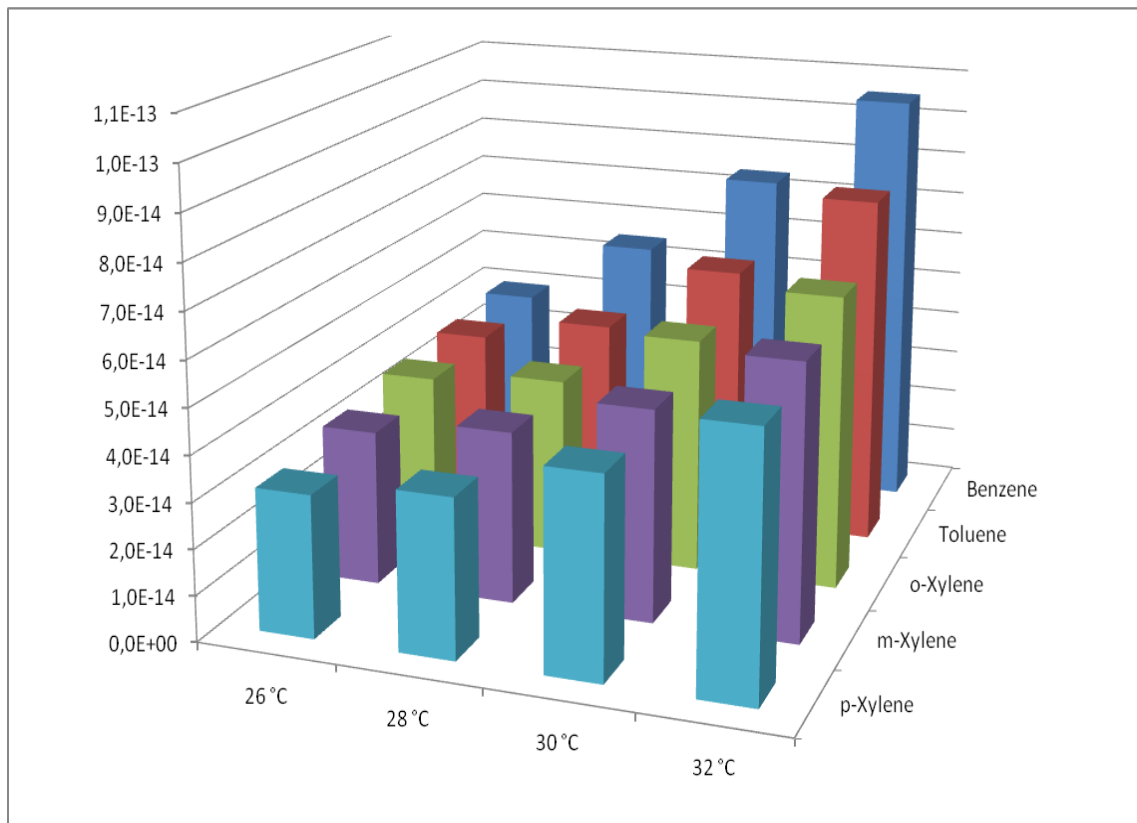
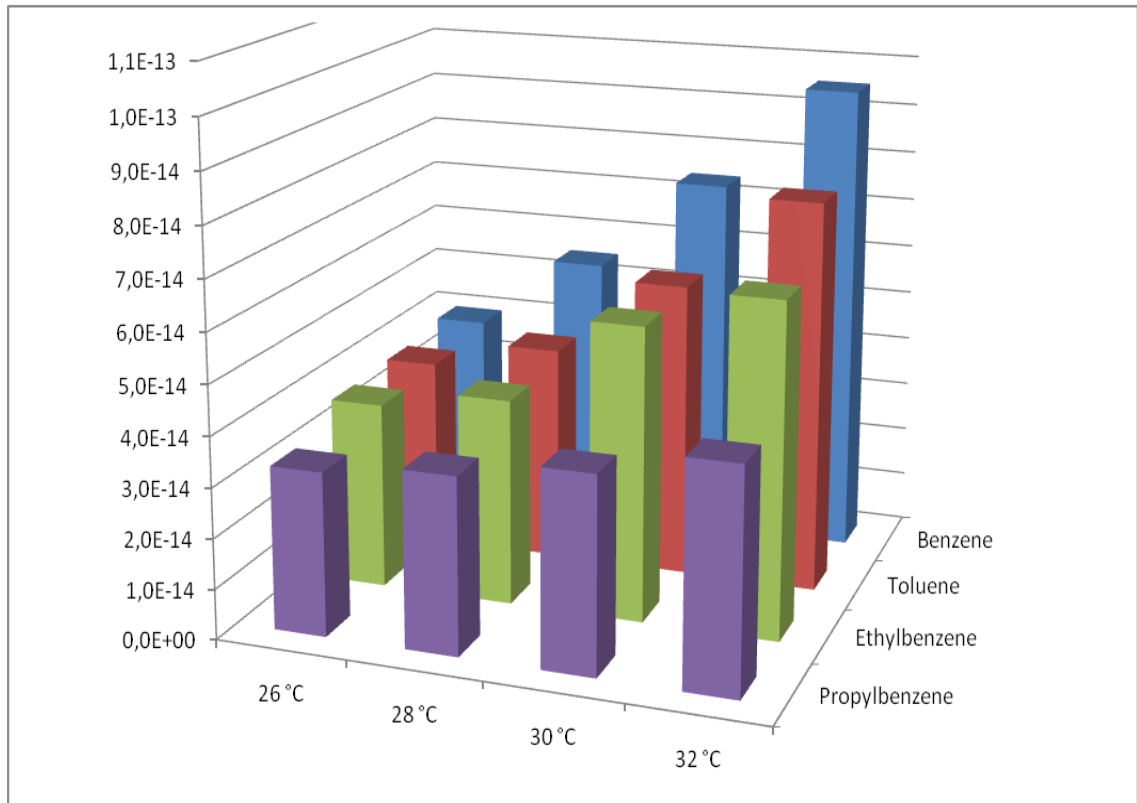


**Figure 4-39** Diffusion coefficients of volatile aromatics in MCM-41

#### 4.3.1.2 Diffusional Rate Constants and Mode of Transport in MCM-41

The diffusion rate constants, diffusion exponents and transport mechanism of alcohols and aromatics in MCM-41 were given in Table 4-10 and Table 4-11, respectively. Linearity analysis of the data gave acceptable regression coefficients ( $R^2$ ) with values greater than 0.98 indicating a linear relationship between  $\ln (M_t/M_{inf})$  vs.  $\ln t$  for diffusion of alcohols and aromatics in mesoporous media.

Diffusion rate constants slightly changed with temperature which might be a reason of using different portion MCM-41 source for each experiment and slight structural varieties within the crystalline structure. Diffusion rate constants slightly increased with temperature within the range of 26-32 °C, and slightly decreased as the molecular weight increased for all samples.

The diffusion rate constant of methanol over MCM-41 was increased from  $2.56 \times 10^{-4}$  to  $1.50 \times 10^{-3} \text{ s}^{-1}$  when diffusion temperature increased from 26 to 32 °C. For the case of benzene, diffusion rate constant increased from  $1.06 \times 10^{-4}$  to  $2.44 \times 10^{-4} \text{ s}^{-1}$  when diffusion temperature increased from 26 to 32 °C.

Diffusion exponents being in the range of 0.99-1.3 indicated an anomalous diffusion mechanism for alcohol diffusion. However for the case of aromatics, diffusion exponents decreased from 1 to 0.7 indicating some change in the diffusion mechanism from anomalous diffusion as the attachments to the benzene ring increased.

In the literature [249], the diffusion exponents of alcohols (methanol, ethanol, n-propanol, i-propanol and n-butanol) in natural zeolites systems were estimated to be between 0.96-1.00 indicating an anomalous diffusion mechanism assuming Fickian diffusion mechanism.

**Table 4-10** Diffusion rate constants, diffusion exponents, and transport mechanism of alcohols in MCM-41

<b>Alcohol</b>	<b>T, °C</b>	<b>k, s<sup>-1</sup></b>	<b>n</b>	<b>R<sup>2</sup></b>
<b>Methanol</b>	26	2.56 x 10 <sup>-4</sup>	1.27	0.999
	28	2.93 x 10 <sup>-4</sup>	1.18	0.985
	30	3.20 x 10 <sup>-4</sup>	1.32	0.993
	32	1.50 x 10 <sup>-3</sup>	1.16	0.997
<b>Ethanol</b>	26	2.16 x 10 <sup>-4</sup>	1.18	0.997
	28	2.23 x 10 <sup>-4</sup>	1.18	0.990
	30	2.36 x 10 <sup>-4</sup>	1.17	0.987
	32	2.69 x 10 <sup>-4</sup>	1.17	0.983
<b>n-Propanol</b>	26	8.35 x 10 <sup>-5</sup>	1.15	0.991
	28	1.12 x 10 <sup>-4</sup>	1.14	0.986
	30	1.35 x 10 <sup>-4</sup>	1.07	0.984
	32	1.70 x 10 <sup>-4</sup>	1.08	0.995
<b>n-Butanol</b>	26	8.84 x 10 <sup>-5</sup>	1.11	0.993
	28	9.84 x 10 <sup>-5</sup>	1.03	0.997
	30	1.09 x 10 <sup>-4</sup>	0.99	0.987
	32	1.25 x 10 <sup>-4</sup>	1.00	0.984

**Table 4-11** Diffusion rate constants, diffusion exponents, and transport mechanism of aromatics in MCM-41

Aromatic	T, °C	k, s <sup>-1</sup>	n	R <sup>2</sup>
<b>Benzene</b>	26	1.06 x 10 <sup>-4</sup>	1.17	0.993
	28	1.92 x 10 <sup>-4</sup>	1.11	0.998
	30	2.39 x 10 <sup>-4</sup>	1.09	0.996
	32	2.44 x 10 <sup>-4</sup>	0.98	0.999
<b>Toluene</b>	26	3.04 x 10 <sup>-5</sup>	1.31	0.997
	28	4.45 x 10 <sup>-5</sup>	1.23	0.998
	30	4.93 x 10 <sup>-5</sup>	1.17	0.997
	32	5.66 x 10 <sup>-5</sup>	0.93	0.998
<b>Ethylbenzene</b>	26	1.42 x 10 <sup>-3</sup>	0.86	0.996
	28	1.55 x 10 <sup>-3</sup>	0.78	0.999
	30	1.61 x 10 <sup>-3</sup>	0.81	0.999
	32	2.80 x 10 <sup>-3</sup>	0.75	0.999
<b>Propylbenzene</b>	26	1.67 x 10 <sup>-3</sup>	0.76	0.999
	28	1.81 x 10 <sup>-3</sup>	0.76	0.998
	30	1.84 x 10 <sup>-3</sup>	0.74	0.998
	32	2.36 x 10 <sup>-3</sup>	0.72	0.999
<b>o-Xylene</b>	26	2.20 x 10 <sup>-3</sup>	0.77	0.999
	28	1.49 x 10 <sup>-3</sup>	0.83	0.999
	30	2.05 x 10 <sup>-3</sup>	0.80	0.998
	32	2.73 x 10 <sup>-3</sup>	0.76	0.999
<b>m-Xylene</b>	26	1.12 x 10 <sup>-3</sup>	0.86	0.999
	28	2.71 x 10 <sup>-3</sup>	0.73	0.999
	30	3.55 x 10 <sup>-3</sup>	0.70	0.998
	32	3.62 x 10 <sup>-3</sup>	0.71	0.995
<b>p-Xylene</b>	26	1.08 x 10 <sup>-3</sup>	0.86	0.999
	28	2.85 x 10 <sup>-3</sup>	0.74	0.998
	30	3.14 x 10 <sup>-3</sup>	0.76	0.997
	32	4.41 x 10 <sup>-3</sup>	0.73	0.997

#### 4.3.1.3 Activation Energies of Diffusion in MCM-41

The activation energy calculations were done from the graph of  $\ln D$  versus  $1/T$  for each alcohol and aromatics. The results were given in Table 4-12 and 4-13 for alcohols and aromatics, respectively.

The slope of the graphs gave activation energies as 65, 76, 93 and 118 kJ/mol for methanol, ethanol, n-propanol, n-butanol, respectively. It is observed that an increase in molecular weight (or chain length) results in an increase in activation energy. Larger activation energies result in relatively small diffusion coefficients for alcohol diffusion measurements in mesoporous media. It can be concluded that there should be a strong relationship between the chain length, critical molecular size on the diffusion coefficients and activation energies. Activation energies of alcohols were also in good agreement with the values of diffusion coefficients of alcohols such that larger activation energies resulted in smaller diffusion coefficients. The activation energy of methanol in MCM-41 was measured to be the smallest of alcohols and diffusion coefficients of methanol were the greatest at all temperatures.

It is interesting that Sakintuna and Yürüm [249] estimated the activation energies of the volatile alcohols diffusion within the natural zeolites as 18.3, 46.4, 79.7 and 90.1 kJ/mol, respectively. Although the operating conditions were the same, the diffused molecules over MCM-41 has to overcome an energy barrier higher than the zeolites. Once the molecules overcome this energy barrier, they move more easily within the mesoporous channels of MCM-41 than microporous channels of zeolites which explains the higher diffusion coefficients of alcohols within MCM-41.

The activation energies of aromatics were 48, 91, 98, 112, 121, 126 and 133 kJ/mol for benzene, toluene, ethylbenzene, propylbenzene, o-xylene, m-xylene and p-xylene, respectively. With increasing molecular weight of the volatile aromatics, the activation energies also increased. The activation energy of benzene in the mesoporous channels of MCM-41 was estimated to be the smallest among those of aromatic solvents and as discussed in the previous sections, diffusion coefficients of benzene were the highest at all temperatures.

**Table 4-12** Activation energies of volatile alcohols in MCM-41

<b>Alcohol</b>	<b>Ea, kJ/mol</b>
<b>Methanol</b>	65
<b>Ethanol</b>	76
<b>n-Propanol</b>	93
<b>n-Butanol</b>	118

**Table 4-13** Activation energies of volatile aromatics in MCM-41

<b>Aromatics</b>	<b>Ea, kJ/mol</b>
<b>Benzene</b>	48
<b>Toluene</b>	91
<b>Ethylbenzene</b>	98
<b>Propylbenzene</b>	112
<b>o-Xylene</b>	121
<b>m-Xylene</b>	126
<b>p-Xylene</b>	133

### 4.3.2 Diffusion in Metal Incorporated MCM-41

#### 4.3.2.1 Diffusion Coefficients in Metal Incorporated MCM-41

The coefficients of diffusion of methanol, ethanol, n-propanol, and n-butanol at 26, 28, 30 and 32 °C into Cu, Ni, Co and Fe incorporated MCM-41 with a Si/Metal mol ratio of 25 and prepared by microwave assisted direct synthesis technique at 120 Watt in 30 minutes were given in Figure 4-40, Figure 4-41, Figure 4-42 and Figure 4-43, respectively. In Appendix C.2, all experimental data was tabulated.

Specific surface area values of all metal incorporated MCM-41 samples were 941, 1047, 1151 and 1299 m<sup>2</sup>/gr and pore volume values were 1.00, 1.13, 0.30 and 0.66 cm<sup>3</sup>/gr while average pore diameter of these samples were 3.07, 3.07, 3.41, and 4.01 nm for Cu, Ni, Co, and Fe incorporated MCM-41 mesoporous molecular sieves, respectively.

For all metal incorporated MCM-41 mesoporous molecular sieves, diffusion coefficients increased with an increase in temperature since the molecules gained higher mobility. For instance, diffusion coefficient of methanol increased from 8.06 x 10<sup>-13</sup> to 1.06 x 10<sup>-12</sup> m<sup>2</sup>/s for Cu, increased from 4.58 x 10<sup>-13</sup> to 5.51 x 10<sup>-13</sup> m<sup>2</sup>/s for Ni, increased from 4.10 x 10<sup>-13</sup> to 6.05 x 10<sup>-13</sup> m<sup>2</sup>/s for Co and increased from 2.83 x 10<sup>-13</sup> to 4.32 x 10<sup>-13</sup> m<sup>2</sup>/s for Fe, from 26 to 32 °C. The diffusion coefficients of methanol for pure MCM-41 increased from 4.01 x 10<sup>-13</sup> to 9.99 x 10<sup>-13</sup> m<sup>2</sup>/s. Cu-MCM-41 had the highest diffusion coefficients for methanol compared to other metal incorporated and pure MCM-41 and Fe-MCM-41 had the lowest.

For the case of ethanol, diffusion coefficient of ethanol increased from 4.12 x 10<sup>-13</sup> to 8.34 x 10<sup>-13</sup> m<sup>2</sup>/s for Cu, increased from 2.23 x 10<sup>-13</sup> to 5.07 x 10<sup>-13</sup> m<sup>2</sup>/s for Ni, increased from 2.27 x 10<sup>-13</sup> to 4.15 x 10<sup>-13</sup> m<sup>2</sup>/s for Co and increased from 2.24 x 10<sup>-13</sup> to 4.05 x 10<sup>-13</sup> m<sup>2</sup>/s for Fe, from 26 to 32 °C. The diffusion coefficients of methanol for pure MCM-41 increased from 1.83 x 10<sup>-13</sup> to 3.38 x 10<sup>-13</sup> m<sup>2</sup>/s. It was interesting to observe that diffusion coefficient of all metal incorporated samples were higher than pure MCM-41.

For the case of ethanol, diffusion coefficient of n-propanol increased from  $2.11 \times 10^{-13}$  to  $3.60 \times 10^{-13} \text{ m}^2/\text{s}$  for Cu, increased from  $1.40 \times 10^{-13}$  to  $2.40 \times 10^{-13} \text{ m}^2/\text{s}$  for Ni, increased from  $1.62 \times 10^{-13}$  to  $2.28 \times 10^{-13} \text{ m}^2/\text{s}$  for Co and increased from  $1.77 \times 10^{-13}$  to  $2.86 \times 10^{-13} \text{ m}^2/\text{s}$  for Fe, from 26 to 32 °C. The diffusion coefficients of methanol for pure MCM-41 increased from  $8.26 \times 10^{-14}$  to  $1.72 \times 10^{-13} \text{ m}^2/\text{s}$ .

For the case of ethanol, diffusion coefficient of n-butanol increased from  $6.94 \times 10^{-14}$  to  $1.02 \times 10^{-13} \text{ m}^2/\text{s}$  for Cu, increased from  $7.85 \times 10^{-14}$  to  $1.39 \times 10^{-13} \text{ m}^2/\text{s}$  for Ni, increased from  $7.77 \times 10^{-14}$  to  $1.62 \times 10^{-13} \text{ m}^2/\text{s}$  for Co and increased from  $7.39 \times 10^{-14}$  to  $1.18 \times 10^{-13} \text{ m}^2/\text{s}$  for Fe, from 26 to 32 °C. The diffusion coefficients of methanol for pure MCM-41 increased from  $2.51 \times 10^{-14}$  to  $6.36 \times 10^{-14} \text{ m}^2/\text{s}$ .

Higher the molecular weight of the alcohol, the lower the diffusion coefficient for all samples. The diffusion coefficients decreased as the molecular weight of alcohols increased for all metal incorporated samples of MCM-41.

It was interesting to observe that, surface modification by metal incorporation increased the diffusion coefficients of alcohol diffusion through mesoporous medium. Functionalization of the walls by incorporation of transition metals enhances the electron-transfer efficiency to design new sorption systems [27]. Increasing the active sites by incorporation of metals, increased the diffusion coefficients of alcohols through mesoporous medium.

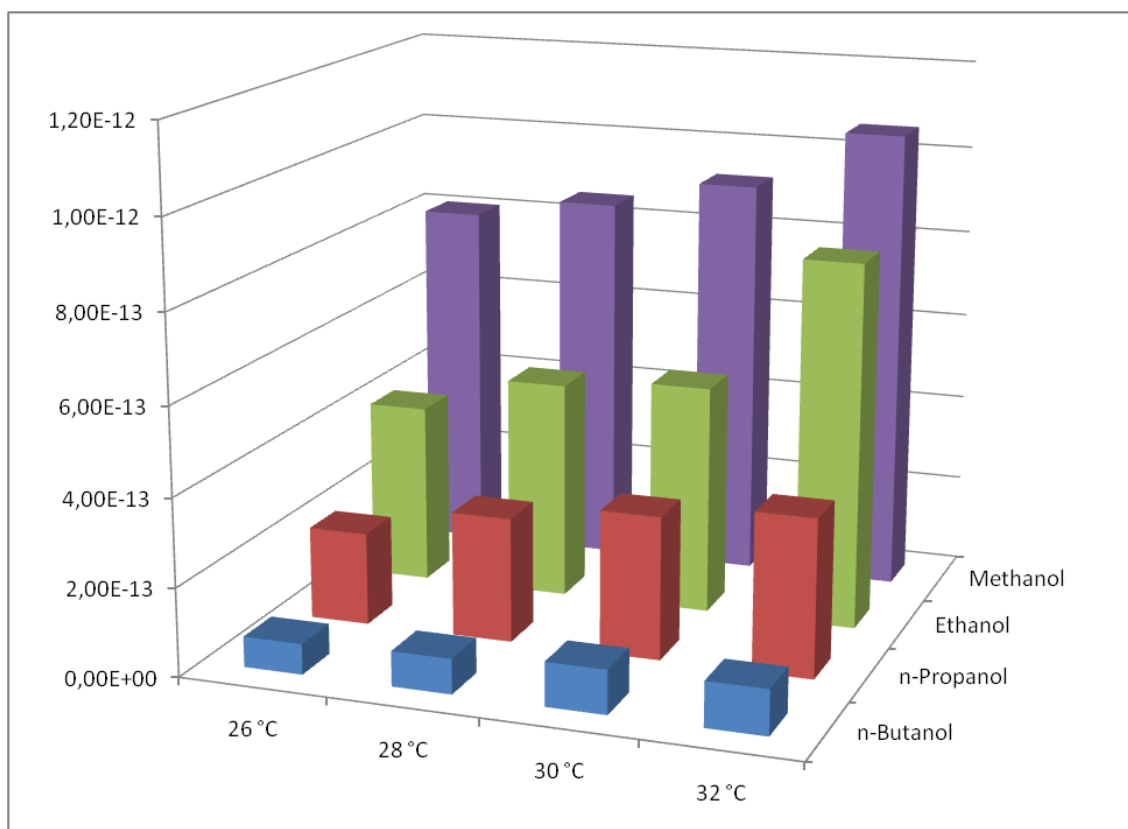


**Figure 4-40** Diffusion coefficients of volatile alcohols in Cu-MCM-41

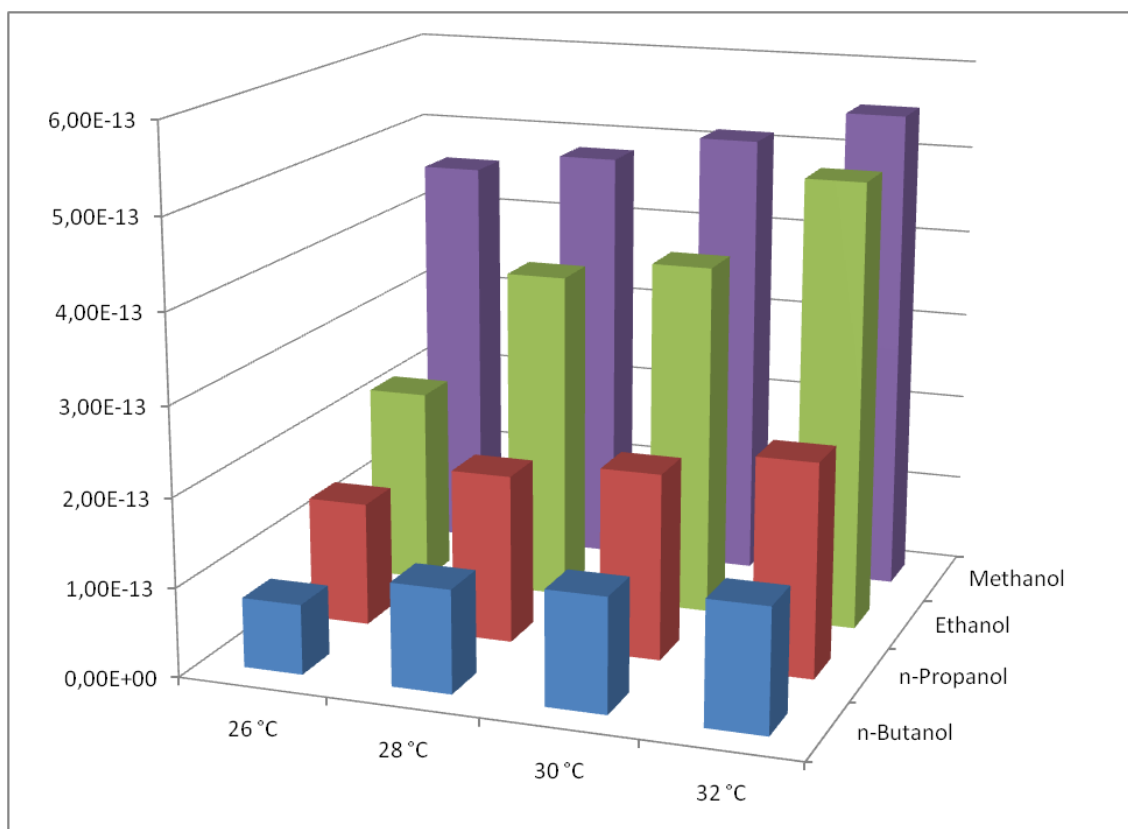


**Figure 4-41** Diffusion coefficients of volatile alcohols in Ni-MCM-41

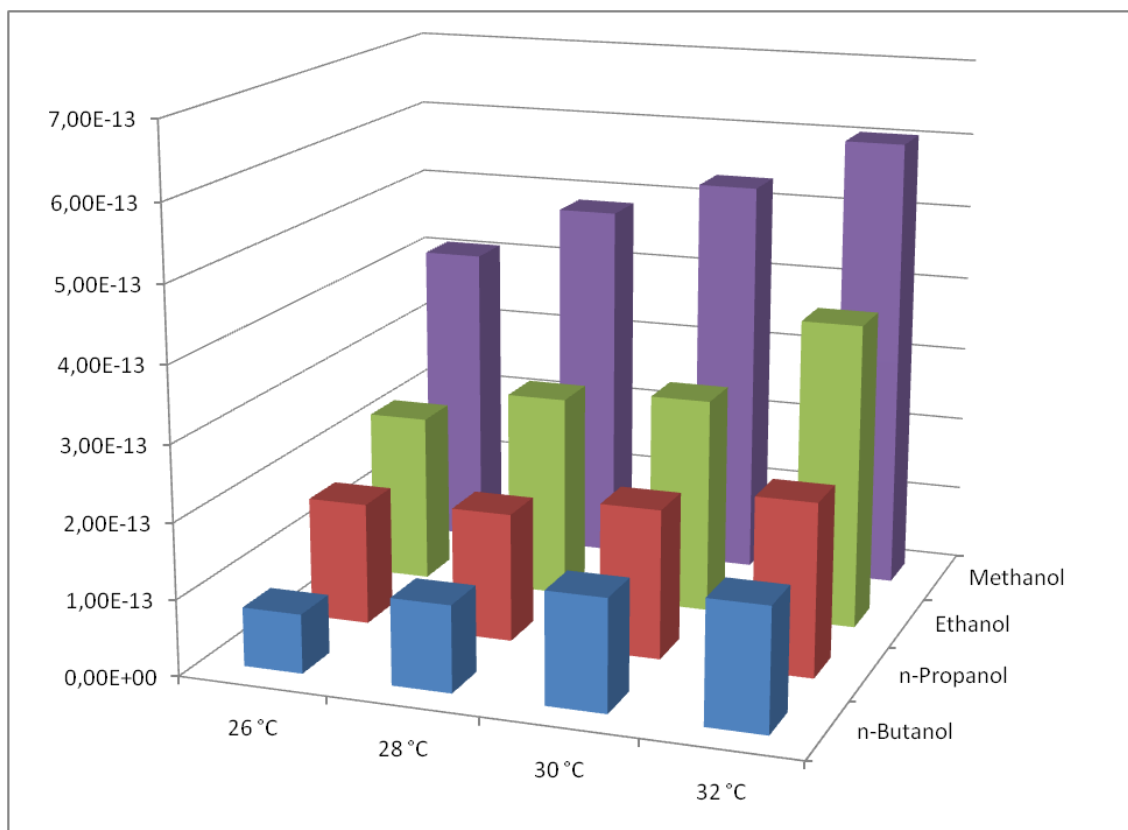


**Figure 4-42** Diffusion coefficients of volatile alcohols in Co-MCM-41

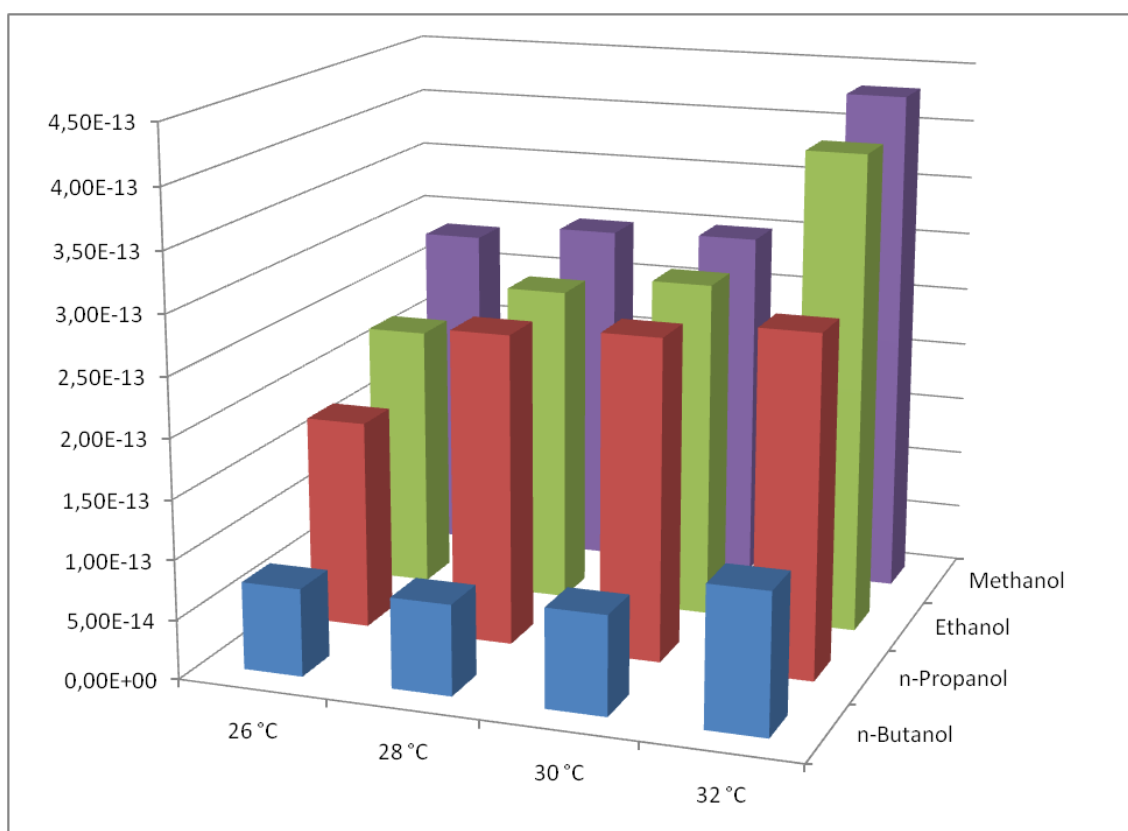


**Figure 4-43** Diffusion coefficients of volatile alcohols in Fe-MCM-41

#### **4.3.2.2 Diffusional Rate Constants and Mode of Transport in Metal Incorporated MCM-41**

The diffusion rate constants, diffusion exponents and transport mechanisms of different alcohols in metal incorporated mesoporous media were presented in Table 4-14, Table 4-15, Table 4-16 and Table 4.17 for Cu, Ni, Co, and Fe samples, respectively. Linearity analysis of the data gave acceptable regression coefficients ( $R^2$ ) with values greater than 0.98 indicating a linear relationship between  $\ln (M_t/M_{inf})$  vs.  $\ln t$  for diffusion of alcohols and aromatics in mesoporous media.

Diffusion rate constants slightly changed with temperature which might be a reason of using different portion MCM-41 source for each experiment and slight structural varieties within the crystalline structure. Diffusion rate constants slightly increased with temperature within the range of 26-32 °C, and slightly decreased as the molecular weight increased for all samples. The diffusion rate constants of Cu-MCM-41 were higher than other metal incorporated MCM-41 mesoporous sieves.

Diffusion exponents being in the range of 0.6-0.8 indicated a diffusion mechanism closer to anomalous type of diffusion for alcohol in metal incorporated mesoporous sieves. The diffusion exponents of metal incorporated samples were lower than that of MCM-41 which showed some difference in the diffusion mechanisms..

**Table 4-14** Diffusion rate constants, diffusion exponents, and transport mechanism of alcohols in Cu-MCM-41

Alcohol	T, °C	k, s <sup>-1</sup>	n	R <sup>2</sup>
<b>Methanol</b>	26	3.73 x 10 <sup>-2</sup>	0.63	0.996
	28	4.08 x 10 <sup>-2</sup>	0.70	0.989
	30	4.34 x 10 <sup>-2</sup>	0.59	0.996
	32	4.46 x 10 <sup>-2</sup>	0.65	0.990
<b>Ethanol</b>	26	2.44 x 10 <sup>-2</sup>	0.58	0.985
	28	2.65 x 10 <sup>-2</sup>	0.63	0.995
	30	2.70 x 10 <sup>-2</sup>	0.60	0.992
	32	2.86 x 10 <sup>-2</sup>	0.68	0.990
<b>n-Propanol</b>	26	1.50 x 10 <sup>-2</sup>	0.58	0.994
	28	1.53 x 10 <sup>-2</sup>	0.55	0.992
	30	1.54 x 10 <sup>-2</sup>	0.67	0.994
	32	1.82 x 10 <sup>-2</sup>	0.64	0.997
<b>n-Butanol</b>	26	1.37 x 10 <sup>-2</sup>	0.60	0.996
	28	1.53 x 10 <sup>-2</sup>	0.60	0.986
	30	1.57 x 10 <sup>-2</sup>	0.61	0.990
	32	1.70 x 10 <sup>-2</sup>	0.62	0.992

**Table 4-15** Diffusion rate constants, diffusion exponents, and transport mechanism of alcohols in Ni-MCM-41

Alcohol	T, °C	k, s <sup>-1</sup>	n	R <sup>2</sup>
<b>Methanol</b>	26	9.51 x 10 <sup>-3</sup>	0.75	0.996
	28	1.06 x 10 <sup>-2</sup>	0.74	0.995
	30	1.33 x 10 <sup>-2</sup>	0.77	0.999
	32	1.65 x 10 <sup>-2</sup>	0.69	0.986
<b>Ethanol</b>	26	9.35 x 10 <sup>-3</sup>	0.69	0.999
	28	9.47 x 10 <sup>-3</sup>	0.70	0.999
	30	9.63 x 10 <sup>-3</sup>	0.72	0.999
	32	9.89 x 10 <sup>-3</sup>	0.75	0.996
<b>n-Propanol</b>	26	5.70 x 10 <sup>-3</sup>	0.79	0.984
	28	6.04 x 10 <sup>-3</sup>	0.75	0.992
	30	6.58 x 10 <sup>-3</sup>	0.75	0.991
	32	7.64 x 10 <sup>-3</sup>	0.74	0.998
<b>n-Butanol</b>	26	5.52 x 10 <sup>-3</sup>	0.68	0.989
	28	6.01 x 10 <sup>-3</sup>	0.79	0.989
	30	6.45 x 10 <sup>-3</sup>	0.74	0.993
	32	7.08 x 10 <sup>-3</sup>	0.68	0.996

**Table 4-16** Diffusion rate constants, diffusion exponents, and transport mechanism of alcohols in Co-MCM-41

Alcohol	T, °C	k, s <sup>-1</sup>	n	R <sup>2</sup>
<b>Methanol</b>	26	7.39 x 10 <sup>-3</sup>	0.76	0.995
	28	8.57 x 10 <sup>-3</sup>	0.76	0.995
	30	1.61 x 10 <sup>-2</sup>	0.68	0.996
	32	1.88 x 10 <sup>-2</sup>	0.65	0.995
<b>Ethanol</b>	26	5.64 x 10 <sup>-3</sup>	0.79	0.999
	28	6.19 x 10 <sup>-3</sup>	0.81	0.997
	30	9.07 x 10 <sup>-3</sup>	0.75	0.999
	32	1.01 x 10 <sup>-2</sup>	0.71	0.995
<b>n-Propanol</b>	26	5.09 x 10 <sup>-3</sup>	0.79	0.991
	28	5.84 x 10 <sup>-3</sup>	0.74	0.994
	30	6.36 x 10 <sup>-3</sup>	0.72	0.996
	32	7.09 x 10 <sup>-3</sup>	0.70	0.994
<b>n-Butanol</b>	26	4.83 x 10 <sup>-3</sup>	0.77	0.982
	28	5.96 x 10 <sup>-3</sup>	0.78	0.981
	30	6.21 x 10 <sup>-3</sup>	0.69	0.971
	32	6.36 x 10 <sup>-3</sup>	0.68	0.999

**Table 4-17** Diffusion rate constants, diffusion exponents, and transport mechanism of alcohols in Fe-MCM-41

Alcohol	T, °C	k, s <sup>-1</sup>	n	R <sup>2</sup>
<b>Methanol</b>	26	7.13 x 10 <sup>-3</sup>	0.78	0.998
	28	8.51 x 10 <sup>-3</sup>	0.76	0.995
	30	1.06 x 10 <sup>-2</sup>	0.72	0.993
	32	1.88 x 10 <sup>-2</sup>	0.65	0.990
<b>Ethanol</b>	26	5.31 x 10 <sup>-3</sup>	0.77	0.997
	28	5.56 x 10 <sup>-3</sup>	0.80	0.997
	30	6.12 x 10 <sup>-3</sup>	0.76	0.999
	32	6.49 x 10 <sup>-3</sup>	0.80	0.987
<b>n-Propanol</b>	26	4.74 x 10 <sup>-3</sup>	0.78	0.988
	28	5.48 x 10 <sup>-3</sup>	0.74	0.991
	30	5.93 x 10 <sup>-3</sup>	0.79	0.988
	32	6.44 x 10 <sup>-3</sup>	0.78	0.972
<b>n-Butanol</b>	26	4.59 x 10 <sup>-3</sup>	0.70	0.995
	28	5.17 x 10 <sup>-3</sup>	0.74	0.981
	30	5.63 x 10 <sup>-3</sup>	0.70	0.988
	32	6.26 x 10 <sup>-3</sup>	0.67	0.989

#### 4.3.2.3 Activation Energies of Diffusion in Metal Incorporated MCM-41

The activation energy calculations were done from the graph of  $\ln D$  versus  $1/T$  for each alcohol and aromatics. The results were given in Table 4-18 for Cu-MCM-41, Ni-MCM-41, Co-MCM-41 and Fe-MCM-41, respectively.

The activation energies were related with the electron configuration of the metals incorporated to the MCM-41 structure. As the number of valance electrons increased in the metal, the activation energy necessary for diffusion decreased. For instance, the activation energies of diffusion for methanol, ethanol, n-propanol and n-butanol were as 34, 45, 47 and 49 kJ/mol, respectively which were much lower than the pure MCM-41 values. Although the operating conditions were the same, the diffused molecules in MCM-41 had to overcome an energy barrier higher than the metal incorporated samples. It can be concluded that surface modification by metal incorporation increased the smoothness of the surface and adsorbent molecules favored to diffuse more easily than pure Si walls .

It is also observed that an increase in molecular weight (or chain length) results in an increase in activation energy. Larger activation energies result in relatively small diffusion coefficients for alcohol diffusion measurements in mesoporous media. It can be concluded that there should be a strong relationship between the chain length, critical molecular size on the diffusion coefficients and activation energies. Activation energies of alcohols were also in good agreement with the values of diffusion coefficients of alcohols such that larger activation energies resulted in smaller diffusion coefficients. The activation energy of methanol in Cu-MCM-41 was measured to be the smallest of alcohols and diffusion coefficients of methanol were the greatest at all temperatures.

**Table 4-18** Activation energies of volatile alcohols in metal incorporated MCM-41

<b>Me-MCM-41</b>	<b>Alcohol</b>	<b>Ea, kJ/mol</b>
<b>Cu-MCM-41</b>	Methanol	34
	Ethanol	45
	n-Propanol	47
	n-Butanol	49
<b>Ni-MCM-41</b>	Methanol	44
	Ethanol	57
	n-Propanol	65
	n-Butanol	69
<b>Co-MCM-41</b>	Methanol	48
	Ethanol	58
	n-Propanol	67
	n-Butanol	70
<b>Fe-MCM-41</b>	Methanol	52
	Ethanol	60
	n-Propanol	65
	n-Butanol	71

### 4.3.3 Diffusion in CNT

#### 4.3.3.1 Diffusion Coefficients in CNT

Diffusion coefficients of methanol, ethanol, n-propanol and n-butanol at 26, 28, 30 and 32 °C into carbon nanotubes were presented in Figure 4.44. In Appendix C, Table C-7 raw data was tabulated. In all samples, diffusion coefficients increased with increasing temperature and decreased as molecular weight increased.

The diffusion coefficient of methanol in carbon nanotube increased from  $5.42 \times 10^{-12}$  to  $9.12 \times 10^{-12} \text{ m}^2/\text{g}$  when the diffusion temperature was elevated from 26 to 32 °C, respectively. Higher the molecular weight of the alcohol, the lower the diffusion coefficient owing to the steric hindrances. The diffusion coefficient of methanol in the carbon nanotube seemed to be highest compared to other alcohols. The diffusion coefficients of methanol, ethanol, n-propanol and n-butanol were  $5.42 \times 10^{-12}$ ,  $4.03 \times 10^{-12}$ ,  $3.75 \times 10^{-12}$ ,  $2.08 \times 10^{-12} \text{ m}^2/\text{g}$  at 26 °C, respectively.

Sakintuna and Yürüm [250] observed that diffusion coefficients of alcohols also increased with increasing temperature in the natural zeolite templated porous carbons which were carbonized at different temperatures, as 700, 800, 900 and 1000 °C with 397, 350, 405, and 367  $\text{m}^2/\text{g}$  surface area values respectively and an average pore diameter of 11 nm. The diffusion coefficients of methanol, ethanol, n-propanol and n-butanol in the porous carbon carbonized at 700°C at 26 °C were  $2.95 \times 10^{-14}$ ,  $1.54 \times 10^{-14}$ ,  $1.96 \times 10^{-14}$  and  $2.97 \times 10^{-15} \text{ m}^2/\text{g}$ , respectively.

When we compare the diffusion coefficients between carbon nanotubes with porous carbons, there was a significant difference between the results. The diffusion coefficients of carbon nanotubes were  $10^3$  times higher than porous carbons even though the same operating conditions were performed. It is known that there is large number of different functional groups on carbon surface; carbonyl, carboxylic acid, hydroxyl, ether, lactone, anhydride... etc. which may result in many types of solute-adsorbent interaction [326] However, these extremely high diffusivities can be attributed to the extraordinary smoothness of the potential-energy surface defined by carbon nanotubes [327].

Skoulidas et al. [327, 328] reported, on the basis of simulation, that the self- and transport-diffusion coefficients of light gases in SWCNs can be orders of magnitude higher than those in any known microporous materials, approaching free diffusion in the bulk gas. The simulation results were also in good agreement with our experimental results for heavier molecules.

It is also interesting to compare the diffusion coefficients of alcohols in carbon nanotubes with MCM-41. Even though they had the same pore diameter and even MCM-41 had higher surface area compared to carbon nanotubes, diffusion coefficients of alcohols in CNTs were at least 10 times higher than in MCM-41.

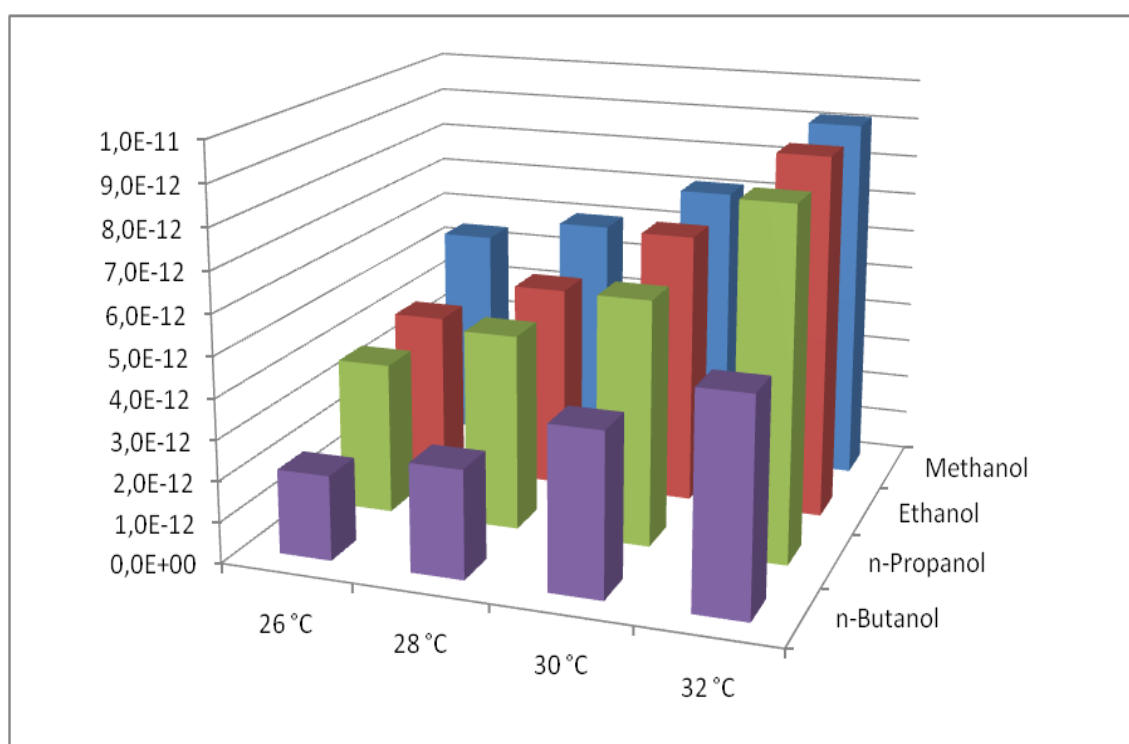


**Figure 4-44** Diffusion coefficients of volatile alcohols in CNT

In this study, the diffusion behavior of aromatic solvents in the nano-channels of carbon nanotubes was also investigated. Diffusion coefficients of benzene, toluene, ethylbenzene, propylbenzene, o-xylene, m-xylene and p-xylene at 26, 28, 30 and 32 °C were presented Figure 4-45. Raw data were given in Appendix C, Table C-8.

It is interesting to observe that benzene diffusions in the nano-channels were even higher than those of methanol at all temperatures. Diffusion coefficients of benzene increased from  $4.67 \times 10^{-12}$  to  $1.62 \times 10^{-11}$   $\text{m}^2/\text{s}$  from 26 to 32 °C. As the molecular weight of aromatic solvent increased, diffusion coefficients decreased. For instance, diffusion coefficients of benzene, toluene, ethylbenzene and propylbenzene were  $3.67 \times 10^{-12}$ ,  $2.85 \times 10^{-12}$ ,  $2.71 \times 10^{-13}$  and  $1.52 \times 10^{-13}$   $\text{m}^2/\text{g}$  at 26 °C, respectively and o-xylene, m-xylene and p-xylene were  $1.81 \times 10^{-12}$ ,  $2.22 \times 10^{-12}$ , and  $2.39 \times 10^{-12}$ , at 26 °C, respectively.

As the chain length of the attachment to the benzene ring increased, the diffusion coefficients significantly decreased, i.e. ethylbenzene and propylbenzene. Aside from MCM-41, diffusion of xylenes within carbon nanotubes showed very different characteristics. Within the xylenes, p-xylene had the highest diffusion coefficients at the same temperatures. When the spacing between the attached molecules decreased, diffusion coefficients decreased. For instance, diffusion coefficients of p-xylene increased from  $2.39 \times 10^{-12}$  to  $9.73 \times 10^{-12}$   $\text{m}^2/\text{s}$  from 26 to 32 °C.

When we compare the diffusion experiments between MCM-41 and carbon nanotubes, there were considerable differences within the results due to the origin of materials, structural behavior, steric hindrances and sorption-adsorbate interactions.

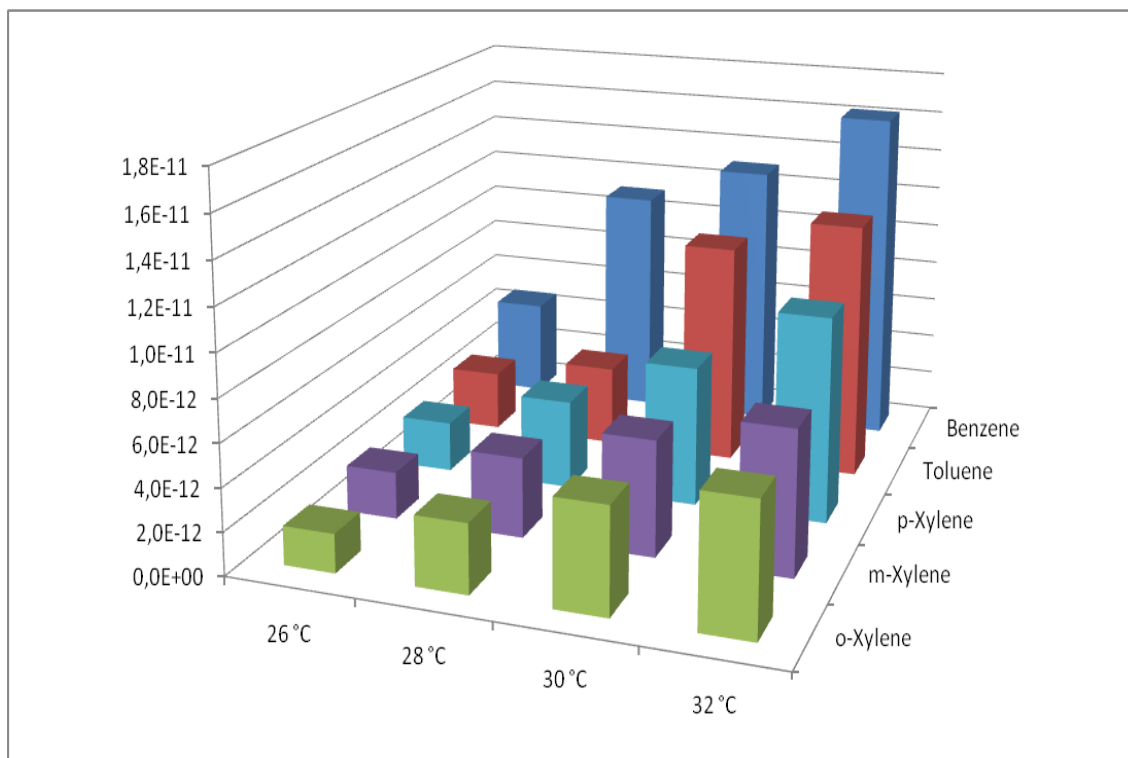
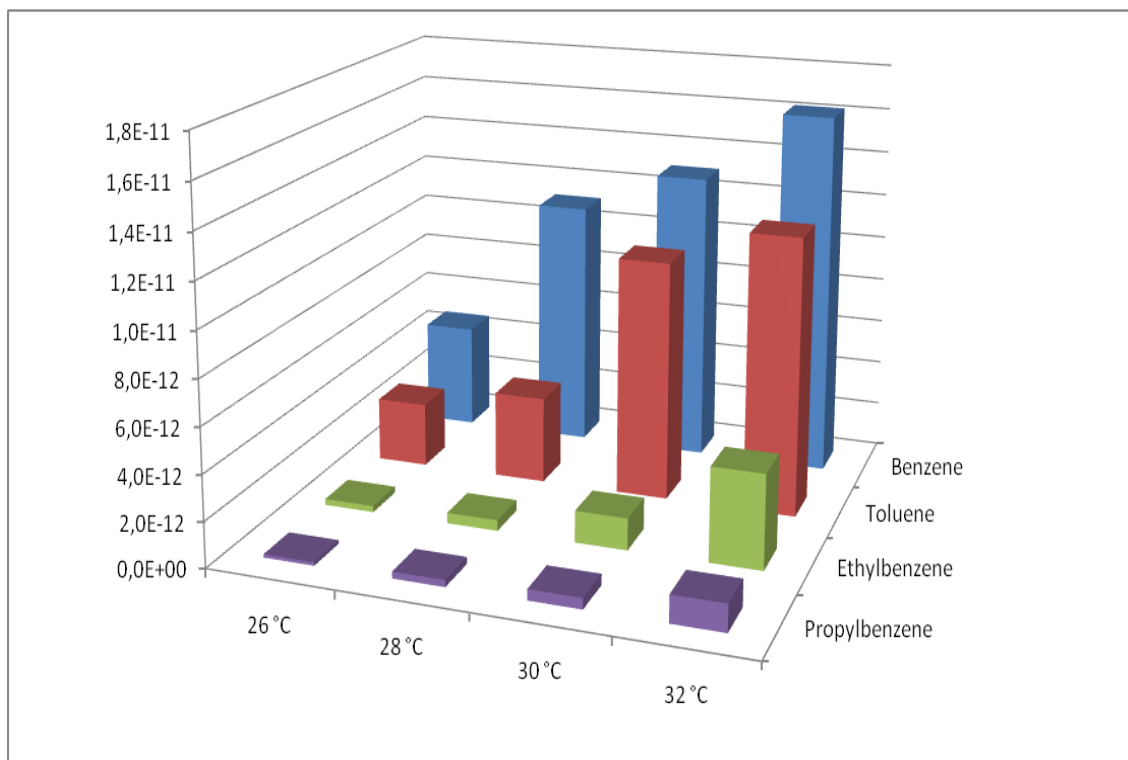


**Figure 4-45** Diffusion coefficients of volatile aromatics in CNT

#### 4.3.3.2 Diffusional Rate Constants and Mode of Transport in CNT

The diffusion rate constants, diffusion exponents and transport mechanism of alcohols and aromatics in CNT were given in Table 4-19 and Table 4-20, respectively. As in the case of MCM-41, linearity analysis of the data gave acceptable regression coefficients ( $R^2$ ) with values greater than 0.98 indicating a linear relationship between  $\ln (M_t/M_{inf})$  vs.  $\ln t$  for diffusion of alcohols and aromatics in nano-channels of carbon nanotubes.

The change in the diffusion rate constants with temperature was more significant compared to MCM-41 which might be a reason of using different portion source for each experiment and slight structural varieties within the crystalline structure. The general trend in diffusion rate constants was a slight increase with temperature within the range of 26-32 °C, and slight decrease as the molecular weight increased for all samples.

The diffusion rate constant of methanol over CNT was increased from  $4.34 \times 10^{-4}$  to  $6.71 \times 10^{-3} \text{ s}^{-1}$  when diffusion temperature increased from 26 to 32 °C. For the case of propylbenzene, diffusion rate constant increased from  $3.90 \times 10^{-6}$  to  $1.49 \times 10^{-4} \text{ s}^{-1}$  when diffusion temperature increased from 26 to 32 °C. The change in the diffusion rate constant with temperature became more significant as the molecular weight of aromatics increased.

Diffusion exponents being in the range of 0.8-1.3 indicated an anomalous diffusion mechanism for both alcohol and aromatic diffusion.

In the literature [250], the diffusion exponents of alcohols (methanol, ethanol, n-propanol, i-propanol and n-butanol) in natural zeolite templated porous carbon systems were estimated to be in a broader range as 0.58-1.00 indicating an anomalous diffusion mechanism assuming Fickian diffusion mechanism. However, for the case of carbon nanotubes, the diffusion exponent values were estimated in a narrow scale.

**Table 4-19** Diffusion rate constants, diffusion exponents, and transport mechanism of alcohols in CNT

Alcohol	T, °C	k, s <sup>-1</sup>	n	R <sup>2</sup>
<b>Methanol</b>	26	4.34 x 10 <sup>-4</sup>	0.97	0.999
	28	6.51 x 10 <sup>-3</sup>	0.95	0.994
	30	5.61 x 10 <sup>-3</sup>	0.97	0.994
	32	6.71 x 10 <sup>-3</sup>	0.99	0.986
<b>Ethanol</b>	26	1.71 x 10 <sup>-4</sup>	1.08	0.995
	28	4.51 x 10 <sup>-4</sup>	0.94	0.995
	30	1.19 x 10 <sup>-3</sup>	0.84	0.995
	32	9.17 x 10 <sup>-4</sup>	0.90	0.995
<b>n-Propanol</b>	26	2.29 x 10 <sup>-4</sup>	1.07	0.996
	28	3.70 x 10 <sup>-4</sup>	0.99	0.999
	30	8.04 x 10 <sup>-4</sup>	0.92	0.997
	32	5.77 x 10 <sup>-5</sup>	1.33	0.993
<b>n-Butanol</b>	26	6.19 x 10 <sup>-5</sup>	1.21	0.999
	28	6.59 x 10 <sup>-5</sup>	1.19	0.997
	30	2.98 x 10 <sup>-4</sup>	0.98	0.999
	32	9.03 x 10 <sup>-4</sup>	0.90	0.995

**Table 4-20** Diffusion rate constants, diffusion exponents, and transport mechanism of aromatics in CNT

Aromatic	T, °C	k, s <sup>-1</sup>	n	R <sup>2</sup>
<b>Benzene</b>	26	1.17 x 10 <sup>-3</sup>	0.95	0.996
	28	1.09 x 10 <sup>-3</sup>	0.98	0.998
	30	4.86 x 10 <sup>-3</sup>	1.13	0.993
	32	4.93 x 10 <sup>-3</sup>	0.81	0.996
<b>Toluene</b>	26	2.49 x 10 <sup>-4</sup>	1.13	0.992
	28	2.71 x 10 <sup>-4</sup>	1.12	0.991
	30	2.19 x 10 <sup>-3</sup>	0.94	0.997
	32	3.37 x 10 <sup>-3</sup>	0.94	0.998
<b>Ethylbenzene</b>	26	5.56 x 10 <sup>-6</sup>	1.56	0.996
	28	2.17 x 10 <sup>-5</sup>	1.37	0.994
	30	3.49 x 10 <sup>-4</sup>	1.01	0.996
	32	4.48 x 10 <sup>-4</sup>	1.03	0.997
<b>Propylbenzene</b>	26	3.90 x 10 <sup>-6</sup>	1.41	0.995
	28	3.34 x 10 <sup>-6</sup>	1.49	0.993
	30	2.60 x 10 <sup>-6</sup>	1.56	0.994
	32	1.49 x 10 <sup>-4</sup>	1.06	0.997
<b>o-Xylene</b>	26	8.05 x 10 <sup>-6</sup>	1.47	0.996
	28	6.10 x 10 <sup>-5</sup>	1.20	0.997
	30	7.75 x 10 <sup>-5</sup>	1.18	0.998
	32	2.28 x 10 <sup>-4</sup>	1.05	0.995
<b>m-Xylene</b>	26	5.49 x 10 <sup>-5</sup>	1.25	0.997
	28	1.94 x 10 <sup>-4</sup>	1.07	0.982
	30	4.64 x 10 <sup>-4</sup>	0.98	0.994
	32	5.95 x 10 <sup>-4</sup>	0.99	0.997
<b>p-Xylene</b>	26	1.94 x 10 <sup>-4</sup>	1.07	0.993
	28	8.02 x 10 <sup>-4</sup>	0.90	0.996
	30	1.35 x 10 <sup>-3</sup>	0.82	0.995
	32	6.33 x 10 <sup>-3</sup>	0.96	0.993

#### 4.3.3.3 Activation Energies of Diffusion in CNT

The activation energy calculations were done from the graph of  $\ln D$  versus  $1/T$  for each alcohol and aromatic. The results were given in Table 4-21 and 4-22 for alcohols and aromatics, respectively.

The slope of the graphs gave activation energies as 81, 102, 103, 120 kJ/mol for methanol, ethanol, n-propanol, n-butanol, respectively in CNTs which were 65, 76, 93 and 118 kJ/mol for MCM-41. As observed from the results, the energy barrier that an alcohol molecule had to overcome to diffuse through MCM-41 and CNT were close to each other. It is also observed that larger activation energies result in relatively small diffusion coefficients for alcohol diffusion measurements in mesoporous media. For both materials, this statement is true within their own results. However, the diffusion coefficients of CNTs were much higher than of MCM-41s even though they had the same activation energy. That situation might be a result of the smoother surface of CNTs which allow the materials diffuse more easily once they overcome the energy barrier.

It can be concluded that there should be a strong relationship between the chain length, critical molecular size on the diffusion coefficients and activation energies. Activation energies of alcohols were also in good agreement with the values of diffusion coefficients of alcohols such that larger activation energies resulted in smaller diffusion coefficients. The activation energy of methanol in MCM-41 was measured to be the smallest of alcohols and diffusion coefficients of methanol were the greatest at all temperatures.

The activation energies of aromatics were 163, 190, 245, 261, 189, 169 and 159 kJ/mol for benzene, toluene, ethylbenzene, propylbenzene, o-xylene, m-xylene and p-xylene, respectively in CNTs as twice as higher than that of in MCM-41s. Even though, the diffusion coefficients of aromatics within CNTs were much higher than MCM-41s, the activation energies of diffusion were also higher. That is most likely due to the interaction between carbon and aromatics in their first contact; once the energy barrier was overcome the molecules diffuse more easily on the smooth surface of CNTs.

**Table 4-21** Activation energies of volatile alcohols in CNT

<b>Alcohol</b>	<b>Ea, kJ/mol</b>
<b>Methanol</b>	81
<b>Ethanol</b>	102
<b>n-Propanol</b>	103
<b>n-Butanol</b>	120

**Table 4-22** Activation energies of volatile aromatics in CNT

<b>Aromatics</b>	<b>Ea, kJ/mol</b>
<b>Benzene</b>	163
<b>Toluene</b>	190
<b>Ethylbenzene</b>	245
<b>Propylbenzene</b>	261
<b>o-Xylene</b>	189
<b>m-Xylene</b>	169
<b>p-Xylene</b>	159

## CONCLUSIONS

1. MCM-41 mesoporous materials were successfully synthesized in very short crystallization times using the microwave method. Apparently, the effect of the microwave heating was to accelerate the condensation reactions of the silicate network. It is thought that the microwave radiation, by stimulating the water molecules around the silicon atoms via vibration and rotation, causes the condensation process of the framework to accelerate.
2. The variation of crystallinity with various reaction conditions suggested that the formation mechanism of MCM-41 under microwave heating was similar to that observed with conventional oven heating.
3. High quality MCM-41 hexagonal mesoporous materials of good thermal stability were obtained in 30 minutes at 120 Watt by microwave assisted heating with specific surface area value of 1438 m<sup>2</sup>/g and average pore diameter of 3.49 nm.
4. When the heating time was too long (or temperature was too high) continued heating resulted in decomposition of the already formed structure. Continued microwave action may cause the meta stable MCM-41 material to collapse into a denser phase in the reaction solution, for example by destroying the surfactant.
5. The samples prepared at 80 Watt for 1 minute and 120 minutes did not give any Bragg peaks by XRD analysis. The reason for the initial case was that the time was not enough to initiate the formation of ordered structure and also it was evidence that no crystalline MCM-41 was formed before the microwave treatment. For the latter case over heating resulted in phase deformation.

6. A hexagonal phase was already formed after heating the gel at 80 Watt for 20 minutes. Increasing the microwave power and time first increase the crystallinity then decrease it after heating for two hours.
7. In MCM-41, a strong low angle XRD diffraction pattern was observed at around  $2.50^\circ$  for  $2\theta$  and this was assigned to a (100) reflection from a hexagonal arrangement of mesopores.
8. In  $N_2$  adsorption-desorption isotherms, all samples had typical Type IV isotherms as expected for mesoporous materials. Between  $P/P_0$  0.3-0.4, a well defined step occurred, representing the spontaneous filling of the mesopores due to capillary condensation. The isotherm corresponding to  $P/P_0 < 0.3$  represented the monolayer adsorption of  $N_2$  on the walls of the mesopores, while that with  $P/P_0 > 0.4$  represented the multilayer adsorption on the outer surface of the materials. The point at which the inflection begins was related to the capillary condensation within the uniform mesopores.
9. For metal incorporated MCM-41 samples, propagation of the metal loading lead to a gradual reduction of intensity and a shift towards the lower angles of the peak in the 100 plane. The aforementioned reduction of intensity was in prospect, as introducing metal based nanoparticles into the pores caused an increase in the phase cancelation, and to this respect, reduced scattering intensities for the Bragg reflections.
10. No peaks were observed at high angle XRDs of the metal incorporated mesoporous materials which indicates the absence of large crystalline metal or metal oxide particles on the silica surface.
11. The lattice parameters of metal incorporated MCM-41 type mesoporous materials were greater than that of pure MCM-41. This was consisted with the Metal-O bonds being longer than that of Si-O bonds and gave an evidence of the metal incorporation into the framework.
12. It was also observed that the lattice parameters increased with the metal content which indicated that the metal content incorporated in the framework increased with increasing amount of metal salt added in the synthesis gel.

13. TEM analyses of the samples with the highest metal loading confirmed the production of nanoparticles on the mesoporous host.
14. N<sub>2</sub> physisorption data showed that a decrease in the pore volume, average pore diameter and surface area with increasing metal content in accordance with expectations as the amount of the metal species increased within the pores. Also, there was a slight shift in the inflection step toward lower P/P<sub>0</sub> upon the introduction of the material.
15. For microwave assisted direct synthesis method, Cu-MCM-41 mesoporous molecular sieves had specific surface areas in a range of 941–1368 m<sup>2</sup>/g and average pore sizes in a range of 3.07–3.49 nm; Ni-MCM-41 mesoporous molecular sieves have specific surface areas in a range of 1047–1431 m<sup>2</sup>/g and average pore sizes in a range of 3.07–3.51 nm; Co-MCM-41 mesoporous molecular sieves have specific surface areas in a range of 1151–1546 m<sup>2</sup>/g and average pore sizes in a range of 3.04–3.44 nm; and Fe-MCM-41 mesoporous molecular sieves have specific surface areas in a range of 1299–1582 m<sup>2</sup>/g and average pore sizes in a range of 3.47–4.01 nm.
16. For microwave assisted impregnation synthesis method, Cu-MCM-41 mesoporous molecular sieves had specific surface areas in a range of 837–1481 m<sup>2</sup>/g and average pore sizes in a range of 3.08–3.52 nm; Ni-MCM-41 mesoporous molecular sieves have specific surface areas in a range of 1060–1485 m<sup>2</sup>/g and average pore sizes in a range of 3.49–3.58 nm; Co-MCM-41 mesoporous molecular sieves have specific surface areas in a range of 656–1420 m<sup>2</sup>/g and average pore sizes in a range of 3.05–3.43 nm; and Fe-MCM-41 mesoporous molecular sieves have specific surface areas in a range of 995–1520 m<sup>2</sup>/g and average pore sizes in a range of 3.46–3.48 nm.
17. The MCM-41 materials obtained from the direct synthesis method had higher specific surface area values compared to impregnated samples. In addition to this, impregnated samples had higher metal content compared to samples obtained from direct synthesis method. This indicated that, higher amount of metal incorporation lead to a decrease in specific surface area values due to blockage of pores.

18. The diffusion behavior (diffusion coefficients, modes of transport, and the activation energies) of linear chain alcohols and aromatic solvents in MCM-41 were investigated by macroscopic method. Also, diffusion of alcohols in metal incorporated MCM-41 with Si/Metal mol ratio of 25, were studied in detail to understand the effect of metal in diffusion process. Beside MCM-41, CNTs with the same inner mean pore diameter of MCM-41 (4 nm) were used in alcohol and aromatic solvent uptake measurements.
19. As the molecular weight of the alcohols and aromatics increased, diffusion coefficients into MCM-41 and CNTs decreased, and the time necessary to reach equilibrium increased.
20. The diffusion of alcohols and aromatics into MCM-41 and CNTs obeyed the anomalous transport mechanism. Diffusion rate constants slightly increased with increasing temperature.
21. It is also observed that an increase in molecular weight (or chain length) results in an increase in activation energy. Larger activation energies result in relatively small diffusion coefficients for alcohol and aromatic diffusion measurements in mesoporous media. It can be concluded that there should be a strong relationship between the chain length, critical molecular size on the diffusion coefficients and activation energies. Activation energies of volatile chemicals were also in good agreement with the values of diffusion coefficients such that larger activation energies resulted in smaller diffusion coefficients.
22. The diffusion coefficients of low chain alcohols in MCM-41 and natural zeolites with 40.2 % micropores, 57.9 % mesopores and 1.9 % macropores and 59 m<sup>2</sup>/g surface area were compared. The diffusion coefficients of methanol, ethanol, propanol and n-butanol in natural zeolites were at least 10 times lower than those measured for MCM-41. It is clearly seen that, larger pore diameter and higher surface area values of MCM-41 make diffusion more suitable for volatile substances.
23. It was interesting to observe that diffusion coefficient of all metal incorporated samples were higher than pure MCM-41 due to the increase in active sites.

24. When we compare the diffusion coefficients between carbon nanotubes with porous carbons, there was a significant difference between the results. The diffusion coefficients of carbon nanotubes were  $10^3$  times higher than porous carbons even though the same operating conditions were performed. It is also interesting to compare the diffusion coefficients of alcohols in carbon nanotubes with MCM-41. Even though they had the same pore diameter and even MCM-41 had higher surface area compared to carbon nanotubes, diffusion coefficients of alcohols in CNTs were at least 10 times higher than in MCM-41. These results can be attributed to the extraordinary smoothness of the potential-energy surface defined by carbon nanotubes.

## REFERENCES

- [1] IUPAC Manual of Symbols and Terminology, Pure Appl. Chem., 1972, 31, 578
- [2] R. Roque-Malherbe, in Handbook of Surfaces and Interfaces of Materials, Vol. 5, Nalwa, H.S. Ed., Academic Press, New York, 2001, 495
- [3] M.E. Davis, C. Saldarriaga, C. Montes, J. Garces, C. Crowder, Zeolites, 1988, 8, 362
- [4] M.E. Davies, Nature, 2002, 417, 813
- [5] C.T. Kresge, et al., Nature, 1992, 359, 710
- [6] J.S. Beck, et. al., J. Am. Chem. Soc., 1992, 114, 10834
- [7] J.S. Beck, Method for synthesizing mesoporous crystalline materials. US Patent 5,057,296, 1991
- [8] C.T. Kresge, M.E. Leonowicz, W.J. Roth, J.C. Vartuli, Composition of synthetic porous crystalline material, its synthesis, US Patent 5,102,643, April 7, 1992
- [9] C.T. Kresge, M.E. Leonowicz, W.J. Roth, J.C. Vartuli, Synthesis of mesoporous crystalline material ,US Patent 5,098,684, March 24, 1992
- [10] Q.S. Huo, et al., Nature, 1994, 368, 317
- [11] Q. Huo, D.I. Margolese, U. Ciesla, D. G. Demuth, P. Feng, T. E. Gier, P. Sieger, A. Firouzi, B. F. Chmelka, F. Schüth, G. D. Stucky, Chem. Mater., 1994, 6, 1176
- [12] J.C. Vartuli, et al., Chem. Mater, 1994, 6, 2070
- [13] J.C. Vartuli, et al., Chem. Mater., 1994. 6, 2317

- [14] J.C. Vartuli, K.D. Schmitt, C.T. Kresge, W.J. Roth, M.E. Leonowicz, S.B. McCullen, S.D. Hellring, J.S. Beck, J.L. Schlenker, D.H. Olsen, and E.W. Sheppard, J. Weitkamp, H.G. Karge, H. Pfeifer, and W. Höderich (Eds.), 1994 Development of a formation mechanism for M41S. Zeolites and Related Microporous Materials: State of Art p. 53. Elsevier , Amsterdam
- [15] V. Chiola, J.E. Ritsko, C.D. Vanderpool, US Patent 3 556 725, 1971
- [16] F. DiRenzo, H. Cambon, R. Dutartre, Microporous Mater., 1997, 10, 283.
- [17] T. Yanagisawa, T. Shimizu, K. Kuroda, C. Kato, Bull. Chem. Soc. Jpn., 1990, 63, 988
- [18] S. Inagaki, Y. Fukushima, K. Kuroda, J. Chem. Soc. Chem. Commun., 1993, 680
- [19] P.T. Tanev, T.J. Pinnavaia, Science, 1995, 267, 865,
- [20] P.T. Tanev, M. Chibwe, T.J. Pinnavaia, Nature, 1994, 368, 321
- [21] S.A Bagshaw, E. Prouzet, T.J. Pinnavaia, Science, 1995, 269, 1242
- [22] D.Y. Zhao, J.L. Feng, Q.S. Huo, N. Melosh, G.H. Fredrickson, B.F. Chmelka, G.D. Stucky, Science, 1998, 279, 548
- [23] M.E. Leonowicz, J.A. Lawton, S.L. Lawton, M.K. Rubin, Science, 1994, 264, 1910
- [24] W.J. Roth, C.T. Kresge, J.C. Vartuli, M.E. Leonowicz, A.S. Fung, S.B. McCullen, Catalysis by Microporous Mesoporous Materials, Stud.Surf. Sci. Catal., Vol 94. , H.K. Beyer, H.G. Karge, I. Kricsi, J.B. Nagy (Eds.), Elsevier Science, 1995, 94, 301
- [25] W.J. Roth, J.C. Vartuli, Stud. Surf. Sci. Catal., 2002, 141, 273
- [26] C.T. Kresge, J.C. Vartuli, W.J., Roth, M.E. Leonowicz, Stud. Surf. Sci. Catal., 2004, 148, 53
- [27] T.A. Konovalova, Y. Gao, R. Schad, L.D. Kispert, C.A. Saylor, L.-C. Brunel, J. Phys. Chem. B, 2001, 105, 7459
- [28] [http://www.exxonmobil.com/apps/refiningtechnologies/catalyst/mn\\_catalyst.html](http://www.exxonmobil.com/apps/refiningtechnologies/catalyst/mn_catalyst.html)
- [29] G. Øye, J. Sjöblom, M. Stöckr, Advances in Colloid and Interphase Science, 2001, 89-90, 439
- [30] C-Y. Chen, H-X. Li, M. E. Davis, Microporous Mater. 1993, 2, 17-26
- [31] C-Y. Chen, S. L. Burkett, H-X. Li, M. E. Davis, Microporous Mater. 1993, 2, 27
- [32] A. Firouzi, D. Kumar, L. M. Bull, T. Besier, P. Sieger, Q. Huo, S. A. Walker, J. A. Zasadzinsky, C. Glinka, J. Nicol, D. Margolis, G. D. Stucky, B. F. Chmelka, Science 1995, 267, 1138

- [33] A. Monnier, F. Schüth, Q. Huo, D. Kumar, D. Margolese, R. S. Maxwell, G. D. Stucky, M. Krishnamurty, P. Petroff, A. Firouzi, M. Janicke, B. F. Chmelka, *Science* 1993, 261, 1299
- [34] J. Fan, S. W. Boettcher, C.-K. Tsung, Q. Shi, M. Schierhorn, G. D. Stucky, *Chem. Mater.*, 2008, 20, 909
- [35] Y. Wan and D. Zhao, *Chem. Rev.*, 2007, 110, 2821
- [36] Y. Sakamoto, M. Kaneda, O. Terasaki, D.Y. Zhao, J.M. Kim, G. Stucky, H.J. Shim, R. Ryoo, *Nature* 2000, 408, 449
- [37] S.D. Shen, A.E. Garcia-Bennett, Z. Liu, Q.Y. Lu, Y.F. Shi, Y. Yan, C.Z. Yu, W.C. Liu, Y. Cai, O. Terasaki, D.Y. Zhao, *Am. Chem. Soc.* 2005, 127, 6780
- [38] B. Tan, A. Dozier, H.J. Lehmler, B.L. Knutson, S.E. Rankin, *Langmuir* 2004, 20, 6981
- [39] S. Che, A.E. Garcia-Bennett, T. Yokoi, K. Sakamoto, H. Kunieda, O. Terasaki, T. Tatsumi, *Nat. Mater.* 2003, 2, 801
- [40] S. Che, Z. Liu, T. Ohsuna, K. Sakamoto, O. Terasaki, T. Tatsumi, *Nature* 2004, 429, 281
- [41] S. Oliver, A. Kuperman, N. Coombs, A. Lough, G.A. Ozin, *Nature* 1995, 378, 47
- [42] T. Abe, A. Taguchi, M. Iwamoto, *Chem. Mater.*, 1995, 7, 1429
- [43] Q.S. Huo, D.I. Margolese, G.D. Stucky, *Chem. Mater.*, 1996, 8, 1147
- [44] D.Y. Zhao, Q.S. Huo, J.L. Feng, J.M. Kim, Y.J. Han, G.D. Stucky, *Chem. Mater.* 1999, 11, 2668
- [45] Q.S. Huo, R. Leon, P.M. Petroff, G.D. Stucky, *Science* 1995, 268, 1324
- [46] T. Yokoi, H. Yoshitake, T. Tatsumi, *Chem. Mater.*, 2003, 15, 4536
- [47] A.E. Garcia-Bennett, K. Miyasaka, O. Terasaki, S.N. Che, *Chem. Mater.* 2004, 16, 3597
- [48] A.E. Garcia-Bennett, N. Kupferschmidt, Y. Sakamoto, S. Che, O. Terasaki, *Angew. Chem., Int. Ed.*, 2005, 44, 5317
- [49] C.B. Gao, Y. Sakamoto, K. Sakamoto, O. Terasaki, S.N. Che, *Angew. Chem., Int. Ed.* 2006, 45, 4295
- [50] J.Y. Ying, C.P. Mehnert, M.S. Wong, *Angew. Chem., Int. Ed.* 1999, 38, 56
- [51] P.T. Tanev, T.J. Pinnavaia, *Science* 1995, 267, 865
- [52] D.Y. Zhao, Q.S. Huo, J.L. Feng, B.F. Chmelka, G.D. Stucky, *J. Am. Chem. Soc.*, 1998, 120, 6024
- [53] C.Z. Yu, Y.H. Yu, D.Y. Zhao, *Chem. Commun.*, 2000, 575

- [54] X.Y. Liu, B.Z. Tian, C.Z. Yu, F. Gao, S.H. Xie, B. Tu, R.C. Che, L.M. Peng, D.Y. Zhao, *Angew. Chem., Int. Ed.*, 2002, 41, 3876
- [55] J. Fan, C.Z. Yu, T. Gao, J. Lei, B.Z. Tian, L.M. Wang, Q. Luo, B. Tu, W.Z. Zhou, D.Y. Zhao, *Angew. Chem., Int. Ed.* 2003, 42, 3146
- [56] F. Kleitz, D.N. Liu, G.M. Anilkumar, I.S. Park, L.A. Solovyov, A.N. Shmakov, R.J. Ryoo, *Phys. Chem. B*, 2003, 107, 14296
- [57] F. Kleitz, S.H. Choi, R. Ryoo, *Chem. Commun.*, 2003, 2136
- [58] A. Shimojima, K. Kuroda, *Angew. Chem., Int. Ed.*, 2003, 42, 4057
- [59] A. Shimojima, Z. Liu, T. Ohsuna, O. Terasaki, K.J. Kuroda, *Am. Chem. Soc.*, 2005, 127, 14108
- [60] N. Coustel, F. Di Renzo, F. Fajula, *Chem. Commun.*, 1994, 967
- [61] C.F. Cheng, W.Z. Zhou, D.H. Park, J. Klinowski, M. Hargreaves, F. Gladden, *J. Chem. Soc. Faraday Trans.*, 1997, 93, 359
- [62] C.F. Cheng, D.H. Park, J. Klinowski, *J. Chem. Soc. Faraday Trans.*, 1997, 93, 193
- [63] R. Ryoo, J.M. Kim, *Chem. Commun.*, 1995, 711
- [64] K.J. Edler, J.W. White, *Chem. Mater.*, 1997, 9, 1226
- [65] L. Chen, T. Horiuchi, T. Mori, K. Maeda, *J. Phys. Chem.*, 1999, B103, 1216
- [66] A. Jentys, N.H. Pham, H. Vinek, *J. Chem. Soc. Faraday Trans.*, 1996, 92, 3287
- [67] A. Jentys, K. Kleesrofer, H. Vinek, *Micropor. Mesopor. Mater.*, 1999, 27, 321
- [68] M. Hunger, U. Schenk, M. Breuninger, R. Gläser, J. Weitkamp, *Micropor. Mesopor. Mater.*, 1999, 27, 261
- [69] M. Janicke, D. Kumar, G.D. Stucky, B.F. Chmelka, *Stud. Surf. Sci. Catal.*, 1994, 84, 243
- [70] F.P. Matthaе, D. Genske, C. Minchev, H. Lechert, *Stud. Surf. Sci. Catal.*, 1998, 117, 223
- [71] R. Schmidt, D. Akporiaye, M. Stöcker, O.H. Ellestad, *J. Chem. Soc. Chem. Commun.*, 1994, 12, 1493
- [72] J.B. Kim, T. Inui, *Catal. Lett.*, 1996, 36, 255
- [73] X.S. Zhao, G.Q. Lu, G.J. Millar, X.S. Li, *Catal. Lett.*, 1996, 38, 33
- [74] N. Constel, F. Di Renzo, F. Fajula, *J. Chem. Soc. Chem. Commun.*, 8, 1994, 967
- [75] C.Y. Chen, H.X. Li, M.E. Davis, *Micropor. Mater.*, 1993, 2, 17
- [76] K.M. Reddy, C. Song, *Catal. Lett.*, 1996, 36, 103
- [77] K.M. Reddy, C. Song, *Stud. Surf. Sci. Catal.*, 1998, 117, 291
- [78] M.D. Alba, Z. Luan, J. Klinowski, *J. Phys. Chem.*, 1996, 100, 2178

- [79] T. Maschmeyer, F. Rey, G. Sankar, J.M. Thomas, *Nature*, 1995, 378, 159
- [80] P.T. Tanev, M. Chibwe, T.J. Pinnavaia, *Nature*, 1994, 368, 321
- [81] S. Gontier, A. Tuel, *Zeolites*, 1995, 15, 601
- [82] T. Blasco, A. Corma, M.T. Navarro, J.P. Pariente, *J. Catal.*, 1995, 156, 65
- [83] M. Morey, A. Davidson, G.D. Stucky, *Micropor. Mater.*, 1996, 6, 99
- [84] W. Zhang, T.J. Pinnavaia, *Catal. Lett.*, 1996, 38, 261
- [85] W. Zhang, M. Fr̄oba, J. Wang, P.T. Tanev, J. Wong, T.J. Pinnavaia, *J. Am. Chem. Soc.*, 1996, 118, 9164
- [86] G. Øye, J. Sjöblom, M. St̄ocker, *J. Disp. Sci. Technol.*, 2000, 27, 49
- [87] W.S. Ahn, D.H. Lee, T.J. Kim, J.H. Kim, G. Seo, R. Ryoo, *Appl. Cat. A Gen.*, 1999, 181, 39
- [88] C.H. Rhee, J.S. Lee, *Catal. Today*, 1997, 38, 213
- [89] E.W. Thomas, J.P.M. Niessen, T. Gjervan, W.F. Hölderich, *Micropor. Mesopor. Mater.*, 1998, 21, 67
- [90] A. Chenite, Y. Le Page, A. Sayari, *Chem. Mater.*, 1995, 7, 1015
- [91] J.S. Reddy, A. Sayari, *J. Chem. Soc. Chem. Commun.*, 1995, 21, 2231
- [92] M. Hartmann, S. Racouchot, C. Bischof, *Micropor. Mesopor. Mater.*, 1999, 27, 309
- [93] Á. Szegedi, M. Popova, V. Mavrodinova, M. Urbán, I. Kiricsi, C. Minchev, *Micro. Meso. Mater.*, 2007, 99, 149
- [94] J.F. Diaz, K.J. Balkus, F. Bedioui, V. Kurshev, L. Kevan, *Chem. Mater.*, 1997, 9, 61
- [95] S.C. Laha, R. Gläser, *Micro. Meso. Mater.*, 2007, 99, 159
- [96] Z.Y. Yuan, S.H. Liu, T.H. Chen, J.Z. Wang, H.X. Li, *J. Chem. Soc. Chem. Commun.*, 1995, 9, 973
- [97] C.F. Cheng, H. He, W. Zhou, J. Klinowski, J.A. Sousa Goncalves, L.F. Gladden, *J. Phys. Chem.*, 1996, 100, 390
- [98] C.F. Cheng, J. Klinowski, *J. Chem. Soc. Faraday Trans.*, 1996, 92, 289
- [99] D. Zhao, D. Goldfarb, *J. Chem. Soc. Chem. Commun.*, 1995, 8, 875
- [100] D.Y. Zhao, D. Goldfarb, *Stud. Surf. Sci. Catal.*, 1995, 97, 181
- [101] A. Sayari, I.L. Moudrakovski, C. Danumah, C.I. Ratcliffe, J.A. Ripmeester, K.F. Preston, *J. Phys. Chem.*, 1995, 99, 16373
- [102] A. Sayari, C. Danumah, I.L. Moudrakovski, *Chem. Mater.*, 1995, 7, 813
- [103] C. Şener, T. Doğu, G. Doğu, *Micro. Meso. Mater.*, 2006, 94, 89

- [104] K. Moller, T. Bein, *Chem. Mater.*, 1998, 10, 2950
- [105] C.-G. Wu, T. Bein, *Science*, 1994, 264, 175
- [106] T.Q. Nguyen, J.J. Wu, V. Doan, B.T. Schwartz, S.H. Tolbert, *Science*, 2000, 288, 652
- [107] X. Hu, S. Qiao, X.S. Zhao, G.Q. Lu, *Ind. Eng. Chem. Res.*, 2001, 40, 862
- [108] P. Selvam, S.K. Bhatia, C.G. Sonwane, *Ind. Eng. Chem. Res.*, 2001, 40, 3237
- [109] X.S. Zhao, G.Q. Lu, X. Hu, *Colloids Surf. A. Physicochem. Eng. Aspects*, 2001, 179, 261
- [110] X.S. Zhao, G.Q. Lu, *J. Phys. Chem. B*, 1998, 102, 1556
- [111] C. R. Buffler, *Microwave Cooking and Processing*, Van Nostrand Reinhold, New York, 1993, 1–68
- [112] Williams, N.H. *J. Microwave Power*, 1967, 2, 123
- [113] M. Bacci, M. Bini, A. Checcucci, A. Ignesti, L. Millanta, N. Rubino, R. Vanni, *J. Chem. Soc. Faraday Tans.* 1981, 77, 150
- [114] G. Roussy, P. Chenot, *J. Phys. Chem.*, 1981, 85, 2199
- [115] M.B. Chanaa, M. Lallemand, M.H. Simonotgrange, G. Bertrand, *Thermochim. Acta*, 1987, 115, 317
- [116] J.M. Thiebaut, C. Akyel, G. Roussy, R.G. Bosisio, *IEEE Trans. Instrument. Measurement*, 1988, 37, 114
- [117] M. Benchanaa, M. Lallemand, M.H. Simonotgrange, *Thermochim. Acta*, 1991, 175, 149
- [118] P. Chu, F.G. Dwyer, J.C. Vartuli, US Patent 4,778,666, 1988
- [119] C.S. Cundy, *Collect Czech. Chem. Commun.*, 1998, 63, 1699
- [120] B. Sakintuna, PhD Dissertation, "Synthesis and characterization of porous carbons using natural zeolites and  $\text{AlPO}_4\text{-5}$  as templates and diffusion of volatile organic chemicals in porous media", Sabanci University, June 2005
- [121] D.M.P. Mingos, D.R. Baghurst, *Chem. Soc. Rev.*, 1991, 20, 1
- [122] A.G. Whittaker, D.M.P. Mingos, *J. Microwave Power Elektromag. Energy*, 1994, 29, 195
- [123] D.M.P. Mingos, *Res. Chem. Intermed.*, 1994, 20, 85
- [124] D.M.P. Mingos, *Chem. Ind. (London)*, 1994, 596
- [125] C. Gabriel, S. Gabriel, E.H. Grant, B.S.J. Halstead, D.M.P. Mingos, *Chem. Soc. Rev.*, 1998, 27, 213
- [126] J. Berlan, *Radiat. Phys. Chem.*, 1995, 45, 581

- [127] D.M.P. Mingos, D.G. Baghurst, Microwave Enhanced Chemistry, ed. H.M. Kingston and St. J. Haswell, ACS, Washington, DC, 1997, p. 3
- [128] P. Lindström, J. Tieney, B. Wathey, J. Westmann, Tetrahedron, 2001, 57, 9225
- [129] W. Lautenschläger and T. Schweizer, Laborpraxis, 1990, 5, 376
- [130] C.S. Cundy, Collect Czech. Chem. Commun., 1998, 63, 1699
- [131] M. Nüchter, B. Ondruschka, W. Bonrath, A. Gum, Green Chem., 2004, 6, 128
- [132] Ch. R. Strauss, R.W. Trainor, Aust. J. Chem., 1995, 48, 1665
- [133] <http://www.peuschner.com/dt/basics>
- [134] G.A. Tompsett, W.C. Conner, K.S. Yngvesson, Chem.Phys. Chem., 2006, 7, 296
- [135] T. Brar, P. France, P. G. Smirniotis, Ind. Eng. Chem. Res. 2001, 40, 1133
- [136] D. Baek, U. Y. Hwang, K. S. Lee, Y. Shul, K. K. Koo, J. Ind. Eng. Chem. 2001, 7, 241–249
- [137] J. Cai, J. Liu, Z. Gao, A. Navrotsky, S. L. Suib, Chem. Mater. 2001, 13, 4595
- [138] J. Chen, D. K. Sun, S. C. Dong, M. Huang, Q. H. Xu, Chin. J. Inorg. Chem., 2000, 16, 769–774
- [139] C. S. Cundy, R. J. Plaisted, J. P. Zhao, Chem. Commun. 1998, 1465
- [140] J. H. Koegler, A. Arafat, H. van Bekkum, J. C. Jansen in Progress in Zeolite and Microporous Materials, Proceedings of the 11th International Zeolite Conference, Seoul, Korea, 1996, Pts. A–C, Vol. 105, 1997, 2163
- [141] P. M. Slangen, J. C. Jansen, H. van Bekkum, Microporous Mater., 1997, 9, 259
- [142] J. P. Zhao, C. Cundy, J. Dwyer in Progress in Zeolite and Microporous Materials, Proceedings of the 11th International Zeolite Conference, Seoul, Korea, 1996, Pts.A–C, Vol. 105, 1997, 181
- [143] X. H. Xu, W. H. Yang, J. Liu, L. W. Lin, Sep. Purif. Technol. 2001, 25, 241
- [144] F. Mizukami in Porous Materials in Environmentally Friendly Processes, Vol. 125, Proceedings of the 1<sup>st</sup> International FEZA Conference, Eger, Hungary, 1999,1
- [145] T. G. Tsai, H. C. Shih, S. J. Liao, K. J. Chao, Microporous Mesoporous Mater., 1998, 22, 333–341
- [146] H. Wang, H. R. Zhang, J. J. Zhu, J. Cryst. Growth 2001, 233, 829–836
- [147] A. Arafat, J. C. Jansen, A. R. Ebaid, H. Vanbekkum, Zeolites, 1993, 13, 162
- [148] C. Chang, W. Y. Zhang, L. H. Zhang, R. S. Li, M. W. Tian, X. W. Yang, L. Hou, Chem. J. Chin. Univ. 1996, 17, 1914–1917

- [149] Introduction to Green Chemistry (Eds.: M. A. Ryan, M. Tinnesand), American Chemical Society, Washington DC, 2002
- [150] C-G. Wu, T.Bein, Chem. Commun., 1996, 925
- [151] S-E. Park, D.S. Kim, J-S. Chang, W. Y. Kim, Catalysis Today, 1998, 44, 301-308
- [152] D.S. Kim, J-S. Chang, W. Y. Kim, H.Y. Kim, S-E. Park, Bull. Korean Chem. Soc., 1999, 20, 408
- [153] U. Oberhagemann, M.Jeschke, H. Papp, 1999, Micro. Mesop. Mater., 33, 165-172
- [154] S.-E. Park, D.S. Kim, J.-S. Chang, W.Y. Kim in L. Bonneviot, F. Beland, C. Danumah, S. Giasson, S. Kaliaguine (Eds.), Mesoporous Molecular Sieves, 1998, Stud. Surf. Sci. Catal., Vol. 117, 1998, 265
- [155] M. Sung-Suh, D.E.S. Kim, Y-K. Park, S.-E. Park, J. Ind. Eng. Chem., 1999, 5, 191
- [156] H.M. Sung-Suh, D.E.S. Kim, Y-K. Park, S.-E. Park, Res. Chem. Intermed., 2000, 26, 283-294
- [157] Y. K. Hwang, J.-S. Chang, Y.-U. Kwon, S.-E. Park, Stud. Sur. Sci. Catal., 2003, 146, 101
- [158] S.H. Jhung, J.-S. Chang, YK Hwang, S.-E. Park, J. Mater. Chem., 2004, 14, 280
- [159] S.-E. Park, Y. K. Hwang, D.S. Kim, J.S. Chang, J.S. Hwang, S.H. Jhung in B. Zhou, S. Hermans, G.A. Somorjai (Eds.), Nanostructure Science and Technology, 2004, Nanotechnology in Catalysis, Vol. 1, 2004, , 329-343
- [160] CAO Yuan, et al., Trans. Nonferrous Met. Soc. China, 2009, 19, 656
- [161] K. Kang, C. Park, W. Ahn, Catalysis Letters, 1999, 59, 45-49
- [162] S.C Laha, R.Glaser, Micro. Mesop. Mater., 2007, 99, 159-166
- [163] T. Jiang, Y, Tang, Q. Zhao, H. Yin, Colloids and Surfaces A: Physicochem. Eng. Aspects, 2008, 315, 299-303
- [164] T. Jiang, Q. Zhao, K. Chen, Y. Tang, L. Yu and H. Yin, Applied Surface Science, 2008, 254, 2575-2580
- [165] T. Jiang, W. Shen, Q. Zhao, M. Li, J. Chu, H. Yin, Journal of Solid State Chemistry, 2008, 181, 2298-2305
- [166] Q. Zhao, Q. Wang, Y. Tang, T. Jiang, C.Li, H. Yin, Korean J. Chem. Eng., 2010, 27, 1310-1315
- [167] J. He, X. Yang, D.G. Evans, X. Duan, Materials Chemistry and Physics, 2002, 77, 270-275
- [168] M. Nüchter, B. Ondruschka, W. Bonrath, A. Gum, Green Chem., 2004, 128-141

- [169] A. Nalbant, T. Doğu, S. Balcı, *Journal of Nanoscience and Nanotechnology*, 2008, 8, 549
- [170] G. Øye, J. Sjoblom, M. Stocker, *Advances in Colloid and Interface Science* 89-90,2001, 439-466
- [171] U. Ciesla, F. Schüth, *Micro. Meso. Mater.*, 1999, 27, 131
- [172] Q. Huo, D.I. Margolese, G.D. Stucky, *Chem. Mater.*, 1996, 8, 1147
- [173] V.B. Fenelonov, V.N. Romannikov, A.Yu. Derevyankin, *Micro. Meso. Mater.*, 1999, 28, 57
- [174] O. Terasaki, T. Ohsuna, Z.Liu, Y.Sakamoto, A.E. Garcia-Bennett, *Stud. Surf. Sci. Catal.*, 2004, 148, 261
- [175] B.D. Cullity, S.R. Stock, *Elements of X-ray Diffraction*, 3<sup>rd</sup> Edition, Prentice Hall Inc., 2001
- [176] C.Y. Chen, S.-Q. Xiao, M.E. Davis, *Microporous Mater.*, 1995, 4, 1
- [177] V. Alfredsson, M. Keung, A. Monnier, G.D. Stucky, K.K. Unger, F. Schüth, *J. Chem. Soc., Chem. Commun.*, 1994, 921
- [178] H.W. Kroto, J.R. Heath, S.C. Obrien, R.F. Curl, R.E. Smalley, *Nature*, 1985, 318, 162
- [179] R.E. Smalley, National Institute of Standards and Technology, Dec. 6-7, 1990
- [180] M.S. Dresselhaus, Oral presentation at fullerene workshop, University of Pennsylvania, 1991
- [181] S. Iijima, *Nature*, 1991, 354, 56
- [182] S Iijima and T Ichihashi *Nature*, 1993, 363, 603
- [183] D.S. Bethune, C.H. Klang, M. S. De Vries, G.Gorman, R. Savoy, J. Vazquez, R. Beyers, *Nature*, 1993, 363, 605
- [184] R. Bacon, *Journal of Applied Physics*, 1960, 31, 283
- [185] A. Oberlin, M. Endo, T. Koyama, *Journal of Crystal Growth*, 1976, 32, 335
- [186] T.W. Ebbesen, P.M. Ajayan, *Nature*, 1993, 358, 220
- [187] R. Saito, M. Fujita, G. Dresselhaus, and M. S Dresselhaus, *Appl. Phys. Lett.*, 1992, 60, 2204
- [188] M.J. O'Connell, *Carbon Nanotubes Properties and Applications*, 2006, CRC Press Taylor & Francis Group, Boca Raton, USA
- [189] A.M. Rao, E. Richter, S. Bandow, B. Chase, P.C. Eklund, K.A. Williams, S. Fang, K.R. subbaswamy, M. Menon, A. Thess, R.E. Smalley, G. Dresselhaus, M.S. Dresselhaus, *Science*, 1997, 275, 187

- [190] H. Kataura, Y. Kumazawa, Y. Maniwa, I. Umezu, S. Suzuki, Y. Ohtsuka, Y. Achiba, *Synthetic Metals*, 1991, 103, 2555
- [191] S. Farhat, M.L. de La Chapelle, A. Loiseau, C.D. Scott, S. Lefrant, C. Journet, P. Bernier, *J. Chem. Phys. Lett.*, 1996, 260, 471
- [192] E.I. Waldorff, A.M. Wass, P.P. Friedmanni M. Keidar, *J. Appl. Phys.*, 2004, 95, 2749
- [193] A. Thess, R. Lee, P. Nikolaev, H. Dai, P. Petit, J. Robert, C.H. Xu, Y. H. Lee, S. G. Kim, A. G. Rinzler, D. T. Colbert, G. Scuseria, D. Tomanek, J. E. Fischer and R.E. Smalley, *Science*, 1996, 273, 483
- [194] M. Endo, K. Takeuchi, S. Igarashi, K. Kobori, M. Shiraishi, H.W. Kroto, *J. Phys. Chem. Solids*, 1993, 54, 1841
- [195] H. Dai, A.G. Rinzler, P. Nikolaev, A. Thess, D.T. Colbert, R.E. Smalley, *Chem. Phys. Lett.*, 1996, 260, 471
- [196] J. Kong, H.T. Soh, A.M. Cassell, C.F. Quate, H.J. Dai, *Nature*, 1998, 395, 878
- [197] W. Kim, H.C. Choi, M. Shim, Y.M. Li, D.W. Wang, H.J. Dai, *Nano Letters*, 2002, 2 703
- [198] B.C. Satishkumar, A. Govindaraj, R. Sen, C.N.R. Rao, *Chem. Phys. Lett.*, 1998, 293, 47
- [199] S. Maruyama, R. Kojima, Y. Miyauchi, S. Chiashi, M. Kohno, *Chem. Phys. Lett.*, 2002, 360, 229
- [200] S. Bai, F. Li, Q.H. Yang, H.M. Cheng, J. Bai, *Chem. Phys. Lett.*, 2003, 376, 83
- [201] A.M. Cassell, J.A. Raymakers, J. Kong, H.J. Dai, *J. Phys. Chem. B*, 1999, 103, 6484
- [202] S.C. Lyu, B.C. Liu, S.H. Lee, C.Y. Park, H.K. Kang, C.W. Yang, C.J. Lee, *J. Phys. Chem. B*, 2004, 108, 1613
- [203] N. Wang, Z.K. Tang, G.D. Li, J.S. Chen, *Nature*, 2000, 408, 50
- [204] P.B. Amama, S. Lim, D. Ciuparu, Y. Yang, L. Pfefferle, G.L. Haller, *J. Phys. Chem. B*, 2005, 109, 2645
- [205] S. Lim, D. Ciuparu, C. Pak, F. Dobek, Y. Chen, D. Harding, L. Pfefferle, G.L. Haller, *J. Phys. Chem. B*, 2003, 107, 11048
- [206] P. Ramesh, N. Kishi, T. Sugai, H. Shinohara, *J. Phys. Chem. B*, 2006, 110, 130
- [207] T. Somanathan, A. Pandurangan, *Applied Surface Science*, 2008, 254, 5643

- [208] A. Jorio, M.D. Dresselhaus, G. Dresselhaus, Topics in Applied Physics: Carbon Nanotubes Advanced Topics in the Synthesis, Structure, Properties and Applications, Springer-Verlag: Berlin Heidelberg, 2008
- [209] S. Arepalli, P. Nikolaev, O. Gorelik, V.G. Hadjiev, W. Holmes, B. Files, L. Yowell, Carbon, 2004, 42, 1783
- [210] 2<sup>nd</sup> Joint Workshop on Measurement Issues in Single Wall Carbon Nanotubes: Purity and Dispersion Part II (NIST Gaithersburg 2005) URL: [http://www.msel.nist.gov/Nanotube2/Carbon\\_NAnotubes.htm](http://www.msel.nist.gov/Nanotube2/Carbon_NAnotubes.htm)
- [211] First International Forum on the Metrology, Standardization and Industrial Quality of Carbon Nanotubes (INMETRO Rio de Janeiro 2007) URL: <http://www.inmetro.gov.br/msin07>
- [212] Third NASA-NIST Workshop on Nanotube Measurements (NIST Gaithersburg 2007) URL: <http://polymers.nist.gov/Nanotube3/Workshop3.htm>
- [213] T. Somanathan, A. Pandurangan, Applied Surface Science, 2008, 254, 5643
- [214] M.S. Dresselhaus, G. Dresselhaus, R. Saito, A. Jorio, Physics Reports, 2005, 409, 47
- [215] A. Jorio, M.A. Pimenta, A.G. Souza Filho, R. Saito, G. Dresselhaus, M.S. Dresselhaus, New J. Phys., 2003, 5, 1.1
- [216] S.H. Shiao, C.W. Liu, C. Gau, B. T. Dai, Nanotechnology, 2008, 19, 105303
- [217] P.T. Araujo, S.K. Doorn, S. Kilina, D. Tretiak, E. Einarsson, S. Maruyama, H. Chacham, M.A. Pimenta, A. Jorio, Phys. Rev. Lett., 2007, 98, 067401
- [218] C. Fantini, A. Jorio, M. Souza, M.S. Strano, M.S. Dresselhaus, M.A. Pimenta, Phys. Rev. Lett., 2004, 93, 147406
- [219] A. Jorio, A.G. Souza Filho, G. Dresselhaus, M.S. Dresselhaus, A.K. Swan, M.S. Ünlü, B. Goldberg, M.A. Pimenta, J.H. Hafner, C.M. Lieber, R. Saito, Phys. Rev. B, 2002, 65, 155412
- [220] L.G. Cançado, M.A. Pimenta, B.R.A. Neves, M.S.S. Dantas, A.Jorio, Phys. Rev. Lett., 2004, 93, 247401
- [221] Z. Zhang, C.M. Lieber, Appl. Phys. Lett., 1993, 62, 2792
- [222] C.H. Olk, J.P. HERemans, J. Mater. Res., 1994, 9, 259
- [223] M. Ge, K. Sattler, Science, 1993, 260, 515
- [224] D.L. Carroll, P. Redlich, P.M. Ajayan, J.C. Charlier, X. Blase, A. De Vita, R. Car, Phys. Rev. Lett., 1997, 78, 2811
- [225] M. Ge, K. Sattler, Appl. Phys. Lett., 1994, 65, 2284

- [226] A. Hassanien, M. Tokumoto, Y. Kumazawa, H. Kataura, Y. Maniwa, S. Suzuki, Y. Achiba, *Appl. Phys. Lett.*, 1998, 73, 3839
- [227] J.W.G. Wilder, L.C.Venema, A.G. Rinzler, R.E. Smalley, C. Dekker, *Nature*, 1998, 391, 59
- [228] T.W. Odom, J.-L. Huang, P. Kim, C.M. Lieber, *Nature*, 391, 62
- [229] A. Hassanien, M. Tokumoto, P. Umek, D. Mihilovic, A. Mrzel, *Appl. Phys. Lett.*, 2001, 78, 808
- [230] R.A. Jishi, M.S. Dresselhaus, G. Dresselhaus, *Phys. Rev. B*, 1993, 48, 11385
- [231] R.M. Barrer, D.M. Grove, *Trans. Faraday Soc.*, 1951, 47, 826
- [232] E.R. Gilliland, R.F. Baddour, J.L. Russell, *AIChE J.* 1958, 4, 90
- [233] P.C. Carman, P. Le R. Malherbe, *Proc. R. Soc. London, Ser. A*, 1950, 203, 165
- [234] C.G. Pope, *Trans. Faraday Soc.* 1967, 63, 734
- [235] J.K. Kelly, O.M. Fuller, *Ind. Eng. Chem. Fundam.* 1980, 19, 11
- [236] R. Aris, *Ind. Eng. Chem. Fundam.* 1983, 22, 150
- [237] R.M. Barrer, *Faraday Discuss.* 1948, 3, 61
- [238] D.M. Ruthven, *Principles of Adsorption and Adsorption Processes*; Wiley: New York, 1984
- [239] H. Pfeifer, *NMR Basic Principles and Progress*; Springer-Verlag: Berlin, 1972, Vol. 7
- [240] J. Kärger, H. Pfeifer, W. Heink, *Adv. Magn. Res.*, 1988, 12, 1
- [241] D.M. Ruthven, *ACS Symp. Ser.*, 1977, 40, 320
- [242] J. Kärger, D.M. Ruthven, *Zeolites* 1989, 9, 267
- [243] J. Kärger, D.M. Ruthven, *Stud. Surf. Sci. Catal.* 1997, 105, 1843
- [244] D. M. Ruthven, *Principles of Adsorption and Adsorption Processes*, John Wiley & Sons, New York, 1984
- [245] J. Kärger and H. Pfeifer, *Zeolites*, 1987, 7, 90
- [246] H. Jobic, M. Beé, and G. J. Kearley, *J. Phys. Chem.*, 1994, 98, 4660
- [247] M. Seferinoğlu, Y. Yürüm, *Energy & Fuels*, 2001, 15, 135
- [248] M. Seferinoğlu, Y. Yürüm, *Energy & Fuels*, 2006, 20, 1150
- [249] B. Sakintuna, O. Çuhadar, Y. Yürüm, *Energy & Fuels*, 2005, 19, 2219
- [250] B. Sakintuna, O. Çuhadar, Y. Yürüm, *Energy & Fuels*, 2006, 20, 1269
- [251] W. Jost, *Diffusion in Solids, Liquids and Gases*, Academic Press, New York, 1960

- [252] R. Reif, *Fundamentals of Statistical and Thermal Physics*, McGraw-Hill, Boston, 1965
- [253] W. Kauzmann, *Kinetic Theory for Atoms in Crystals*, Van Nostrand, Princeton, 1968
- [254] J. Crank, *The Mathematics of Diffusion*, 2<sup>nd</sup> Edition, Oxford University Press, Oxford, 1975
- [255] B.S. Bokstein, M.I. Mendeleev, D.J. Srolovitz, *Thermodynamics and Kinetics in Material Science*, Oxford University Press, Oxford, 2005
- [256] D.M. Ruthven, *Principles of Adsorption and Adsorption Processes*, Butterworths, Boston, 1987
- [257] M.F.M. Post, *Stud. Surf. Sci. Catal.*, 1991, 58, 391
- [258] J. Xiao, J. Wei, *Chem. Eng. Sci.*, 1992, 47, 1123
- [259] N.Y. Chen, T.F. Jr. Degnan, C.M. Smith, *Molecular Transport and Reaction in Zeolites*, VCH Publishers, New York, 1994
- [260] R.T. Yang, *Gas Separation by Adsorption Processes*, Butterworths, Boston, 1987
- [261] A. Einstein, *Ann. Phys.*, 1855, 94, 59
- [262] J. Karger, D.M. Ruthven, *Diffusion in Zeolites and Other Microporous Solids*, J. Wiley & Sons, New York, 1992
- [263] R.B. Bird, W.E. Stewart, E.N. Lightfoot, *Transport Phenomena*, 2<sup>nd</sup> Edition, J. Wiley & Sons, New York, 2002
- [264] P. Brauer, S. Fritzsche, J. Karger, G. Schutz, S. Vasenkov, *Lect. Notes Phys.*, 2004, 634, 89
- [265] P. Heitjans, J. Karger (Eds.), *Diffusion in Condensed Matter*, Springer, Berlin, 2005
- [266] A. Fick, *Ann. Phys.*, 1855, 94, 59
- [267] L. Onsager, *Phys. Rev.*, 1931, 37, 405
- [268] L. Onsager, *Phys. Rev.*, 1932, 38, 2265
- [269] R.M.A. Roque-Malherbe, *Adsorption and diffusion in Nanoporous Materials*, CRC Press, Taylor & Francis Group, Boca Raton, USA, 2007
- [270] R. Roque-Malherbe, *Micro. Meso. Mater.*, 2000, 41, 227
- [271] J. Karger, S. Vasenkov, S.M. Auerbach, in *Handbook of Zeolite Science and Technology*, S. Auerbach, K.A. Carrado, P.K. Dutta (Eds.), Marcell Dekker Inc., New York, 2003, p. 341
- [272] D.M. Ruthven, M. Eic, *Zeolites*, 1988, 8, 40

- [273] Y. Yasuda, *J. Phys. Chem.*, 1982, 86, 1913
- [274] N.G. van den Begin, L.V.C. Rees, *Stud. Surf. Sci. Catal.*, 1989, 49B, 915
- [275] H.G. Karge, W. Niessen, *Catal. Today*, 1991, 8, 451
- [276] W. Niessen, H.G. Harge, *Stud. Surf. Sci. Catal.*, 1991, 60, 213
- [277] R. Roque-Malherbe, R. Wendelbo, A. Mifsud, A. Corma, *J. Phys. Chem.*, 1995, 99, 14064
- [278] R. Roque-Malherbe, *Micro. Meso. Mater.*, 2002, 56, 321
- [279] R. Roque-Malherbe, V. Ivanov, *Micro. Meso. Mater.*, 2001, 47, 25
- [280] G. Sastre, N. Raj, C. Richard, C. Catlow, R. Roque-Malherbe, A. Corma, *J. Phys. Chem. B*, 1998, 102, 3198
- [281] R. Wendelbo, R. Roque-Malherbe, *Mic. Mat.*, 1997, 10, 231
- [282] H. Pfeifer, in *NMR Basic Principles*, P. Diehl, E. Fluck, R. Kosfeld (Eds.), Springer, Berlin, 1972, p. 53
- [283] J. Karger, *J. Surf. Sci.*, 1973, 36, 797
- [284] A. Burggraaf, *Fundamentals of Inorganic Membrane Science and Technology*, in: A. Burggraaf, L. Cot, (Eds.), *Membrane Science and Technology Series 4*. Elsevier, Amsterdam, 1996
- [285] C.N. Satterfield, *Heterogeneous Catalysis in Practice*, Mc Graw-Hill, New York, 1980
- [286] M.R. Wang, Z.X. Li, *Phys. Rev. E.*, 2003, 68, 046704
- [287] J.-G Choi, D.D. Do, H.D. Do, *Ind. Eng. Chem. Res.*, 2001, 40, 4005
- [288] S.-T Hwang, K. Kammermeyer, *Techniques in Chemistry: Membranes in Separation*, J. Wiley & Sons, New York, 1975
- [289] A. Kapoor, R.T. Yang, C. Wong, *Catal. Rev. Sci. Eng.*, 1989, 129, 31
- [290] P.J. Hall, K.M. Thomas, H. Marsh, *Fuel*, 1992, 71, 1271
- [291] N.A. Peppas, L.M. Lucht, *Chem. Eng. Commun.*, 1985, 37, 333
- [292] V.J. Inglezakis, H.P. Grigoropoulou, *J. Colloid Interface Sci*, 2001, 234, 434
- [293] J. Crank, *The Mathematics of Diffusion*, London, Clarendon Press, Oxford, 1976
- [294] F.E. Ndaji, K.M. Thomas, *Fuel*, 1993, 72, 1525
- [295] J.M. Thomas, W.J. Thomas, *Principles and Practice of Heterogeneous Catalysis*, VCH Publishers Inc., New York, 1996
- [296] J. Karger, P. Heitjans, R. Haberlandt, *Diffusion in Condensed Matter*, Braunschweig/Weisbaden: Vieweg, 1998
- [297] L. Riekert, *Adv. Catal.*, 1970, 21, 281

- [298] N.A. Peppas, N.M. Franson, *Polymer Phys. Ed.*, 1983, 21, 983
- [299] Y. Otake, E.M. Suuberg, *Energy Fuels*, 1997, 11, 1155
- [300] H. Gao, M. Nolura, S. Murata, L. Artok, *Energy Fuels*, 1999, 13, 518
- [301] C.A. Koh, R. Nooney, S. Tahir, *Catal. Lett.*, 1997, 47, 199
- [302] A. S. Araujo, M. Jaroniec, *Thermochimica Acta*, 2000, 363, 175
- [303] V.L. Zholobenko, S.M. Holmes, C.S. Cundy, J. Dwyer, *Micropor. Mesopr. Mater.*, 1998, 11, 83
- [304] S. M. Holmes, V. L. Zholobenko, A. Thursfield, R. J. Plaisted, C. S. Cundy, J. Dwyer, *J. Chem. Soc., Faraday Trans.*, 1998, 94, 2025
- [305] K. Hadjiivanov, T. Tsoncheva, M. Dimitrov, C. Minchev and H. Knözinger, *Appl. Catal. A: General*, 2003, 241, 331
- [306] Qiang Wu, Xijun Hu, Po Lock Yue, Xiu Song Zhao and Gao Qing Lu, *Appl. Catal. B: Environmental*, 2001, 32, 151
- [307] M. Broyer, J.P. Bellat, O. Heintz, C. Paulin, S. Valange and Z. Gabelica, *Stud. Surf. Sci. Catal.*, 2002, 142, 1101
- [308] Z. Ozaydin, S. Yasyerli, G. Doğu, *Ind. Eng. Chem. Res.*, 2008, 47, 1035
- [309] G. Zhang, J. Long, X. Wang, Z. Zhang, W. Dai, P. Liu, Z. Li, L. Wu, X. Fu, *Langmuir*, 2010, 26, 1362
- [310] J.S. Jung, W.S. Chae, R.A. McIntyre, C.T. Seip, J.B. Wiley, C.J. O'Connor, *Mater. Res. Bul.*, 1999, 34, 1353
- [311] R. M. Krishna, L. Kevan, *Phys. Chem. Chem. Phys.*, 2001, 3, 5348
- [312] M. Hartmann, A. Pöppel, L. Kevan, *J. Phys. Chem.*, 1996, 100, 9906
- [313] T. Kang, Y. Park, J. Yi, *J. Mol. Catal. A: Chem.*, 2006, 244, 151
- [314] S. Banerjee, A. Santhanam, A. Dhathathreyan, P.M. Rao, *Langmuir*, 2003, 13, 5522
- [315] S. Suvanto, J. Hukkamäki, T.T. Pakkanen, T.A. Pakkanen, *Langmuir*, 2000, 16, 4109
- [316] Z. Deng, G.R. Dieckmann, S.H. Langer, *Chem. Commun.*, 1997, 1789
- [317] A. Jentys, N.H. Pham, H. Vinek, M. English, J.A. Lercher, *Micropor. Mesopr. Mater.*, 1996, 6, 13
- [318] J. El Haskouri, S. Cabrera, C.J. Gomez-Garcia, C. Guillem, J. Latorre, A. Beltran, D. Beltran, M.D. Marcos, P. Amoros, *Chem.Mater.*, 2004, 16, 2805
- [319] S.Y. Lim, D. Ciuparu, C.H. Pak, F. Dobek, Y. Chen, D. Harding, L. Pfefferle, G. Haller, *J. Phys. Chem. B*, 2003, 107, 11048

- [320] W.A. Carvalho, M. Wallau, U. Schuhardt, *J. Mol. Catal. A*, 1999, 144, 91-99
- [321] S.-T. Wong, J.F. Lee, S. Cheng, C.-Y. Mou, *Appl. Catal. A*, 2000, 198, 115
- [322] N.X. He, S.L. Bao, Q.H. Xu, in H. Chou, S.K. Ihm, Y.S. Uh (Eds.), *Stud. Surf. Sci. Catal.*, 1997, 105, 85
- [323] A. De Stafanis, S. Kaciulis, L. Pandolfini, *Micropor. Mesopor. Mater.*, 2007, 99, 140
- [324] N. Gokulakrishnan, A. Pandurangan, P.K. Sinha, *J. Chem. Technol. Biotechnol.*, 2007, 82, 25
- [325] M. Stockenhuber, *Micropore Mesopore Mat.*, 2001, 44-45, 367
- [326] S. Anandan, M. Okazaki, *Micropore Mesopore Mat.*, 2005, 87, 77
- [327] A.I. Skoulidas, D.M. Ackerman, J.K. Johnson, D.S. Sholl, *Phys. Rev. Lett.*, 2002, 89, 185901
- [328] D.M. Ackerman, A.I. Skoulidas, D.S. Sholl, J.K. Johnson, *Mol.Simul.*, 2003, 29, 677
- [329] V.P. Sokhan, D. Nicholson, N. Quirke, *J. Chem. Phys.*, 2004, 120, 3855
- [330] H. Chen, D. S. Sholl, *J. Am. Chem. Soc.*, 2004, 126, 7778
- [331] P.J. Branton, P.G. Hall, K.S.W. Sing, H. Reichert, F. Schüth, K.K. Unger, *J. Chem. Soc., Faraday Trans.* 1994, 90, 2965
- [332] P.L. Liewellyn, Y. Grillet, F. Schüth, H. Reichert, K.K. Unger, *Microp. Mesop. Mater.* 1994, 3, 345
- [333] Zhu, H. Y.; Zhao, X. S.; Lu, G. Q.; Do, D. D. *Langmuir* **1996**, 12, 6513.
- [334] M. Kruk, M. Jaroniec, A. Sayari, *J. Phys. Chem. B* 1997, 101, 583
- [335] P.I. Ravicovitch, D. Wei, W.T. Chuch, G.L. Haller, A.V. Neimark, *J. Phys. Chem. B* 1997, 101, 3671
- [336] P.L. Llewellyn, F. Schüth, Y.Grillet, F. Rouquerol, J. Rouquerol, K.K. Unger, *Langmuir* 1995, 11, 574
- [337] A. Cauvel, D. Brunel, F. Di Renzo, E. Garrone, B. Fubini, *Langmuir* 1997, 13, 2773
- [338] J. Janchen, H. Stach, M. Busio, J.H.M.C. Van Wolput, *Thermochim. Acta* 1998, 312, 33
- [339] C. Nguyen, C.G. Sonwane, S.K. Bhatia, D.D. Do, *Langmuir*, 1998, 14, 4950
- [340] T. Boger, R. Roesky, R. Glaeser, S. Ernst, G. Eigenberger, Wietkamp, J. *Microporous Mater.* 1997, 8, 79

- [341] J. Rathousky, A. Zukal, O. Franke, G. Schulz-Ekloff, G. J. Chem.Soc., Faraday Trans. 1995, 91, 937
- [342] O. Franke, G. Schulz-Ekloff, J. Rathousky, J. Starech, A. Zukal, J. Chem. Soc., Chem. Commun. 1993, 724
- [343] J. Rathousky, A. Zukal, O. Franke, G. Schulz-Ekloff, J. Chem. Soc., Faraday Trans. 1995, 91, 937
- [344] O. Franke, G. Schulz-Ekloff, J. Rathousky, J. Starech, A. Zukal, J. Chem. Soc., Chem. Commun. 1993, 724
- [345] Glaser, R.; Roesky, R.; Boger, J.; Eigerberger, G.; Ernst, S.; Weitkamp, J. Stud. Surf. Sci. Catal. 1997, 105A, 695
- [346] Maddox, M. W.; Sowers, S. L.; Gubbins, K. E. Adsorption 1996, 2, 23
- [347] Loneva, M. A.; Newman, G. K.; Harwell, J. H. AIChE Symp. Ser. 1995, 309, 40
- [348] S. Wang, Z.-fei Ma, H.-qing Yao, Chem. Eng. Sci., 2009, 24, 1318
- [349] V.-Thang Hoang, Q. Huang, A. Malekian, M. Eic, T-On Do, S. Kaliaguine, Adsorption, 2006, 11, 421

## APPENDIX A

### A.1 Exxon Mobil Patents on Selected Applications of M41S Molecular Sieves [26]

**Table A-1** Selected Exxon Mobil Patents on Catalytic Applications

U.S. Patent Number	Description
5,134,243	Olefin Oligomerization over MCM-41
5,174,888	Organic conversion over M41S
5,183,561	Hydrocracking using M41S/Zeolite Combined Catalyst
5,196,633	Organic Conversion over MCM-41
5,238,676	Post-synthesis Addition of Activating Metals to M41S
5,264,641	Aromatic Saturation over M41S Materials
5,451,312	Use of M41S Materials to Produce Low Aromatic Distillates
5,475,178	Organic Conversion over Heteropoly Acid Catalysts Supported on M41S Materials
5,837,639	Metal-containing M41S Compositions as Hydroprocessing Catalysts

**Table A-2** Selected Exxon Mobil Patents on Other Applications

U.S. Patent Number	Description
5,143,707	Use of M41S in NO <sub>x</sub> Reduction
5,220,101	Sorption/Separation
5,348,687	M41S Materials Having Nonlinear Optical Properties
5,364,797	Sensor Device Containing M41S
5,378,440	Separation over M41S Material

## A.2 TGA analysis of MCM-41

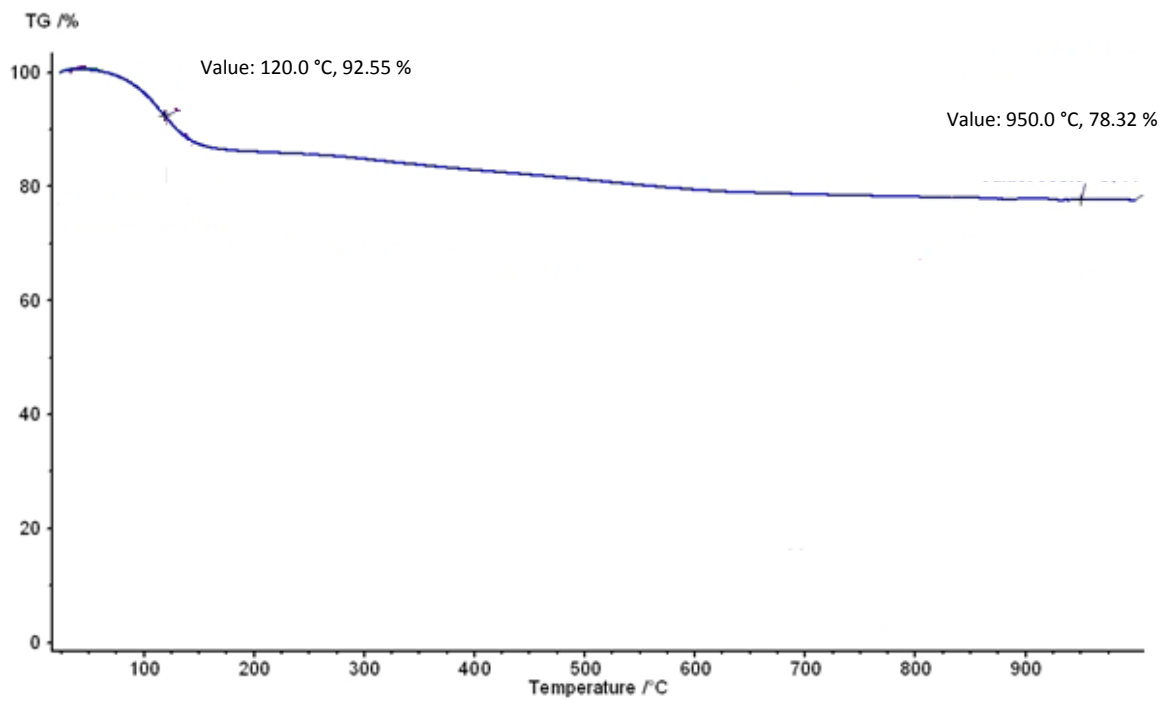


**Figure A-1** TGA thermogram of MCM-41 (120/30)

## APPENDIX B

### B.1 Calculating Diffusion Coefficients

The uptake measurements of volatile solvents into the mesoporous structures were recorded until the equilibrium was attained. As an example, ethanol uptake measurement in MCM-41 at 26 °C was given in Figure B-1.

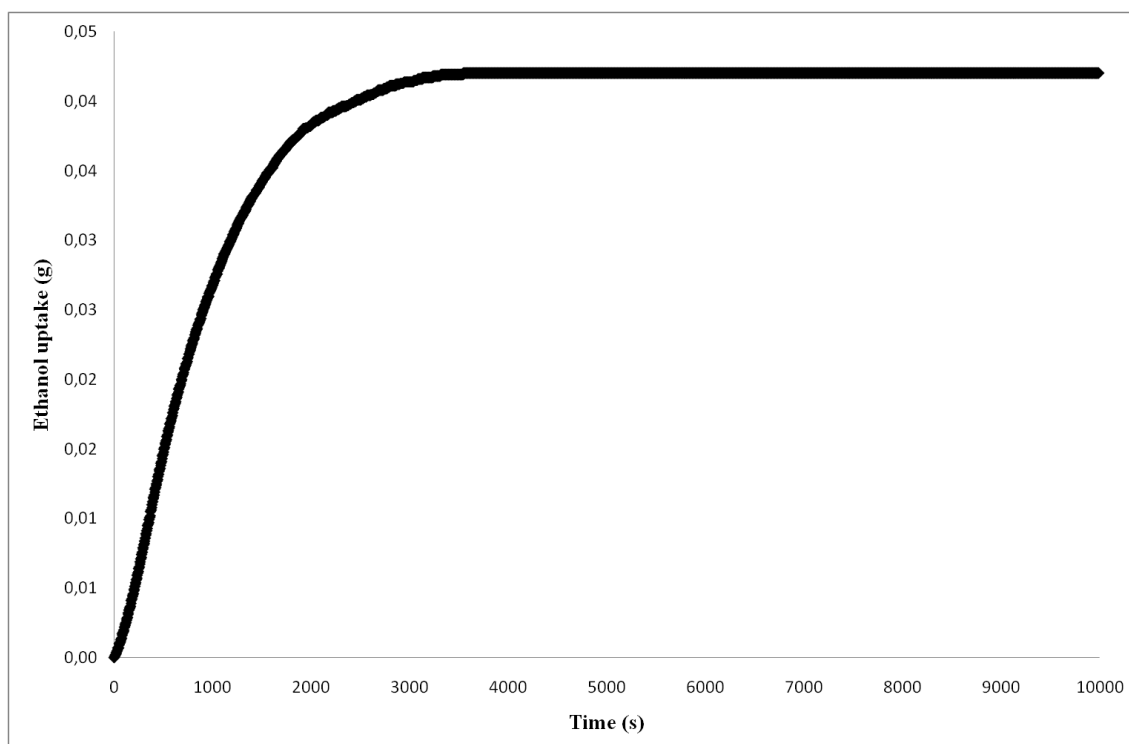


**Figure B-1** Ethanol uptake of MCM-41 at 26 °C

All the calculations based on diffusion coefficients and activation energies were calculated from the region where diffusion was assumed to be occurred linearly during the first 60 percent of the ramp of uptake versus time graph.

Graphs of  $M_t/M_\infty$  versus  $t^{1/2}$  for the solvent diffusion in mesopores were plotted in order to calculate the coefficient of diffusion (Figure B-2).

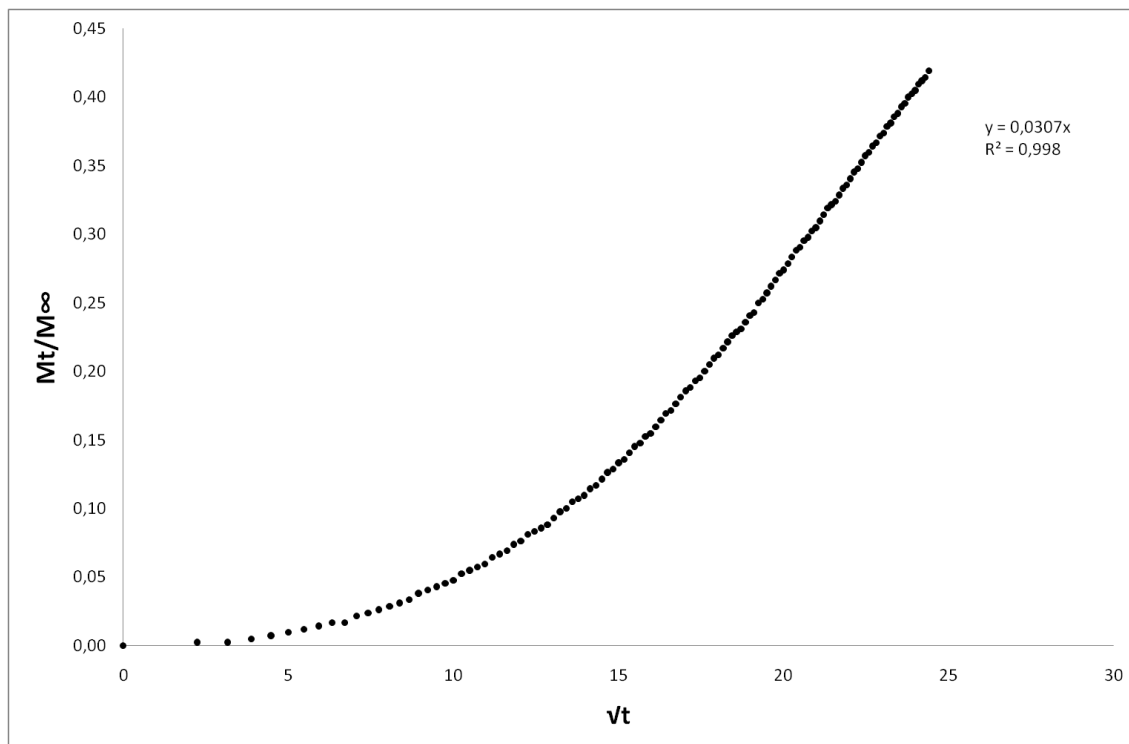


**Figure B-2**  $M_t/M_\infty$  vs.  $t^{1/2}$  graph of ethanol diffusion in MCM-41 at 26 °C

The slope of this graph was used to calculate diffusion coefficient.

## B.2 Calculating Diffusion Rate Constants and Diffusion Exponents

The type of transport mechanisms of volatile solvents in the mesopores of MCM-41 and CNT materials were predicted from the values of diffusion rate constants,  $k$ , and diffusion exponents,  $n$ , which were calculated from the graphs of  $\ln(M_t/M_\infty)$  vs.  $\ln(t)$  (Figure B-3).

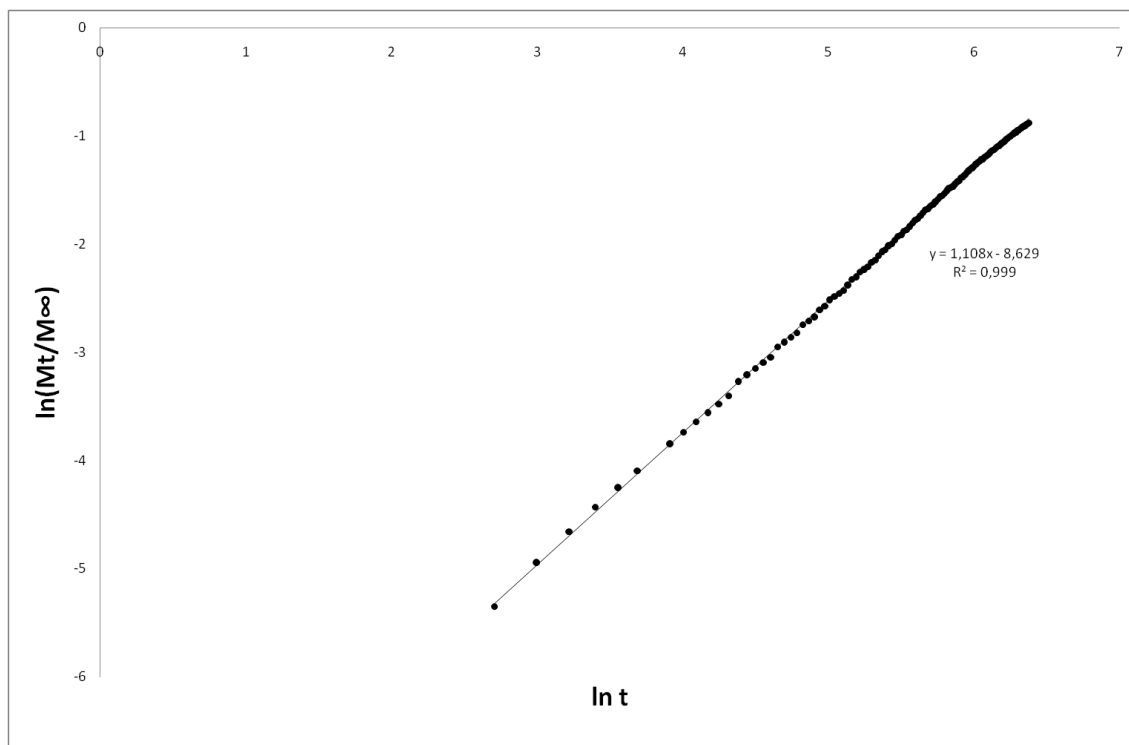


**Figure B-3**  $\ln(M_t/M_\infty)$  vs.  $\ln(t)$  graph of ethanol diffusion in MCM-41 at 26 °C

## APPENDIX C

### C.1 Diffusion Measurements in MCM-41

**Table C-1** Diffusion coefficients of alcohols in MCM-41

Alcohols/T	26 °C	28 °C	30 °C	32 °C
<b>Methanol</b>	$4.01 \times 10^{-13}$	$4.38 \times 10^{-13}$	$8.43 \times 10^{-13}$	$9.99 \times 10^{-13}$
<b>Ethanol</b>	$1.83 \times 10^{-13}$	$2.34 \times 10^{-13}$	$2.70 \times 10^{-13}$	$3.38 \times 10^{-13}$
<b>n-Propanol</b>	$8.26 \times 10^{-14}$	$1.09 \times 10^{-13}$	$1.40 \times 10^{-13}$	$1.72 \times 10^{-13}$
<b>n-Butanol</b>	$2.51 \times 10^{-14}$	$4.13 \times 10^{-14}$	$5.68 \times 10^{-14}$	$6.36 \times 10^{-14}$

**Table C-2** Diffusion coefficients of aromatics in MCM-41

Aromatics/T	26 °C	28 °C	30 °C	32 °C
<b>Benzene</b>	$3.96 \times 10^{-14}$	$5.47 \times 10^{-14}$	$7.38 \times 10^{-14}$	$9.52 \times 10^{-14}$
<b>Toluene</b>	$3.79 \times 10^{-14}$	$4.35 \times 10^{-14}$	$5.94 \times 10^{-14}$	$7.85 \times 10^{-14}$
<b>Ethylbenzene</b>	$3.74 \times 10^{-14}$	$4.12 \times 10^{-14}$	$5.87 \times 10^{-14}$	$6.64 \times 10^{-14}$
<b>Propylbenzene</b>	$3.26 \times 10^{-14}$	$3.52 \times 10^{-14}$	$3.90 \times 10^{-14}$	$4.41 \times 10^{-14}$
<b>o-Xylene</b>	$3.68 \times 10^{-14}$	$3.96 \times 10^{-14}$	$5.21 \times 10^{-14}$	$6.50 \times 10^{-14}$
<b>m-Xylene</b>	$3.42 \times 10^{-14}$	$3.79 \times 10^{-14}$	$4.65 \times 10^{-14}$	$6.01 \times 10^{-14}$
<b>p-Xylene</b>	$3.11 \times 10^{-14}$	$3.47 \times 10^{-14}$	$4.35 \times 10^{-14}$	$5.67 \times 10^{-14}$

## C.2 Diffusion Measurements in Metal Incorporated MCM-41

**Table C-3** Diffusion coefficients of alcohols in Cu-MCM-41-DS-25 (120/30)

Alcohols/T	26 °C	28 °C	30 °C	32 °C
<b>Methanol</b>	$8.06 \times 10^{-13}$	$8.52 \times 10^{-13}$	$9.18 \times 10^{-13}$	$1.06 \times 10^{-12}$
<b>Ethanol</b>	$4.12 \times 10^{-13}$	$4.99 \times 10^{-13}$	$5.23 \times 10^{-13}$	$8.34 \times 10^{-13}$
<b>n-Propanol</b>	$2.11 \times 10^{-13}$	$2.83 \times 10^{-13}$	$3.25 \times 10^{-13}$	$3.60 \times 10^{-13}$
<b>n-Butanol</b>	$6.94 \times 10^{-14}$	$7.93 \times 10^{-14}$	$9.94 \times 10^{-14}$	$1.02 \times 10^{-13}$

**Table C-4** Diffusion coefficients of alcohols in Ni-MCM-41-DS-25 (120/30)

Alcohols/T	26 °C	28 °C	30 °C	32 °C
<b>Methanol</b>	$4.58 \times 10^{-13}$	$4.81 \times 10^{-13}$	$5.13 \times 10^{-13}$	$5.51 \times 10^{-13}$
<b>Ethanol</b>	$2.23 \times 10^{-13}$	$3.75 \times 10^{-13}$	$3.99 \times 10^{-13}$	$5.07 \times 10^{-13}$
<b>n-Propanol</b>	$1.40 \times 10^{-13}$	$1.90 \times 10^{-13}$	$2.10 \times 10^{-13}$	$2.40 \times 10^{-13}$
<b>n-Butanol</b>	$7.85 \times 10^{-14}$	$1.16 \times 10^{-13}$	$1.29 \times 10^{-13}$	$1.39 \times 10^{-13}$

**Table C-5** Diffusion coefficients of alcohols in Co-MCM-41-DS-25 (120/30)

Alcohols/T	26 °C	28 °C	30 °C	32 °C
<b>Methanol</b>	$4.10 \times 10^{-13}$	$4.85 \times 10^{-13}$	$5.33 \times 10^{-13}$	$6.05 \times 10^{-13}$
<b>Ethanol</b>	$2.27 \times 10^{-13}$	$3.77 \times 10^{-13}$	$3.97 \times 10^{-13}$	$4.15 \times 10^{-13}$
<b>n-Propanol</b>	$1.62 \times 10^{-13}$	$1.70 \times 10^{-13}$	$1.97 \times 10^{-13}$	$2.28 \times 10^{-13}$
<b>n-Butanol</b>	$7.77 \times 10^{-14}$	$1.14 \times 10^{-13}$	$1.47 \times 10^{-13}$	$1.62 \times 10^{-13}$

**Table C-6** Diffusion coefficients of alcohols in Fe-MCM-41-DS-25 (120/30)

Alcohols/T	26 °C	28 °C	30 °C	32 °C
<b>Methanol</b>	$2.83 \times 10^{-13}$	$2.97 \times 10^{-13}$	$3.00 \times 10^{-13}$	$4.32 \times 10^{-13}$
<b>Ethanol</b>	$2.24 \times 10^{-13}$	$2.70 \times 10^{-13}$	$2.86 \times 10^{-13}$	$4.05 \times 10^{-13}$
<b>n-Propanol</b>	$1.77 \times 10^{-13}$	$2.63 \times 10^{-13}$	$2.72 \times 10^{-13}$	$2.86 \times 10^{-13}$
<b>n-Butanol</b>	$7.39 \times 10^{-14}$	$7.62 \times 10^{-14}$	$8.33 \times 10^{-14}$	$1.18 \times 10^{-13}$

### C.3 Diffusion Measurements in CNT

**Table C-7** Diffusion coefficients of alcohols in CNT

Alcohols/T	26 °C	28 °C	30 °C	32 °C
<b>Methanol</b>	$5.42 \times 10^{-12}$	$5.98 \times 10^{-12}$	$7.13 \times 10^{-12}$	$9.15 \times 10^{-12}$
<b>Ethanol</b>	$4.03 \times 10^{-12}$	$5.09 \times 10^{-12}$	$6.75 \times 10^{-12}$	$9.00 \times 10^{-12}$
<b>n-Propanol</b>	$3.75 \times 10^{-12}$	$4.83 \times 10^{-12}$	$6.04 \times 10^{-12}$	$8.58 \times 10^{-12}$
<b>n-Butanol</b>	$2.08 \times 10^{-12}$	$2.66 \times 10^{-12}$	$3.99 \times 10^{-12}$	$5.20 \times 10^{-12}$

**Table C-8** Diffusion coefficients of aromatics in CNT

Aromatics/T	26 °C	28 °C	30 °C	32 °C
<b>Benzene</b>	$4.67 \times 10^{-12}$	$1.11 \times 10^{-11}$	$1.30 \times 10^{-11}$	$1.62 \times 10^{-11}$
<b>Toluene</b>	$2.85 \times 10^{-12}$	$3.85 \times 10^{-12}$	$1.06 \times 10^{-11}$	$1.23 \times 10^{-11}$
<b>Ethylbenzene</b>	$2.71 \times 10^{-13}$	$4.68 \times 10^{-13}$	$1.40 \times 10^{-12}$	$4.13 \times 10^{-12}$
<b>Propylbenzene</b>	$1.52 \times 10^{-13}$	$2.97 \times 10^{-13}$	$4.79 \times 10^{-13}$	$1.19 \times 10^{-12}$
<b>o-Xylene</b>	$1.81 \times 10^{-12}$	$3.22 \times 10^{-12}$	$4.93 \times 10^{-12}$	$6.10 \times 10^{-12}$
<b>m-Xylene</b>	$2.22 \times 10^{-12}$	$3.75 \times 10^{-12}$	$5.42 \times 10^{-12}$	$6.75 \times 10^{-12}$
<b>p-Xylene</b>	$2.39 \times 10^{-12}$	$4.23 \times 10^{-12}$	$6.63 \times 10^{-12}$	$9.73 \times 10^{-12}$

## APPENDIX D

### CURRICULUM VITAE

#### ASLI NALBANT ERGÜN

Sabancı University,

Faculty of Engineering and Natural Sciences,

Orhanli, Tuzla, 34956 Istanbul TURKEY

[aslin@sabanciuniv.edu](mailto:aslin@sabanciuniv.edu)

#### **Education:**

**Ph.D.** Sabancı University, Material Science and Engineering Department, Faculty of Engineering and Natural Sciences, Istanbul, Turkey, 2005-Recent

**M.S.** Middle East Technical University, Chemical Engineering Department, Faculty of Engineering, Ankara, Turkey, 2003-2005

**B.S.** Middle East Technical University, Chemical Engineering Department, Faculty of Engineering, Ankara, Turkey, 1999-2003

#### **Work Experience:**

- ❖ Teaching Assistant, Faculty of Engineering and Natural Sciences, Sabancı University, Istanbul, Turkey, 2005-Recent

*Teaching Experience:* MAT 202- Kinetics and Kinetics Lab, CHEM 301-Inorganic Chemistry and Lab, MAT 401-Surface Chemistry, NS 207-Organic Chemistry and Lab, ENS 205-Material Science I

*Hands on experience:* XRD, SEM, FTIR, TGA/DSC, Gas Sorption Analyzer, IGA, GCMS, Calorimeter, Sulphur Analyzer

- ❖ Researcher at BOREN Project: Catalytic Synthesis of Boron Nitride Nanotubes with Hydrothermal and Microwave Energy and Application of BNTs in Hydrogen Storage
- ❖ Editorial Board of EMCC-6 Conference
- ❖ Researcher at COPOWER Project: European Union Sixth Framework Program, Sustainable Energy Systems
- ❖ Supervisor at Undergraduate Project: Biodiesel Production, 2005
- ❖ Internship, UNILEVER Co, Kocaeli, Turkey, 6-8 2002
- ❖ Internship, YASAŞ Paint and Chemicals Co., Kocaeli, Turkey, 6-8 2001

### **Scholarships:**

- ❖ Full scholarship from Sabancı University, Istanbul, Turkey, 2005-Recent

### **Awards:**

- ❖ Sabancı University Travel Award
- ❖ ICAM Junior Travel Award
- ❖ Best Oral Presentation, School of Catalysis Conference, Russia
- ❖ Tubitak Travel Award

### **Memberships:**

- ❖ Member of American Chemical Society (ACS)
- ❖ Member of Material Research Society (MRS)
- ❖ Member of Catalysis Society of Turkey
- ❖ Member of Complex Adaptive Matter (ICAM)

### **Journal Articles:**

1. A. Nalbant, T. Doğu, S. Balcı, "Ni and Cu Incorporated Mesoporous Nanocomposite Catalytic Materials", Journal of Nanoscience and Nanotechnology, 2008, Vol 8., pp. 549-556
2. Ö. Haklı, A. G. Dumanlı, A. Nalbant, F. Okyay, And Y. Yürüm, "Conversion of Low-rank Kilyos Coal to Nitrogeneous Fertilizers", Energy Sources, Part A, 2010, 32, 19, pp.1-7

### **Journal Articles in Progress:**

1. A. Nalbant Ergün, Y. Yürüm, “Microwave Assisted Synthesis of MCM-41 Mesoporous Molecular Sieves”, in progress
2. A. Nalbant Ergün, Y. Yürüm, “Microwave Assisted Synthesis of Metal Incorporated MCM-41 Mesoporous Molecular Sieves”, in progress
3. A. Nalbant Ergün, Y. Yürüm, “Diffusion of Alcohols in Mesoporous Media: MCM-41 and CNT”, in progress
4. A. Nalbant Ergün, Y. Yürüm, “Diffusion of Aromatics in Mesoporous Media: MCM-41 and CNT”, in progress
5. A. Nalbant Ergün, Y. Yürüm, “Investigation of Alcohol Diffusion in Metal Incorporated MCM-41”, in progress

### **Conference Proceedings:**

1. A. Nalbant Ergün, Y. Yürüm, 6<sup>th</sup> Chemical Engineering Conference for Collaborative Research in Eastern Mediterranean Countries, EMCC-6, March 7-12, 2010, Antalya, Turkey, “Carbon Nanotube Production over MCM-41 Type Catalytic Materials via CVD Method”,
2. A. Nalbant Ergün, Y. Yürüm, 3<sup>rd</sup> International School-Conference on Catalysis for Young Scientists “Catalyst Design”, July 13-18 2009, “Chusovaya”, Ekaterinburg region, Russia, “MCM-41 Type Catalytic Materials via Microwave Synthesis”
3. A. Nalbant, Y. Yürüm, Gordon Research Conferences (GRC) Hydrocarbon Resources, January 11-16, 2009, Ventura Beach Marriott, California, USA, “Use of Metal-MCM-41 Type of Catalysts in the Synthesis of CNTs by CVD”
4. A. Nalbant, Y. Yürüm, NCC-2, 2<sup>nd</sup> National Catalysis Conference, June 18-21, 2008, Erzurum, Turkey, “MCM-41 Type Catalytic Materials via Impregnation and Microwave Assisted Synthesis Methods”
5. A. Nalbant, A.G. Dumanlı, Y. Yürüm, EMCC 5, 5th Chemical Engineering Conference for Collaborative Research in Eastern Mediterranean Countries, May 24-29 2008, Cetraro, Italy, “ MCM-41 Type Catalytic Materials Synthesized by Microwave Radiation and Utilization of these in CNT/CNF and Mesoporous Carbon Production”

6. A.G. Dumanlı, B.Sakintuna, A. Nalbant, A. Erden, Y. Yürüm, EMCC 5, 5th Chemical Engineering Conference for Collaborative Research in Eastern Mediterranean Countries, May 24-29 2008, Cetraro, Italy, "Carbon Nanofibers, Templated Mesoporous Carbons and Supercapacitors"
7. A.G. Dumanlı, A. Nalbant, Y. Yürüm, Somer Symposium Series 1, May 14-15 2007, Ankara, Turkey, "Utilization of MCM-41 Type Catalytic Materials Synthesized by Microwave Induced Heating in the Production of Carbon Nanotubes"
8. A. Nalbant, y. Yürüm, First National Catalysis Conference , NCC-1, 18-21 January 2007, Northern Cyprus, "Co-MCM-41 Type Catalytic Materials via Impregnation & Microwave Assisted Synthesis Methods
9. A. Nalbant, Y. Yürüm, ACS, Division of Industrial & Engineering Chemistry, Membrane Materials and Applications, Sponsored by Separation Science and Technology Sub-Division 232nd National Meeting & Exposition, September 10-14, 2006, San Francisco, USA, "Microwave Assisted Synthesis of MCM-41 & Diffusion of Organic Solvents in Porous Media"
10. Y. Güçbilmez, C. Şener, A. Nalbant, T. Doğu, International Workshop on Nanostructured Materials, NANOMAT, June 20-23, 2006, Antalya, Turkey, "Ni and Cu Incorporated Mesoporous Nanocomposite Catalytic Materials"
11. A. Nalbant, Y. Yürüm, International Workshop on Nanostructured Materials, NANOMAT, June 20-23, 2006, Antalya, Turkey "Microwave Assisted Synthesis of Copper and Nickel Incorporated Materials"
12. A. Nalbant, C. Şener, Y. Güçbilmez, T. Doğu, 4th Eastern Mediterranean Chemical Engineering Conference ,EMCC-4, Dead Sea, Israel, 2006, pp. 378-379, "Metal & Metal Oxide Incorporated MCM-41 Type Mesoporous Materials and Their Catalytic Applications"
13. A. Nalbant, T. Doğu, Microporous and Mesoporous Materials Meeting, Rome, Italy, December 2004, "Synthesis and Characterization of Cu-MCM-41 Type Catalytic Materials"